



U.S. Department
of Transportation
Federal Railroad
Administration

EVALUATION OF TWO PROTOTYPE DEVICES FOR NON-DESTRUCTIVELY MEASURING STRESSES IN RAILROAD WHEELS

Office of Research and
Development
Washington D.C. 20590

R. L. Higgins and B. R. Rajkumar

**Association of American Railroads
Transportation Test Center
Pueblo, Co 81001**

DOT/FRA/ORD-92/15

October 1992
Final Report

This document is available to the
U.S. public through the National
Technical Information Service
Springfield, Virginia 22161

DISCLAIMER

This document is disseminated under the sponsorship of the Department of Transportation in the interest of information exchange. The United States Government assumes no liability for the contents or use thereof. The United States Government does not endorse products or manufacturers. Trade or manufacturers' names appear herein solely because they are considered essential to the object of this report.

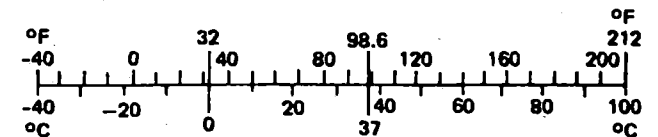
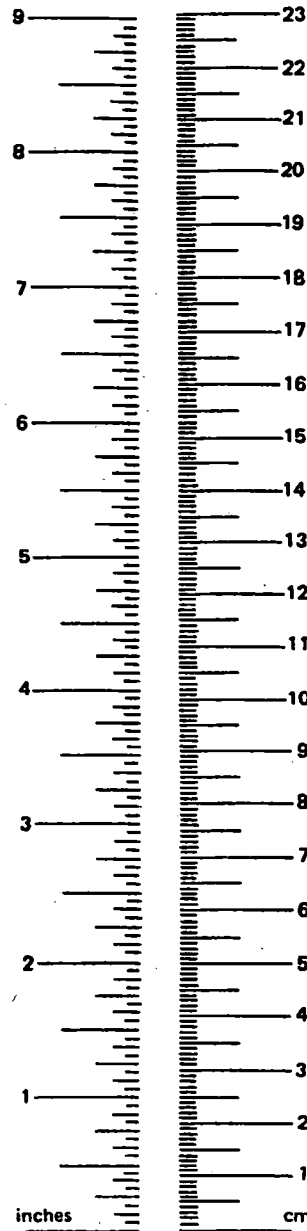
METRIC CONVERSION FACTORS

Approximate Conversions to Metric Measures

Symbol	When You Know	Multiply by	To Find	Symbol
LENGTH				
in	inches	*2.50	centimeters	cm
ft	feet	30.00	centimeters	cm
yd	yards	0.90	meters	m
mi	miles	1.60	kilometers	km
AREA				
in ²	square inches	6.50	square centimeters	cm ²
ft ²	square feet	0.09	square meters	m ²
yd ²	square yards	0.80	square meters	m ²
mi ²	square miles	2.60	square kilometers	km ²
	acres	0.40	hectares	ha
MASS (weight)				
oz	ounces	28.00	grams	g
lb	pounds	0.45	kilograms	kg
	short tons	0.90	tonnes	t
	(2000 lb)			
VOLUME				
tsp	teaspoons	5.00	milliliters	ml
Tbsp	tablespoons	15.00	milliliters	ml
fl oz	fluid ounces	30.00	milliliters	ml
c	cups	0.24	liters	l
pt	pints	0.47	liters	l
qt	quarts	0.95	liters	l
gal	gallons	3.80	liters	l
ft ³	cubic feet	0.03	cubic meters	m ³
yd ³	cubic yards	0.76	cubic meters	m ³
TEMPERATURE (exact)				
'F	Fahrenheit temperature	5/9 (after subtracting 32)	Celsius temperature	'C

Approximate Conversions from Metric Measures

Symbol	When You Know	Multiply by	To Find	Symbol
LENGTH				
mm	millimeters	0.04	inches	in
cm	centimeters	0.40	inches	in
m	meters	3.30	feet	ft
m	meters	1.10	yards	yd
km	kilometers	0.60	miles	mi
AREA				
cm ²	square centim.	0.16	square inches	in ²
m ²	square meters	1.20	square yards	yd ²
km ²	square kilom.	0.40	square miles	mi ²
ha	hectares (10,000 m ²)	2.50	acres	
MASS (weight)				
g	grams	0.035	ounces	oz
kg	kilograms	2.2	pounds	lb
t	tonnes (1000 kg)	1.1	short tons	
VOLUME				
ml	milliliters	0.03	fluid ounces	fl oz
l	liters	2.10	pints	pt
l	liters	1.06	quarts	qt
l	liters	0.26	gallons	gal
m ³	cubic meters	36.00	cubic feet	ft ³
m ³	cubic meters	1.30	cubic yards	yd ³
TEMPERATURE (exact)				
'C	Celsius temperature	9/5 (then add 32)	Fahrenheit temperature	'F



* 1 in. = 2.54 cm (exactly)

1. Report No. FRA/ORD-92/15	2. Government Accession No.		3. Recipient's Catalog No.	
4. Title and Subtitle EVALUATION OF TWO PROTOTYPE DEVICES FOR NON-DESTRUCTIVELY MEASURING STRESSES IN RAILROAD WHEELS			5. Report Date October 1992	
			6. Performing Organization Code	
7. Author(s) R.L. Higgins B.R. Rajkumar			8. Performing Organization Report No.	
			10. Work Unit No. (TRAIS)	
9. Performing Organization Name and Address Association of American Railroads Transportation Test Center P.O. Box 11130 Pueblo, CO 81001			11. Contract or Grant No. DTFR53-82-C-00282 Task Order 32	
			13. Type of Report or Period Covered Final Report	
12. Sponsoring Agency Name and Address U.S. Department of Transportation Federal Railroad Administration Office of Research and Development 400 7th St. SW Washington, D.C. 20590			14. Sponsoring Agency Code	
			15. Supplementary Notes	
16. Abstract Two devices designed to non-destructively determine the residual stress state of railroad wheels were evaluated. The first device was a magnetoacoustic design developed by the National Aeronautics and Space Administration, Langley Research Center in conjunction with the Association of American Railroads, Chicago Technical Center. The second device was an acoustic birefringence device developed by the National Institute of Standards and Technology. The evaluation involved comparison of results from the non-destructive devices with results from more conventional destructive analysis.				
17. Key Words Non-Destructive Evaluation, NDE, Railroad Wheel Stress, Residual Stress Measurement			18. Distribution Statement This document is available through National Technical Information Service Springfield, VA 22161	
19. Security Classification (of the report)	20. Security Classification (of this page)		21. No. of Pages	22. Price

Form DOT F 1700.7 (8-72)

EXECUTIVE SUMMARY

The Association of American Railroads (AAR) carried out an extensive research program entitled Wheel Failure Mechanisms, funded by the Federal Railroad Administration (FRA) to study the causes of wheel thermal failure. Under this program, an investigation of promising methodologies was made to review and evaluate available nondestructive techniques for isolating critically stressed wheels. Subsequently, FRA funded the current program at the Transportation Test Center (TTC), Pueblo, Colorado, to evaluate two prototype devices designed to non-destructively measure the residual stresses in the rims of the railroad wheels. The two prototypes tested were an acoustic birefringence device developed by the National Institute of Standards and Technology (NIST), and a magnetoacoustic device developed by the National Aeronautics and Space Administration (NASA) Langley Laboratories in collaboration with the AAR's Chicago Technical Center (CTC).

Under this project, test procedures were developed with these two techniques to estimate the average residual stresses in the rims of selected wheels. The type of transducers, their orientation with reference to the rim of a railroad wheel, and the respective fixtures were standardized for optimum results. The residual stress measurements with these two techniques were compared with the estimated stresses from semi-destructive and destructive stress evaluation techniques (the hole-drilling/strain-gaging technique and saw-cut/displacement technique, respectively) for evaluating the accuracy and reliability of the two non-destructive evaluation (NDE) techniques.

Test specimens were comprised of an assortment of 17 railroad wheels: Class U, Class C, straight plate, curved plate, as manufactured, drag braked and inductively heated. The summary of test results with the prototypes from NIST and NASA are as follows:

- The acoustic birefringence method is capable of distinguishing between tensile and compressive residual stresses in the rims of railroad wheels reliably, given a proper value of stress free birefringence (B_0). This technique demonstrated an accuracy of more than 70 percent when compared to the estimated residual stresses from the destructive technique.
- A proper value of stress free birefringence B_0 is apparently in some doubt.
- Acoustic birefringence as currently defined is not, in general, a reliable indicator of actual residual stress value.

- **The results from the magnetoacoustic method show some correlation with the results obtained using saw cutting when the wheel has a net residual tension according to the saw cut data.**
- **The magnetoacoustic method, in its current configuration, cannot reliably distinguish between compressive and tensile stresses in a railroad wheel.**
- **The magnetoacoustic method in its current configuration is not, in general, a reliable indicator of actual residual stress values in the rim of a railroad wheel.**

Table of Contents

1.0 INTRODUCTION	1
2.0 OBJECTIVES	2
3.0 METHODOLOGY	2
3.1 MAGNETOACOUSTIC TECHNIQUE	2
3.2 ACOUSTIC BIREFRINGENCE TECHNIQUE	2
3.3 DESTRUCTIVE TECHNIQUE USING SAW-CUT DISPLACEMENT DATA	3
4.0 INSTRUMENTATION	8
4.1 MAGNETOACOUSTIC	8
4.2 ACOUSTIC BIREFRINGENCE	9
4.3 HOLE DRILLING STRAIN GAGING	11
4.4 SAW CUTTING	11
5.0 TEST PROCEDURES	12
5.1 NON DESTRUCTIVE EVALUATION	12
5.1.1 Magnetoacoustic (NASA)	12
5.1.2 Acoustic Birefringence (NIST)	16
5.2 SEMI-DESTRUCTIVE AND DESTRUCTIVE EVALUATION	18
5.2.1 Hole Drilling Procedure	18
5.2.2 Saw Cutting Procedure	21
6.0 PRELIMINARY NDE MEASUREMENTS WITH WHEEL RIM FLEXING DEVICE	21
6.1 MAGNETOACOUSTIC MEASUREMENTS	22
6.2 ACOUSTIC BIREFRINGENCE MEASUREMENTS	24
7.0 DATA	25
7.1 DATA MEASUREMENT LOCATIONS ON TEST WHEELS	26
7.2 ACOUSTIC BIREFRINGENCE DATA	28
7.3 MAGNETOACOUSTIC DATA	28
7.4 HOLE DRILLING DATA	28
7.5 SAW-CUT DATA	28

8.0 DATA ANALYSIS	30
8.1 ACOUSTIC BIREFRINGENCE DATA	30
8.2 MAGNETOACOUSTIC DATA	31
8.3 HOLE DRILLING DATA	32
8.4 SAW-CUT DATA	33
9.0 RESULTS	33
9.1 SAW CUTTING VS. ACOUSTIC BIREFRINGENCE	33
9.2 SAW CUTTING VS. MAGNETOACOUSTIC TECHNIQUE	37
10.0 DISCUSSION	37
11.0 RECOMMENDATIONS	39
APPENDIX A -- COMPARISON OF 3D FINITE ELEMENT MODEL AND TTC CLOSED FORM SOLUTION	A1
APPENDIX B -- DATA MEASUREMENT LOCATION MAPS	B1
APPENDIX C -- ACOUSTIC BIREFRINGENCE DATA	C1
APPENDIX D -- MAGNETOACOUSTIC DATA	D1
APPENDIX E -- HOLE-DRILLING STRAIN-GAGE DATA	E1
APPENDIX F -- SAW-CUT DATA	F1
APPENDIX G -- HOLE-DRILLING STRAIN-GAGE DATA ANALYSIS	G1
APPENDIX H -- COMPUTED STRESSES FROM HOLE DRILLING STRAIN- GAGE DATA	H1
APPENDIX I -- RESIDUAL STRESSES COMPUTED FROM SAW-CUT DATA USING TTC'S "CLOSED FORM" SOLUTION	I1
APPENDIX J -- INTERIM REPORT AND ANALYSIS OF W1, W5, W6, AND W7 BY NIST	J1

List of Figures

Figure 1. Typical Responses of Wheel Flange Tip During Saw Cut	5
Figure 2. Saw Cut Displacement and Corresponding Hoop Stress	6
Figure 3. Residual Circumferential Stresses (KSI) from 3D Finite Element Analysis.	7
Figure 4. Magnetoacoustic Cabling Configuration	8
Figure 5. Acoustic Birefringence System Configuration	9
Figure 6. Acoustic Birefringence EMAT Mounting Arrangement.....	10
Figure 7. Schematic of Saw Cutting unit at TTC.....	12
Figure 8. Typical 5 MHz Shear Wave Magnetoacoustic Data.....	15
Figure 9. Acoustic Birefringence EMAT Echo Signal.....	17
Figure 10. Acoustic Birefringence First Echo Pulse (Enlarged)	17
Figure 11. Residual Stresses Strain Gage Rosette Arrangement	20
Figure 12. Schematic of Applied Load Fixture.....	22
Figure 13. Frequency Shift for Circumferentially Polarized Shear Waves	23
Figure 14. Frequency Shift for Radially Polarized Shear Waves.....	23
Figure 15. Birefringence Change With Increasing Compressive Hoop Stress	24
Figure 16. Typical Measurement Locations on the Test Wheels	27
Figure 17. Analysis of 5 MHz Magnetoacoustic Data	31
Figure 18. Hole Drilling Stress vs. Saw Cut Net Rim Force	32
Figure 19. Acoustic Birefringence vs. Destructive Methods.	35
Figure 20. Rim Block (B_o) Values.....	36
Figure 21. NDE Measurement Regimes	38

List of Tables

Table 1. Test Matrix.....	25
Table 2. Wheel Specifications.....	26
Table 3. Comparison of Acoustic Birefringence and Saw Cutting Results	29
Table 4. Comparisons of Magnetoacoustic and Saw Cutting Results	29

1.0 INTRODUCTION

The Wheel Failure Mechanisms Program, funded by the Federal Railroad Administration (FRA)¹ has shown that the stresses most likely to lead to wheel failure are the after-effects of thermal abuse such as defective air brakes, unreleased handbrakes or other unusual braking conditions, all of which generate large heat inputs. It is customary in railroad operation to apply prolonged drag braking in terrains with steep slopes, and if braking continues for a long time, wheels are severely heated. On these occasions, wheel temperature is raised and compressive thermal stresses higher than the yield stresses of the material may be produced in the rim of a railroad wheel. When the wheels are cooled a tensile residual stress field in the wheel rim may result. The higher the amount of tensile residual stress in the rim, the greater the risk of wheel fracture initiated from a thermal crack.

Currently, wheels are removed from service when they reach a designated level of plate discoloration due to heat developed during braking. It has been found that many discolored wheels are still safe even though the discoloration rule would have categorized them as dangerous. Conversely, several non-discolored wheels have been found to have high residual stresses. These findings were reported by the Association of American Railroads (AAR) under the Wheel Failure Mechanisms program, where more than 500 freight car wheels (taken out of service by various railroads) were saw cut and the residual stresses were computed using an AAR-developed computer model.²

For these reasons, the FRA funded the current project at the Transportation Test Center (TTC) to investigate two promising non-destructive evaluation (NDE) devices to quantify the wheel rim stresses and provide more effective means of reducing the frequency of catastrophic wheel failures in service. This report describes the test procedures and results of two prototypes in the evaluation of residual stresses in selected wheels as compared with the results of destructive techniques developed during the Wheel Failure Mechanisms program. The following two prototype devices were investigated for the evaluation of residual stresses in railroad wheels:

- Magnetoacoustic, developed by the National Aeronautics and Space Administration (NASA) Langley Laboratories.
- Acoustic birefringence, developed by the National Institute of Standards and Technology (NIST).

The work described in this report was performed by the Association of American Railroads at the TTC, Pueblo, Colorado.

2.0 OBJECTIVES

Residual stresses in selected railroad wheels with different designs (straight, curved, and S plate), heat treatment (Class U and Class C), and various thermal histories (new, drag braked, and inductively heated) were determined with two prototype devices (magnetoacoustic and acoustic birefringence). These results were compared with the estimated stress as determined by the destructive saw cutting technique to determine the efficacy of the prototype devices.

3.0 METHODOLOGY

A brief description of the two NDE techniques and the destructive method for determining the level of residual stresses in the rims of railroad wheels is presented below:

3.1 MAGNETOACOUSTIC TECHNIQUE

The residual stress characterization by the magnetoacoustic method was developed at the NASA Langley Research Center under laboratory conditions and subsequently adapted for railroad wheels in collaboration with AAR's Chicago Technical Center. In this method, the state of internal stress in steel is determined by measuring the material magnetic domain interaction with both stress field and the ultrasonic wave propagation. The tests conducted in the laboratory on a standard steel specimen indicated that this technique was capable of identifying both tensile and compressive stresses in steel.

This technique measures small changes in ultrasonic wave velocity under various stress conditions during application of an external magnetic field. The fractional change in the natural ultrasonic velocity ($\Delta V/V$) of a wave propagating perpendicular to the magnetic field direction is affected by the uniaxial stress (applied parallel to the field). The adaptation of this method for residual hoop stress measurements in railroad wheels required the design of special magnets and the reassessment of acoustic transducer configurations (compressional wave, surface wave, and shear wave transducers) for optimum results.

3.2 ACOUSTIC BIREFRINGENCE TECHNIQUE

This technique uses an electromagnetic acoustic transducer (EMAT) applied to the front rim face of a railroad wheel to produce and orthogonally polarized shear horizontal waves which are propagated through the thickness of the wheel rim. The arrival times through the wheel rim are measured (in pulse-echo mode) and the

difference in arrival time in two orthogonal directions (birefringence) is related to the difference in the principal stresses measured in the hoop and radial directions of the wheel rim.

3.3 DESTRUCTIVE TECHNIQUE USING SAW-CUT DISPLACEMENT DATA

During the implementation of FRA funded Wheel Failure Mechanisms program, the TTC developed a closed form analytical method to evaluate the average distribution of residual hoop stresses in the wheel from the saw-cut displacement data. This analytical model assumes that the cut portion of the wheel consists of several interconnected rings, with the adjacent rings developing interactive shear and radial stresses at the interface, depending on the magnitude of relative displacements between them. Equations, based on the theory of elasticity, were developed to determine the forces acting on the cut as a function of tip displacements. It was possible to compute average residual stress and the net rim force in the wheel for various saw-cut displacement behaviors.

If a rail car wheel is cut radially, one of the three general types of behavior will be observed as presented in Figure 1. The flange tip of a thermally damaged wheel (tensile residual stress) will open continuously as the cut proceeds inwards. The flange tip of a new, heat treated wheel (Class-B or Class-C) in compressive stress will close continuously as the cut proceeds inwards. A new or undamaged Class-U wheel will exhibit a closing of the flange tip as the cut proceeds into the rim (up to 2 inches), with the flange tip opening as the cut proceeds inwards into the plate.

Figure 2 presents an example of the average hoop stress distribution and the net rim force calculation (Appendix A) in a 36-inch diameter Class-U wheel for a given saw-cut displacement. Even though the above analysis does not show the stress gradient across the cross section of a railroad wheel, it was extremely useful in interpreting the saw-cut displacement data for more than 500 freight car wheels in the Wheel Failure Mechanisms program.

In collaboration with the Illinois Institute of Technology Research Institute (IITRI), the AAR developed a second technique which was a more comprehensive analysis using a three-dimensional finite element approach. This procedure required measurement of the saw-cut opening displacement on both sides of the wheel along the entire length of a cut. A circumferential displacement loading was

assumed on the free surface to close the cut. Stresses calculated for the plane of the cut were then an indication of the stresses that existed before the wheel was cut. Figure 3 shows a typical residual stress distribution predicted by this analysis.

The results of the three dimensional (3D) finite element analysis and the closed form solution developed at TTC were compared for five wheels (Appendix A) which were saw cut under the Wheel Failure Mechanisms program. The stress contours from the 3D stress analysis were integrated over the rim surface and multiplied by the incremental cross section area of the wheel to determine the effective rim force acting on the rim cross sectional area. These results were very close to the results of the closed form solution developed at TTC; with the assurance that the simple closed form solution does give reasonable predictions of rim force based only on the flange tip displacement history. In view of the above agreement with the more extensive three-dimensional finite element analysis, the closed form solution has been used for saw cutting analysis of 17 wheels and the results were used as a basis for comparison with the NDE measurements in the current program.

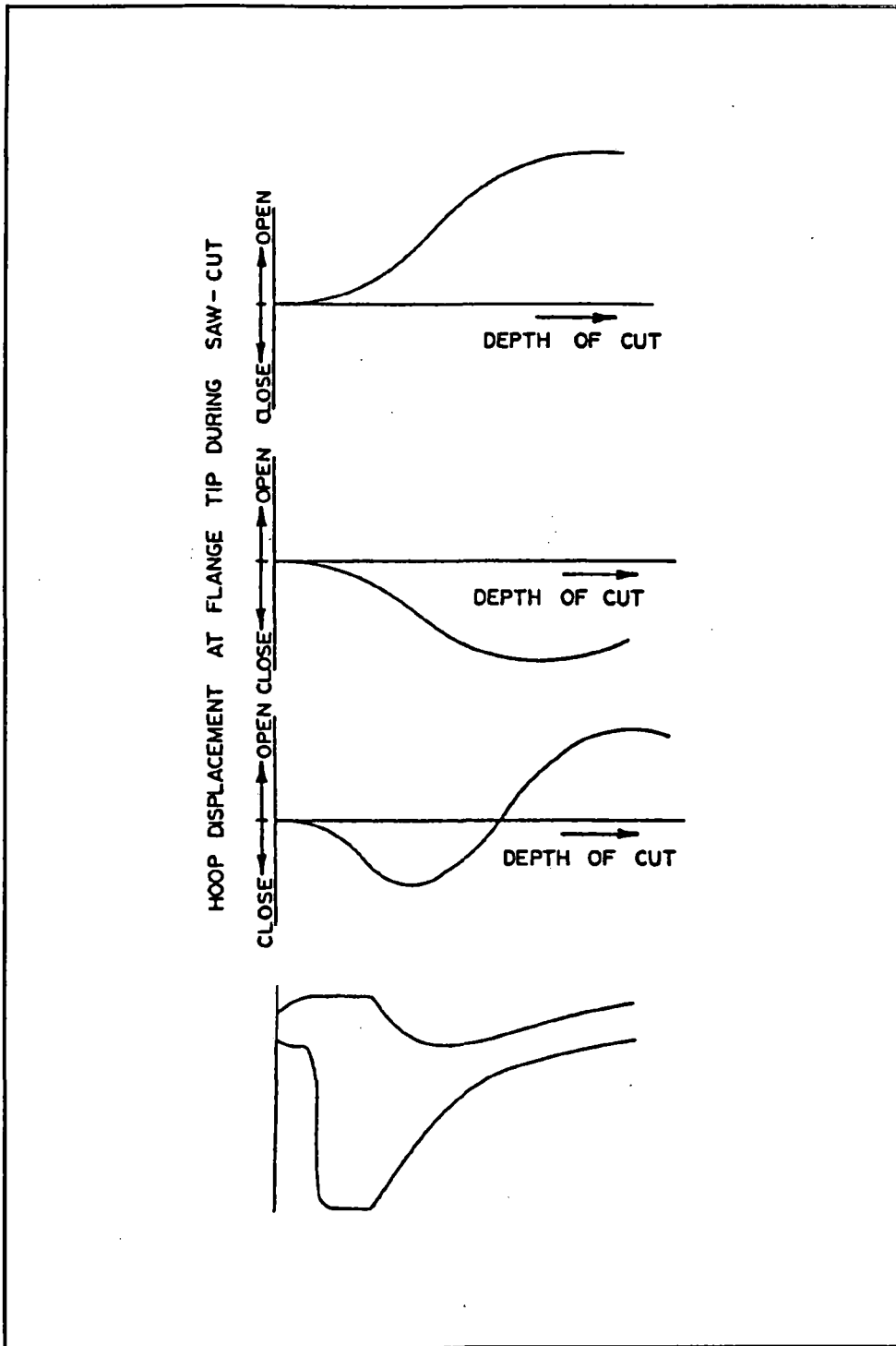


Figure 1. Typical Responses of Wheel Flange Tip During Saw Cut

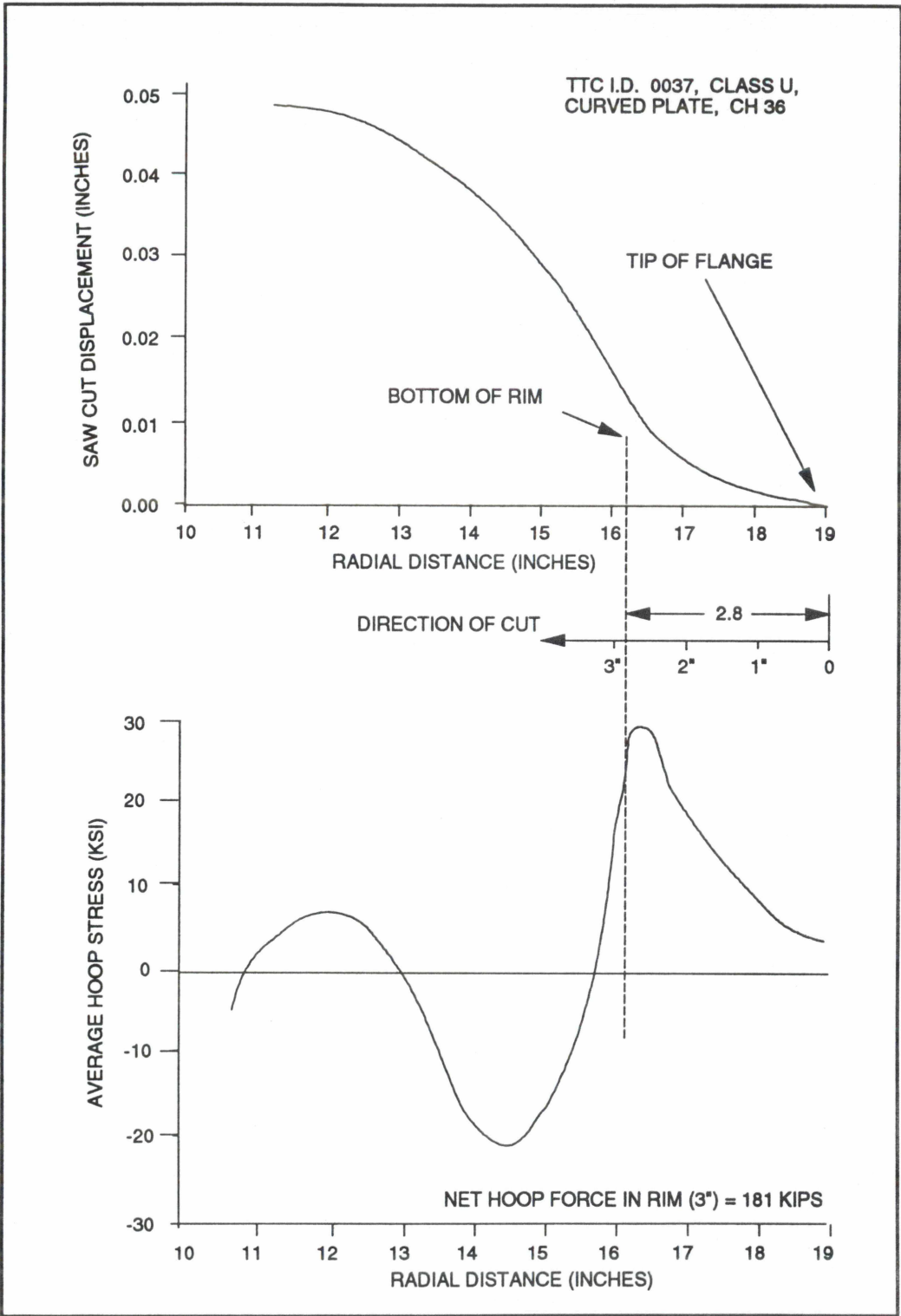


Figure 2. Saw Cut Displacement and Corresponding Hoop Stress

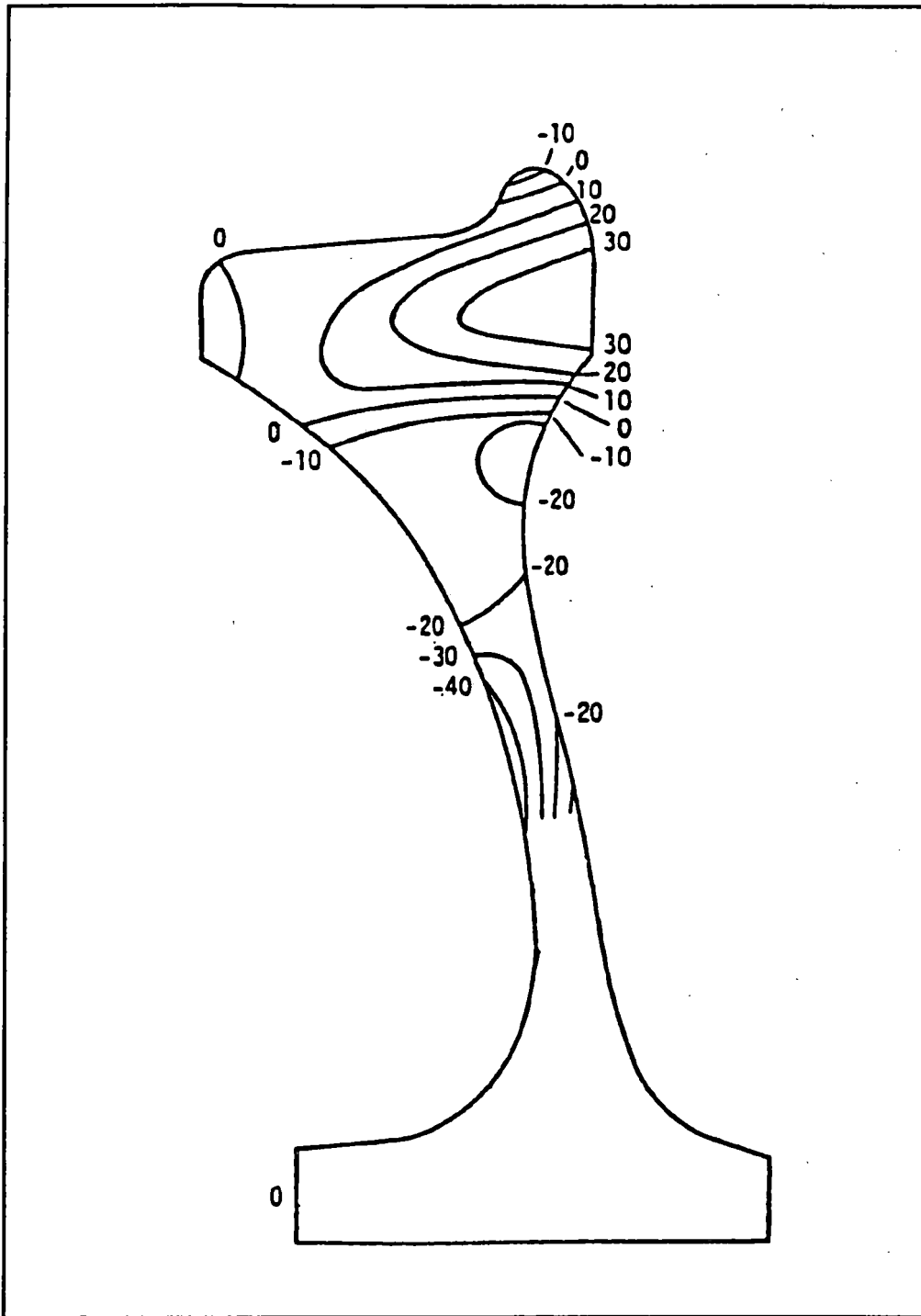


Figure 3. Residual Circumferential Stresses (KSI) from 3D Finite Element Analysis

4.0 INSTRUMENTATION

4.1 MAGNETOACOUSTIC

Figure 4 is a schematic representation of the magnetoacoustic equipment. This equipment was delivered as an integral unit to the TTC in May 1991 from NASA Langley through AAR's Chicago Technical Center. The prototype device consists primarily of:

- Electronic equipment required to produce the properly polarized acoustic wave via piezoelectric transducer
- Pulsed phase lock loop (P2L2) interferometer
- Data collection and analysis computer
- Specially designed electromagnet with pole pieces shaped to fit against the rim of a railroad wheel

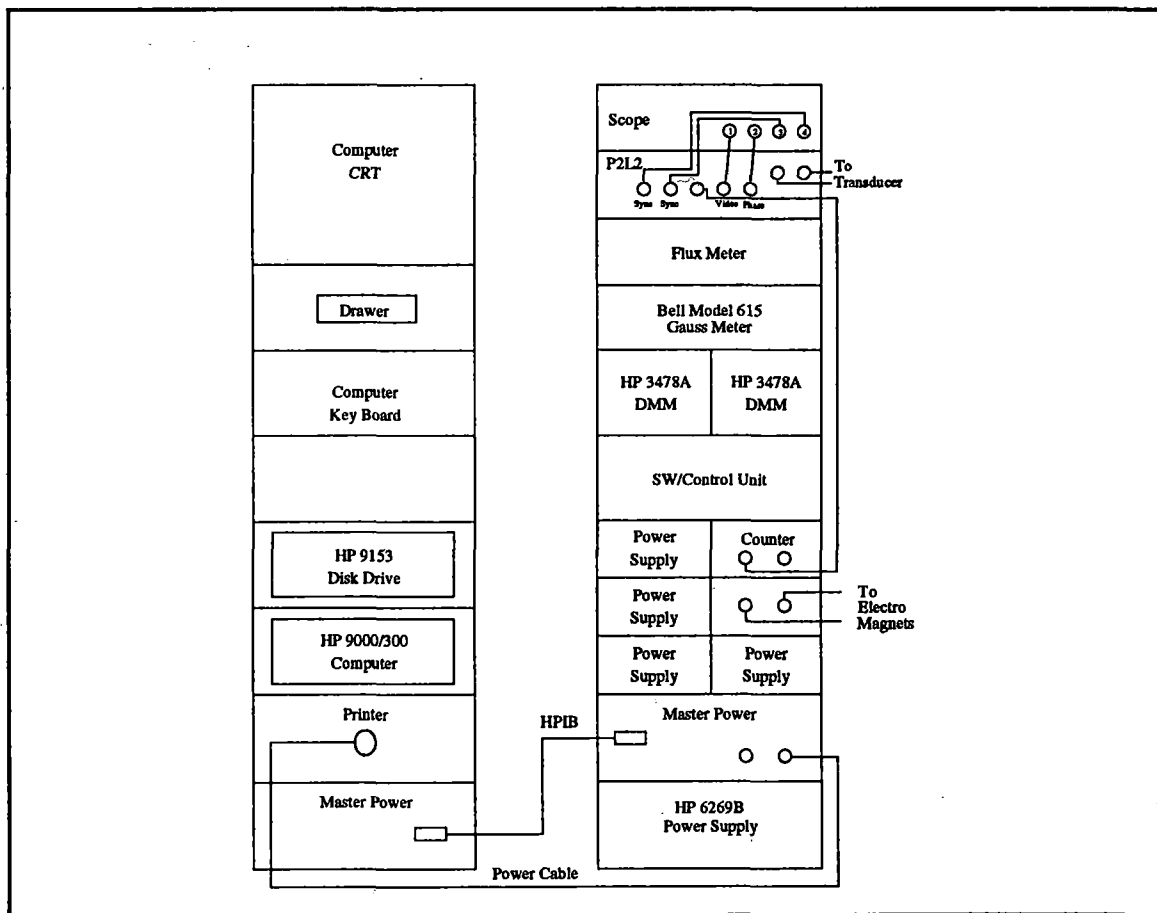


Figure 4. Magnetoacoustic Cabling Configuration

4.2 ACOUSTIC BIREFRINGENCE

Figure 5 is a schematic representation of the acoustic birefringence equipment. This equipment was delivered as a integral unit to the TTC in March 1991 and consists primarily of:

- Electronic equipment required to produce a polarized acoustic pulse via the EMAT
- Time interval counter
- Specially designed fixture to hold the EMAT in the required position on a railroad wheel (Figure 6)

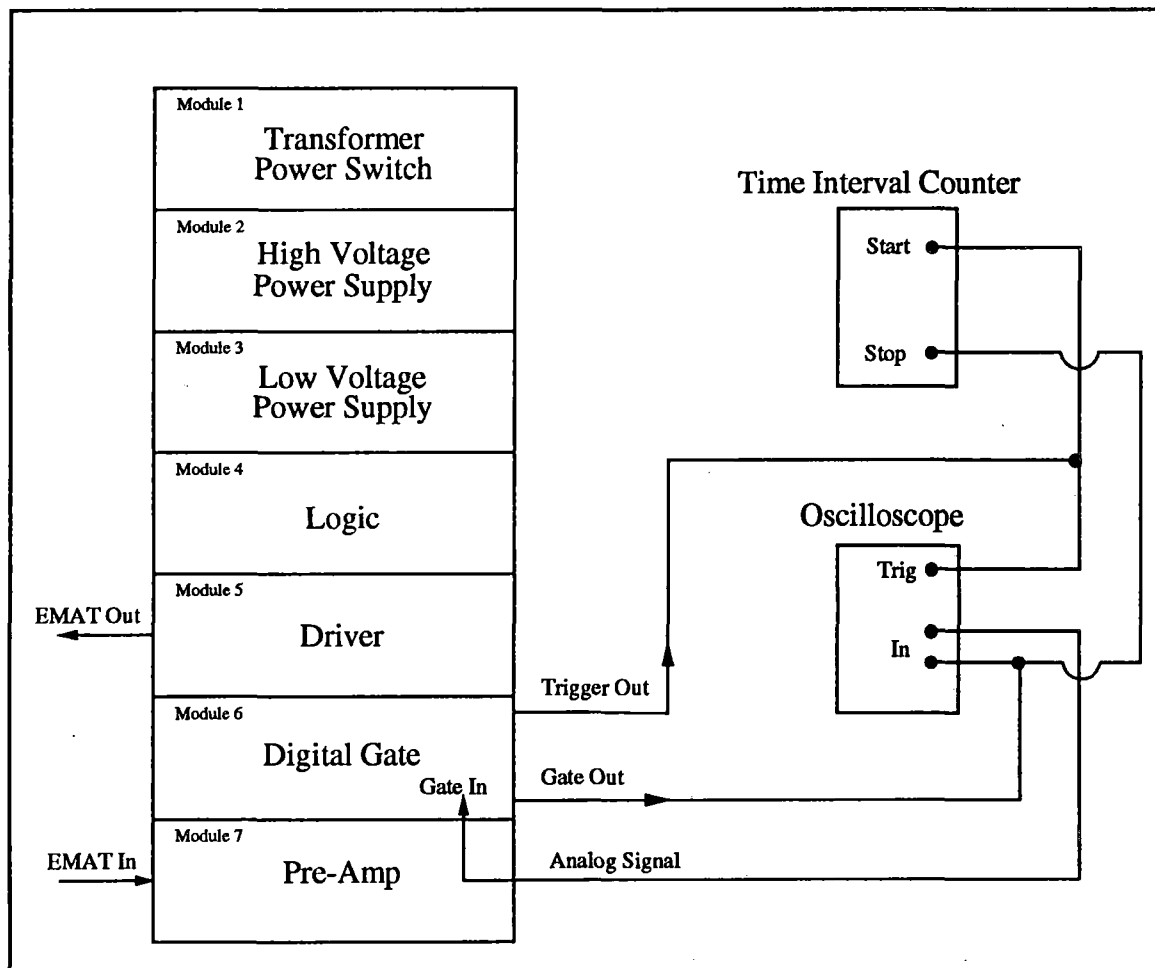


Figure 5. Acoustic Birefringence System Configuration

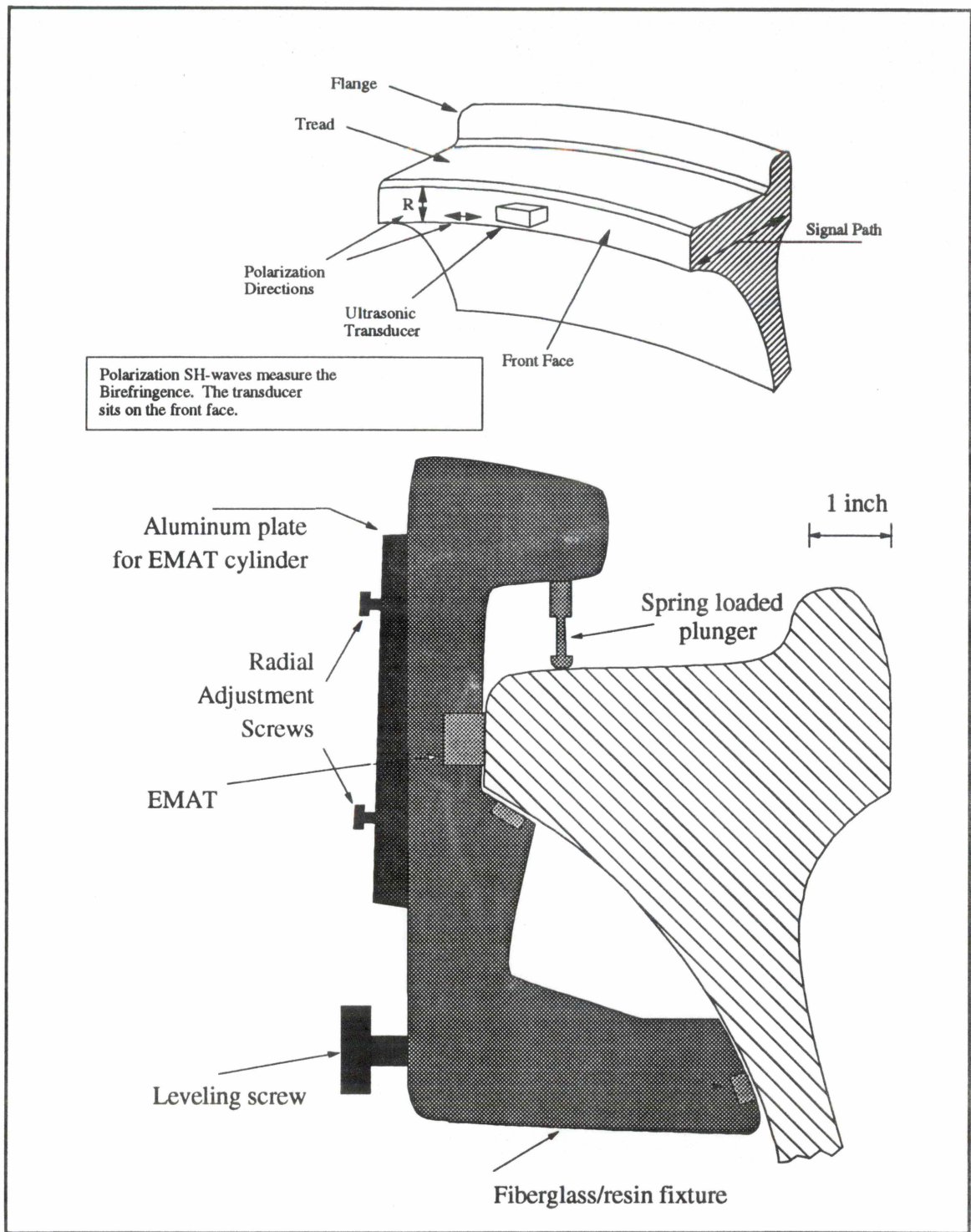


Figure 6. Acoustic Birefringence EMAT Mounting Arrangement

4.3 HOLE DRILLING STRAIN GAGING

The hole drilling strain gaging technique is essentially identical to that described in Tech Note TN-503-3 *Residual Stress Measurement* published by the Measurements Group, Inc. The instrumentation required for this technique essentially consists of:

- Specially designed milling guide (Measurements Group Model RS-200) which provides a firm mounting for the high speed drill and microscope
- Residual stress strain gage rosettes (Measurements Group CEA-XX-062UM-120)
- External electronics which provide strain gage excitation and measure relieved strain

4.4 SAW CUTTING

After the completion of NDE and hole drilling strain gaging measurements, all the test wheels were subjected to radial saw cutting. The saw cutting instrumentation consists of:

- Band saw with linear bearing table to support the test wheel
- Specially machined brackets which are tack welded to the rim of the test wheel to support MTS extensometer
- Extensometer (MTS model 632.02B-20) and associated electronics to measure saw-cut displacement
- 10 inch string pot and associated electronics to measure the depth of the saw cut
- Calibrated pen plotter

A standard band saw was modified at TTC, to facilitate radial saw-cutting of railroad wheels. This band saw has a movable table which was retrofitted with linear bearings (Figure 7). A constant force feed was provided by a pulley and weight system.

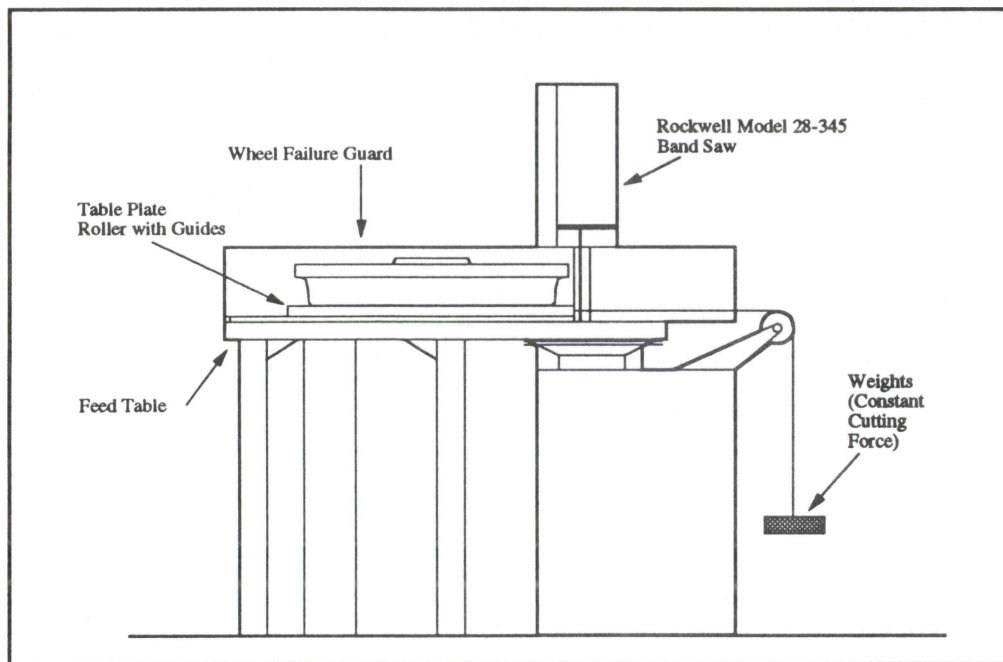


Figure 7. Schematic of Saw Cutting unit at TTC

5.0 TEST PROCEDURES

5.1 NON DESTRUCTIVE EVALUATION

5.1.1 Magnetoacoustic (NASA)

WHEEL SURFACE PREPARATION

- (1) Prepare the wheel surface for measurement by removing any surface contamination using a power grinder equipped with 60 grit paper followed by additional grinding with 120 grit paper until a smooth surface is obtained.

EQUIPMENT POWER UP PROCEDURE

- (1) Master power (Computer Rack) - ON
- (2) HP 9000 - 300 - ON
- (3) HP 9153 (Drive Unit) - ON
- (4) Monitor - ON (If not already on)
- (5) Printer (Lower Drawer) - ON (If not already on). NOTE: Hold "FF" Button while turning power on. This will run a printer self-test and check the ink-jet head for proper operation.
- (6) Master power (Electronics Rack) - ON

- (7) Two HP 6002A power supplies (704 & 705) - ON
- (8) HP 5316 frequency counter (720) - ON
- (9) HP 3488A (relay switch box) - ON
- (10) Two HP 3478A digital multi-meter's (DMM) (707 & 708) - ON
- (11) Black "pulse phase lock unit" - ON
- (12) Tektronix 2445 oscilloscope - ON
- (13) Allow electronics to warm up for at least 30 minutes to stabilize.

COMPUTER BOOT UP PROCEDURE

- (1) Press "F2" on keyboard to boot up with HP Basic 4.0 when prompted. The computer will then begin AUTOBOOT and a series of beeps will be heard as files are loaded.
- (2) After the prompt "the BASIC system is now loaded for your use", type:
SET TIMEDATE DATE ("DD MMM YEAR") - Use current date.
- (3) Type: SET TIME ("HH:MM:SS") - Use current time.
- (4) Type: PRINT DATE\$(TIMEDATE), TIME\$(TIMEDATE) to display the date and time. Re-do if incorrect or does not print on CRT.

POSITION ELECTROMAGNET ASSEMBLY ON TEST WHEEL

- (1) Depending upon the position of the wheel being tested, the pole pieces may have to be reversed.
- (2) Ensure that the contoured surfaces of the pole pieces fit snugly against the wheel tread, including adjacent to the flange. This must be accomplished by raising, lowering, pivoting, and/or tilting the magnet assembly against the wheel.
- (3) Ensure that the section under test is centered between the pole pieces and the magnet assembly is secure on the cart.
- (4) Connect the two power cables from the relay panel just below the Frequency Counter to the XLR-3 Switch Craft jacks on the electromagnets, one to each.

PREPARE FOR TEST

- (1) Install transducer(s) in fixture and affix to wheel in location(s) to be measured (locations 0°, 90°, 180°, and 270°) using the correct coupling fluid.
 - (a) Shear wave transducers - use Panametrics SWC Couplant.
 - (b) Compression wave transducers - use Sonotech Inc. Ultrasonic Couplant.
 - (c) Surface wave transducers - use Sonotech Inc. Ultrasonic Couplant.
- (2) Check all cabling and system presets (see configuration in Figure 4).
- (3) Set correct frequency on P2L2 Panel using VCO Range and Tune controls and monitoring on Frequency Counter.
 - (a) Shear wave transducers - 2.25 MHz or 5.0 MHz
 - (b) Compression wave transducers - 2.25 MHz or 5.0 MHz
 - (c) Surface wave transducers - 2.25 MHz
- (4) Position transducer(s) on test surface to obtain maximum amplitude of echo/received signal on channel 1 on oscilloscope.
- (5) Fine tune P2L2 frequency using TUNE control to the transducer's nominal frequency while monitoring the frequency counter.
- (6) Adjust S/H (Sample & Hold) pulse using P2L2 panel thumb wheel monitoring channel 2 and channel 3 on oscilloscope. Set the S/H pulse (ch 3) to a stable portion (approx. center) of the Phase waveform (ch 2).
- (7) On P2L2 panel, throw the lock switch to the UP position and monitor the frequency counter for any frequency drift. If the frequency drifts more than +/- 2 Hz to 5 Hz then the transducer(s) need more time to set in. Check for adequate couplant.
 - (a) Shear and Compression wave transducers need 5 minutes to 10 minutes to settle in.
 - (b) Surface Wave transducers need approximately 15 minutes to 30 minutes to settle in.

NOTE: With surface wave transducers it is necessary to clean the couplant from around the acrylic interface especially in front and around the sides where they contact the wheel.

- (8) Once again, insure that the frequency is not drifting when in LOCKED position.

BEGIN TEST

- (1) Type LOAD "WHEELBULK", <CR>, then RUN. The acquisition program will load, then answer prompts as they appear on the CRT.

NOTE: Ensure that there is a disk in the HP 9153 drive for the data files.

- (2) The test will automatically begin after answering the prompt concerning continuous runs. The usual matrix of tests is four runs: two continuous and two noncontinuous. After each run, the computer will write raw data to the disk and print out a graph of the data points (Figure 8). The program then runs through a DE-MAG (demagnetization) cycle and begins another test.
- (3) After the series of tests has been completed for the initial location (0°), move transducers to the next location (90°) and repeat beginning with step 1 under WHEEL SURFACE PREPARATION.

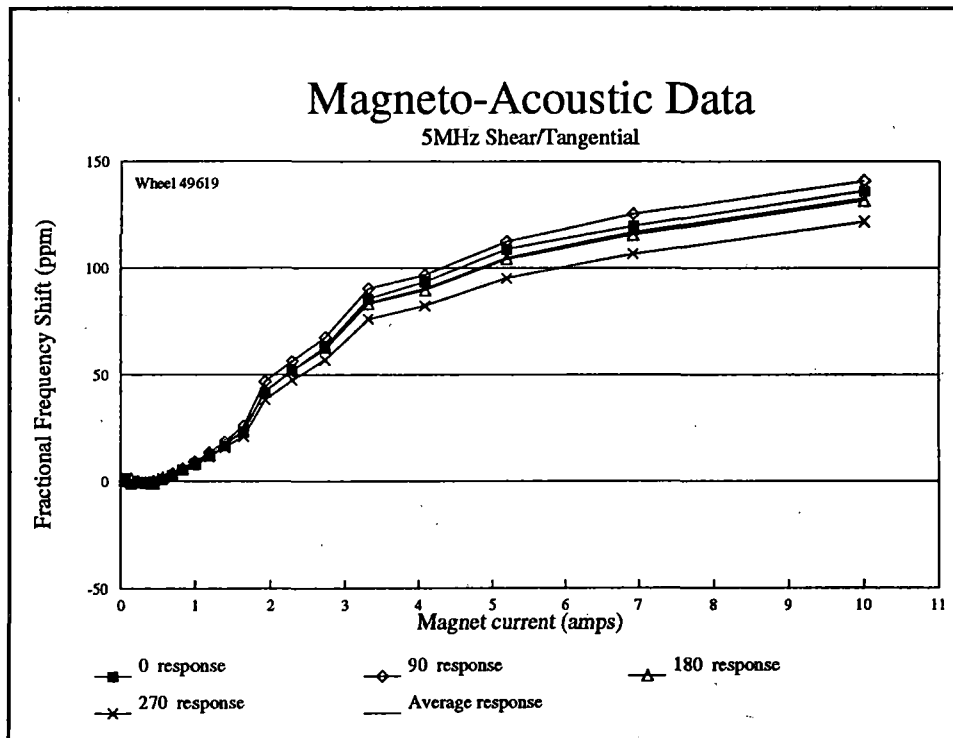


Figure 8. Typical 5 MHz Shear Wave Magnetoacoustic Data

5.1.2 Acoustic Birefringence (NIST)

WHEEL SURFACE PREPARATION

- (1) Prepare the wheel surface for measurement by removing any surface contamination using a power grinder equipped with 60 grit paper followed by additional grinding with 120 grit paper until a smooth surface is obtained.

EQUIPMENT POWER-UP PROCEDURE (REFER TO FIGURE 5)

- (1) Main Power Switch in rear of NIST Unit - ON
(Green Indicator Light on front of unit will illuminate)
- (2) Power Switch on front of NIST Unit - ON
(Red Indicator Light on front of unit will illuminate)
- (3) Power Switch on Tektronix TM5006 Bucket - ON
(Indicator lights and LEDs will illuminate)
- (4) Check all cabling and all presets on frequency counter and oscilloscope.
- (5) Allow at least 30 minutes for electronics to warm up before proceeding to test mode.

PREPARE FOR TEST (REFER TO FIGURE 6)

- (1) Position EMAT fixture on wheel, as illustrated in Figure 6, at the locations to be tested.
- (2) Set the adjustable "aluminum plate" to the desired radial measurement location. Zero (0) on the indicator rules positions the center of the EMAT on the inner lip ("surface corner") of the front rim face.
- (3) Use the "leveling screw" to ensure that the EMAT fixture is parallel to the wheel rim face, thus allowing a perpendicular orientation of the EMAT cylinder to rim face. Check both radial and tangential alignment.
- (4) Ensure that the fixture is indexed on the inner lip of the wheel rim and that rim face index is flush with rim face.
- (5) Adjust the pre-amp gain (Module 7, Figure 5) for a good signal, approximately 1 volt to 2 volts peak-to-peak without over driving or introducing distortion. Be sure to use the first echo pulse after the "main bang" of the acoustic signal as illustrated in Figures 9 and 10.

NOTE: The EMAT cylinder must be in the fixture mounted on the wheel for this adjustment since this waveform is the echo signal.

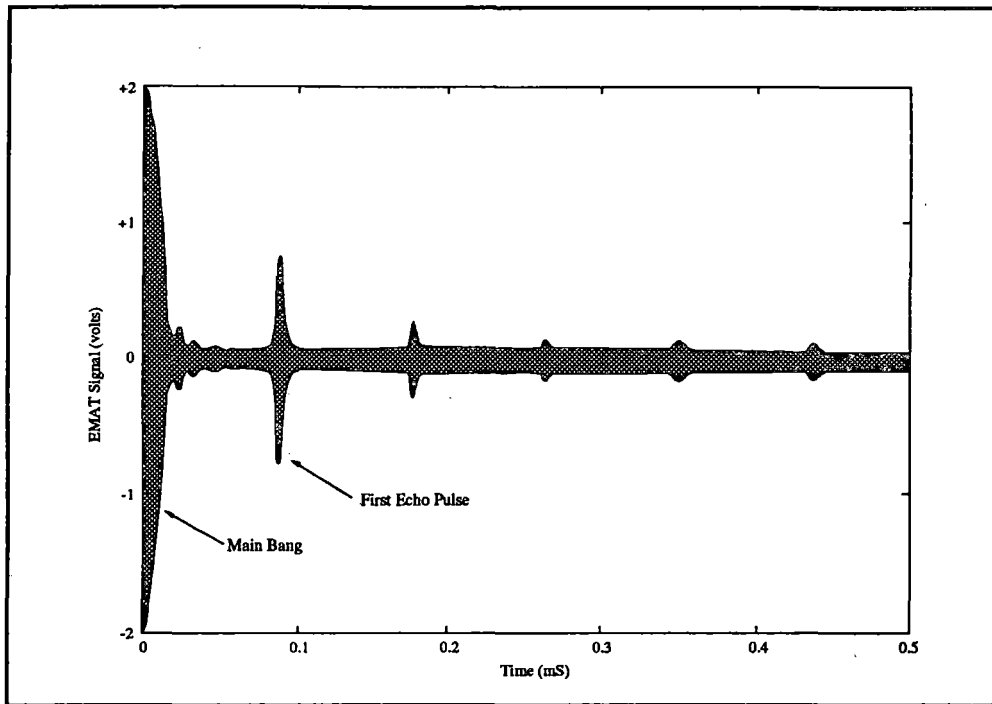


Figure 9. Acoustic Birefringence EMAT echo Signal

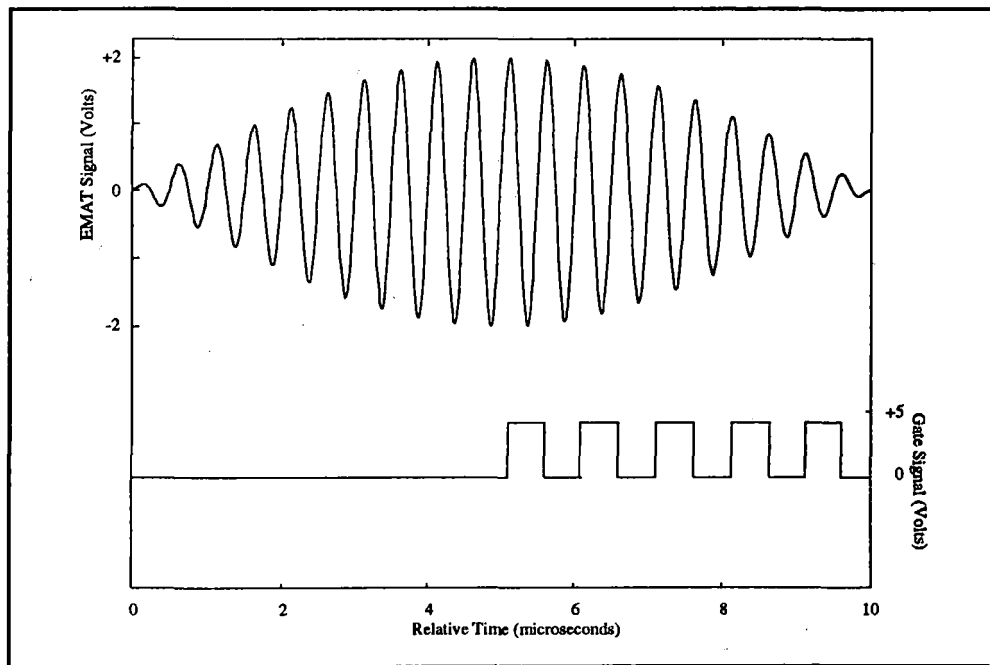


Figure 10. Acoustic Birefringence First Echo Pulse (Enlarged)

- (6) With the fixture and EMAT located on the wheel adjust the gate pulse train, using coarse and fine controls (Module 6, Figure 5), so that the first gate pulse coincides with the center of the first echo pulse and that it is stable (leading gate pulse coincident with the echo pulse maximum amplitude and not jumping between adjacent pulses). This sets the counter's stop pulse (the start pulse being the "main bang"). Ensure that when the EMAT is rotated 90 degrees between tangential (circumferential) and radial orientations, the gate pulse does not jump to an adjacent pulse. This may need adjustment from time to time but it must not be adjusted when taking measurements between the two orientations.

BEGIN TEST

- (1) Ensure that the EMAT and fixture are mounted securely on the test wheel. Rotate the EMAT cylinder between tangential and radial orientations while monitoring the oscilloscope. Be sure that the leading gate pulse does not jump between adjacent echo pulses.
- (2) Ensure that the frequency counter/timer is operating properly, i.e. "gating" approximately every 12 or 13 seconds (average switch should be set to "10³").
- (3) The first measurement, for the sake of convention, should be tangential.

NOTE: Arrow on transducer box indicates polarization of transducer (indicators also on EMAT cylinder and cylinder plate).

Watch approximately 3 to 5 "updates" on the timer and record a nominal average. Variation between these readings should be no more than 5 nanoseconds.

- (4) The second measurement should be radial. Again note 3 to 5 updates on the counter/timer and record an average. The sum and difference of these two values are used in the calculation of birefringence. The difference between the two recorded times should be no more than 300 nanoseconds.
- (5) Repeat steps 1 through 4 for each location to be measured.

5.2 SEMI-DESTRUCTIVE AND DESTRUCTIVE EVALUATION

5.2.1 Hole Drilling Procedure

The procedure for the semi-destructive evaluation using the hole-drilling strain-gage method is described by the *American Society for Testing and Materials (ASTM)* standard E 837 - 85. The adaptation of the hole drilling technique for the measurement of residual stresses in railroad wheels has been described in a paper presented to the American Society of Mechanical Engineers (ASME).³

The rim of the wheel is first prepared as described in *Measurements Group Instruction Bulletin B-129*. A strain gage rosette (*Measurements Group CEA-XX-062UM-120*) is then applied with gage number "one" oriented radially. Provisions are made for the electrical connections between the external electronics and the strain gage terminals.

After the strain gage has been attached to the back side of the rim the RS-200 base plate is centered over the gage and attached to the wheel with dental cement. The measuring microscope is inserted in the base plate and the assembly is centered over the gage using the x-y adjustment screws. The microscope is removed and the high speed drill is inserted.

The wheel is drilled in increments of 0.01 inch as measured on the RS-200 depth micrometer. At each incremental drilling, the strain gage outputs are recorded. This process is repeated until the full hole depth of 0.1 inch is reached.

The hole-drilling/strain-gaging method is a semi-destructive method for measuring residual stresses near the surface of isotropic elastic material. The method involves placing a strain gage rosette (Figure 11) on the surface, drilling a hole in the vicinity of the gages to a depth greater than its diameter and measuring the relaxation strains. Residual stresses in the area surrounding the drilled hole relax, and the relaxation is nearly complete when the depth of the drilled hole approaches 1.2 times the diameter. Measured strains are then related to relieved principal stresses, through a series of equations based on principles of elasticity.

Measuring the relieved radial strain ϵ_1 , ϵ_2 and ϵ_3 as a function of hole depth provides sufficient information to calculate the principal stresses, σ_{\max} and σ_{\min} , and their orientation, α , with respect to a selected reference.

$$\sigma_{\max} = \frac{\epsilon_1 + \epsilon_3}{4A} + \frac{\sqrt{2}}{4B} \sqrt{(\epsilon_1 - \epsilon_2)^2 + (\epsilon_2 - \epsilon_3)^2} \quad (1)$$

$$\sigma_{\min} = \frac{\epsilon_1 + \epsilon_3}{4A} - \frac{\sqrt{2}}{4B} \sqrt{(\epsilon_1 - \epsilon_2)^2 + (\epsilon_2 - \epsilon_3)^2} \quad (2)$$

$$\tan 2\alpha = \frac{\epsilon_1 - 2\epsilon_2 + \epsilon_3}{\epsilon_3 - \epsilon_1} \quad (3)$$

where:

$$\alpha = \alpha_{\max} \quad \text{if} \quad \frac{\epsilon_1 + \epsilon_3}{2} < \epsilon_1$$

$$\alpha = \alpha_{\min} \quad \text{if} \quad \frac{\epsilon_1 + \epsilon_3}{2} > \epsilon_1$$

$$\alpha = 45^\circ \quad \text{if} \quad \epsilon_1 = \epsilon_3$$

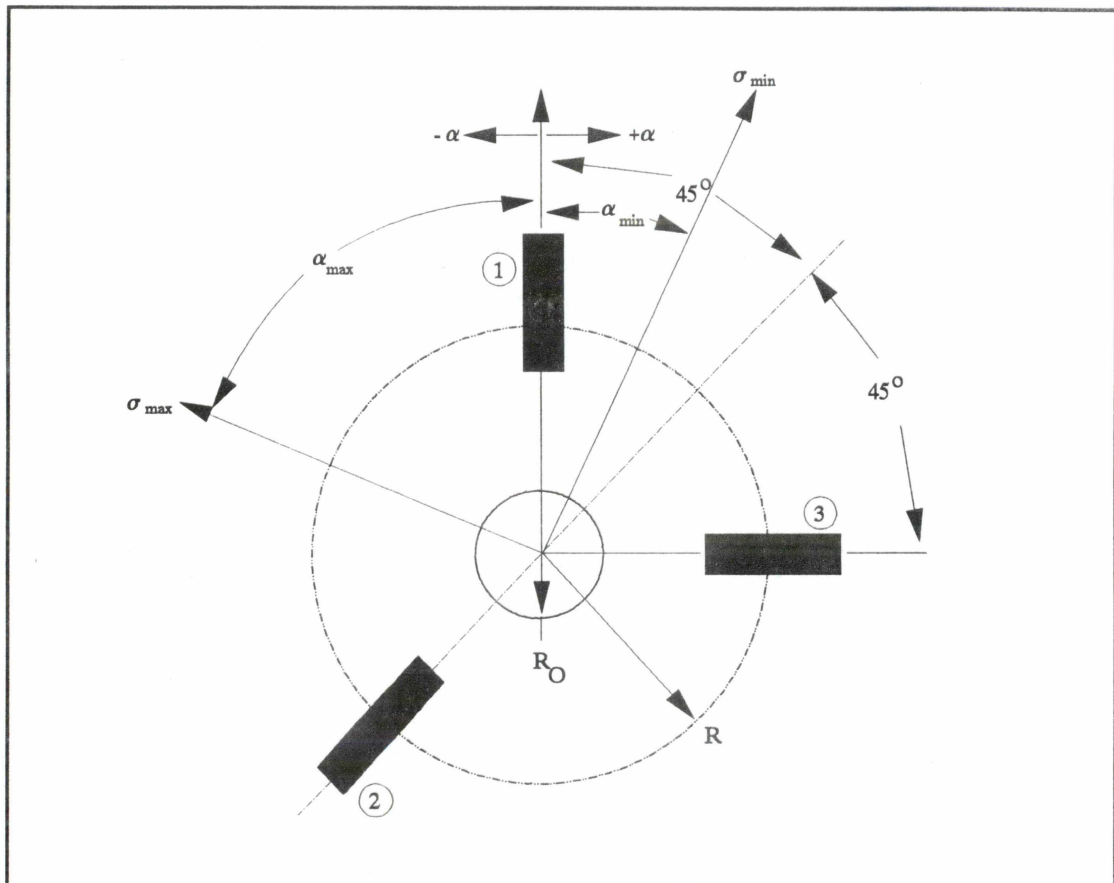


Figure 11. Residual Stresses Strain Gage Rosette Arrangement

Equations (1) and (2) define the maximum and minimum principal stresses. The data reduction coefficients \bar{A} and \bar{B} are described in Tech Note TN-503-3 *Residual Stress Measurement*, published by Measurements Group, Inc.

5.2.2 Saw Cutting Procedure

The extensometer mounting bracket is tack welded to the rim of the wheel under test. The wheel is then placed on the linear bearing table, attached to the band saw, and oriented so that the saw cut will be radial and at the desired location. The extensometer is attached to the bracket and a single 10 pound weight is placed on the pulley mechanism to pull the linear bearing table with the wheel against the power saw blade.

Operation of the band saw is controlled remotely from the control room. Before the actual start of the radial cutting of the wheel, both the extensometer (displacement across the saw cut) and the string potentiometer (depth of the radial cut into the wheel) are zeroed on the pen plotter. At this point the saw is remotely activated and the saw cutting process begins. Data acquisition is completely automated and should require no further operator intervention until the full depth of 10 inches is reached.

6.0 PRELIMINARY NDE MEASUREMENTS WITH WHEEL RIM FLEXING DEVICE

Before the magnetoacoustic and acoustic birefringence devices were shipped to TTC, preliminary measurements with railroad wheels were made at the Chicago Technical Center and NIST respectively. A method for changing the apparent stress in a wheel rim was developed. This entailed machining a portion of the rim out of the wheel and inserting a hydraulic load cylinder in a circumferential orientation in the wheel (Figure 12).

A saw cut through the plate and hub of the wheel was made as shown in Figure 12. By applying various pressure levels to the hydraulic cylinder, incremental circumferential compressive stresses were produced in the rim of the wheel. The above method demonstrated a serious limitation since the plate of the wheel appeared to be "in-bending" giving rise to a stress gradient in the rim of the wheel.

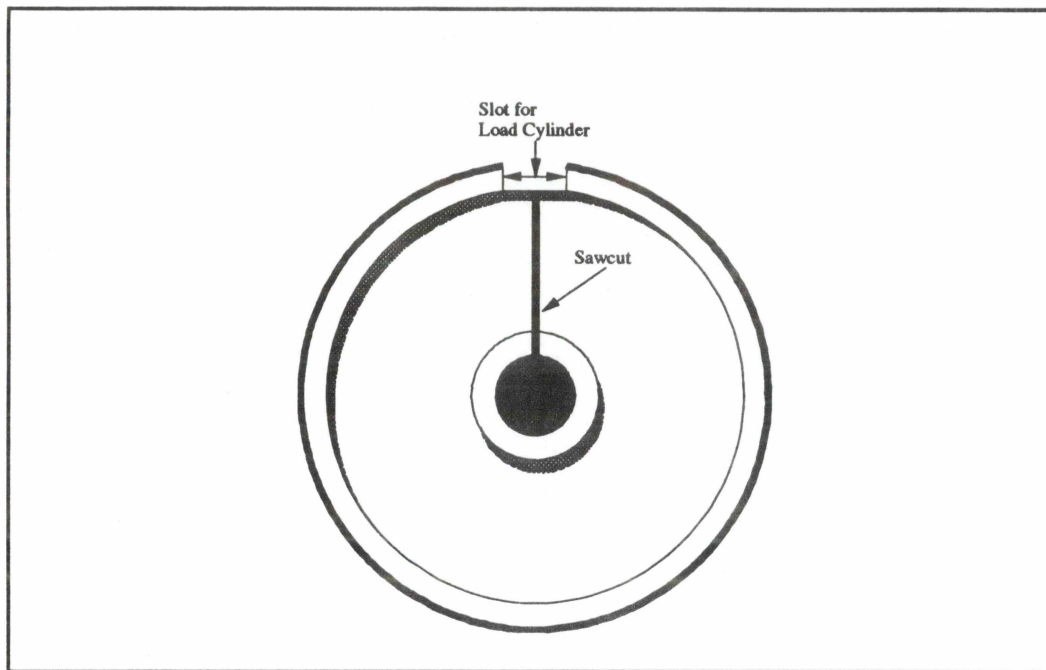


Figure 12. Schematic of Applied Load Fixture

6.1 MAGNETOACOUSTIC MEASUREMENTS

The use of compressional waves in the rim yielded no difference in response under the range of applied loads. The use of surface waves also yielded no difference in response under the range of applied loads.

The use of shear waves, however, yielded systematic changes in test response at the various pressure levels applied to the load cylinder as shown in Figures 13 and 14. These figures show the averaged results of two separate test runs. Using wave polarizations in the circumferential and radial directions, higher pressure to the load cylinder (increasing compression in the rim) caused a decrease in the fractional frequency shift for both polarizations of the shear wave.

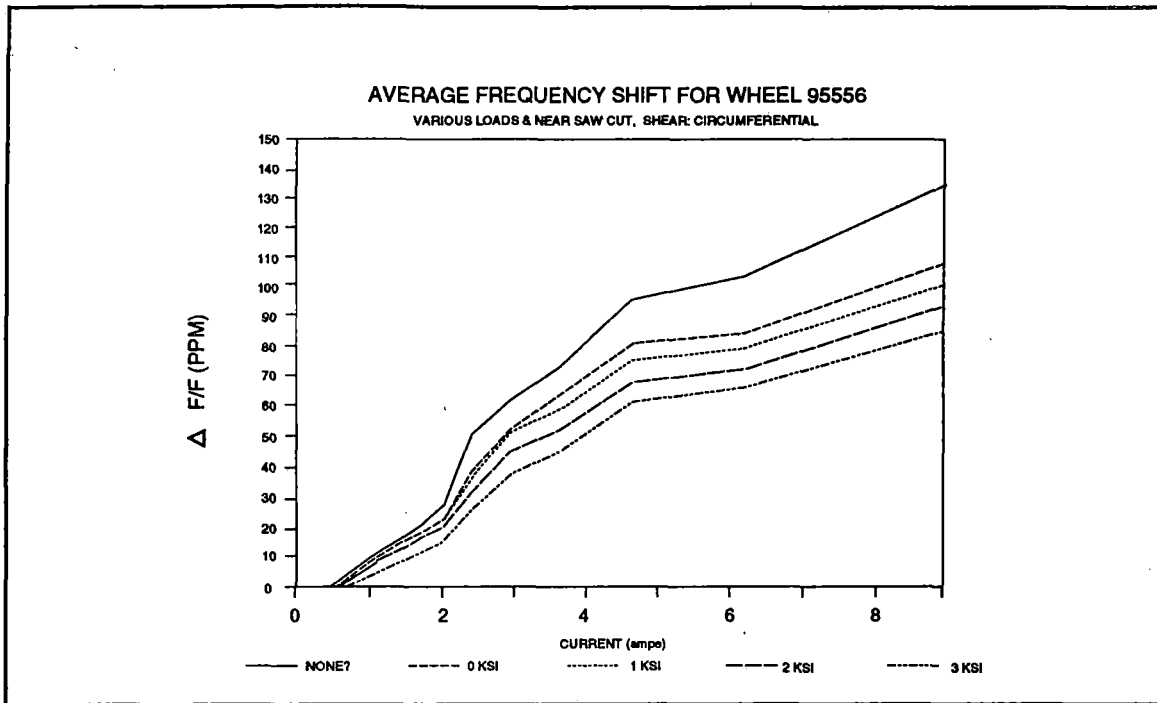


Figure 13. Frequency Shift for Circumferentially Polarized Shear Waves

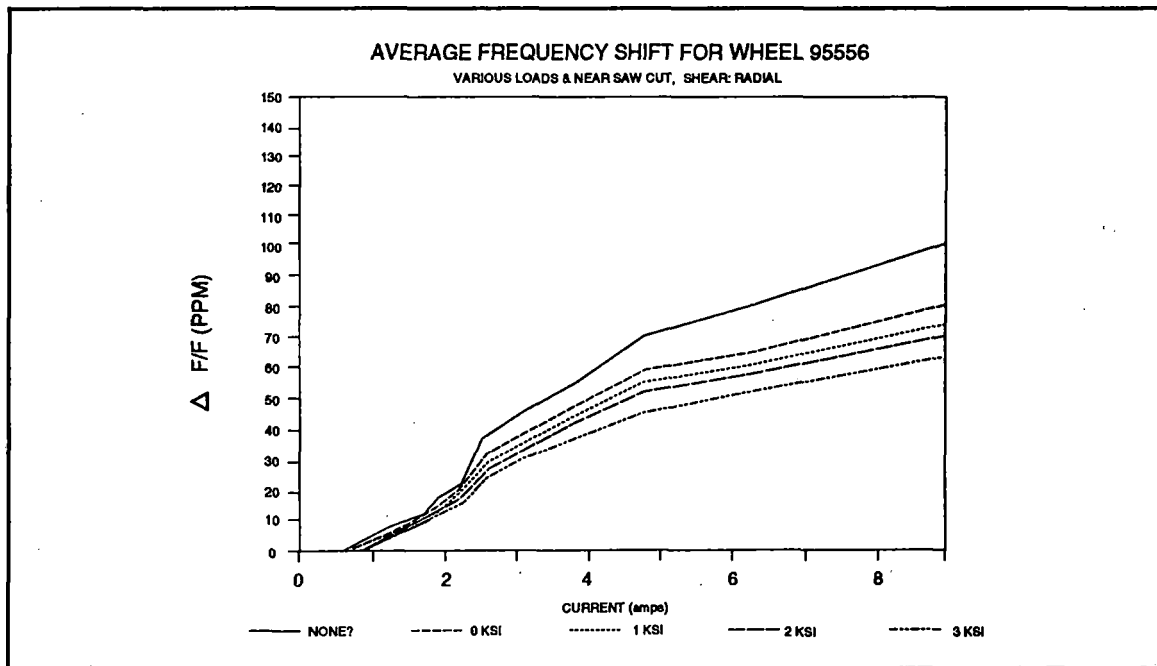


Figure 14. Frequency Shift for Radially Polarized Shear Waves

6.2 ACOUSTIC BIREFRINGENCE MEASUREMENTS

A pair of test wheels, saw cut from the tread to the hub, were shipped to NIST along with the rim flexing hydraulic press.

Measurements were made with the acoustic birefringence device under increasing hydraulic pressure levels which produced incrementally increasing hoop compressive stresses in the rim. Figure 15 presents the results of measured birefringence at the midline of the front face of both test wheels after increasing the hydraulic pressure to predetermined levels.

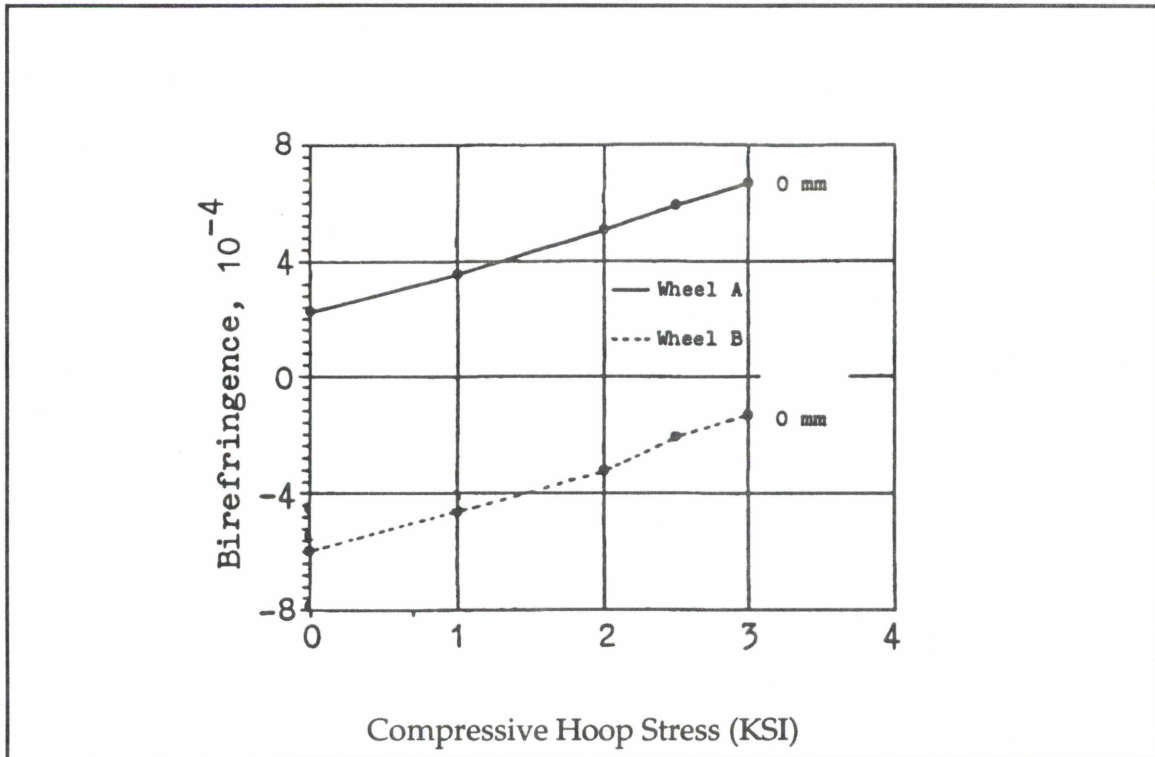


Figure 15. Birefringence Change With Increasing Compressive Hoop Stress⁵

Based on the above preliminary experiments NIST concluded the following:

- (1) Birefringence increases with greater compressive stresses in the rim.
- (2) Birefringence in the rim is linear with applied stress.
- (3) The birefringence measurements at zero hydraulic pressure from the two wheels are considerably different. This is probably due to different residual stresses still remaining in wheels A and B after the radial saw cut and/or due to different metallurgical textures between the two.

7.0 DATA

Table 1 summarizes the tests performed on each wheel included in this report. A number of tests were performed in order to establish the test procedures described in Sections 5.1.1 and 5.1.2. Seventeen different wheels were tested in this program. Three of these wheels were donated by Griffin Wheel, Inc. Of these three, one wheel (28609) was an "as manufactured" Class C wheel. The other two wheels (28603 and 28605) were inductively heated by Griffin to simulate different levels of thermal brake cycling to change the residual stress state.

Table 1. Test Matrix

WHEEL NUMBER	ACOUSTIC BIREFRINGENCE (Intact Wheel)	ACOUSTIC BIREFRINGENCE (Rim Block)	MAGNETO- ACOUSTIC	HOLE DRILLING	SAW CUT
5556	X	X	X	X	X
49619	X	X	X	X	X
95411	‡	‡	X	‡	X
94575	X	†	X	†	†
49547	X	X	X	X	X
49550	X	X	X	X	X
43928	X	X	X	X	X
5576	X	X	X	X	X
5584	X	X	X	X	X
95554(W1)	NIST	X	*	X	X
95551(W2)	X	X	X	X	X
94559(W5)	NIST	X	*	X	X
94550(W6)	X	X	*	X	X
94565(W7)	NIST	X	*	X	X
28609	X	X	X	X	X
28605	X	X	X	X	X
28603	X	REFERENCE	X	X	REFERENCE

- * Wheels cut prior to availability of magnetoacoustic system to support NIST testing
† Wheel inadvertently mounted on axle in preparation for phase two testing.
‡ Wheel inadvertently saw cut prior to acoustic birefringence or hole drilling measurements.

Acoustic birefringence data of intact wheels and rim blocks for wheels 95554(W1), 94559(W5), 94550(W6), and 94565(W7) was collected by NIST prior to delivery of the equipment to TTC. NIST's analysis of this data is included in Appendix J.

Table 2 provides details of each of the test wheels analyzed in the current program.

Table 2. Wheel Specifications

SERIAL NUMBER	MANUFACTURER	CLASS	DESIGN	STATUS	PLATE
5556	Standard	C	J33	New	S
49619	Canadian	C	J33	New	Straight
95411	Griffin	C	CJ33	New	Straight
94575	Griffin	U	J33	New	Parabolic
49547	Canadian	C	J33	Drag Braked	Straight
49550	Canadian	C	J33	Drag Braked	Straight
43928	Canadian	U	J33	Drag Braked	Straight
5576	Standard	C	J33	Drag Braked	S
5584	Standard	C	J33	Drag Braked	S
95554(W1)	Griffin	U	CJ33	Drag Braked	Parabolic
95551(W2)	Griffin	U	CJ33	Drag Braked	Parabolic
94559(W5)	Griffin	U	CJ33	Drag Braked	Parabolic
94550(W6)	Griffin	U	CJ33	Drag Braked	Parabolic
94565(W7)	Griffin	U	CJ33	Drag Braked	Parabolic
28609	Griffin	C	CJ33	Inductively Heated	Parabolic
28605	Griffin	C	CJ33	Inductively Heated	Parabolic
28603	Griffin	C	CJ33	New	Parabolic

7.1 DATA MEASUREMENT LOCATIONS ON TEST WHEELS

Figure 16 presents the typical locations for magnetoacoustic, acoustic birefringence, and hole drilling measurements on a given test wheel (Serial No. 5556). Appendix B contains schematic diagrams indicating the location of all measurements for each wheel in this study.

Measurement Locations

Wheel 5556

 = Hole Drilling

MA = Magnetoacoustic

UB = Acoustic Birefringence

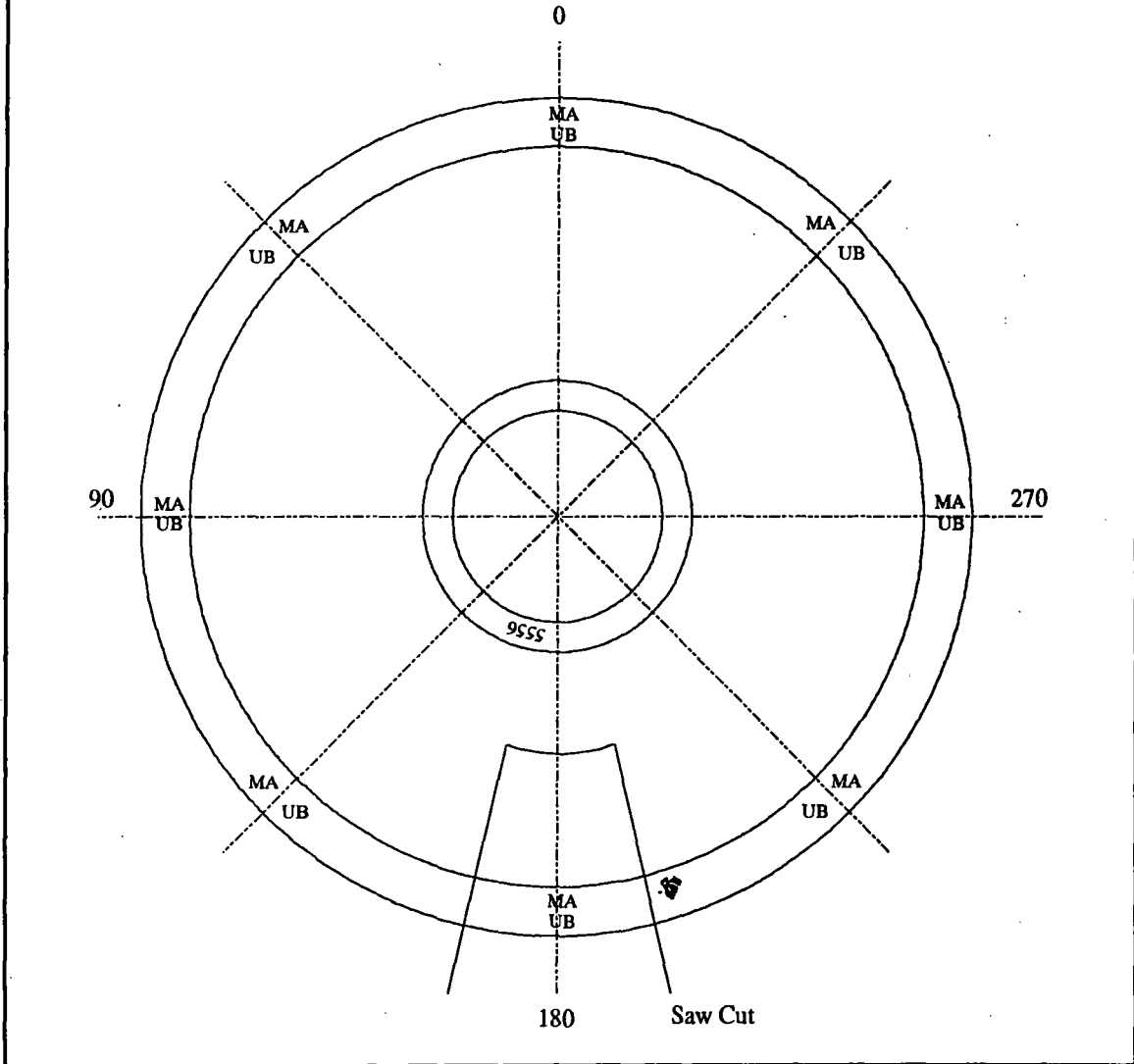


Figure 16. Typical Measurement Locations on Test Wheels

7.2 ACOUSTIC BIREFRINGENCE DATA

The acoustic birefringence data consists of relative transit times for radially and circumferentially polarized ultrasonic waves. These times are in microseconds and are included with the computed stress values in Appendix C. Table 3 presents the average birefringence value obtained from each wheel and the corresponding computed residual stress compared to the results from saw cutting.

7.3 MAGNETOACOUSTIC DATA

In total, data from nearly 1500 complete magnetoacoustic runs was collected on the 17 test wheels. Many of these data runs were primarily intended to ensure that there was no residual magnetization of the wheel. It was decided that analysis be restricted to only the fourth data run from each test configuration. In addition, many of the data runs were performed to establish the test procedures in Section 5.1.1 (investigating the effects of surface preparation, the response from various types of ultrasonic transducers and their frequencies in determining residual stress, and radial positioning of the transducer on the wheel rim). For this report only the fourth data run of those configurations conforming to the established procedures has been included.

During the course of this investigation, it was established that the 5 MHz tangentially polarized shear wave data produced the optimum results for the evaluation of circumferential rim stress.⁴ Appendix D contains the 5 MHz tangentially polarized shear wave data which conforms to the established test procedures. Table 4 presents the average maximum fractional frequency shift for each wheel and the corresponding results from saw cutting.

7.4 HOLE DRILLING DATA

The hole drilling data consists of Measurements Group RS-200 data forms providing the incremental hole depth (Z) and the measured strains ($\epsilon_1, \epsilon_2, \epsilon_3$) at each depth. This data is presented in Appendix E.

7.5 SAW-CUT DATA

Saw-cut data consists of plots of flange tip displacements (from the extensometer) as a function of saw-cut radial position. This data is contained in Appendix F.

Table 3. Comparison of Acoustic Birefringence and Saw Cutting Results

WHEEL NO.	SAW CUT DISPLACEMENT ANALYSIS		ACOUSTIC BIREFRINGENCE		
	Net Rim Force up to 3" below flange tip (KIPS)	Average Hoop Stress at the Location of NDE Measurement (KSI)	Measured B ($\times 10^{-4}$)	Measured B_o ($\times 10^{-4}$)	Computed Stress (KSI)
5556	-164	-28.0	7.5	4.5	-26.0
49619	-156	-18.0	-22.0	16.0	+40.0
49547	-93	-12.0	22.0	-5.0	-50.0
49550	113	+10.0	25.0	-5.0	-60.0
5576	-180	-18.0	13.0	6.34	-15.0
5584	+32	+3.0	-1.5	4.65	+10.0
95551	+87	+7.0	-1.0	4.33	+11.0
28609	-92	-11.0	11.0	12.0	+3.0
28605	+99	+9.0	10.0	12.0	+4.0

Table 4. Comparisons of Magnetoacoustic and Saw Cutting Results

WHEEL NO.	SAW CUT DISPLACEMENT ANALYSIS		MEASURED AVERAGE MAGNETOACOUSTIC FRACTIONAL FREQUENCY SHIFT (PPM)
	Net Rim Force up to 3" below flange tip (KIPS)	Average Hoop Stress at the Location of NDE Measurement (KSI)	
5556	-164	-28.0	115
49619	-156	-18.0	130
95411	+10	+1.0	125
49547	-93	-12.0	140
49550	113	+10.0	155
5576	-180	-18.0	115
5584	+32	+3.0	115
95551	+87	+7.0	110
28609	-92	-11.0	35
28605	+99	+9.0	35

8.0 DATA ANALYSIS

8.1 ACOUSTIC BIREFRINGENCE DATA

The acoustic birefringence is defined as⁵:

$$B = 2 \times \frac{(V_\theta - V_R)}{(V_\theta + V_R)} = 2 \times \frac{(t_R - t_\theta)}{(t_R + t_\theta)} \quad (4)$$

where:

$B \equiv$ birefringence

$V \equiv$ velocity

$t \equiv$ transit time

The relationship between birefringence and stress is:

$$B = B_0 + C_A(\sigma_\theta - \sigma_R) \quad (5)$$

where:

$B_0 \equiv$ birefringence due to metallurgical texture

$C_A \equiv$ stress acoustic constant $\approx -4.8 \times 10^{-5} (\text{ksi})^{-1}$

$\sigma_\theta, \sigma_R \equiv$ stress in the circumferential and radial directions

If B_0 is known (by measuring a zero stress sample) the stress is:

$$\sigma_\theta - \sigma_R = \frac{(B - B_0)}{C_A} \quad (6)$$

An assumption inherent in the birefringence technique is that the radial component of the stress σ_R is negligible. If this assumption is valid, the birefringence method provides a direct measure of the circumferential rim stress.

Each of the transit times across the wheel rim shown in Appendix C represents three or more measured times which have been averaged to produce the recorded time. These readings are themselves averaged to produce the value used to compute the birefringence and ultimately the residual stress in the rim of the wheel.

Two values are included for the computed stress from the measurements: one with the actual B_0 (when applicable), and one with a constant B_0 value. As with any nondestructive method, the acoustic birefringence method must be able to determine the actual stress state (within acceptable uncertainty) with little or no prior knowledge of the wheel material. NIST has sampled a number of wheel rim blocks from various manufacturers and attempted to determine an average B_0 value. This

value $\approx -5 \times 10^{-4}$ was used in the computation of the constant B_0 computed stress value. The computed birefringence and corresponding stress values are shown in Appendix C.

8.2 MAGNETOACOUSTIC DATA

At this time the magnetoacoustic system is not capable of quantifying the stress state of the wheel. It is, at best, a relative indicator of stress state. Figure 17 was produced by Mr. David Utrata during his analysis of the magnetoacoustic results in support of this program. In order to qualify this method's ability to determine the sign of the stress, Mr. Utrata has averaged the results from the 5 MHz tests which were performed. In two cases 2.25 MHz data was used because 5 MHz data was unavailable. The maximum and minimum values from the data are used as a measure of the scatter in the data (indicated by the solid line on each data point). The fractional frequency shift is then compared to the rim force as computed by the saw cutting method.

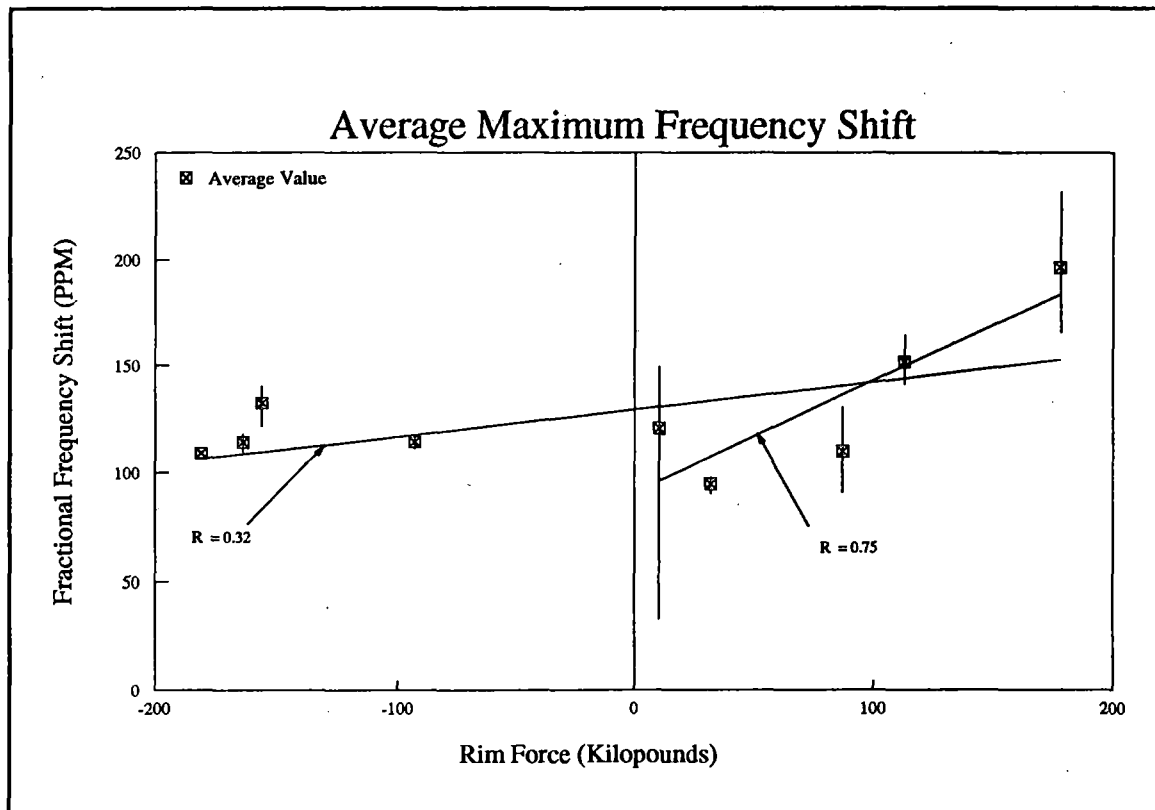


Figure 17. Analysis of 5 MHz Magnetoacoustic Data

8.3 HOLE DRILLING DATA

The first step in the hole drilling data reduction process is to determine the relative percent strain relieved at each depth. The primary purpose of this exercise is to detect the presence of stress gradients. A primary assumption in the hole-drilling strain-gaging method is that the stress is uniform throughout the depth of the hole. If a stress gradient is present, this method will lead to errors in the computed stress. Appendix G contains the normalized relieved strains which have been plotted with the scatterband plot from the *ASTM E837-85* standard. The occurrence of data points outside these scatterbands are indicative of the presence of stress gradients.

The next step in the hole-drilling strain-gaging data analysis is to compute the equivalent uniform stress and the angle (α) of the principle stress axis from the directions of interest. Plots of equivalent uniform stress as a function of hole depth are included in Appendix H along with the computed angle (α).

The final step involves a Mohr's circle calculation of the stress along the axis of interest based on the equivalent uniform stress and the angle (α). These values are labeled circumferential stress and radial stress on the equivalent uniform stress data plots in Appendix H. Figure 18 presents the relationship between the hoop stress component, computed from the hole drilling data, and the average stress computed from saw cutting data.

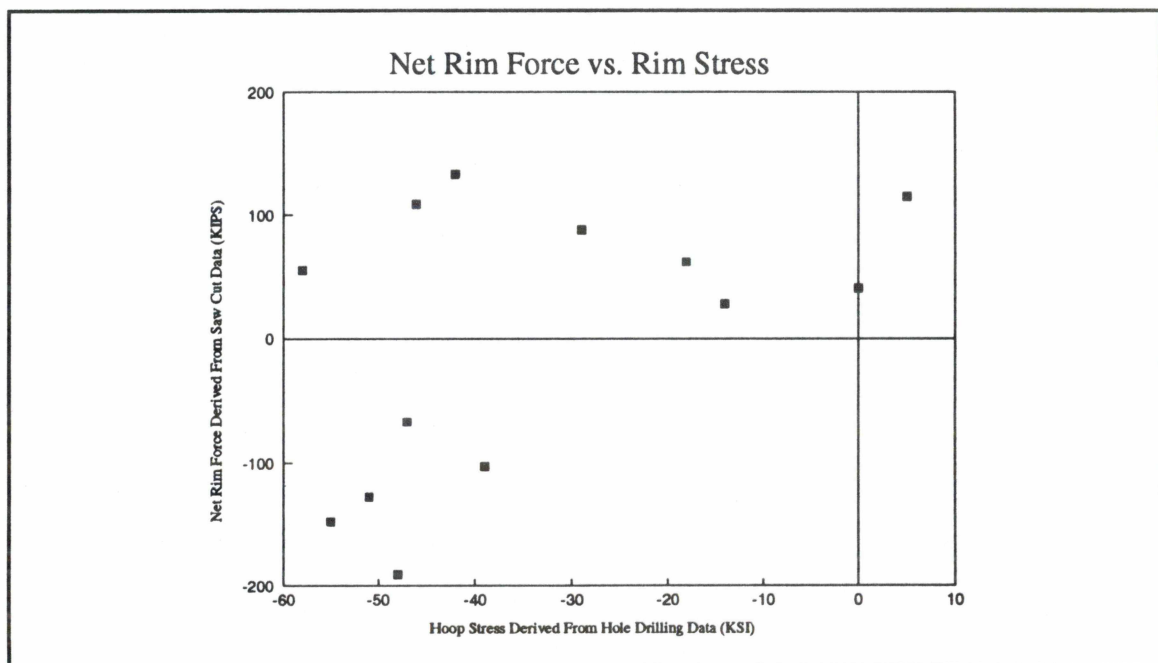


Figure 18. Hole Drilling Stress vs. Saw Cut Net Rim Force

8.4 SAW-CUT DATA

Flange tip displacement data shown in Appendix F is used as input to the AAR's computer program which converts it to average hoop stress as a function of depth of cut. Plots of rim stress vs. radius are included in Appendix I. In addition, the computer program computes the net rim force up to 3 inches below the flange tip. A comparison of the model output with three dimensional finite element analysis is presented in Appendix A.

In the results presented in Appendix I, the computed average stresses in the region of application of the two NDE devices are indicated on the stress vs. radius plots.

9.0 RESULTS

9.1 SAW CUTTING VS. ACOUSTIC BIREFRINGENCE

A scatter plot of the results from saw cutting and acoustic birefringence are presented in Figure 19. Two sets of stress values attributed to the acoustic birefringence method are presented; one using the measured B_o value and one using the average NIST B_o . Error bars of ± 10 ksi are centered on the birefringence data which uses the NIST average B_o . NIST estimates that their system currently should be accurate to within 10 ksi.

There are 11 wheels for which data from hole-drilling strain-gaging, saw cut, and acoustic birefringence exists. In five of these eleven cases the computed stress from the acoustic birefringence data was within 10 ksi of the saw cut value (45%) when using the measured B_o value. When using the average NIST B_o value the birefringence stress and the saw cut stress agree in only two of eleven cases (18%).

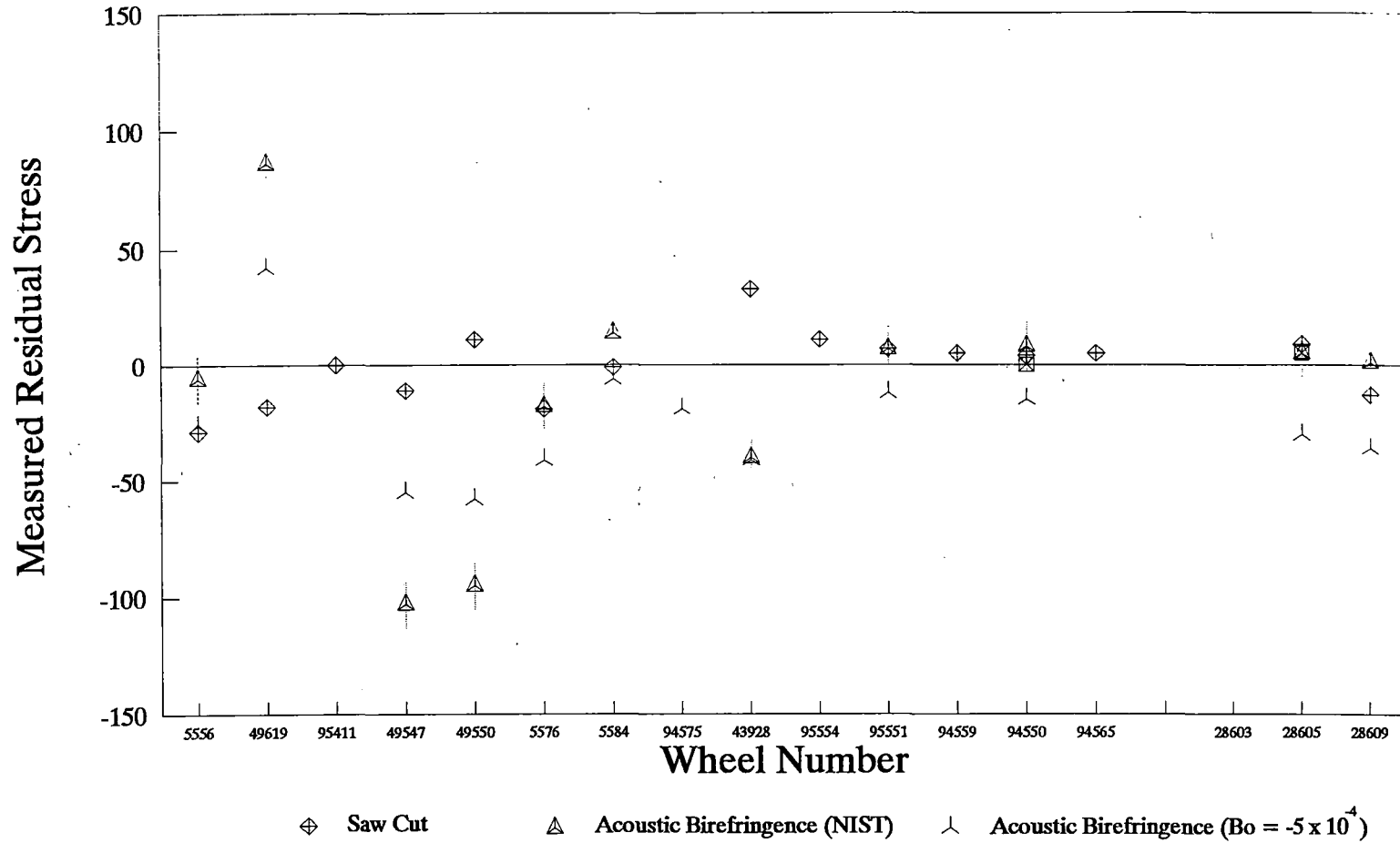
When used strictly to determine the sign of the circumferential rim stress (tension vs. compression) the birefringence method agrees with the saw cut method (within experimental error) in eight of eleven cases (73%) when measured B_o values are used. When the NIST average B_o values are used this agreement drops to five of eleven cases (45%).

Figure 20 shows the computed values of B_o for each of the rim blocks measured by the TTC. Data shows a considerable amount of scatter and is in generally poor agreement with the average B_o as measured by NIST. As seen above, the assumed B_o value can dramatically influence the computed stress value.

An independent evaluation of wheels W1 (serial no. 95554) W5 (serial no. 94559) W6 (serial no. 94550) and W7 (serial no. 94565) was carried out at NIST before the acoustic birefringence device was shipped to TTC. This evaluation is presented in Appendix J.

Residual Stress Measurement Comparison

Destructive and Non-destructive



-35-

Figure 19. Acoustic Birefringence vs. Destructive Methods

Computed Birefringence

Rim Blocks (Bo)



Figure 20. Rim Block (Bo) Values

9.2 SAW CUTTING VS. MAGNETOACOUSTIC TECHNIQUE

A number of interesting features are presented in Figure 17 which shows the correlation between the saw cutting and magnetoacoustic data. Two linear least squares lines have been plotted through the data. The coefficient of determination (R^2) for the line passing through the entire data set is 0.32. This would seem to indicate very little relationship exists between the frequency shift and the net rim force. If, however, only data from those wheels which demonstrated a net tensile (positive) rim force is considered, a slightly more positive picture emerges. The coefficient of determination for this line is 0.75, indicating a substantially stronger linear relationship. When the scatter in the data is considered the coefficient of determination will be considerably higher for these data points.

The new Griffin wheels (28603, 28605, and 28609) appear to have presented something of a problem for the magnetoacoustic system. In each case fractional frequency shift is considerably lower than expected. This phenomenon manifests itself not only on the inductively heated wheels (28603 and 28605) but also on the as manufactured wheel (28609). At this point the behavior does not have a satisfactory explanation.

10.0 DISCUSSION

It is difficult to draw statistically valid conclusions about the adequacy of either of the two NDE devices with the limited sample size available in this study.

Analysis of the data presented in this report is complicated by a number of factors. Results from the hole-drilling strain-gage method show limited correlation with the saw cut displacement analysis due primarily to the complex state of stresses in the wheel rim, as well as the presence of stress gradients. Comparisons of the non-destructive methods must, by necessity, depend exclusively on the saw cutting analysis. Additionally, both non-destructive methods seem to indicate that there may be dramatic differences in the residual stress at different circumferential locations around the wheel. This kind of phenomenon was observed in a number of test wheels which were drag braked during the Wheel Failure Mechanisms test at TTC.¹

Figure 21 is a schematic cross sectional representation of the rim of a railroad wheel with the radial location of the NDE measurements indicated. It is known that both the acoustic birefringence and the magnetoacoustic methods interrogate a relatively small volume, approximated as a cylindrical cross section, in the rim adjacent to

the transducer as shown in Figure 21. Residual stresses in portions of the wheel away from the measurement region will have little effect on the measured stress. In addition, each of the methods discussed (both destructive and non-destructive) will have a tendency to average the stresses seen through the rim. Three dimensional finite element analysis has shown that, in general, stress gradients will exist through the wheel rim. The presence of stress gradients and the tendency of each of these methods to average stresses (in potentially different ways) adds uncertainty to the comparisons between methods.

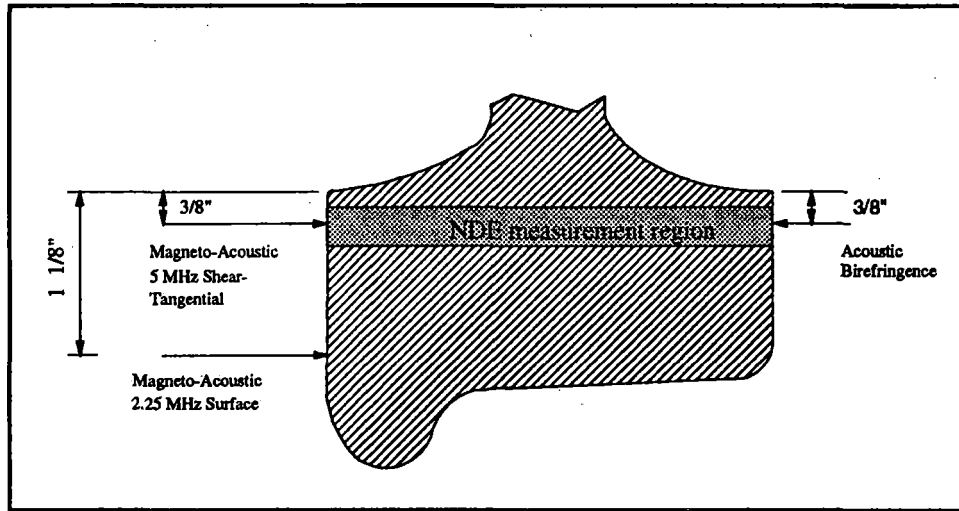


Figure 21. NDE Measurement Regimes

The results for the acoustic birefringence method are mixed. When the actual measured B_o values are used in the stress calculations the system appears to predict the sign of the stress a majority of the time. However, in an operational sense a more realistic analysis can be obtained with the constant B_o value (because there will be no opportunity to measure B_o). When a constant B_o value is used, the ability of the birefringence method to predict the sign of the wheel stress drops significantly. It is interesting to note from Figure 20 that the average B_o value measured by the TTC for this set of wheels differs markedly from the average B_o previously established by NIST.⁵ At this point there is no adequate explanation for this difference.

The primary difficulty with the current magnetoacoustic system seems to be the inability to distinguish frequency shifts caused by stress from those due to differences in material properties. This strong dependence on material properties causes considerable ambiguity when attempting to analyze measurements because there is not a clear

indication that any state of stress exists in the wheel. While it may be possible to determine changes in stress state by periodically measuring wheels with known original stresses, it is not currently possible to measure an unknown wheel and determine its stress state.

The current configuration of the magnetoacoustic device did not lend itself to use on the rim block portions of the wheels. It is possible that if the magnetoacoustic system had been first used on the intact wheel, and those results compared to results obtained from the zero stress rim blocks, the material property influence could be eliminated. In this case the magnetoacoustic system may have been able to determine the sign of the stress in the wheel in much the same way as the acoustic birefringence system.

It is clear that neither of the systems examined is currently capable of reliably determining the stress state of a railroad wheel in an operational sense. Under controlled conditions the acoustic birefringence system can be used to establish the sign of the stress (compression or tension) but only after determining a B_0 value appropriate for that particular wheel. Presently, the magnetoacoustic system does not attempt to assign a value to the wheel stress or even determine the sign. In this sense then, the acoustic birefringence system is much closer to being an operational system.

11.0 RECOMMENDATIONS

- NIST has recommended that a number of changes be made to the acoustic birefringence hardware to improve reliability. Among these are an edge finding tool to increase reliability in positioning the EMAT and crossed EMAT coils to eliminate the need to physically rotate the transducer. Both of these changes are well considered and are likely to further enhance the performance of the NIST system.
- The value of a reasonable birefringence constant (B_0) is apparently in some doubt. Before this system can be made operational the variations observed in this study must be understood and/or accounted for.
- There is some question as to the exact stress state of the rim blocks which were removed from the wheels. It is theorized that they may still contain a considerable amount of residual stress. In future studies if rim blocks are to be used as reference they should be annealed to remove any residual stress.

- The principals involved with the design of the magnetoacoustic system (Min Namkung, NASA and David Utrata, CTC) have recommended a number of improvements to this system. Future study is required to investigate the electromagnet configuration and its relationship to the magnetic field inside the wheel rim. This would seem a reasonable first step in improving the performance of this system.
- The cause of the anomalous magnetoacoustic readings from the inductively heated Griffin wheels should be investigated.
- Future work with the magnetoacoustic system should include the measuring of zero stress rim blocks to establish the systems sensitivity to stress state and to determine if it is possible to eliminate material property uncertainties from the measurement.
- The possibility that residual stress may vary dramatically around the circumference of the wheel must be investigated thoroughly. A fundamental understanding of this phenomenon is essential in order to determine the number of locations which must be examined to ascertain the overall stress state.
- Upon completion of the modifications to each of the systems, the sample size needs to be increased significantly to establish a statistical basis for determining the efficacy of each system.

REFERENCES

1. Rajkumar, B.R. and D.H. Stone. "Wheel Failure Mechanisms of Railroad Cars," FRA Contract No. DTFR53-82-C-00282, July 1987.
2. Rajkumar, B.R., D.H. Stone, C.P. Gannet; "Analysis of Residual Stresses in Railroad Wheel From Sawcutting Displacement Data Using Newly Developed Analytical Approach," IEEE-ASME Joint Railroad Conference, April 21-23, 1987, Toronto, Canada.
3. Rajkumar, B.R. and D.H. Stone; "Measurement Approaches For Determining Thermally Induced Residual Stresses in Railroad Wheels," ASME Winter Annual Meeting (85-WA/RT-16), Miami Beach, Florida, Nov. 17-21, 1985.
4. Letter from D. Utrata to D. Gray (FRA), dated June 19, 1991.
5. Schramm, R.E., Clark, A.V. Jr., Mirrakovic, D.V., Schaps, S.R., McGuire, T.J., "Residual Stress Detection in Railroad Wheels: An Ultrasonic System Using EMATS," National Institute of Standards and Technology Report No. 23, NISTIR 3968, May 1991.

ACKNOWLEDGEMENTS

The authors would like to thank Mr. David Utrata, Dr. Min Namkung, and Mr. Ray Shramm for their valuable contribution in the development of two NDE devices and the standardization of the test procedures evaluated in this program.

The authors would like to acknowledge and thank Griffin Wheel Inc., for their generous donation of three wheels, two of which were inductively heated at their facilities.

The AAR would like to thank Mr. Don Gray and Ms. Claire Orth of the Federal Railroad Administration for their continued support and guidance to the NDE Program and their excellent coordination of various agencies involved in the project.

APPENDIX A

**COMPARISON OF 3D FINITE ELEMENT MODEL
AND
TTC CLOSED FORM SOLUTION**

A1.0 RE-EXAMINATION OF WHEEL STRESS CALCULATIONS FROM TWO DIFFERENT MATHEMATICAL APPROACHES USING SAW CUT DISPLACEMENT DATA

A1.1 THE TRANSPORTATION TEST CENTER'S CLOSED FORM SOLUTION.

During the implementation of the Wheel Failure Mechanisms Program, the AAR performed saw-cutting of more than 500 freight car wheels to evaluate the state of residual stresses by destructive testing. The approach taken to evaluate residual stresses from the saw-cut displacement data was to develop a simple mathematical model for determining the average hoop stress distribution in the test wheel.

The model assumes that the cut portion of the wheel consists of several interconnected rings. Using the reverse saw-cut displacement response, the rings are brought to their original positions. When the radial saw-cut is made, hoop and shear stresses are released on the cut surface, causing individual rings to displace circumferentially and radially. If the cut surfaces are subjected to the released stress distribution, they will merge and the wheel would assume its original shape (before the saw-cut). During this process, radial and shear stresses are developed on the interface of adjacent rings, due to relative displacements. The hoop and shear stresses acting on the tip of an individual ring can then be determined as a function of the tip displacement and the stresses on the interface. For this purpose, an individual ring is separated from the rest; and equations based on the theory of elasticity are developed for determining stresses acting on the tip, which equilibrate with the stresses on the outer and inner interface, and are compatible with tip displacements. Finally, all the individual rings are reconnected. In the process, the complete hoop and shear stress distribution in the radial direction is generated for the depth of the saw-cut.

The saw-cut displacement in the hoop direction, as recorded by the clip gage for each wheel, was used as input to the numerical procedure and the average stress distribution in the wheel (before saw-cut) was estimated. An integration was performed from the flange tip to a depth of three inches, so as to evaluate the net force in the rim.

In this approach, the results from the analyses were used to calculate the total circumferential force in the rim of the wheel and this force is suggested as a measure of the safety of the wheel. A typical average stress distribution and total circumferential force predicted by this model are presented in Figure A1. The complete

details of the above analytical method for determining average residual stress in railroad wheels is described in a paper presented at the 1987 IEEE/ASME Joint Railroad Conference at Toronto, Ontario.

Even though the above model does not show the stress gradient across the cross section of the wheel, it is indeed helpful in interpreting the saw-cut displacement data for a large number of railroad wheels in terms of the average rim residual stress and the net rim force in a test wheel (before the saw-cut), without involving expensive computational procedures such as the Three Dimensional Finite Element Model.

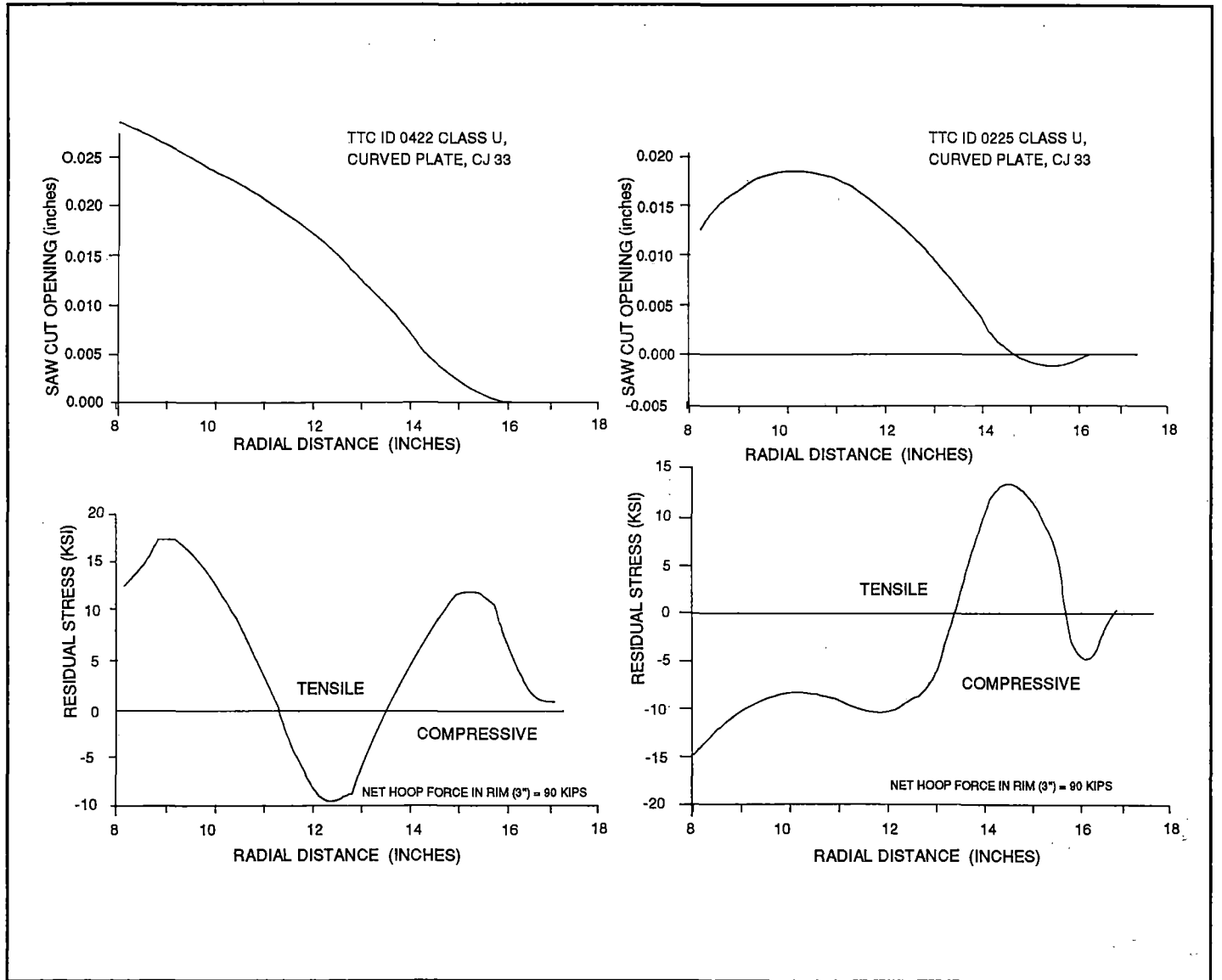
A1.2 THREE-DIMENSIONAL FINITE ELEMENT MODEL

The AAR also developed a more comprehensive analysis of the data obtained from radial saw cutting of selected railroad wheels using a three dimensional (3D) finite element approach in collaboration with the Illinois Institute of Technology Research Institute (IITRI). For this second approach, the saw-cut opening displacement is measured on both sides of the wheel along the entire length of a cut. Then a three dimensional finite element analysis is performed to determine the stresses that result when the cut is closed (as a result of circumferential displacement loading on the free surface).

The stresses that are calculated for the plane of the cut are then an indication of the stresses that existed before the wheel was cut.

The results of the 3D-Finite Element Analysis and the method based on the closed form solution were compared for six wheels that were saw-cut. The stress contours from 3-dimensional stress analysis were integrated over the rim surface and multiplied by the incremental cross section area to determine the effective rim force acting on the rim cross sectional area. The results from both the methods were very close with the assurance that the TTC's closed form solution does give reasonable predictions of average residual stresses based on the flange tip displacement during saw cutting.

Figure A1. Average Hoop Stress Distribution and
 Net Rim Forces for Two 33 Inch Diameter Curved Plate Wheel
 TTC'S Closed Form Solution Model



A1.3 RESULTS FROM BOTH APPROACHES

Five cases from the analysis of saw-cut data using the 3-D finite element model and TTC's closed form solution are presented below.

A1.3.1 Case 1 (TTC ID No. 29)

A thirty-six inch diameter curved-plate wheel (Class U) with discoloration was saw-cut for destructive analysis using the 3D-finite element method and TTC's closed form solution. The saw-cut opening at the tip of the flange with the clip gage versus the saw-cut depth curve is presented in Figure A2, with a total opening of 0.048". Figure A3 shows the net opening displacement of the 10-inch saw-cut as a function of depth into the wheel. There are data for both the inside and outside surfaces of the wheel.

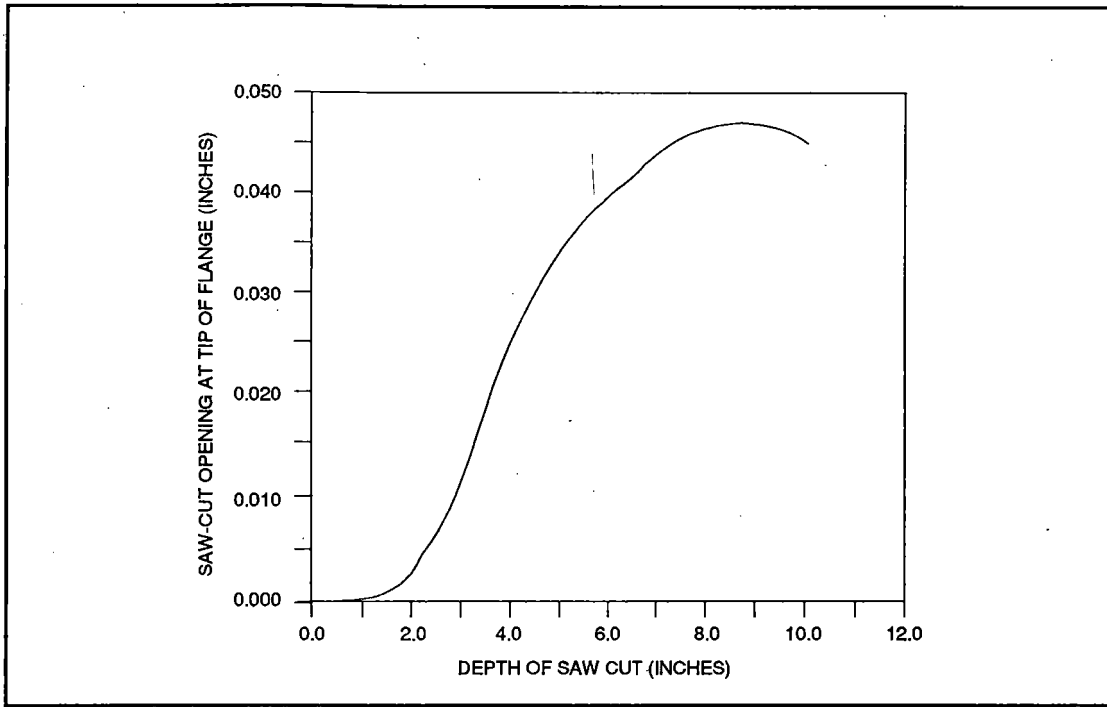


Figure A2. Saw cut Opening at Tip of Flange as a Function of Depth of Saw Cut, 36-inch Diameter Curved Plate Wheel (TTC ID No. 29)

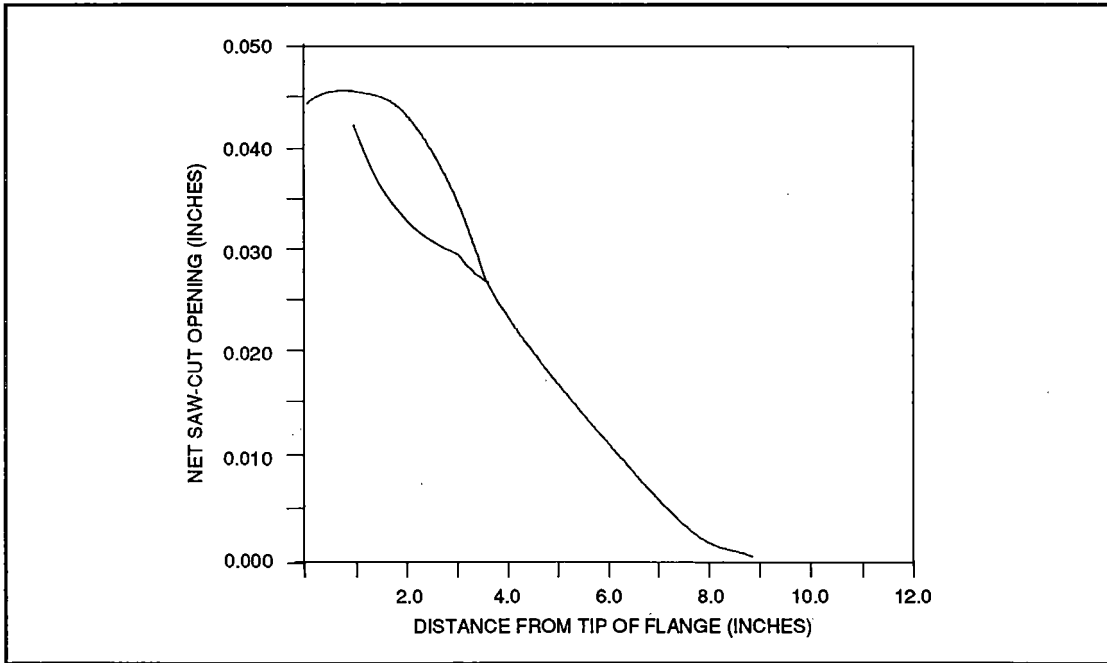


Figure A3. Net Saw Cut as a Function of Cut into Wheel, 36-inch Diameter, Curved-Plate Wheel

Calculations were performed using a 3D finite element code (ANSYS). Figure A4 shows the circumferential residual stress distribution calculated from this approach. The stress contours from the predicted distribution (Figure A3) were integrated over the rim surface and multiplied by the incremental cross sectional area to estimate the effective rim force (135.5 kips).

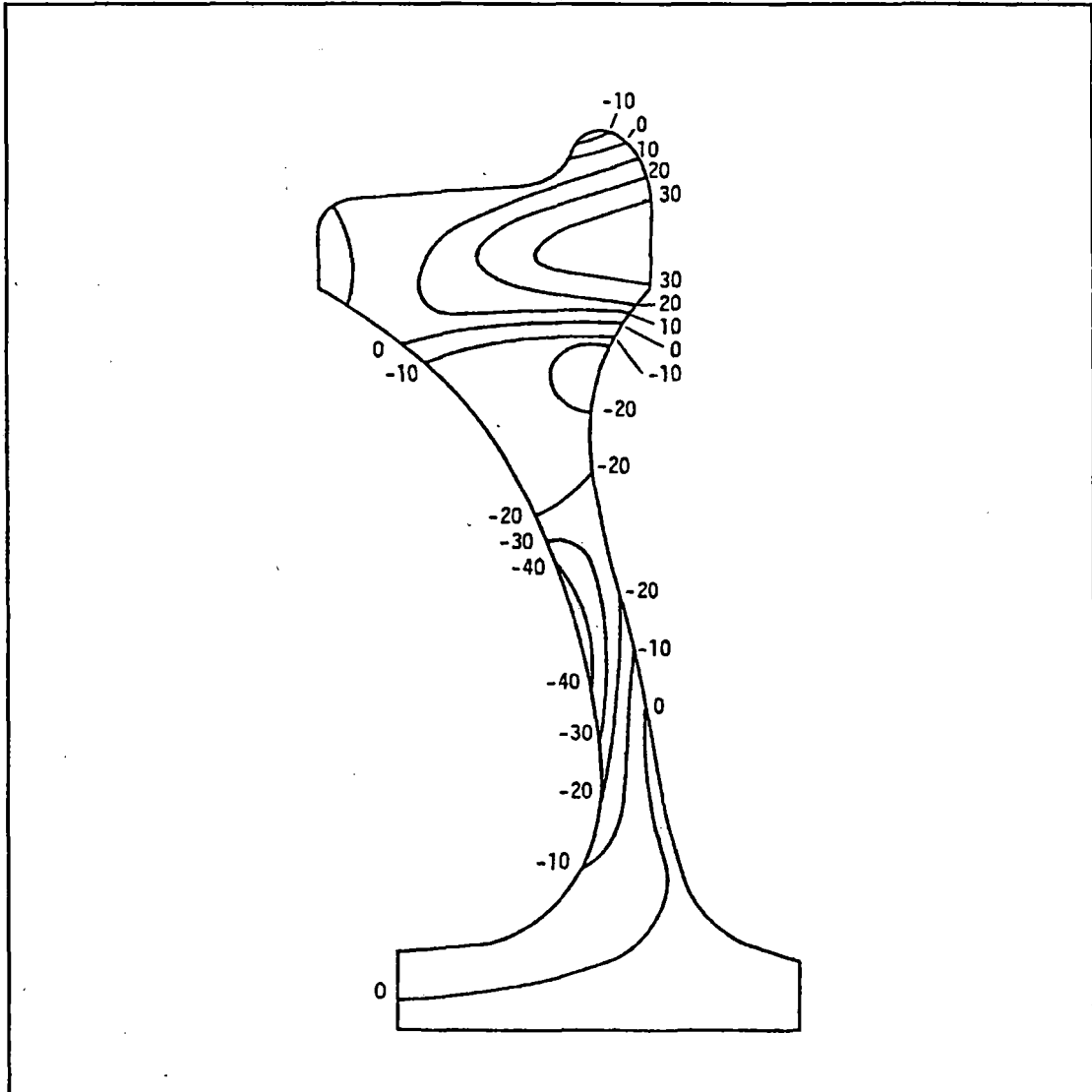


Figure A4. Residual Circumferential Stress Distribution Predicted for a 36-inch Diameter Curved Plate Wheel from Saw Cut Displacement Data, (ksi)

The saw-cut displacement in the hoop direction was recorded by the clip gage for wheel No. 29. Figure 1 was used as input to the numerical procedure for TTC's closed form solution and the average stress distribution in the wheel was computed as shown in Figure A4. This procedure also calculates the net force in the rim by performing an integration from flange tip to a depth of three inches; (132 Kips).

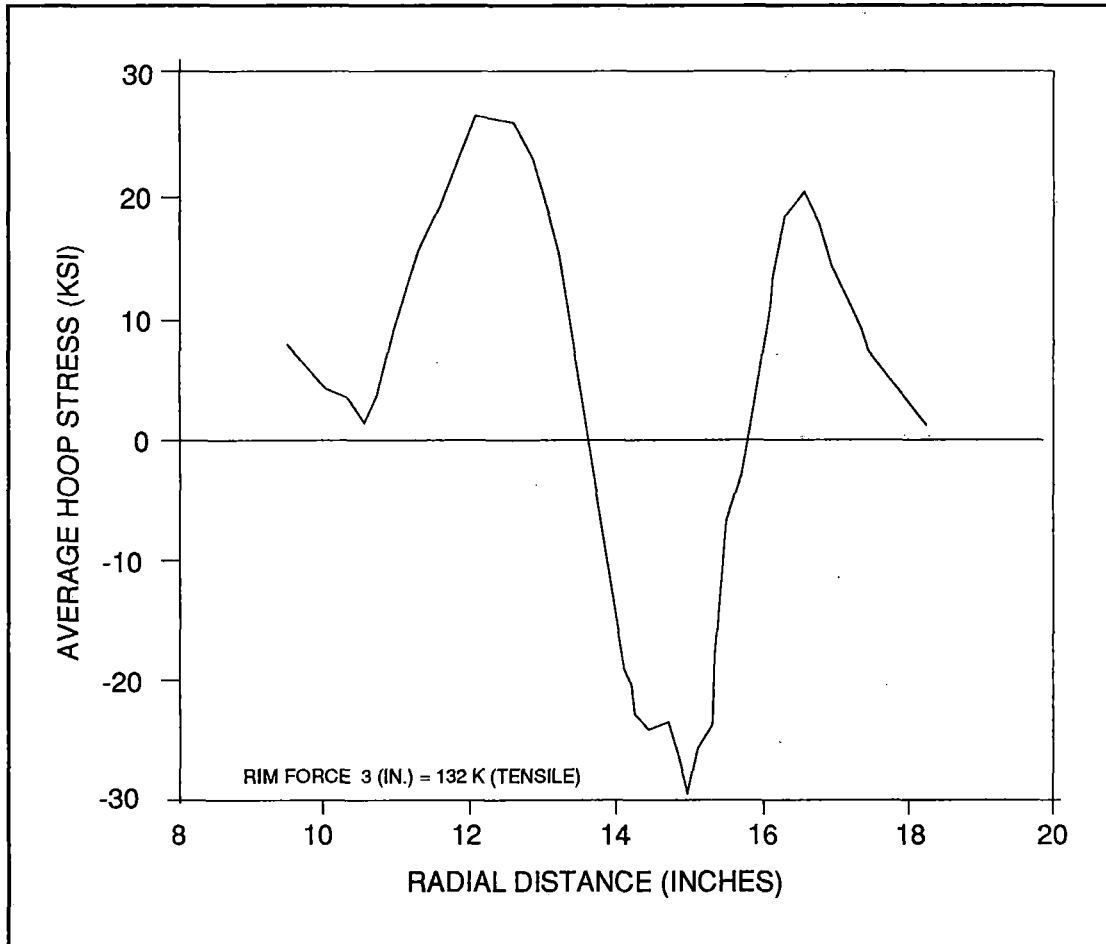


Figure A5. Average Hoop Stress Distribution in CH 36 Class U Wheel, TTC ID No. 0029.

A1.3.2 Case 2 (TTC I.D. No. 072)

"Thirty six inch Diameter Straight Plate Wheel." Figure A6 shows the saw-cut opening at the tip of the flange versus saw-cut depth for a 10.5-inch saw-cut into a 36-inch diameter straight plate wheel.

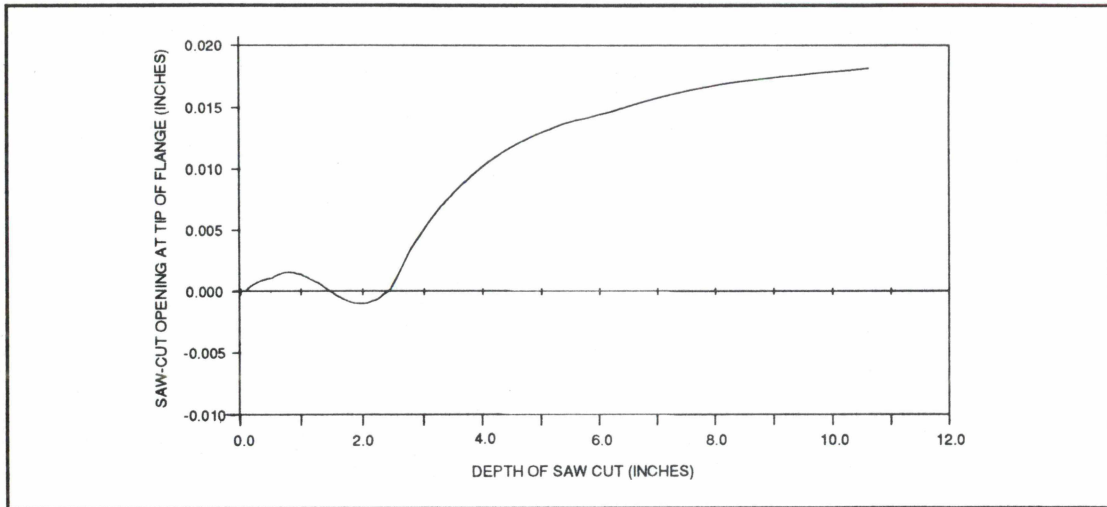


Figure A6. Saw Cut Opening at Tip of Flange as Function of Depth of Saw Cut, 36-inch Diameter Straight-plate Wheel.

Figure A7 shows the net opening displacement of the saw-cut as a function of depth of the 10.5-inch saw-cut into the wheel.

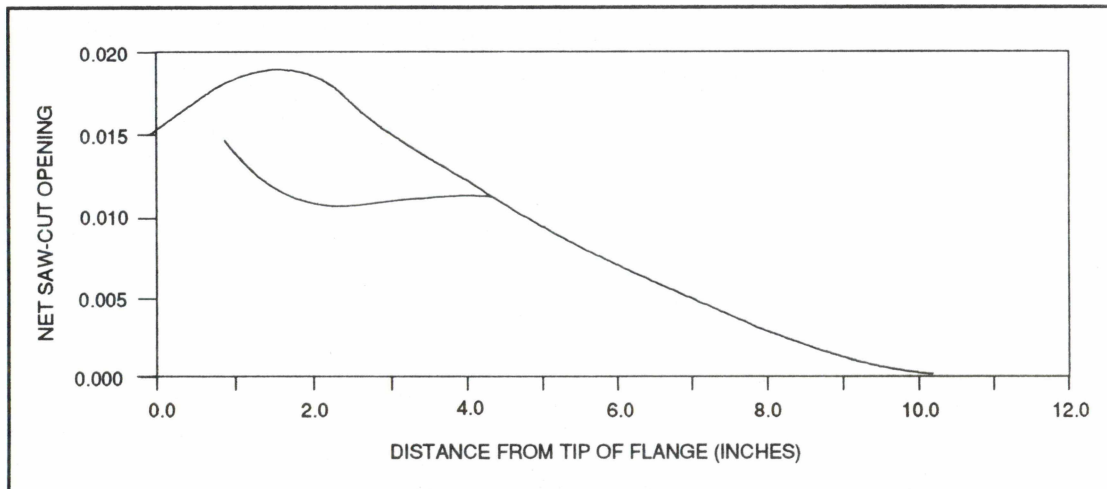


Figure A7. Net Saw Cut Opening as Function of Depth of Cut into Wheel, 36-inch Diameter Straight-Plate Wheel.

Results from the 3-D finite element calculation for closing the cut are shown in Figure 8. This figure shows the predicted circumferential residual stresses. The distribution in the rim is similar to that shown in Figure A3, except that the magnitudes are lower. The maximum stress is again on the back rim face and is predicted to be approximately 19 ksi.

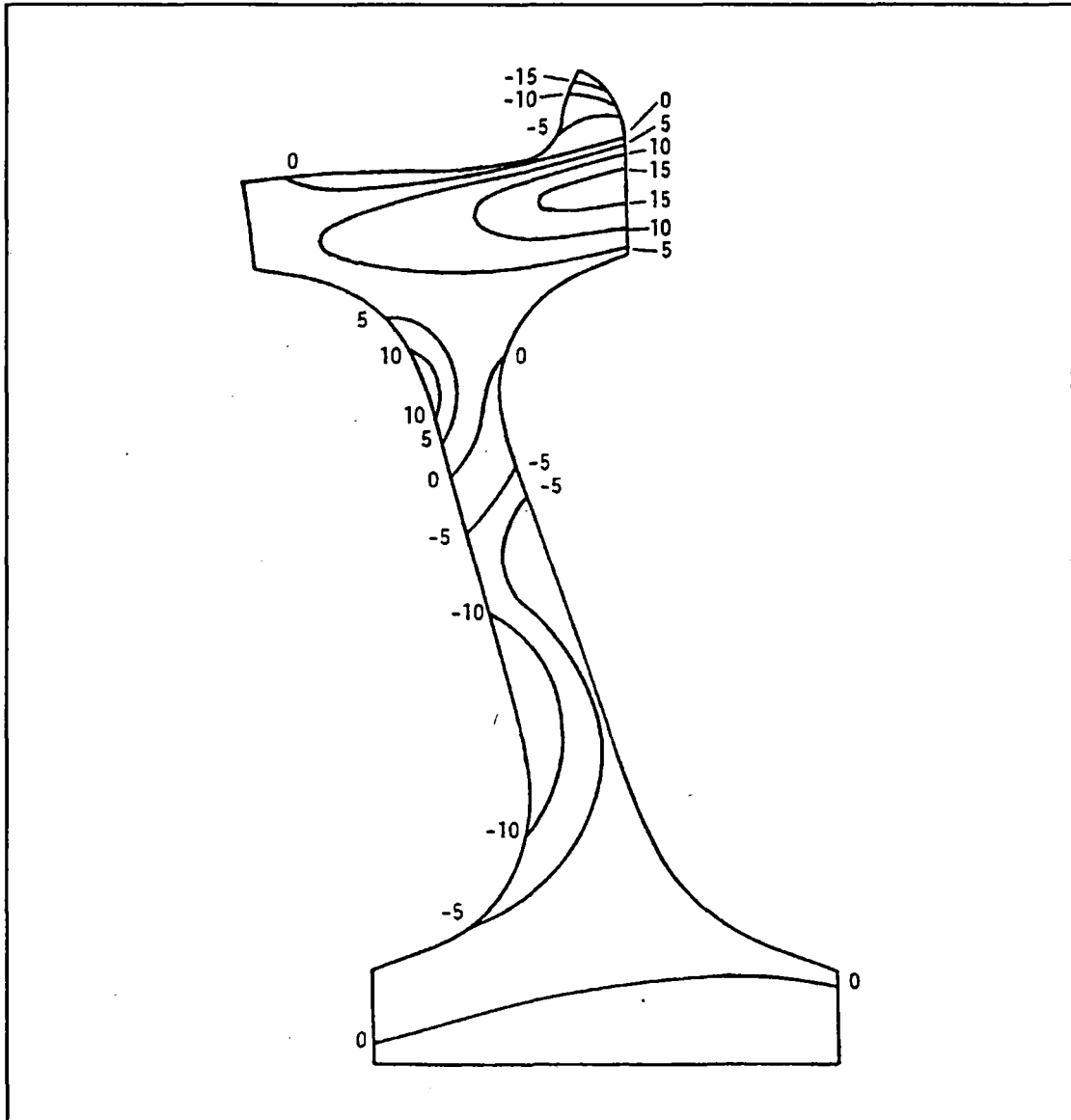


Figure A8. Residual Circumferential Stress Distribution Predicted for 36 inch Diameter Straight-Plate Wheel from Saw Cut Displacement Data (stresses in ksi)

The stress contours from the predicted distribution (Figure A8) were integrated over the rim surface and multiplied by the incremental cross sectional area to estimate the net rim force (43.2 kips).

The saw-cut displacement in the hoop direction as recorded by the clip gage for wheel No. 72 (Figure A6) was used as input to the numerical procedure for TTC's closed form solution and the average stress distribution in the wheel was computed as shown in Figure A9. This procedure calculated the net force in the rim by performing an integration from flange tip to a depth of 3 inches as 43 kips (tensile).

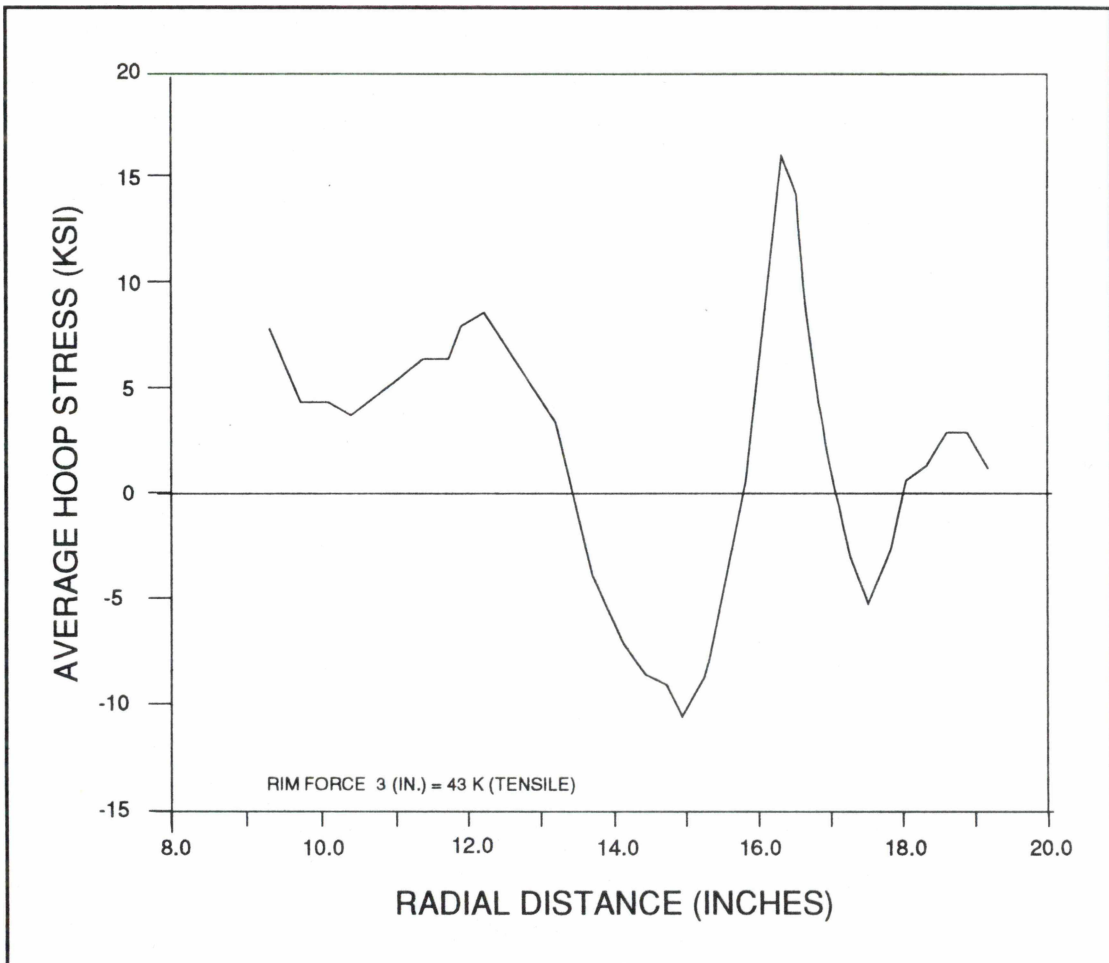


Figure A9. Average Hoop Stress Distribution in 36-inch Diameter Straight-Plate Wheel (TTC ID 0072)

A1.3.3 Case 3

"Thirty-three-inch Diameter Curved-Plate Wheel." Figure A10 shows the saw-cut opening at the tip of the flange versus the saw-cut depth for an 8.5-inch saw-cut into a 33-inch diameter curved-plate wheel. This wheel was subjected to controlled braking cycles in tests conducted on the Roll Dynamics Unit at the Transportation Test Center in Pueblo, Colorado. The wheel was subjected to over 25 simulated drag braking cycles of approximately 60 minutes each at power levels from 25 to 50 braking horse power. Figure A11 shows the net opening displacement of the 8.5-inch saw-cut as a function of depth into the wheel. Note again that there is a significant difference in the displacement data for the opposite sides of the rim of the wheel.

Figure A12 shows the circumferential stresses that are predicted by 3-D finite element analysis when the cut is closed. The stress distribution pattern in the rim is similar to those shown for the other wheels. The maximum circumferential residual stress predicted for the back rim face is approximately 30 ksi.

The stress contours from the predicted distribution (Figure A1) were integrated over the rim surface and multiplied by the incremental cross section area to estimate the net rim force as 65.5 kips.

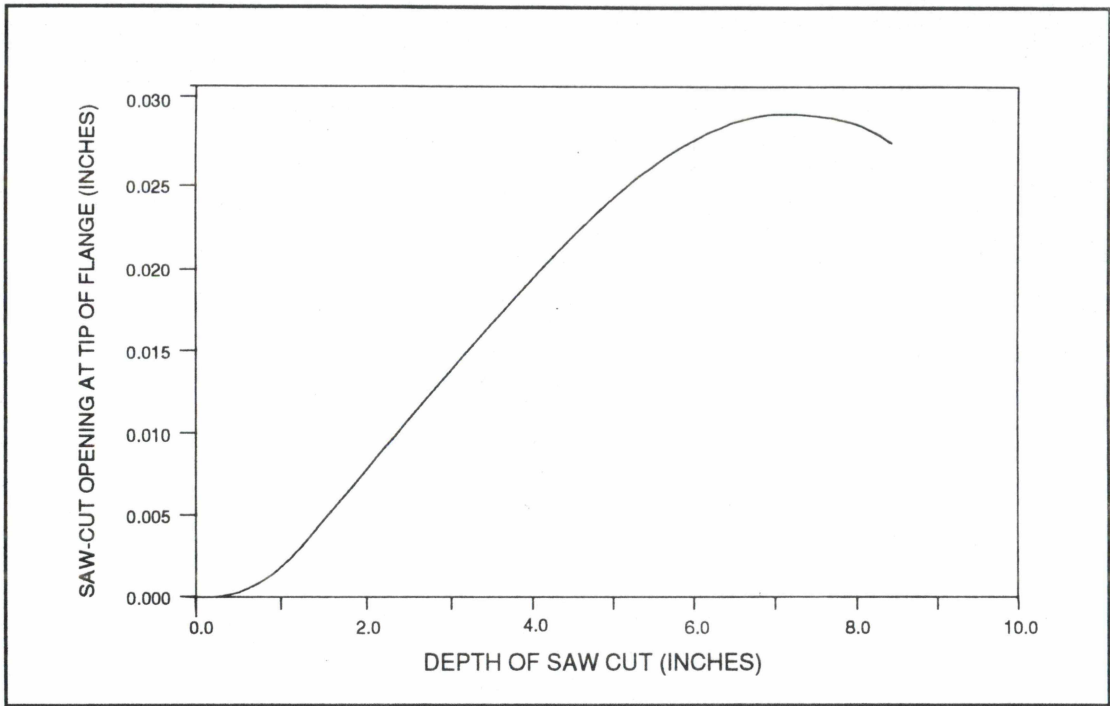


Figure A10. Saw Cut Opening At Tip of Flange as Function of Depth of Saw Cut, 33-inch Diameter, Curved-Plate Wheel

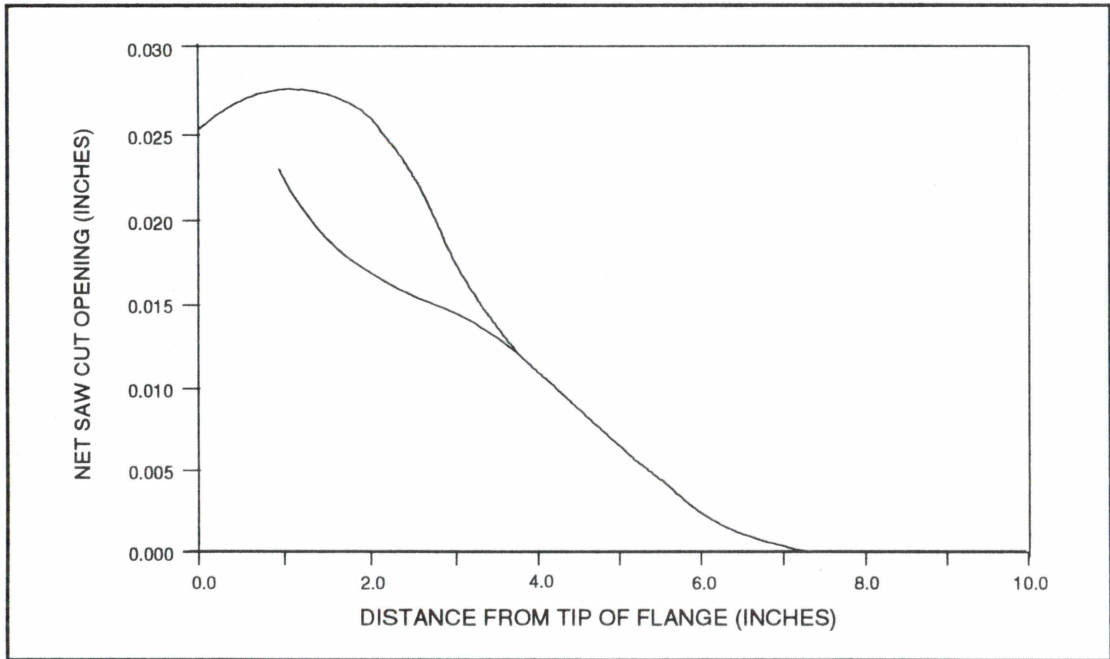


Figure A11. Net Saw Cut Opening as Function of Depth of Saw Cut into Wheel, 33-inch Diameter, Curved-Plate Wheel

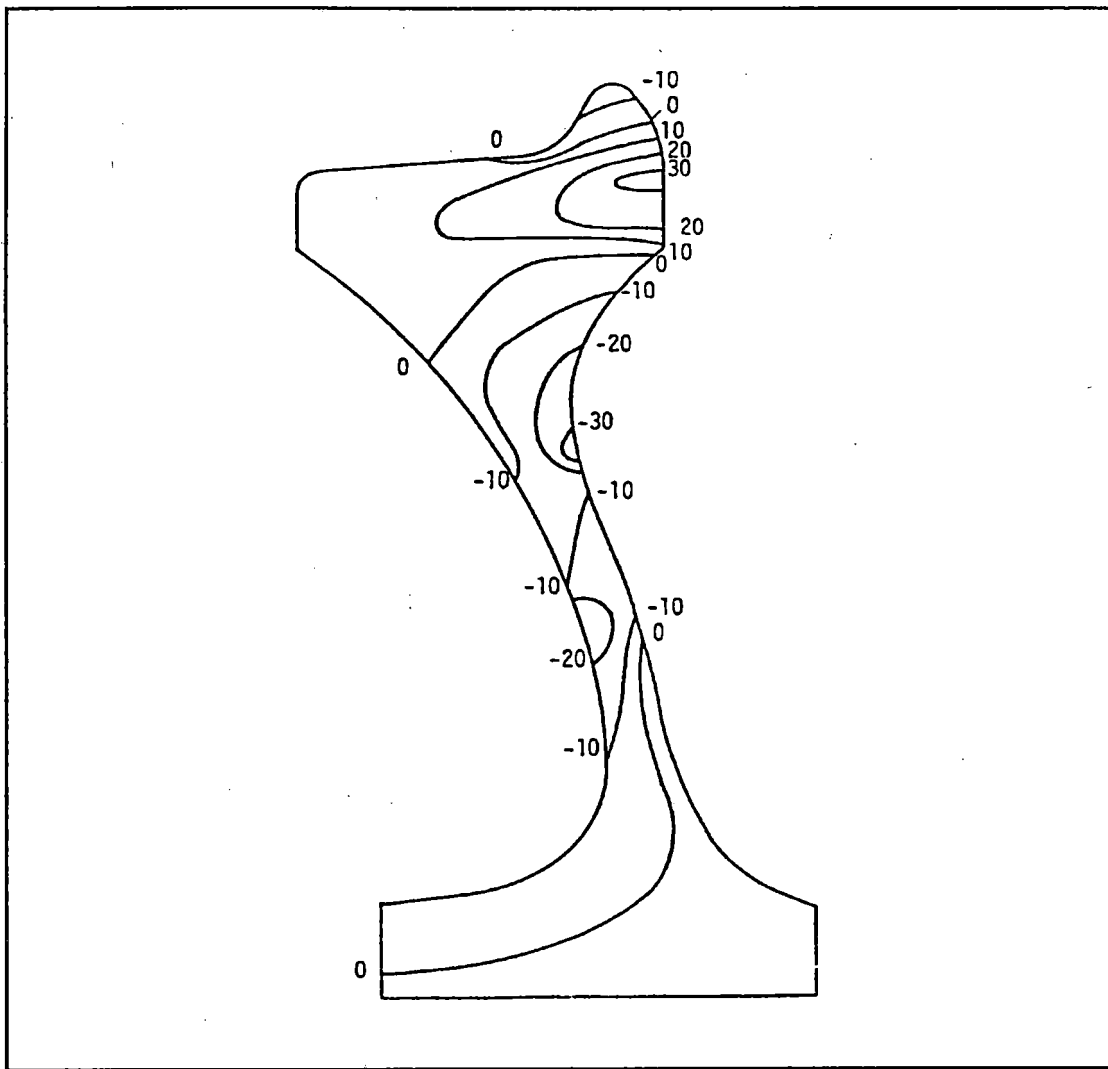


Figure A12. Residual Circumferential Stress Distribution Predicted for 33-inch Diameter, Curved-Plate Wheel from Saw Cut Displacement Data, TTC I.D. No. 003. (ksi)

The saw cut displacement in the hoop direction as recorded by the clip gage for wheel No. 003 (Figure A10) was used as input for TTC's closed form model and the average stress distribution in the total was computed as shown in Figure A13. This procedure calculated the net rim force by performing an integration from flange tip to a depth of 3-inches as 63 kips.

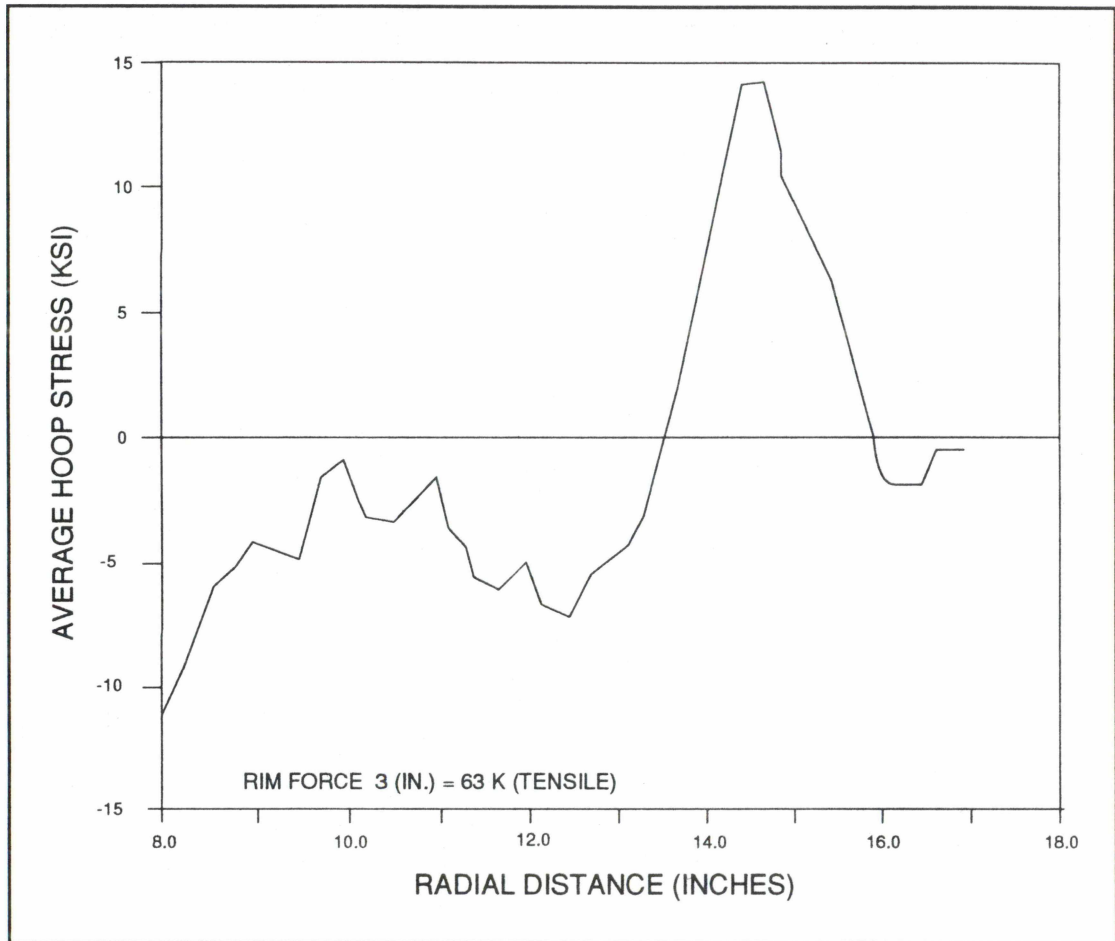


Figure A13. Average Hoop Stress Distribution in 33-inch Diameter Curved-Plate Wheel (TTC I.D. No. 003)

A1.3.4 Case 4: 33-inch Diameter Curved Plate, Class U, New Wheel, TTC I.D. No. 156.

Three dimensional finite element procedures were used to predict the static residual stress in a new 33-inch diameter Class U wheel for which the saw-cut displacement curves are shown Figure A14, and the corresponding computed stress distribution is presented in Figure A15.

The computed net rim force in the above wheel by integration of stress contours (Figure A14) is -15.5 kips (compressive).

The saw-cut displacement as recorded by the clip gage on the flange tip of wheel No. 156 was used as the input for TTC's closed form solution and the average hoop stress distribution in the wheel was computed as shown in Figure A16 along with the calculation of net rim force as -11 kips (compressive).

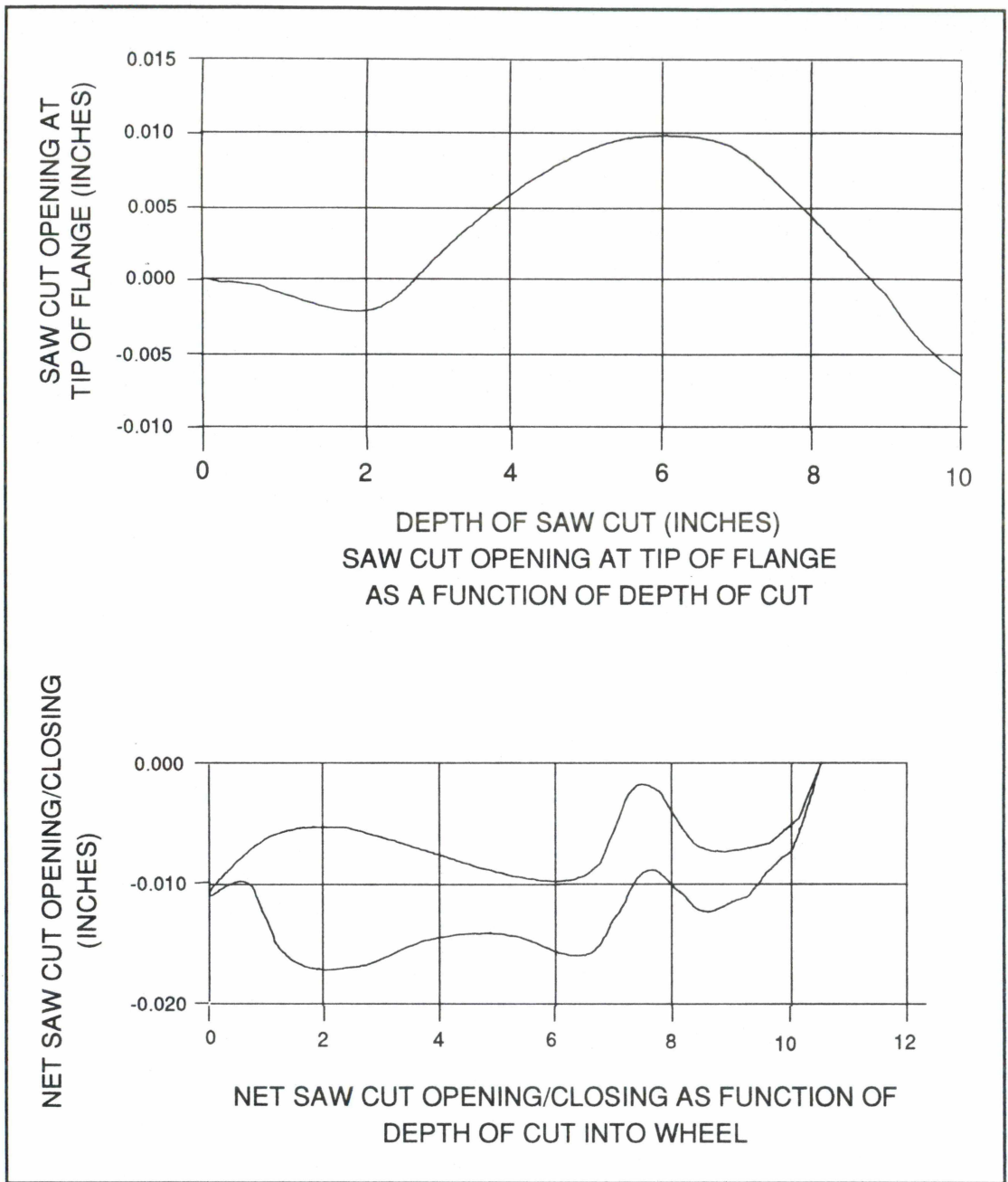
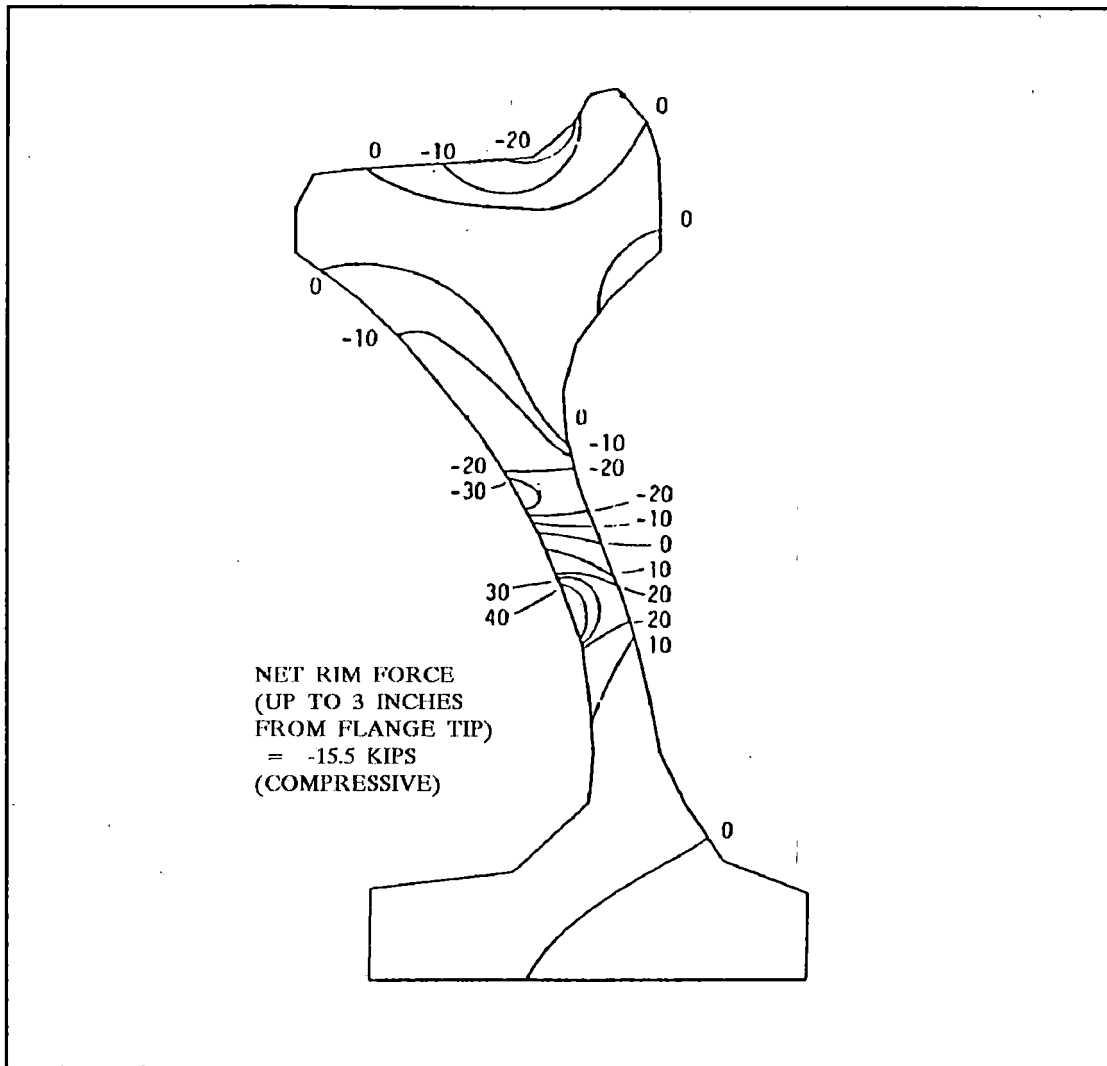
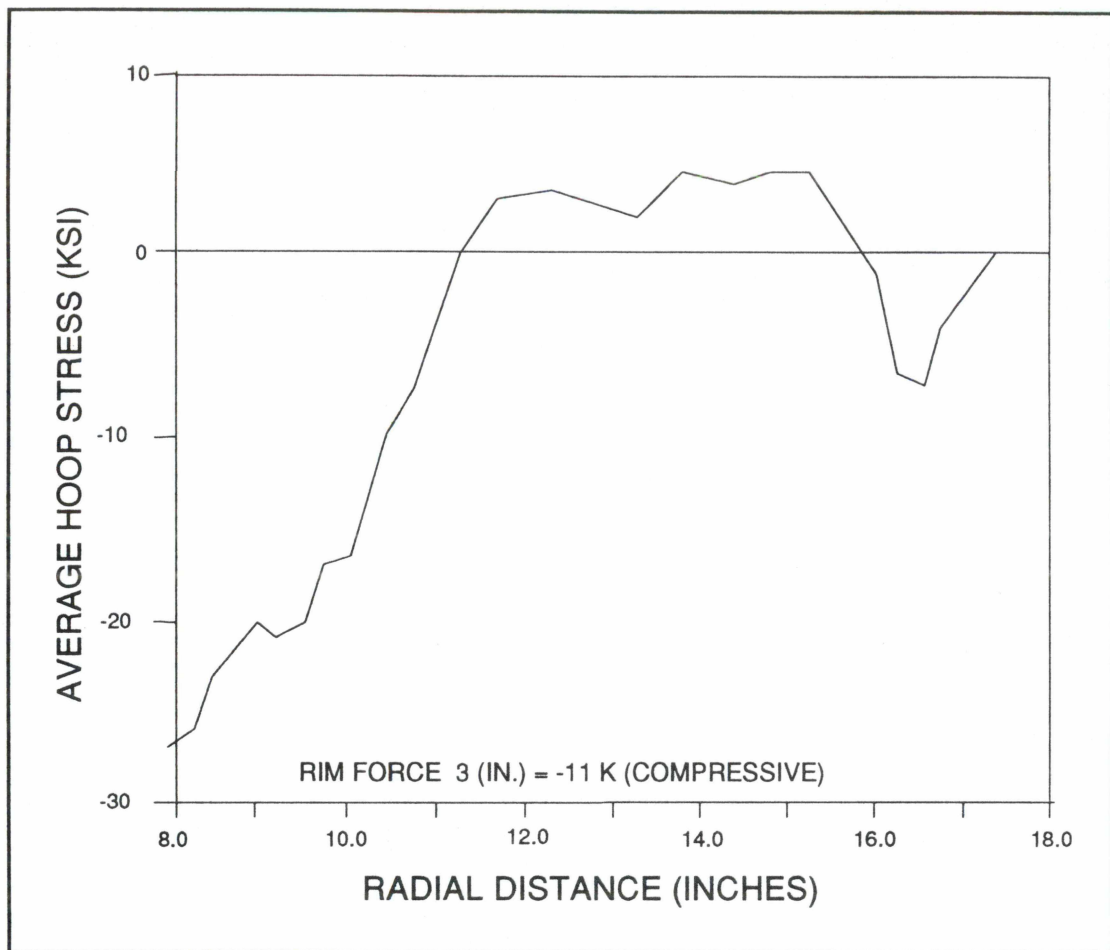


Figure A14. Saw Cut Data for Wheel No. 156, 33-inch Diameter, Curved-Plate Wheel, As Manufactured



**Figure A15. Predicted Residual Circumferential Stress Distribution
for Wheel No. 156, 33-inch Diameter, Curved Plate Wheel using
3-D Finite Element Analysis**



**Figure A16. Average Hoop Stress Distribution in a new 33-inch Diameter, Curved Plate Class U Wheel.
(TTC I.D. No. 156)**

A1.3.5 Case 5: 36-inch Diameter, Curved-Plate Wheel, Class U TTC I.D. 21.

Figure A17 presents the saw-cut displacement responses for the CH 36 Class U wheel and the results of 3D finite element analysis in the form of predicted stress contours. The computed net rim force by the integration of stress contours (Figure A18) is 52.5 kips (tensile).

The results of TTC's closed form solution in terms of average hoop stress distribution in the wheel along with the computed net rim force (42 kips tensile) are presented in Figure A19.

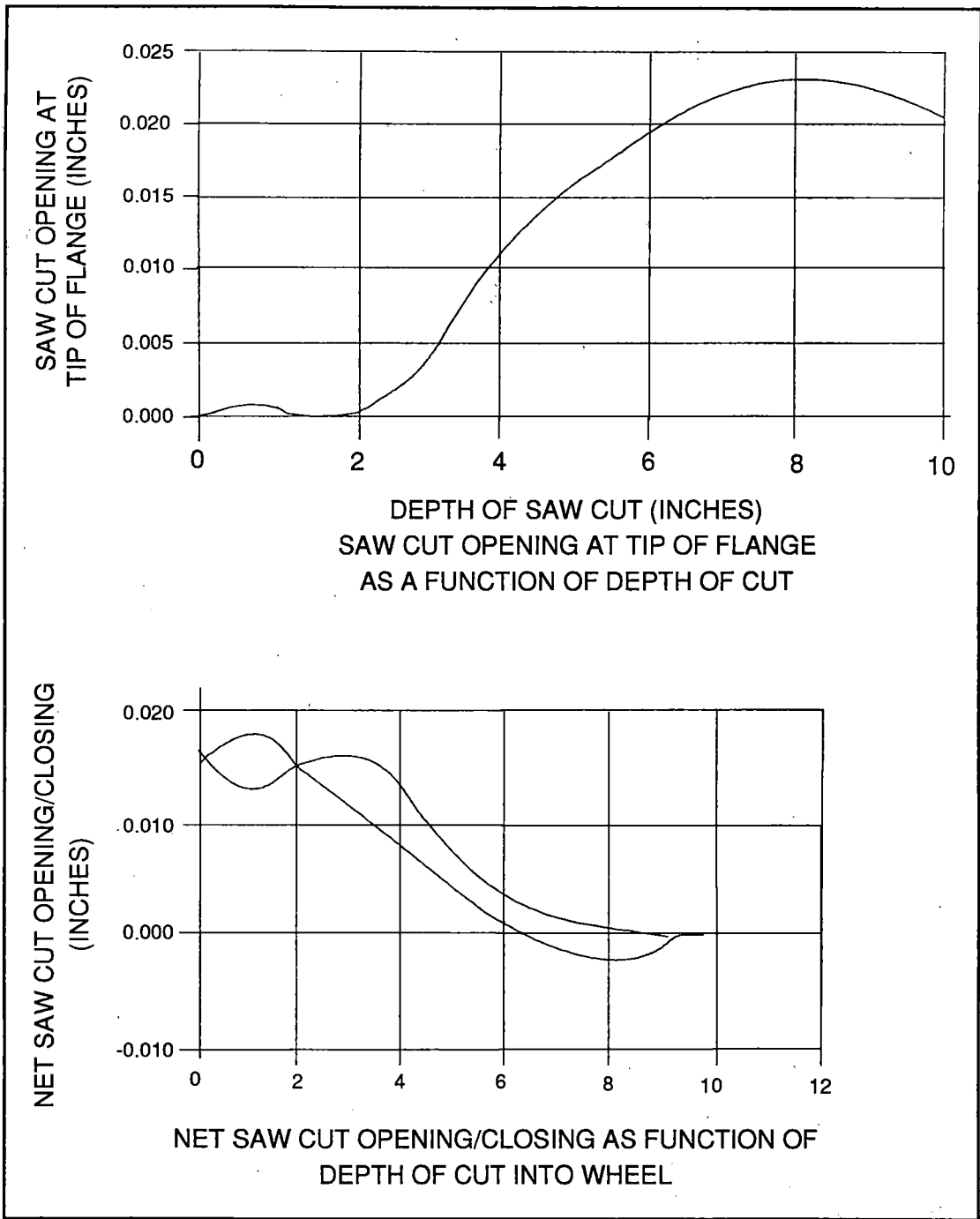


Figure A17. Saw Cut Data for CH36, Class U Wheel (TTC I.D. No. 0021)

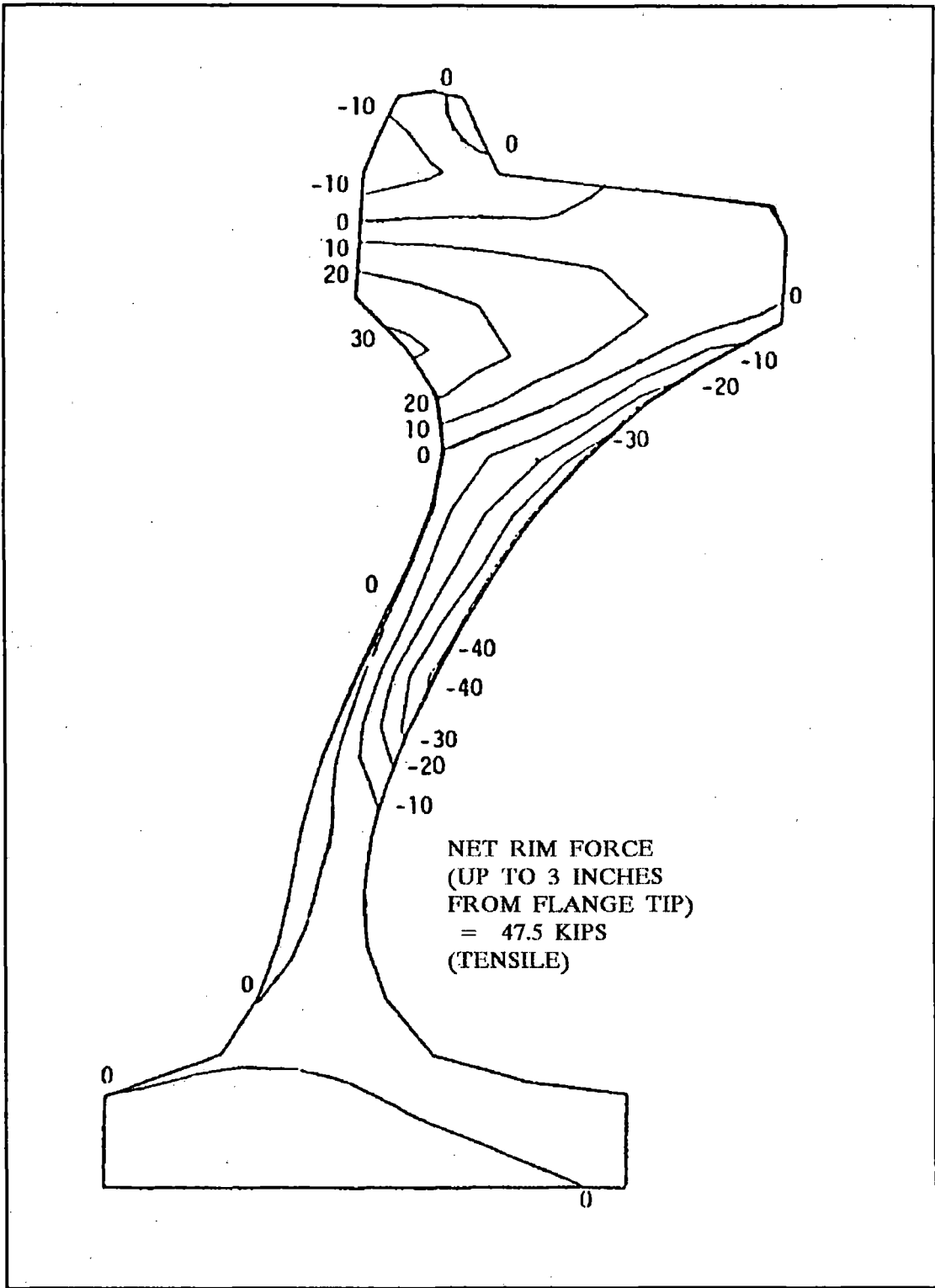


Figure A18. Residual Circumferential Stresses in CH36, Class U Wheel (TTC I.D. No. 0021) from 3D Finite Element Analysis

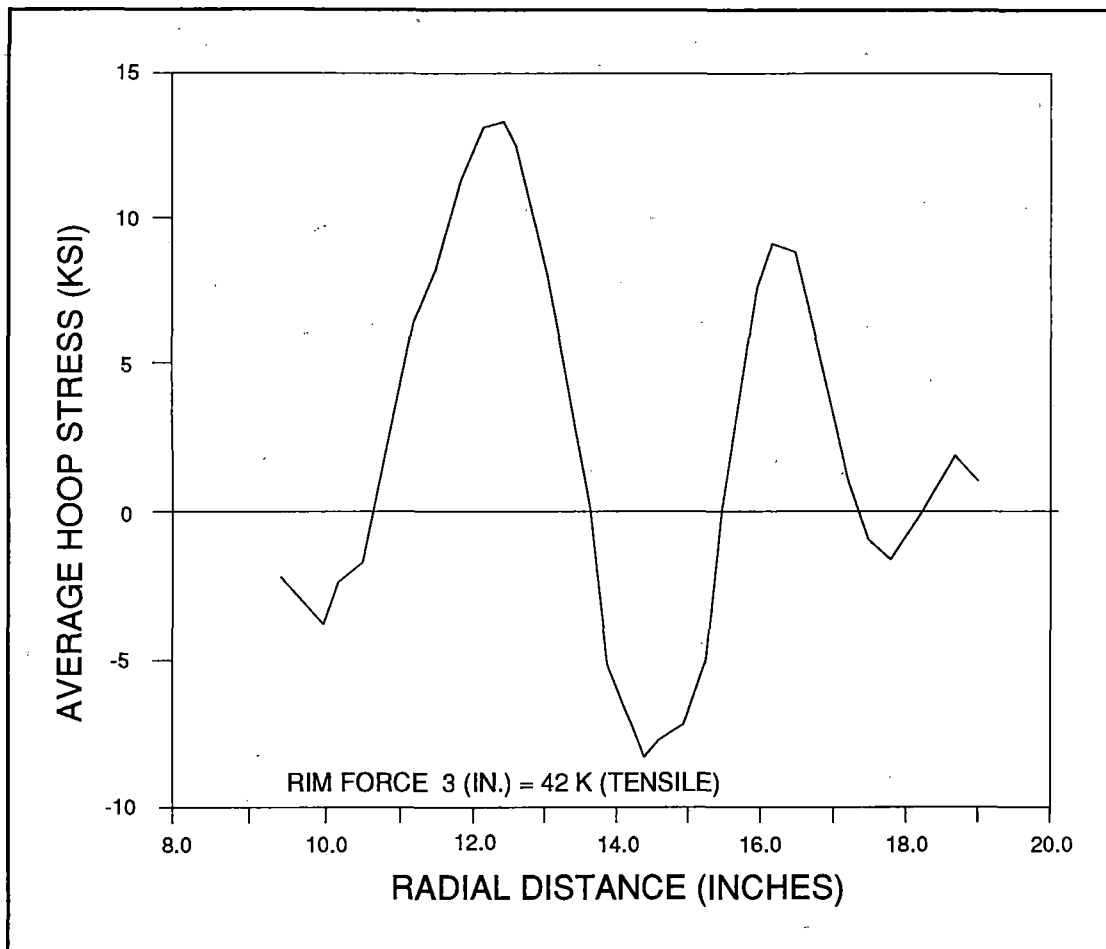


Figure A19. Average Hoop Stress Distribution in CH36, Curved Plate Class U Wheel (TTC I.D. No. 0021)

A2.0 CONCLUSIONS

The re-examination of residual stress calculations from both 3-D finite element analysis and TTC's closed form solution for the above five railroad wheels from their saw-cut displacement behaviors, reveals that even though TTC's closed form solution comprises a more simpler numerical procedure as compared to the intensive 3-D analysis, the net rim forces in the respective wheels computed from both the procedures compare extremely well. For this reason, the results of NDE measurements using magneto-acoustic and acoustic birefringence devices were compared to the net rim force calculations of TTC's closed form solution.

Table 1 predicts the comparison net rim forces computed from 3-D finite element analysis and TTC's closed form solution for five case histories discussed in this appendix.

Table A1. Finite Element and "Closed Form" Comparison


WHEEL NO.(TTC ID)	TYPE	CLASS	NET RIM FORCE (KIPS)	
			3-D Finite Element Analysis	TTC's closed form solution
29	CH36	U	136.5	132
72	H36	U	43.2	43
3	CJ33	U	65.5	63
156	CJ33	U	-15.5	-11
21	CH36	U	47.5	42

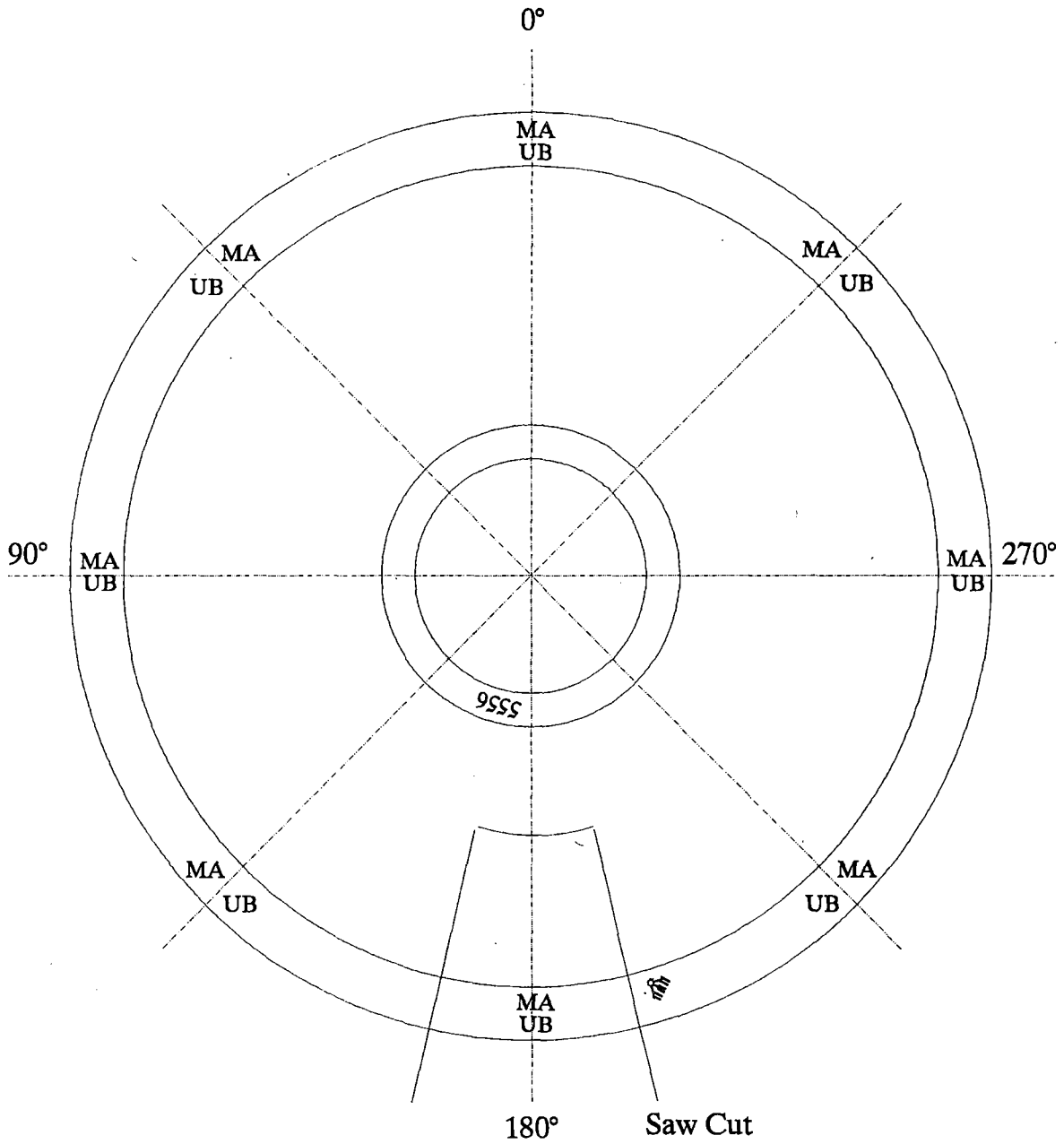
APPENDIX B

DATA MEASUREMENT LOCATION MAPS

Measurement Locations


Wheel 5556

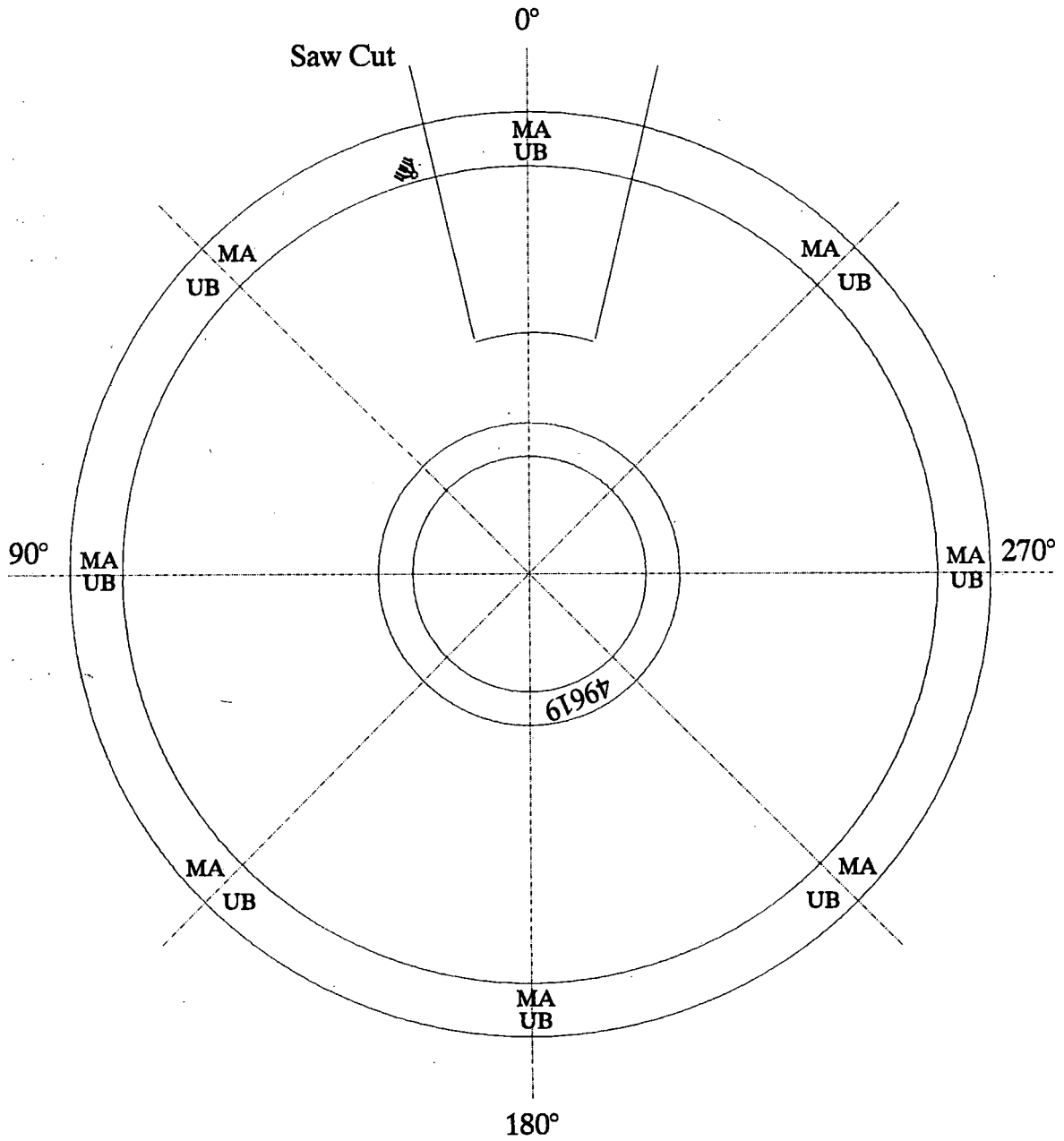
 = Hole Drilling MA = Magnetoacoustic UB = Acoustic Birefringence



Measurement Locations

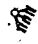
Wheel 49619

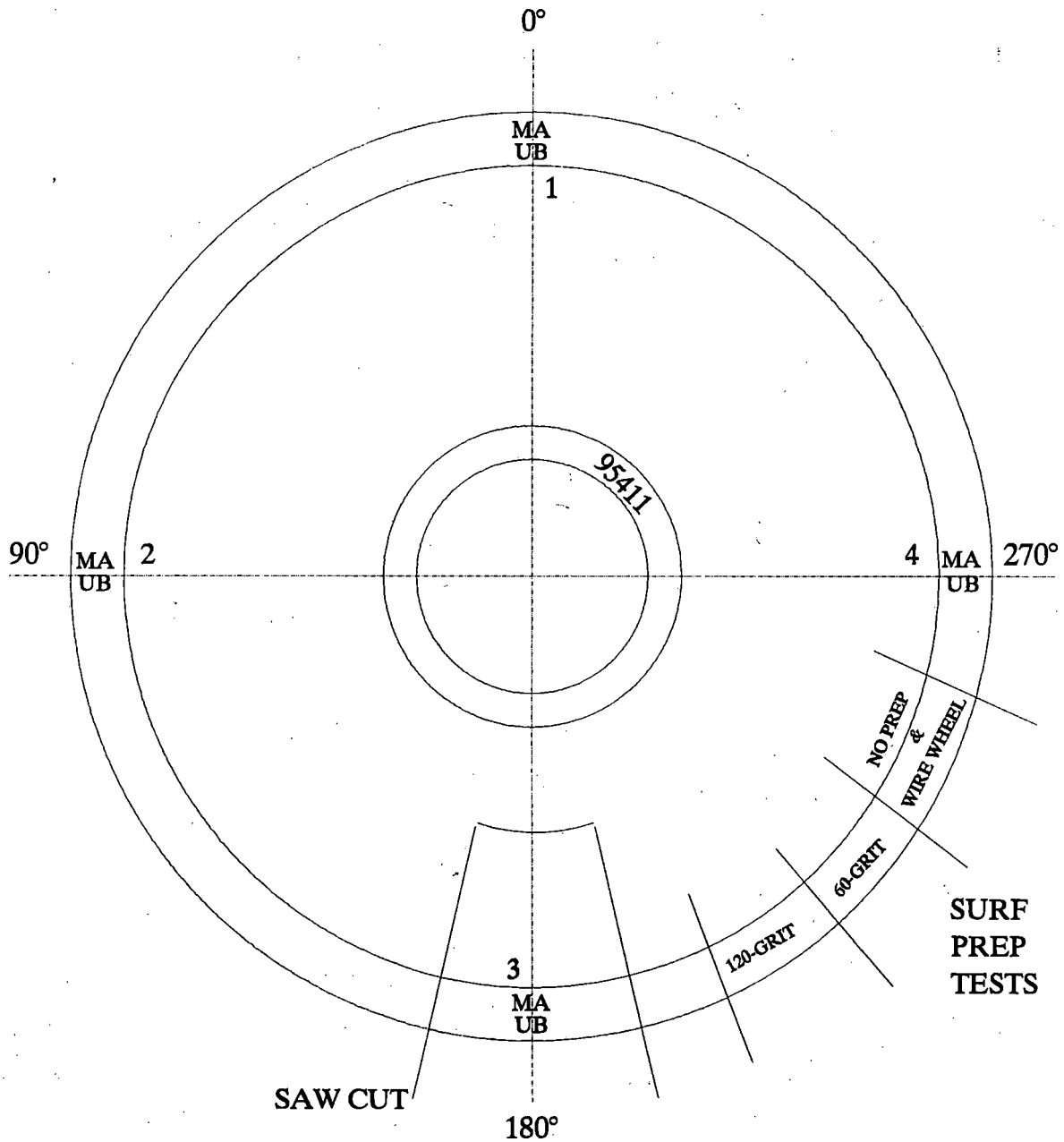
 = Hole Drilling MA = Magnetoacoustic UB = Acoustic Birefringence



Measurement Locations


Wheel 95411

 = Hole Drilling MA = Magnetoacoustic UB = Acoustic Birefringence



Measurement Locations

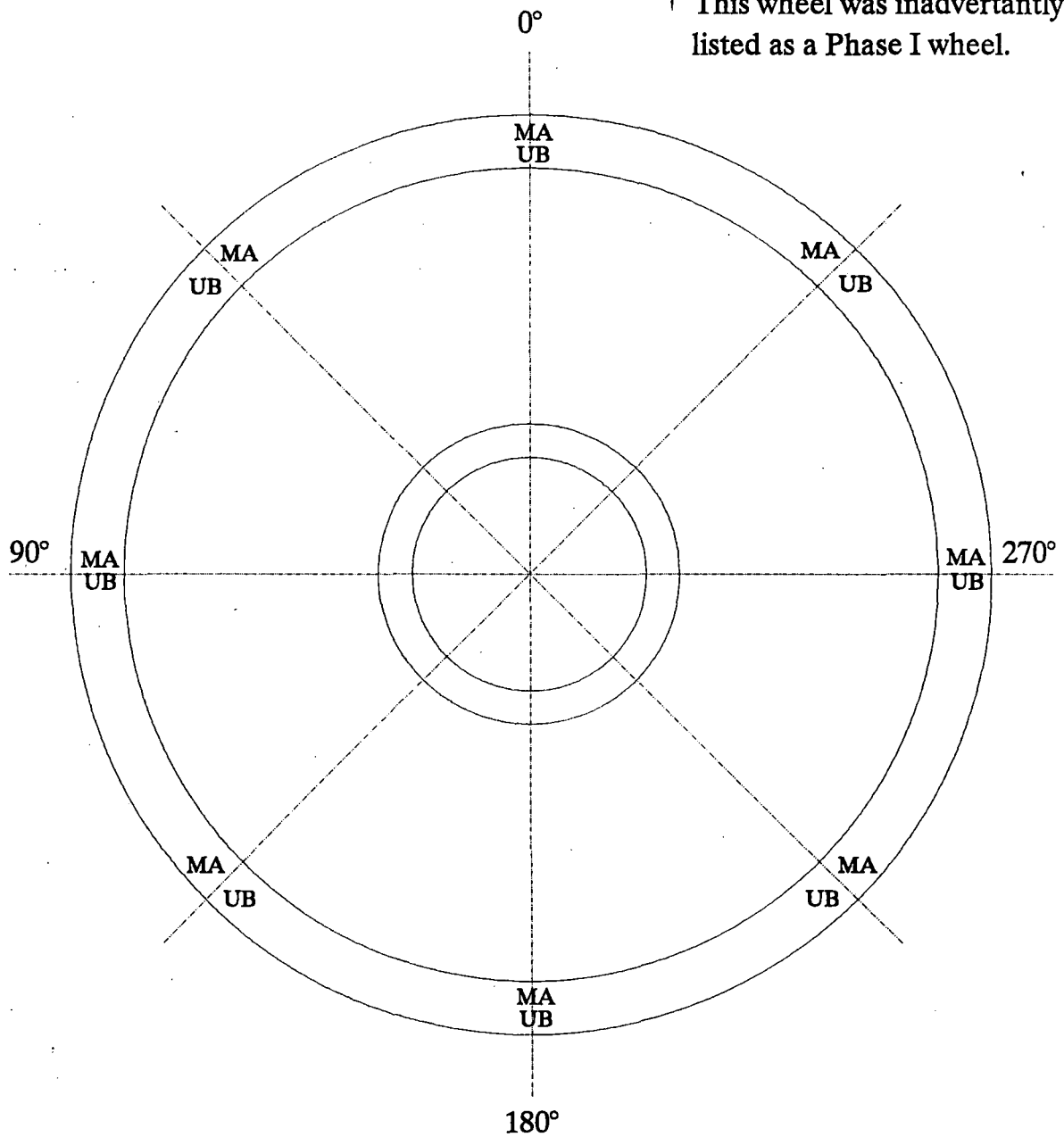
Wheel 94575[†]

 = Hole Drilling

MA = Magnetoacoustic


UB = Acoustic Birefringence

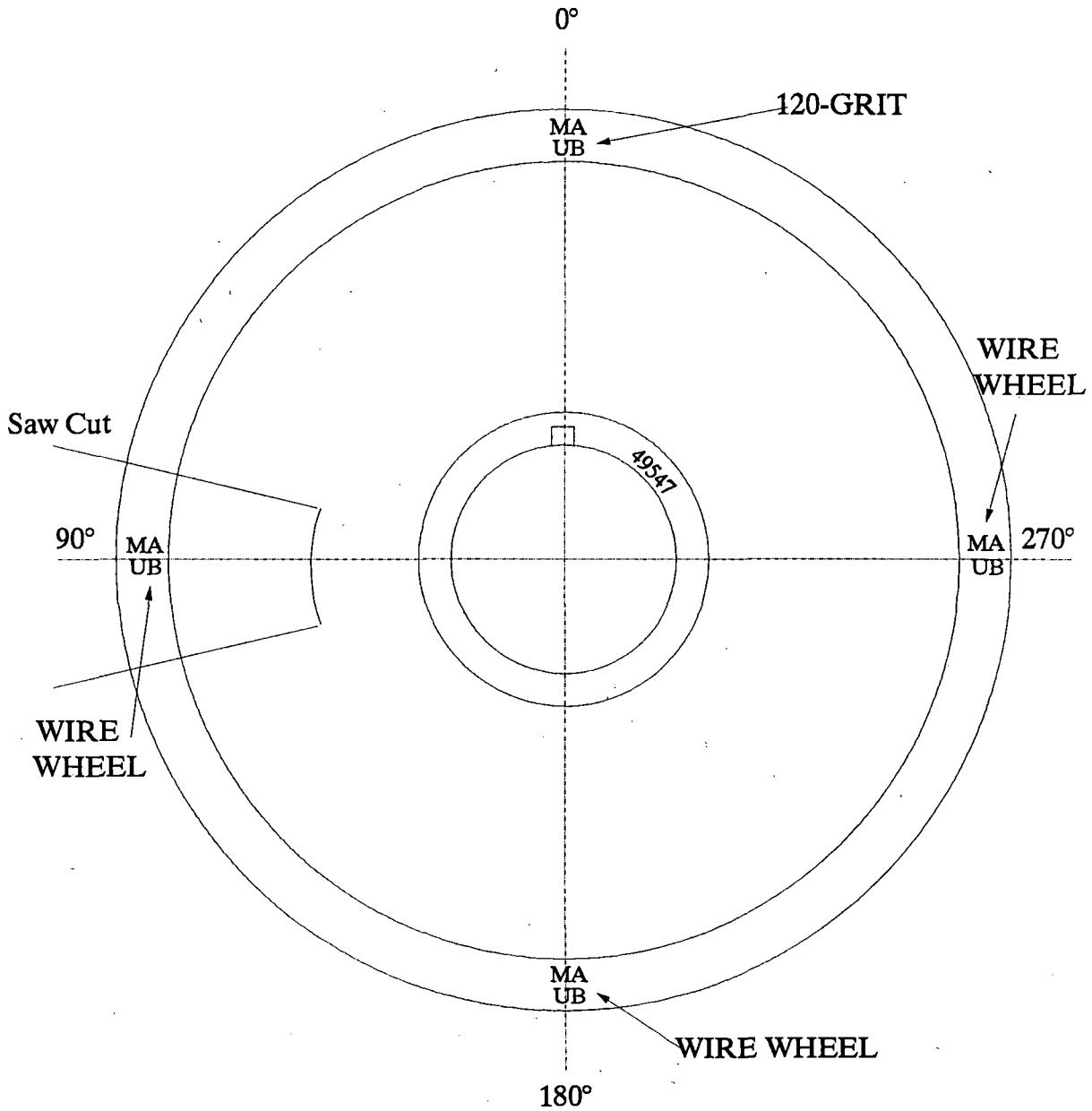
[†] This wheel was inadvertently listed as a Phase I wheel.



Measurement Locations

Wheel 49547

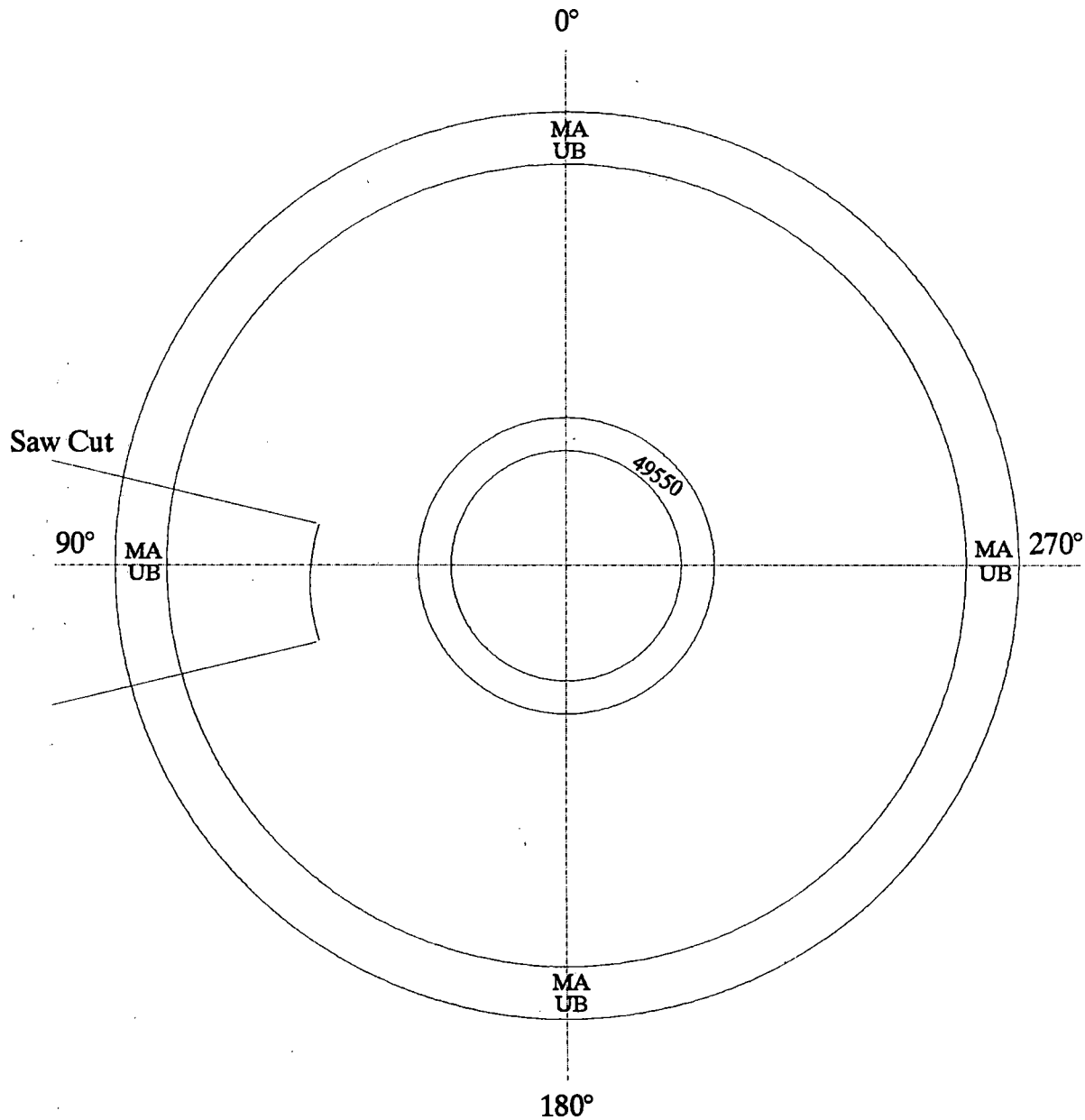
 = Hole Drilling MA = Magnetoacoustic UB = Acoustic Birefringence



Measurement Locations

Wheel 49550

 = Hole Drilling MA = Magnetoacoustic UB = Acoustic Birefringence



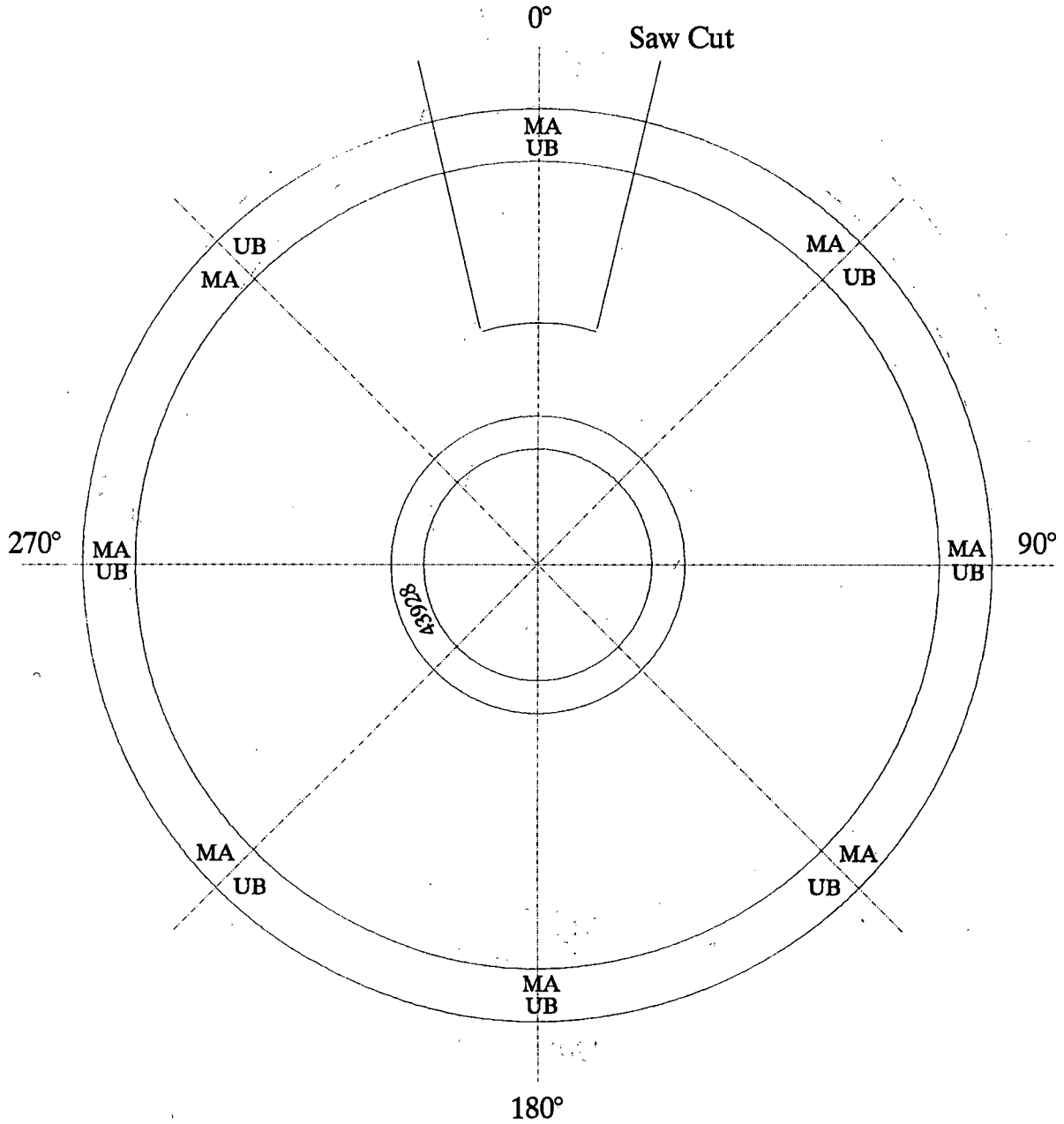
Measurement Locations

Wheel 43928

 = Hole Drilling
Not Drilled


MA = Magnetoacoustic

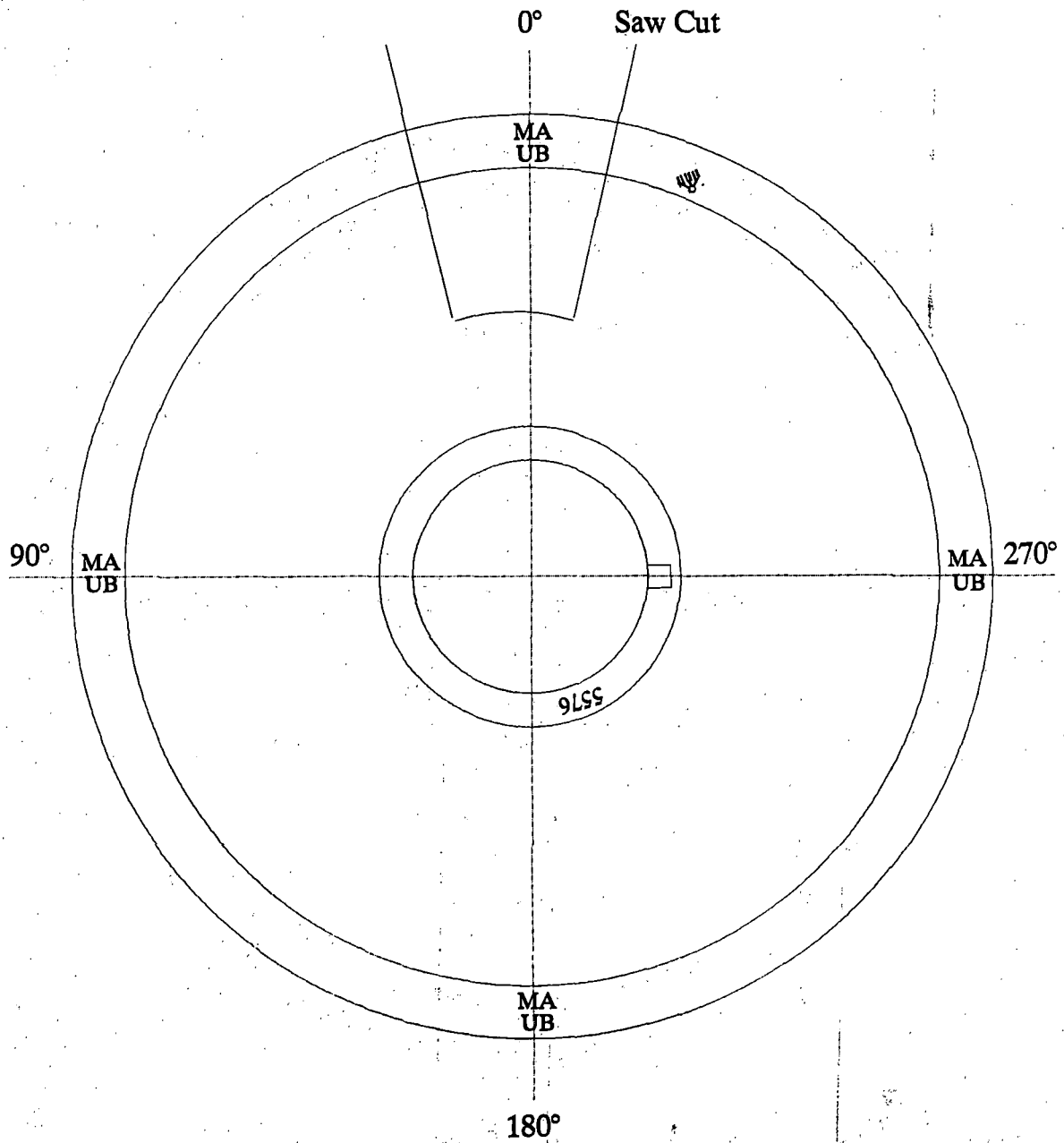
UB = Acoustic Birefringence



Measurement Locations


Wheel 5576

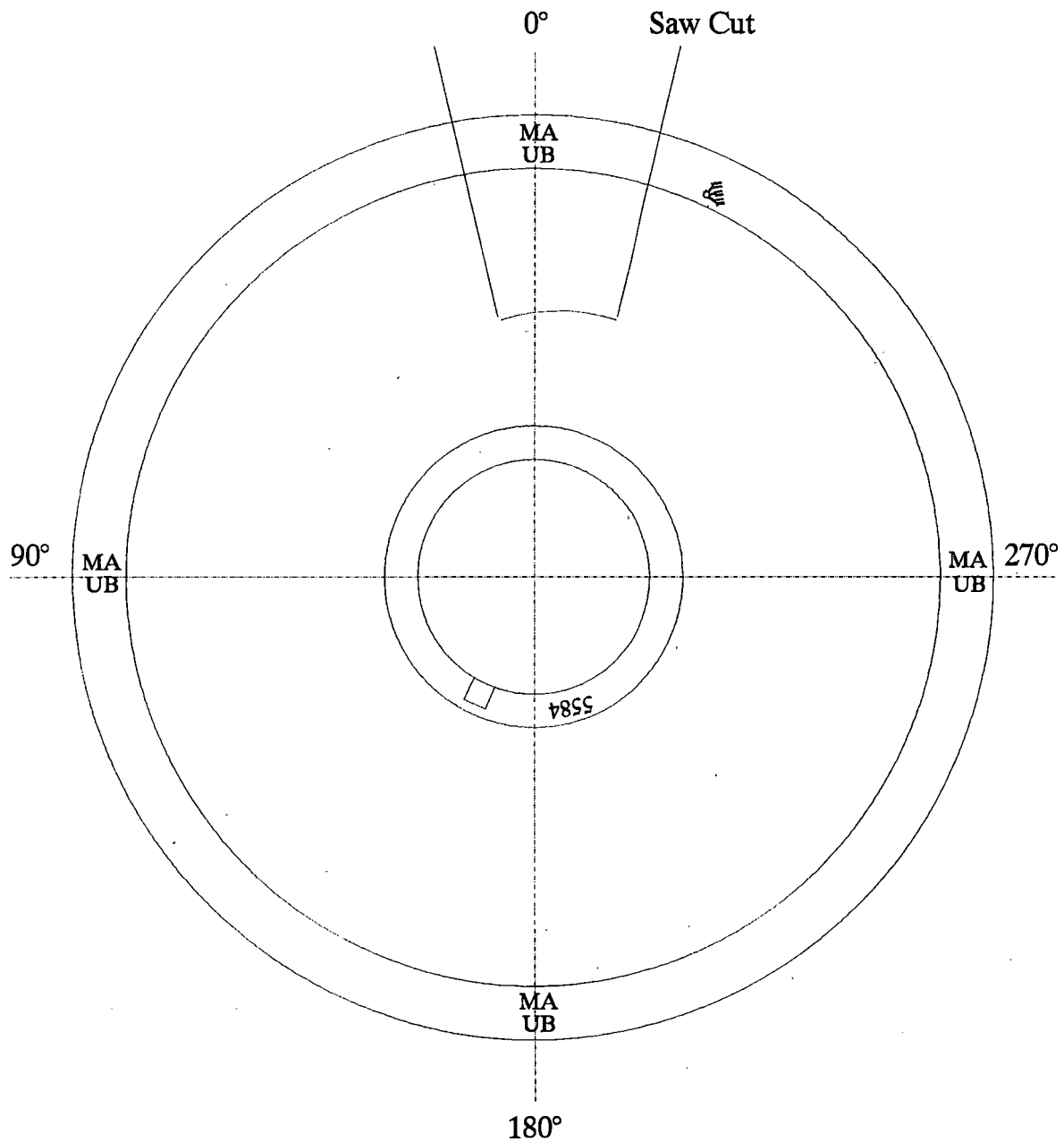
 = Hole Drilling MA = Magnetoacoustic UB = Acoustic Birefringence



Measurement Locations


Wheel 5584

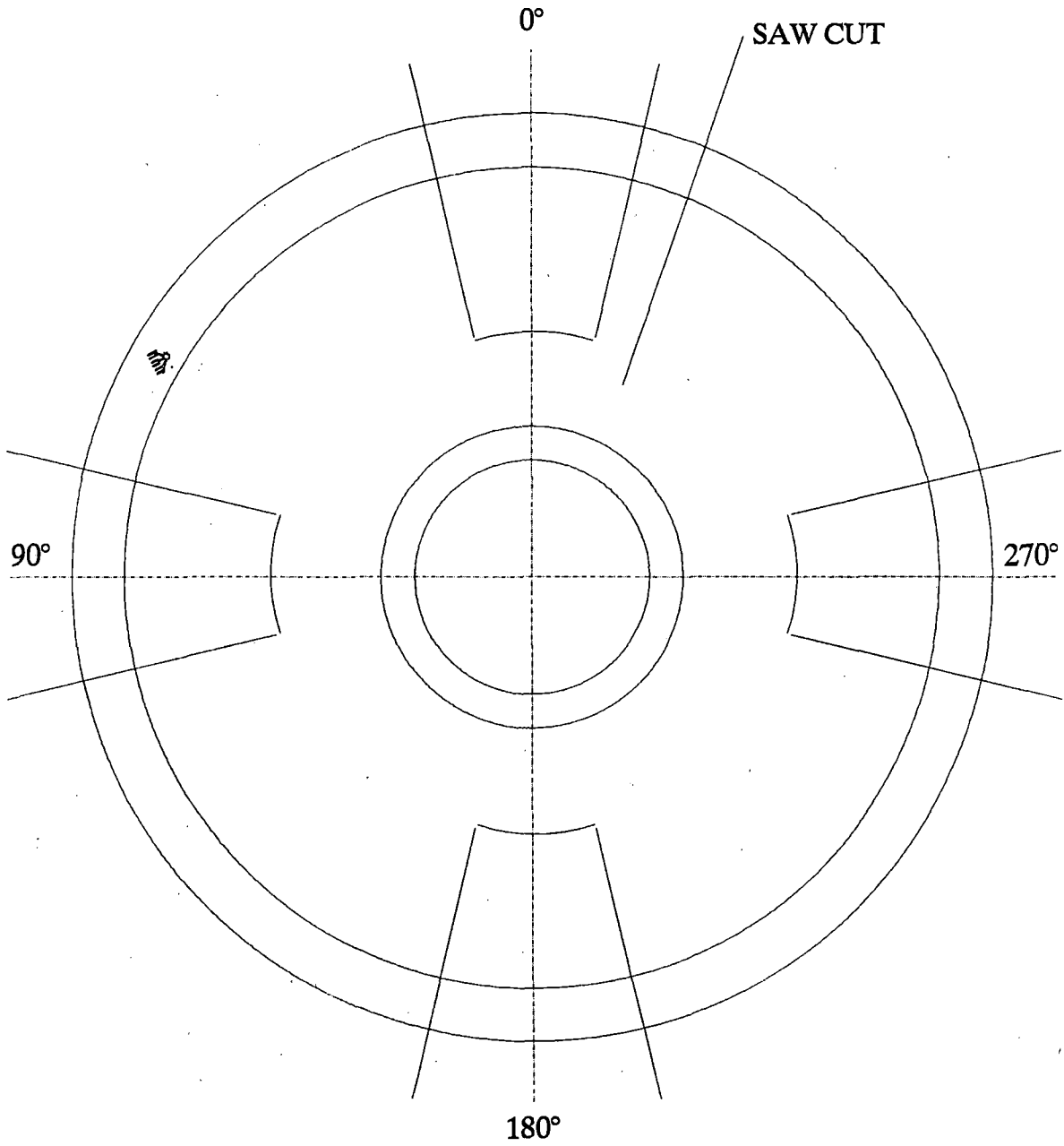
 = Hole Drilling MA = Magnetoacoustic UB = Acoustic Birefringence



Measurement Locations


Wheel 95554 W-1

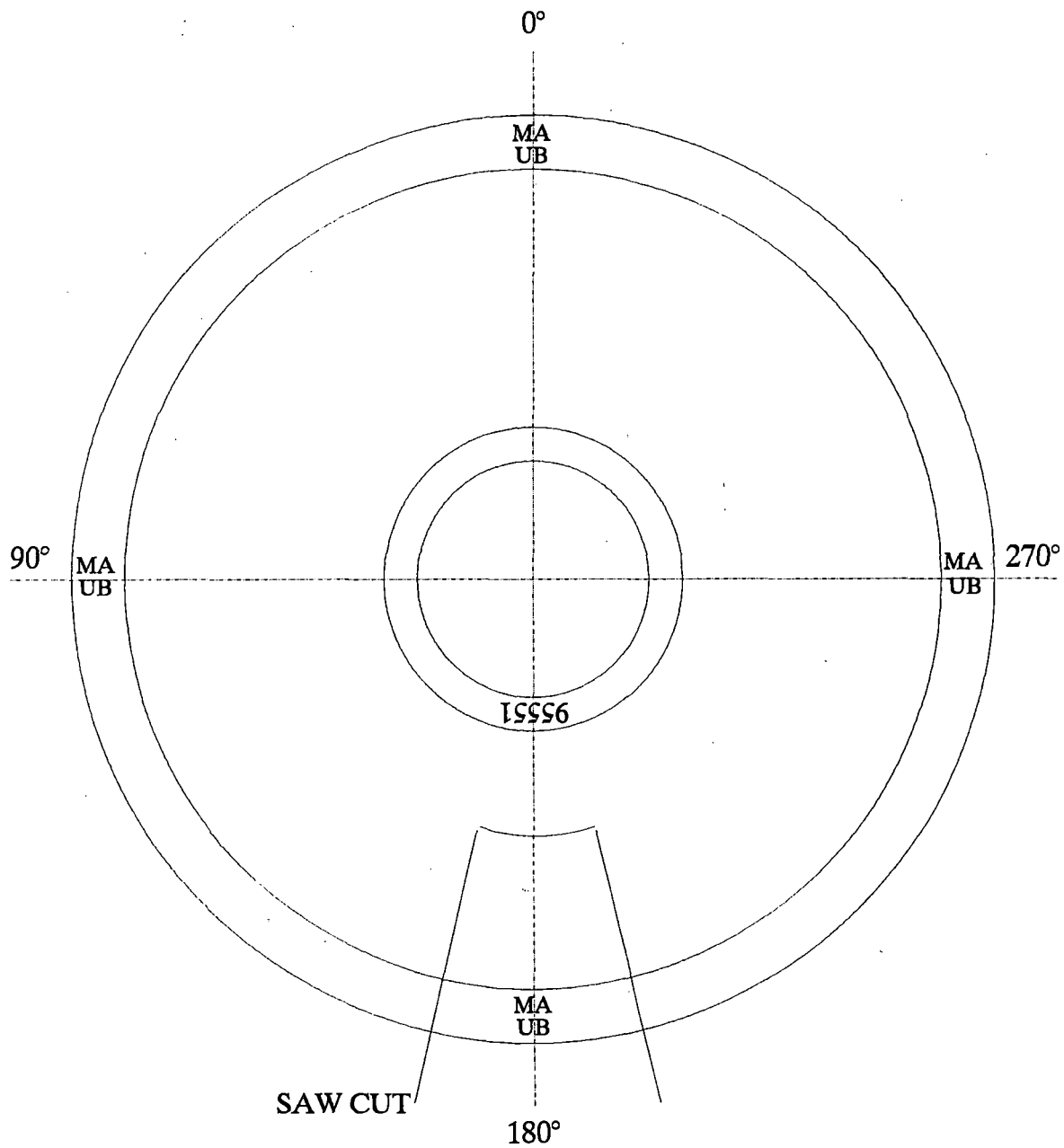
 = Hole Drilling MA = Magnetoacoustic UB = Acoustic Birefringence



Measurement Locations


Wheel 95551 W-2

 = Hole Drilling MA = Magnetoacoustic UB = Acoustic Birefringence



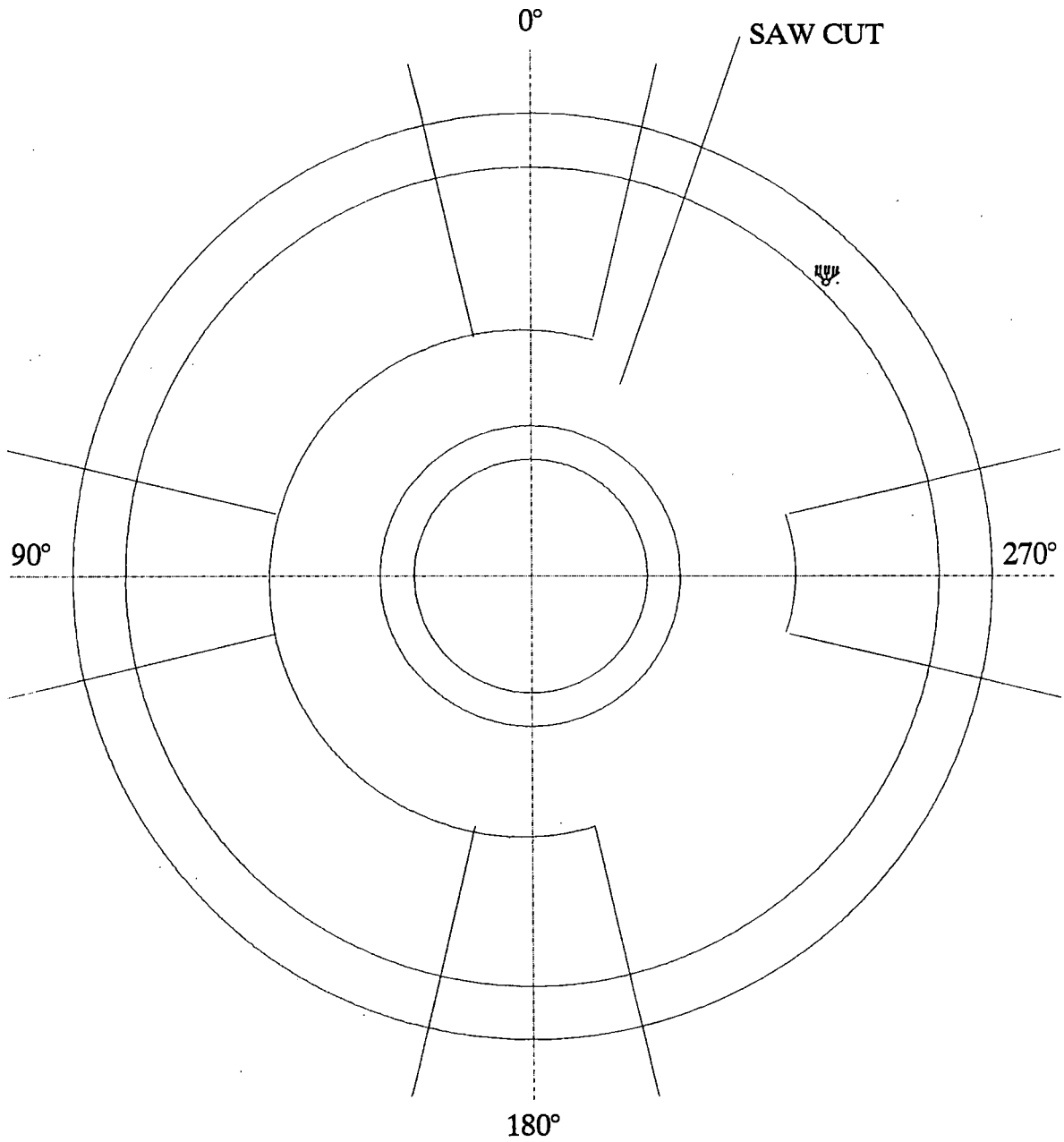
Measurement Locations

Wheel 94559 · W-5

 = Hole Drilling


MA = Magnetoacoustic

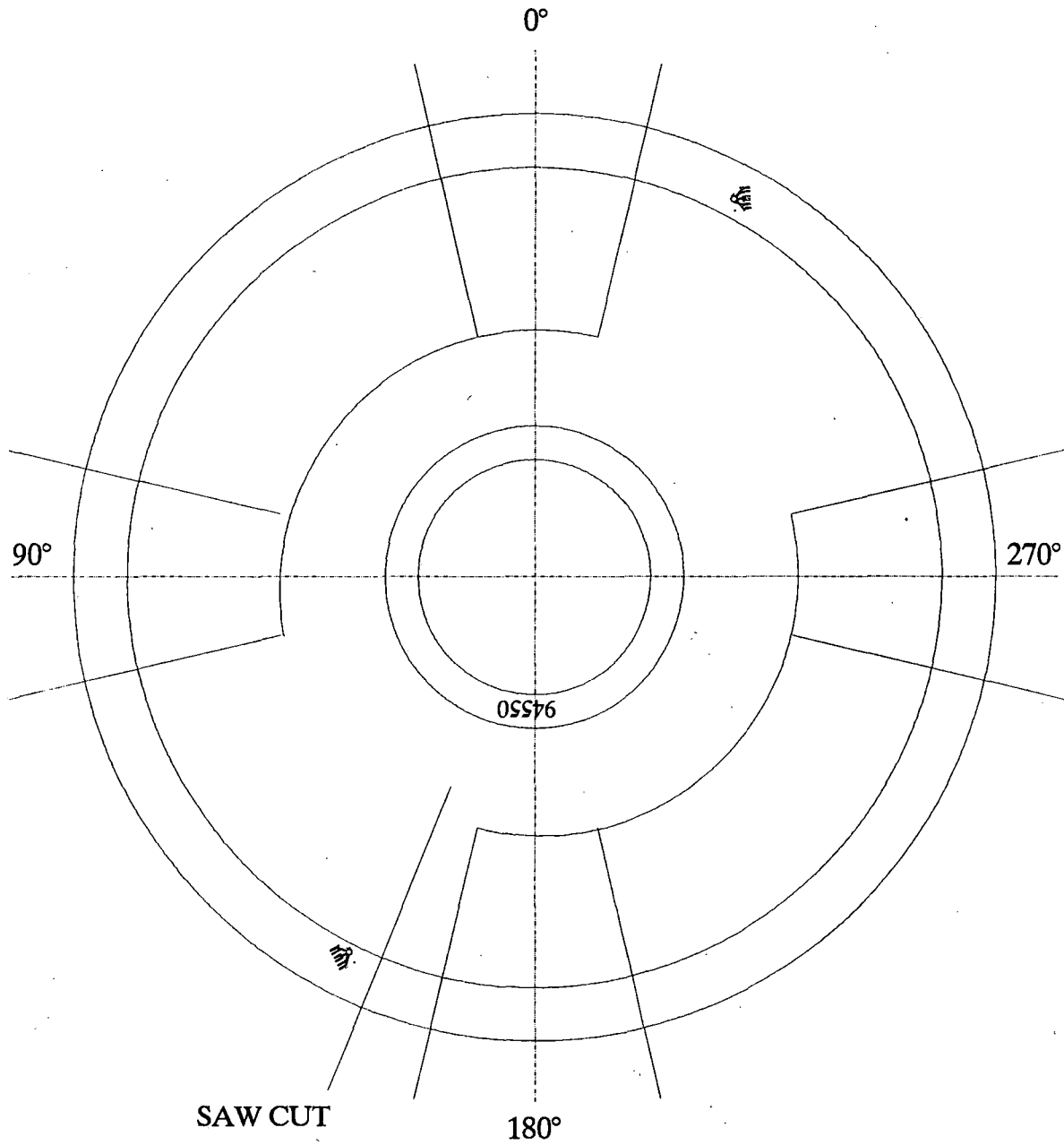
UB = Acoustic Birefringence



Measurement Locations


Wheel 94550 W-6

 = Hole Drilling MA = Magnetoacoustic UB = Acoustic Birefringence



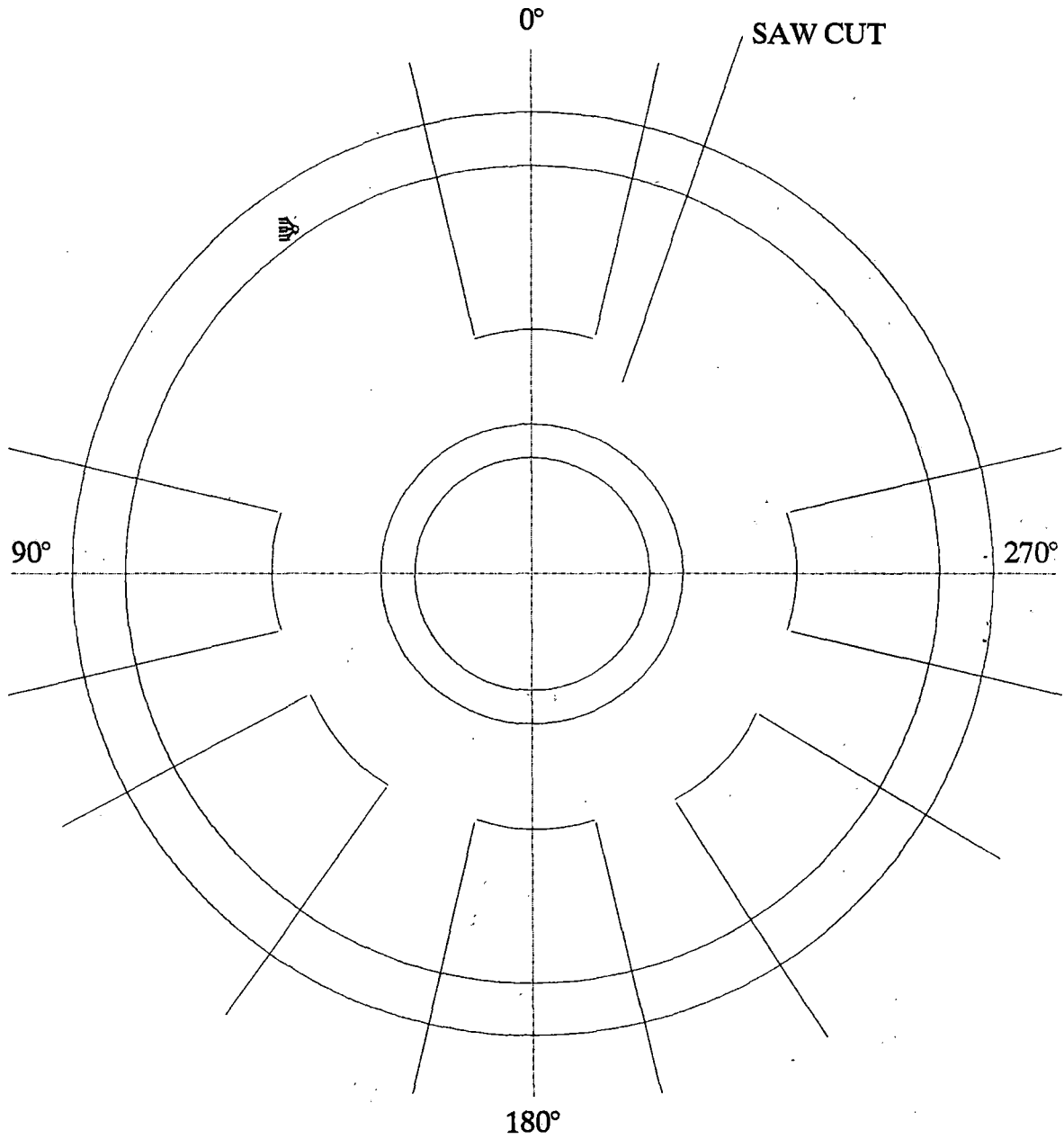
Measurement Locations

Wheel 94565 W-7

 = Hole Drilling


MA = Magnetoacoustic

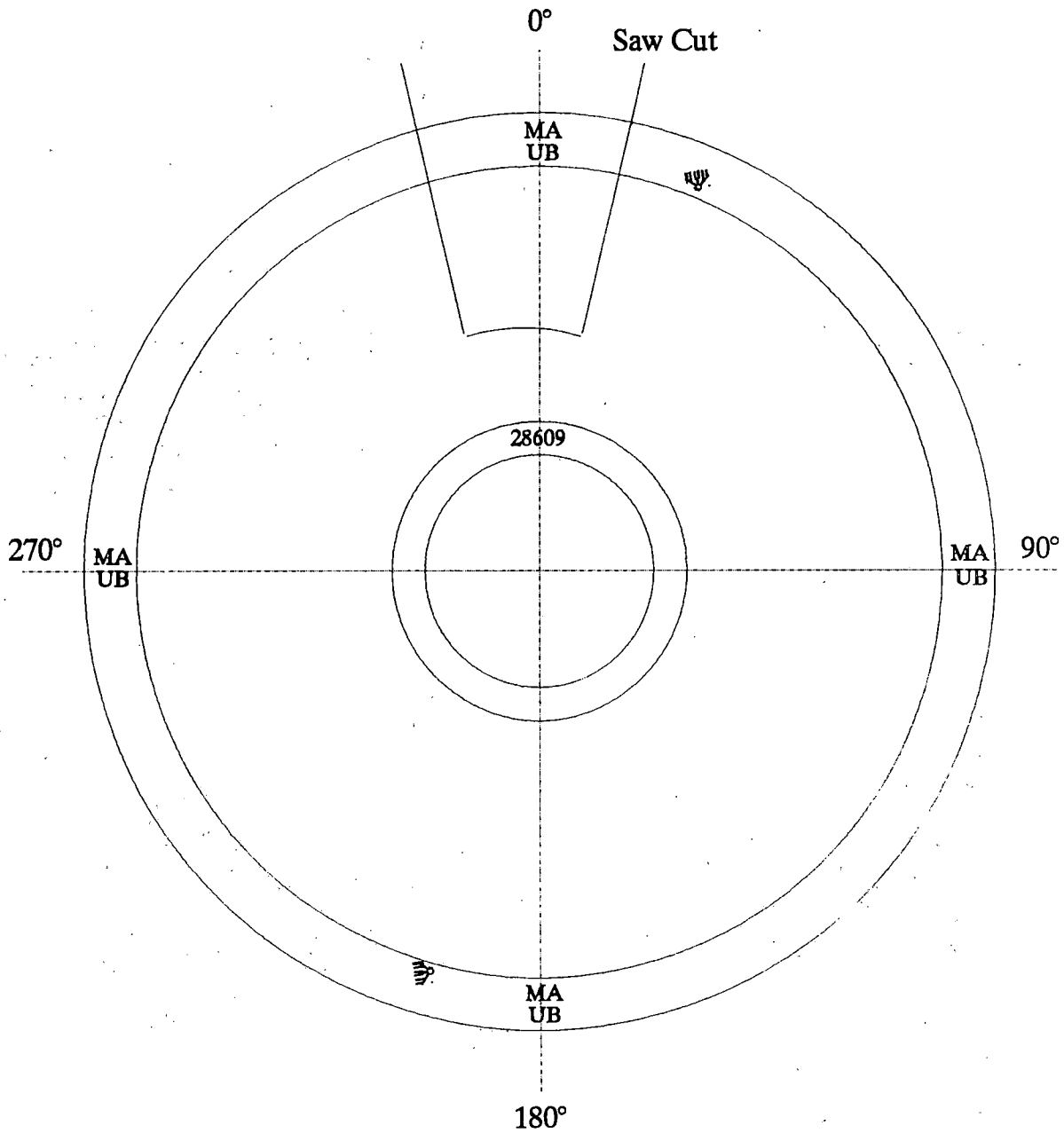
UB = Acoustic Birefringence



Measurement Locations


Wheel 28609

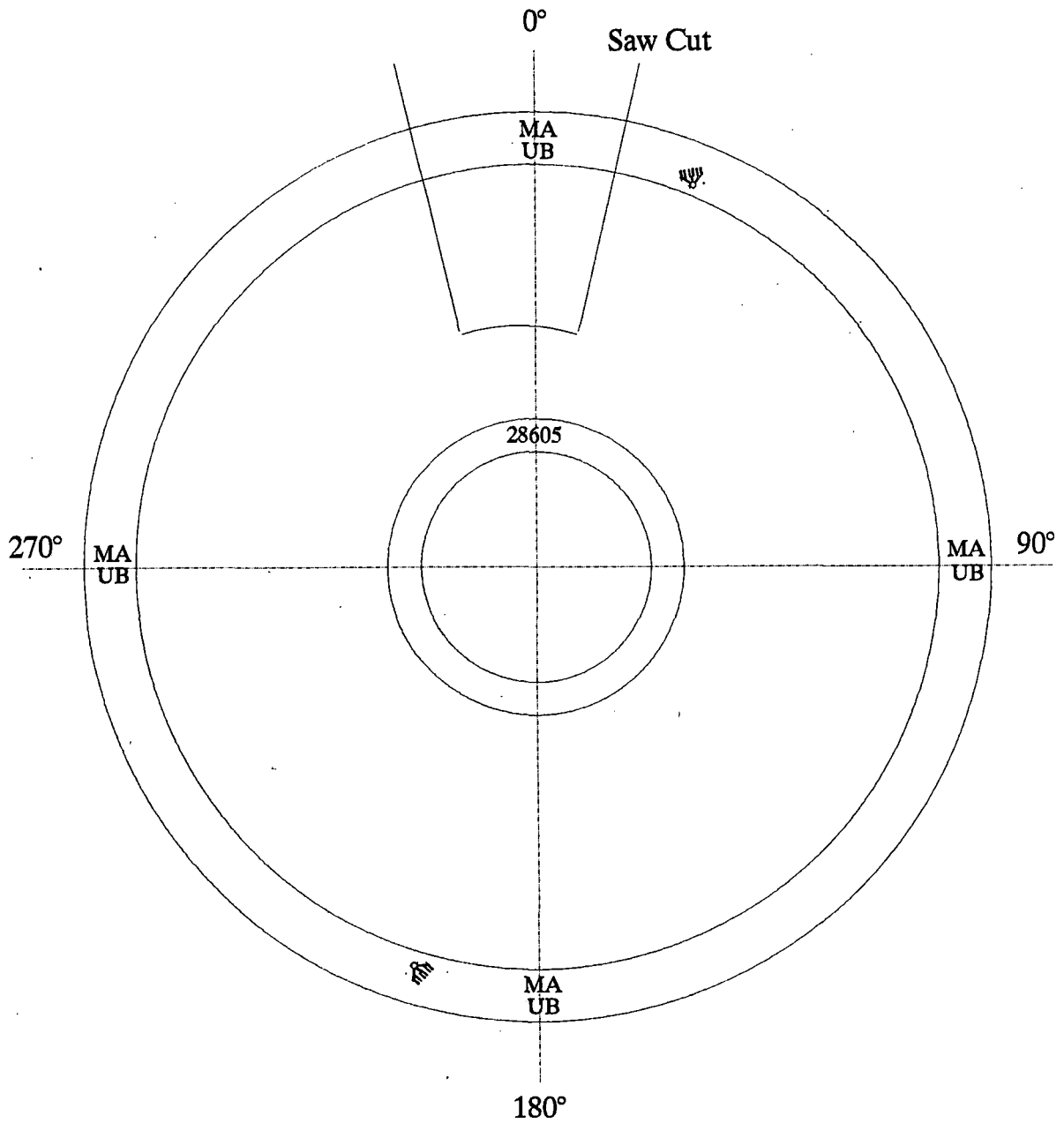
 = Hole Drilling MA = Magnetoacoustic UB = Acoustic Birefringence



Measurement Locations

Wheel 28605

 = Hole Drilling MA = Magnetoacoustic UB = Acoustic Birefringence



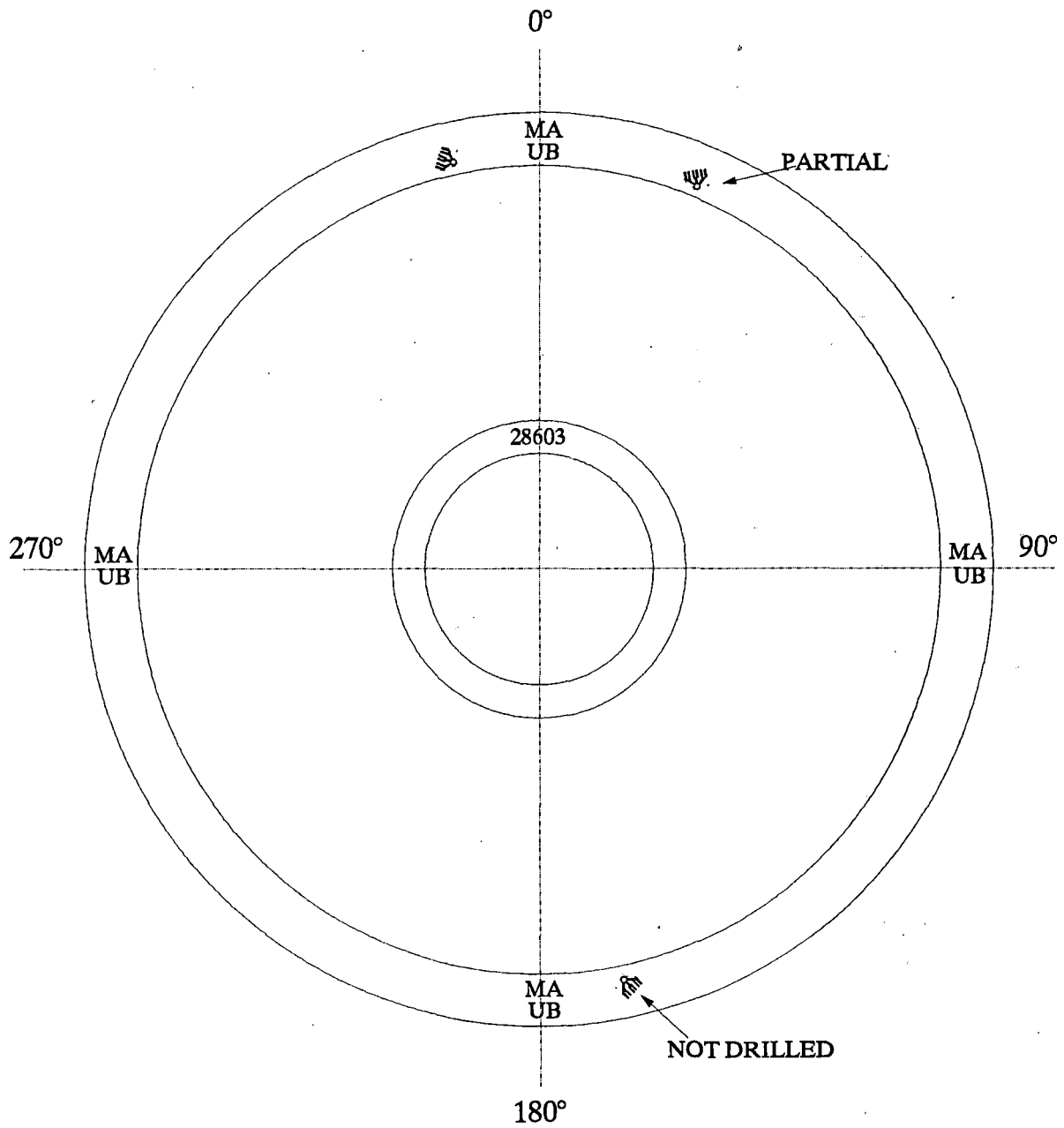
Measurement Locations

Wheel 28603

 = Hole Drilling
NO SAWCUT

MA = Magnetoacoustic

UB = Acoustic Birefringence



APPENDIX C

ACOUSTIC BIREFRINGENCE DATA

NIST Acoustic Birefringence Data

All measurements at 3/8 inch radial location

All times in (μ S)

Wheel 5556

	<i>Intact Wheel</i>		<i>Birefringence</i>	<i>Computed Stress (ksi)</i> <i>(Actual Bo value)</i>	<i>Computed Stress (ksi)</i> <i>(Constant Bo value)</i>
	<i>Circumferential</i>	<i>Radial</i>			
0°	95.4874	95.5511			
	<u>95.4898</u>	<u>95.5489</u>			
<i>average</i>	95.4886	95.5500	<i>B=</i> 6.43E-04	-4	-24
90°	95.5299	95.6016			
	<u>95.5276</u>	<u>95.6037</u>			
<i>average</i>	95.5288	95.6027	<i>B=</i> 7.73E-04	-7	-27
180°	95.5494	95.6218			
	<u>95.5488</u>	<u>95.6216</u>			
<i>average</i>	95.5491	95.6217	<i>B=</i> 7.60E-04	-6	-26
270°	95.5451	95.6117			
	<u>95.5453</u>	<u>95.6118</u>			
<i>average</i>	95.5452	95.6118	<i>B=</i> 6.96E-04	-5	-25
	<i>Rim Block</i>				
	<i>Circumferential</i>	<i>Radial</i>			
0°	96.8250	96.8660			
	<u>96.8270</u>	<u>96.8730</u>			
<i>average</i>	96.8260	96.8695	<i>Bo=</i> 4.49E-04		

NIST Acoustic Birefringence Data

All measurements at 3/8 inch radial location

All times in (μ S)

Wheel 49619

	<i>Intact Wheel</i>		<i>Birefringence</i>	<i>Computed Stress (ksi)</i> <i>(Actual Bo value)</i>	<i>Computed Stress (ksi)</i> <i>(Constant Bo value)</i>
	<i>Circumferential</i>	<i>Radial</i>			
0°	96.3920	96.1490			
	<u>96.3900</u>	<u>96.1440</u>			
<i>average</i>	96.3910	96.1465	$B = -2.54E-03$	86	42
90°	96.3910	96.1560			
	<u>96.3900</u>	<u>96.1560</u>			
<i>average</i>	96.3905	96.1560	$B = -2.44E-03$	84	40
180°	96.0060	95.7730			
	<u>96.0060</u>	<u>95.7770</u>			
<i>average</i>	96.0060	95.7750	$B = -2.41E-03$	83	40
270°	95.9800	96.1470			
	<u>95.9790</u>	<u>96.1500</u>			
<i>average</i>	95.9795	96.1485	$B = 1.76E-03$	-3	-47
	<i>Rim Block</i>				
	<i>Circumferential</i>	<i>Radial</i>			
0°	96.7590	96.9130			
	<u>96.7560</u>	<u>96.9110</u>			
<i>average</i>	96.7575	96.9120	$Bo = 1.60E-03$		

Acoustic Birefringence Data

All measurements at 3/8 inch radial location
All times in (μS)

Wheel 94575

	<i>Intact Wheel</i>		<i>Birefringence</i>	<i>Computed Stress (ksi)</i> <i>(Actual Bo value)</i>	<i>Computed Stress (ksi)</i> <i>(Constant Bo value)</i>
	<i>Circumferential</i>	<i>Radial</i>			
0°	93.7370	93.7760			
	<u>93.7390</u>	<u>93.7780</u>			
<i>average</i>	93.7380	93.7770	<i>B=</i> 4.16E-04	<i>N/A</i>	-19
90°	93.7450	93.7620			
	<u>93.7400</u>	<u>93.7590</u>			
<i>average</i>	93.7425	93.7605	<i>B=</i> 1.92E-04	<i>N/A</i>	-14
180°	94.0730	94.0200			
	<u>94.0620</u>	<u>94.0220</u>			
<i>average</i>	94.0675	94.0210	<i>B=</i> -4.94E-04	<i>N/A</i>	-0
270°	94.2410	94.2600			
	<u>94.2450</u>	<u>94.2600</u>			
<i>average</i>	94.2430	94.2600	<i>B=</i> 1.80E-04	<i>N/A</i>	-14
	<i>Rim Block</i>				
	<i>Circumferential</i>	<i>Radial</i>			
0°	0.0000	0.0000			
	0.0000	0.0000			
	0.0000	0.0000			
	<u>0.0000</u>	<u>0.0000</u>			
<i>average</i>	0.0000	0.0000	<i>Bo=</i> <i>N/A</i>		

NIST Acoustic Birefringence Data

All measurements at 3/8 inch radial location

All times in (μ S)

Wheel 49547

<i>Intact Wheel</i>			<i>Birefringence</i>	<i>Computed Stress (ksi)</i> <i>(Actual Bo value)</i>	<i>Computed Stress (ksi)</i> <i>(Constant Bo value)</i>
	<i>Circumferential</i>	<i>Radial</i>			
0°	95.1650	94.8900			
	<u>95.1800</u>	<u>94.8980</u>			
<i>average</i>	95.1725	94.8940	$B = -2.93E-03$	3	51
90°	94.9720	95.1790			
	<u>94.9800</u>	<u>95.1840</u>			
<i>average</i>	94.9760	95.1815	$B = 2.16E-03$	-103	-55
180°	94.9060	95.1290			
	<u>94.9160</u>	<u>95.1340</u>			
<i>average</i>	94.9110	95.1315	$B = 2.32E-03$	-106	-59
270°	95.1050	94.8430			
	<u>95.1110</u>	<u>94.8500</u>			
<i>average</i>	95.1080	94.8465	$B = -2.75E-03$	-1	47
<i>Rim Block</i>					
	<i>Circumferential</i>	<i>Radial</i>			
90°	95.4930	95.2300			
	<u>95.4900</u>	<u>95.2230</u>			
<i>average</i>	95.4915	95.2265	$Bo = -2.78E-03$		

NIST Acoustic Birefringence Data

All measurements at 3/8 inch radial location

All times in (μ S)

Wheel 49550

	<i>Intact Wheel</i>		<i>Birefringence</i>	<i>Computed Stress (ksi)</i> <i>(Actual Bo value)</i>	<i>Computed Stress (ksi)</i> <i>(Constant Bo value)</i>
	<i>Circumferential</i>	<i>Radial</i>			
0°	96.0190	96.2900			
<i>average</i>	96.0190	96.2900	<i>B=</i> 2.82E-03	-106	-69
90°	96.0820	96.3040			
<i>average</i>	96.0820	96.3040	<i>B=</i> 2.31E-03	-95	-58
180°	96.0400	96.2970			
<i>average</i>	96.0400	96.2970	<i>B=</i> 2.67E-03	-103	-66
270°	96.3840	96.1680			
<i>average</i>	96.3840	96.1680	<i>B=</i> -2.24E-03	-1	36
	<i>Rim Block</i>				
	<i>Circumferential</i>	<i>Radial</i>			
0°	96.5020	96.2810			
	<u>96.4980</u>	<u>96.2810</u>			
<i>average</i>	96.5000	96.2810	<i>Bo=</i> -2.27E-03		

NIST Acoustic Birefringence Data

All measurements at 3/8 inch radial location

All times in (μ S)

Wheel 43928

	<i>Intact Wheel</i>		<i>Birefringence</i>	<i>Computed Stress (ksi)</i> <i>(Actual Bo value)</i>	<i>Computed Stress (ksi)</i> <i>(Constant Bo value)</i>
	<i>Circumferential</i>	<i>Radial</i>			
0°	95.3140	95.4540			
	<u>95.3090</u>	<u>95.4510</u>			
<i>average</i>	95.3115	95.4525	$B = 1.48E-03$	-40	-41
90°	95.3250	95.5030			
	<u>95.3270</u>	<u>95.5150</u>			
<i>average</i>	95.3260	95.5090	$B = 1.92E-03$	-50	-50
180°	95.3920	95.3090			
	<u>95.3970</u>	<u>95.3330</u>			
<i>average</i>	95.3945	95.3210	$B = -7.71E-04$	6	6
270°	95.6370	95.7780			
	<u>95.6220</u>	<u>95.7710</u>			
<i>average</i>	95.6295	95.7745	$B = 1.52E-03$	-41	-42
	<i>Rim Block</i>				
	<i>Circumferential</i>	<i>Radial</i>			
0°	96.2150	96.1760			
	96.2120	96.1740			
	96.2170	96.1640			
	<u>96.2120</u>	<u>96.1630</u>			
<i>average</i>	96.2140	96.1693	$Bo = -4.65E-04$		

NIST Acoustic Birefringence Data

All measurements at 3/8 inch radial location

All times in (μ S)

Wheel 5576

	<i>Intact Wheel</i>		<i>Birefringence</i>	<i>Computed Stress (ksi)</i> <i>(Actual Bo value)</i>	<i>Computed Stress (ksi)</i> <i>(Constant Bo value)</i>
	<i>Circumferential</i>	<i>Radial</i>			
0°	95.0791	95.2203			
	95.0781	95.2203			
<i>average</i>	95.0786	95.2203	<i>B=</i> 1.49E-03	-18	-41
90°	95.1370	95.2543			
	95.1387	95.2555			
<i>average</i>	95.1379	95.2549	<i>B=</i> 1.23E-03	-12	-36
180°	95.0193	95.1427			
	95.0214	95.1453			
<i>average</i>	95.0204	95.1440	<i>B=</i> 1.30E-03	-14	-38
270°	94.9376	95.0264			
	94.9388	95.0290			
<i>average</i>	94.9382	95.0277	<i>B=</i> 9.42E-04	-6	-30
	<i>Rim Block</i>				
	<i>Circumferential</i>	<i>Radial</i>			
0°	95.0200	95.0750			
	95.0150	95.0760			
	95.018	95.08			
	95.0130	95.0760			
<i>average</i>	95.0165	95.0768	<i>Bo=</i> 6.34E-04		

NIST Acoustic Birefringence Data

All measurements at 3/8 inch radial location

All times in (μ S)

Wheel 5584

<i>Intact Wheel</i>			<i>Birefringence</i>	<i>Computed Stress (ksi)</i> <i>(Actual Bo value)</i>	<i>Computed Stress (ksi)</i> <i>(Constant Bo value)</i>
	<i>Circumferential</i>	<i>Radial</i>			
0°	95.0670	95.0490	$B = -2.16E-04$	14	-6
	95.0610	95.0380			
<i>average</i>	95.0640	95.0435			
90°	94.7010	94.6970	$B = -1.06E-04$	12	-8
	94.6980	94.6820			
<i>average</i>	94.6995	94.6895			
180°	94.6520	94.6590	$B = 1.32E-04$	7	-13
	94.6430	94.6610			
<i>average</i>	94.6475	94.6600			
270°	95.0750	95.0590	$B = -3.68E-05$	10	-10
	95.0630	95.0720			
<i>average</i>	95.0690	95.0655			
<i>Rim Block</i>					
	<i>Circumferential</i>	<i>Radial</i>			
0°	<i>time(t)</i>	<i>time(r)</i>			
	95.2410	95.2890			
	95.2390	95.2830			
	95.2290	95.2770			
	95.2370	95.2740			
<i>average</i>	95.2365	95.2808	$Bo = 4.65E-04$		

NIST Acoustic Birefringence Data

All measurements at 3/8 inch radial location

All times in (μ S)

95554 – Wheel #1

	<i>Intact Wheel</i>		<i>Birefringence</i>		<i>Computed Stress (ksi)</i>	<i>Computed Stress (ksi)</i>
	<i>Circumferential</i>	<i>Radial</i>			<i>(Actual Bo value)</i>	<i>(Constant Bo value)</i>
0°	N/A	N/A	B=	N/A	N/A	N/A
90°	N/A	N/A	B=	N/A	N/A	N/A
180°	N/A	N/A	B=	N/A	N/A	N/A
270°	N/A	N/A	B=	N/A	N/A	N/A
<i>Rim Block</i>						
	<i>Circumferential</i>	<i>Radial</i>				
0°	93.7237	93.7749				
	<u>93.7262</u>	<u>93.7739</u>				
average	93.7250	93.7744	Bo=	5.3E-04		
	93.6527	93.7041				
	<u>93.6505</u>	<u>93.7062</u>				
	93.6516	93.7052	Bo=	5.7E-04		
	93.7021	93.7356				
	<u>93.7025</u>	<u>93.7351</u>				
	93.7023	93.7354	Bo=	3.5E-04		
	93.9220	93.9664				
	<u>93.9233</u>	<u>93.9665</u>				
	93.9227	93.9665	Bo=	4.7E-04		

NIST Acoustic Birefringence Data

All measurements at 3/8 inch radial location

All times in (μS)

95551 – Wheel #2

	<i>Intact Wheel</i>		<i>Birefringence</i>	<i>Computed Stress (ksi)</i> <i>(Actual Bo value)</i>	<i>Computed Stress (ksi)</i> <i>(Constant Bo value)</i>
	<i>Circumferential</i>	<i>Radial</i>			
0°	93.6450	93.6430			
	<u>93.6450</u>	<u>93.6420</u>			
<i>average</i>	93.6450	93.6425	<i>B=</i> -2.67E-05	10	-10
90°	93.7200	93.7070			
	<u>93.7220</u>	<u>93.7170</u>			
<i>average</i>	93.7210	93.7120	<i>B=</i> -9.60E-05	11	-8
180°	93.7520	93.7600			
	<u>93.7590</u>	<u>93.7690</u>			
<i>average</i>	93.7555	93.7645	<i>B=</i> 9.60E-05	7	-12
270°	93.7830	93.7510			
	<u>93.7780</u>	<u>93.7430</u>			
<i>average</i>	93.7805	93.7470	<i>B=</i> -3.57E-04	16	-3
<i>Rim Block</i>					
	<i>Circumferential</i>	<i>Radial</i>			
0°	94.5910	94.6330			
	94.5920	94.6330			
	94.5900	94.6310			
	<u>94.5920</u>	<u>94.6320</u>			
<i>average</i>	94.5913	94.6323	<i>Bo=</i> 4.33E-04		

NIST Acoustic Birefringence Data

All measurements at 3/8 inch radial location

All times in (μ S)

94559 – Wheel #5

	<i>Intact Wheel</i>		<i>Birefringence</i>		<i>Computed Stress (ksi)</i>	<i>Computed Stress (ksi)</i>
	<i>Circumferential</i>	<i>Radial</i>	<i>B=</i>		<i>(Actual Bo value)</i>	<i>(Constant Bo value)</i>
0°	N/A	N/A	B=	N/A	N/A	N/A
90°	N/A	N/A	B=	N/A	N/A	N/A
180°	N/A	N/A	B=	N/A	N/A	N/A
270°	N/A	N/A	B=	N/A	N/A	N/A
<i>Rim Block</i>						
	<i>Circumferential</i>	<i>Radial</i>				
0°	93.1893	93.2429				
	93.1884	93.2441				
<i>average</i>	93.1889	93.2435	<i>Bo=</i>	5.9E-04		
90°	93.6836	93.6145				
	93.6845	93.6156				
<i>average</i>	93.6841	93.6151	<i>Bo=</i>	-7.4E-04		
180°	93.2268	93.3249				
	93.2243	93.3229				
<i>average</i>	93.2256	93.3239	<i>Bo=</i>	1.1E-03		
270°	93.1272	93.1699				
	93.1243	93.1681				
<i>average</i>	93.1258	93.1690	<i>Bo=</i>	4.6E-04		

NIST Acoustic Birefringence Data

All measurements at 3/8 inch radial location

All times in (μ S)

94550 - W6

	<i>Intact Wheel</i>		<i>Birefringence</i>	<i>Computed Stress (ksi)</i> <i>(Actual Bo value)</i>	<i>Computed Stress (ksi)</i> <i>(Constant Bo value)</i>
	<i>Circumferential</i>	<i>Radial</i>			
0°	94.5660	94.5880			
	<u>94.5650</u>	<u>94.5840</u>			
average	94.5655	94.5860	$B = 2.17E-04$	8	-15
90°	N/A	N/A	$B = N/A$	N/A	N/A
180°	N/A	N/A	$B = N/A$	N/A	N/A
270°	N/A	N/A	$B = N/A$	N/A	N/A
<i>Rim Block</i>					
	<i>Circumferential</i>	<i>Radial</i>			
0°	93.7879	93.8498			
	93.7805	93.8268			
	93.7862	93.8465			
	<u>93.7876</u>	<u>93.8409</u>			
average	93.7856	93.8410	$Bo = 5.91E-04$		
90°	93.7369	93.6899			
	93.7377	93.6911			
	93.7405	93.7126			
	<u>93.7422</u>	<u>93.7081</u>			
average	93.7393	93.7004	$Bo = -4.15E-04$		
180°	93.7626	93.8199			
	<u>93.7604</u>	<u>93.8198</u>			
average	93.7615	93.8199	$Bo = 6.22E-04$		

270°

NIST Acoustic Birefringence Data

All measurements at 3/8 inch radial location

All times in (μ S)

94565 – W7

0°	N/A	N/A	B=	N/A	N/A	N/A
90°	N/A	N/A	B=	N/A	N/A	N/A
180°	N/A	N/A	B=	N/A	N/A	N/A
270°	N/A	N/A	B=	N/A	N/A	N/A

Rim Block

	<i>Circumferential</i>	<i>Radial</i>		
0°	93.3146	93.3266		
	<u>93.3111</u>	<u>93.3256</u>		
average	93.3129	93.3261	Bo=	1.42E-04
90°	93.2325	93.3004		
	<u>93.2317</u>	<u>93.3008</u>		
average	93.2321	93.3006	Bo=	7.34E-04
180°	94.1656	94.1930		
	<u>94.1674</u>	<u>94.1922</u>		
average	94.1665	94.1926	Bo=	2.77E-04
270°	94.2958	94.2645		
	<u>94.2967</u>	<u>94.2638</u>		
average	94.2963	94.2642	Bo=	-3.40E-04

NIST Acoustic Birefringence Data

All measurements at 3/8 inch radial location

All times in (μ S)

Wheel 28609

<i>Intact Wheel</i>			<i>Birefringence</i>
	<i>Circumferential</i>	<i>Radial</i>	
0°	96.5450	96.6650	
	<u>96.5490</u>	<u>96.6640</u>	
average	96.5470	96.6645	$B = 1.22E-03$
90°	96.4440	96.5500	
	96.4450	96.5510	
	<u>96.4400</u>	<u>96.5540</u>	
average	96.4430	96.5517	$B = 1.13E-03$
180°	96.6400	96.7390	
	96.6430	96.7410	
	<u>96.6370</u>	<u>96.7370</u>	
average	96.6400	96.7390	$B = 1.02E-03$
270°	96.5730	96.6800	
	96.5750	96.6830	
	<u>96.5680</u>	<u>96.6780</u>	
average	96.5720	96.6803	$B = 1.12E-03$
<i>Rim Block</i>			
	<i>Circumferential</i>	<i>Radial</i>	
0°	96.4950	96.6110	
	96.4760	96.6070	
	96.4790	96.6050	
	96.4830	96.6040	
	<u>96.4850</u>	<u>96.6050</u>	
average	96.4836	96.6064	$B_0 = 1.27E-03$

Computed Stress (ksi)
(Actual Bo value)

Computed Stress (ksi)
(Constant Bo value)

1 -36

3 -34

5 -32

3 -34

NIST Acoustic Birefringence Data

All measurements at 3/8 inch radial location

All times in (μ S)

Wheel 28605

<i>Intact Wheel</i>			<i>Birefringence</i>
	<i>Circumferential</i>	<i>Radial</i>	
0°	96.0750	96.1670	
	96.0740	96.1640	
<i>average</i>	<u>96.0720</u>	<u>96.1670</u>	<i>B=</i> 9.61E-04
	96.0737	96.1660	
90°	96.0270	96.1260	
	96.0300	96.1340	
<i>average</i>	<u>96.0270</u>	<u>96.1280</u>	<i>B=</i> 1.05E-03
	96.0280	96.1293	
180°	96.0470	96.1350	
	96.0480	96.1370	
<i>average</i>	<u>96.0480</u>	<u>96.1350</u>	<i>B=</i> 9.16E-04
	96.0477	96.1357	
270°	96.0340	96.1380	
	96.0340	96.1400	
<i>average</i>	<u>96.0310</u>	<u>96.1360</u>	<i>B=</i> 1.09E-03
	96.0330	96.1380	
<i>Rim Block</i>			
	<i>Circumferential</i>	<i>Radial</i>	
0°	96.5490	96.6620	
	96.5500	96.6590	
	96.5430	96.6600	
	96.5460	96.6630	
	96.5440	96.6630	
<i>average</i>	<u>96.5490</u>	<u>96.6630</u>	<i>Bo=</i> 1.19E-03
	96.5468	96.6617	

Computed Stress (ksi) **Computed Stress (ksi)**
(Actual Bo value) *(Constant Bo value)*

5 -30

3 -32

6 -29

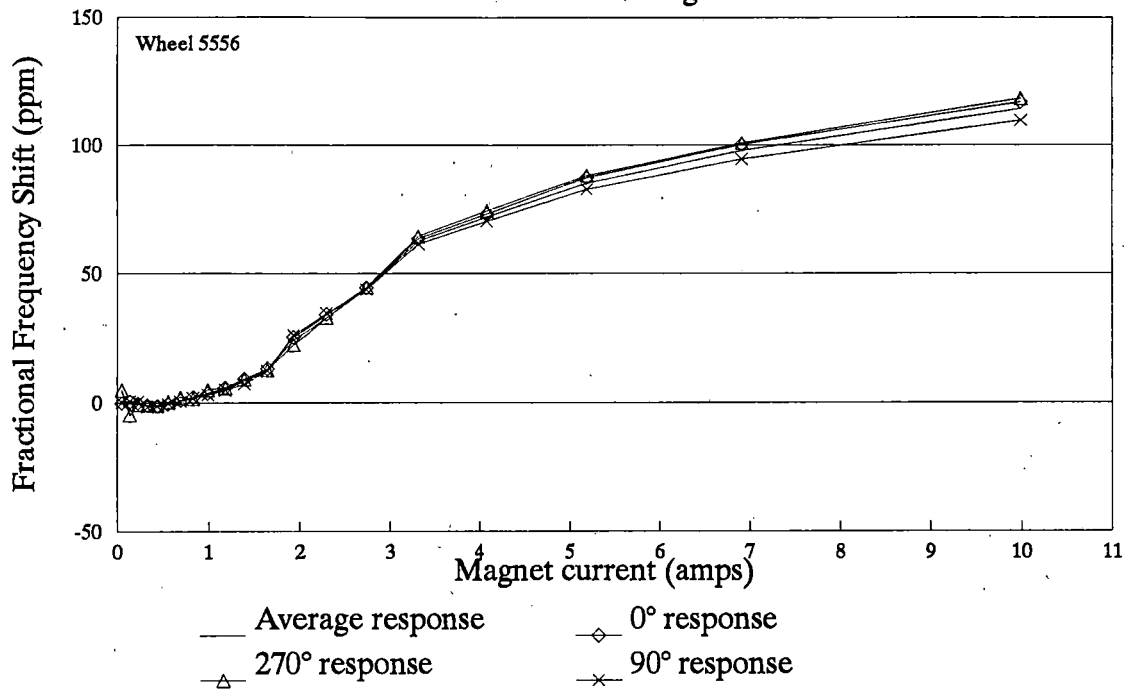
2 -33

APPENDIX D

MAGNETOACOUSTIC DATA

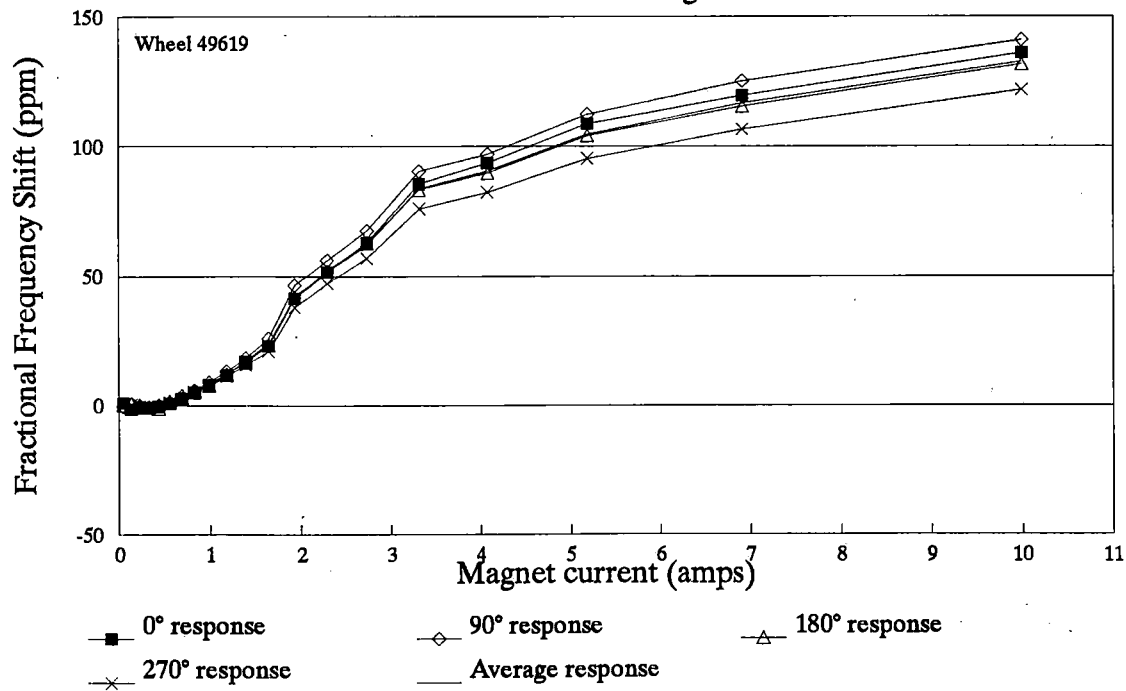
Magneto-Acoustic Data

5MHz Shear/Tangential



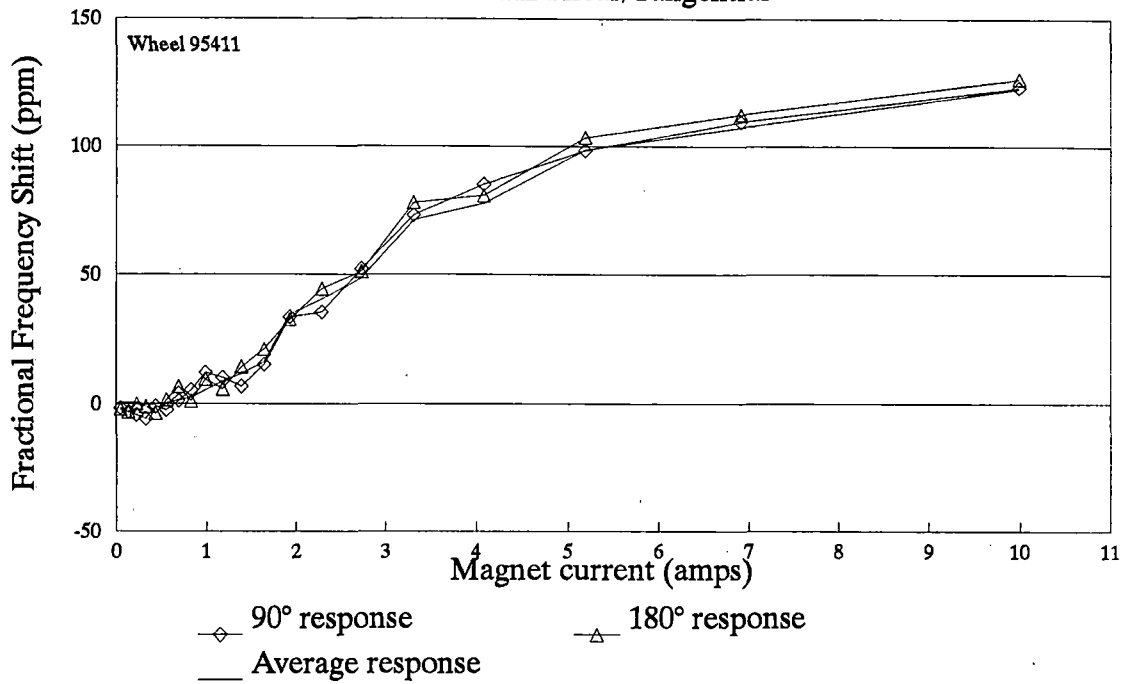
Magneto-Acoustic Data

5MHz Shear/Tangential



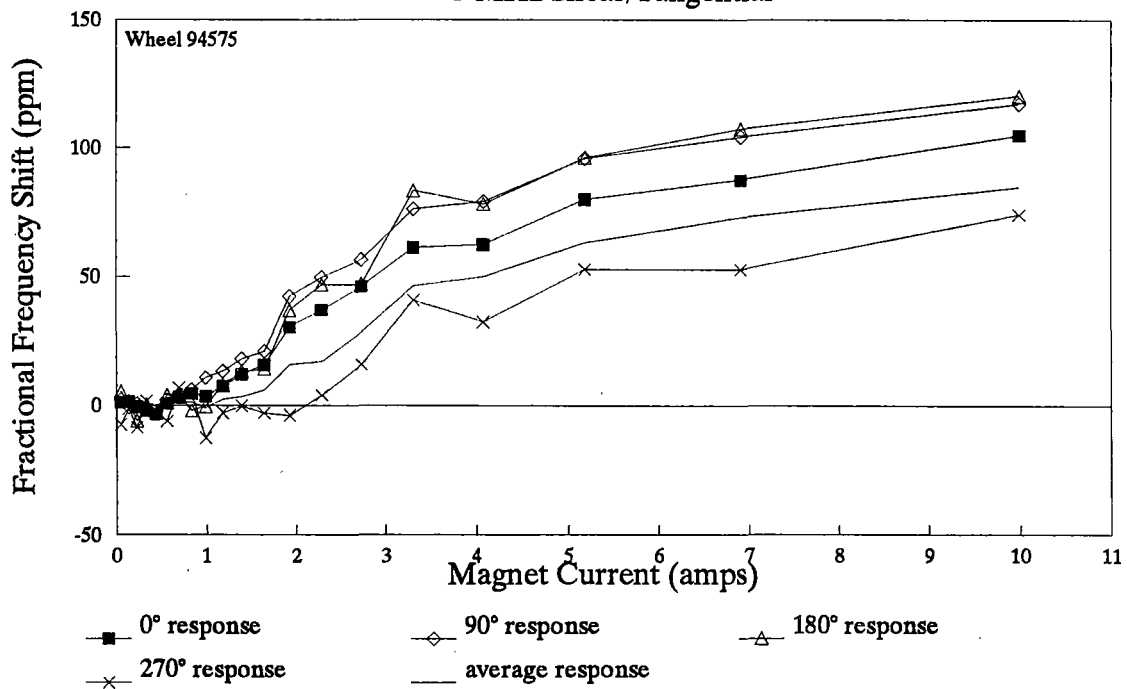
Magneto-Acoustic Data

5MHz Shear/Tangential



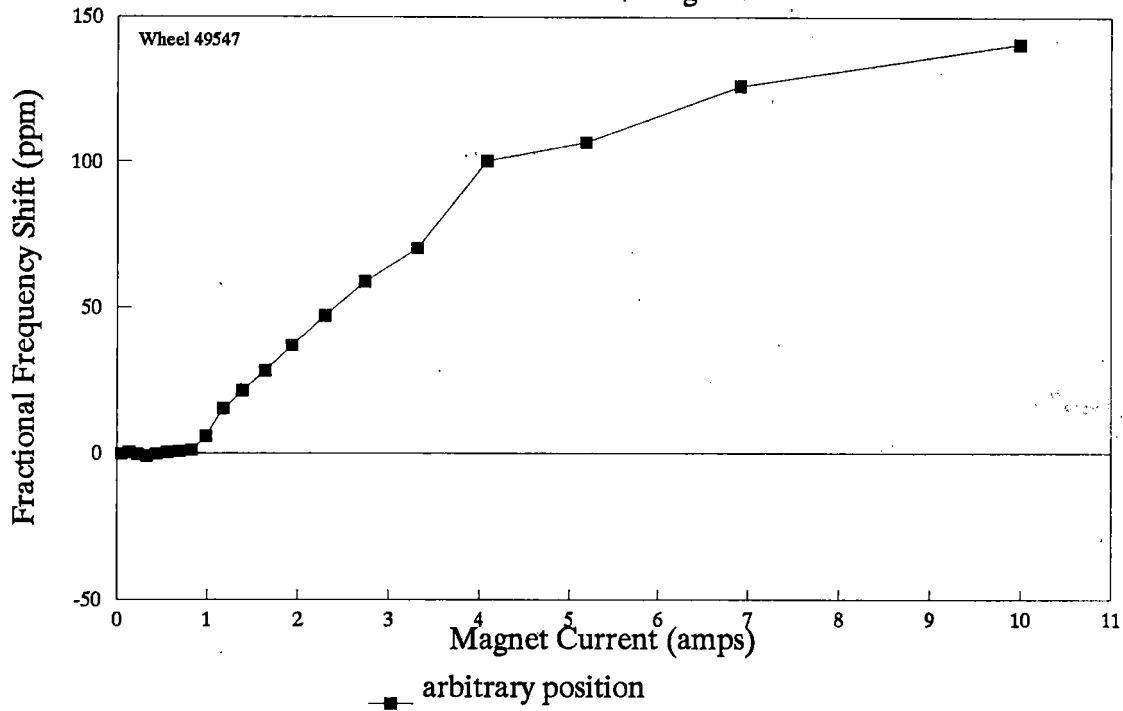
Magneto-Acoustic Data

5 MHz Shear/Tangential



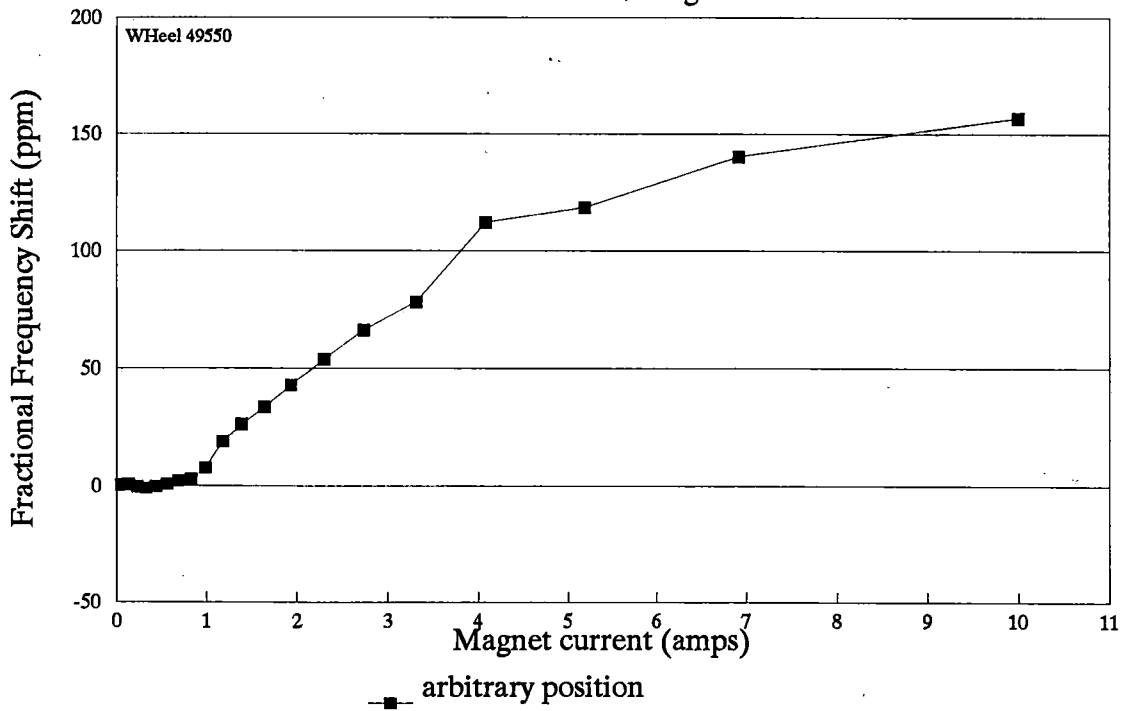
Magneto-Acoustic Data

5MHz Shear/Tangential



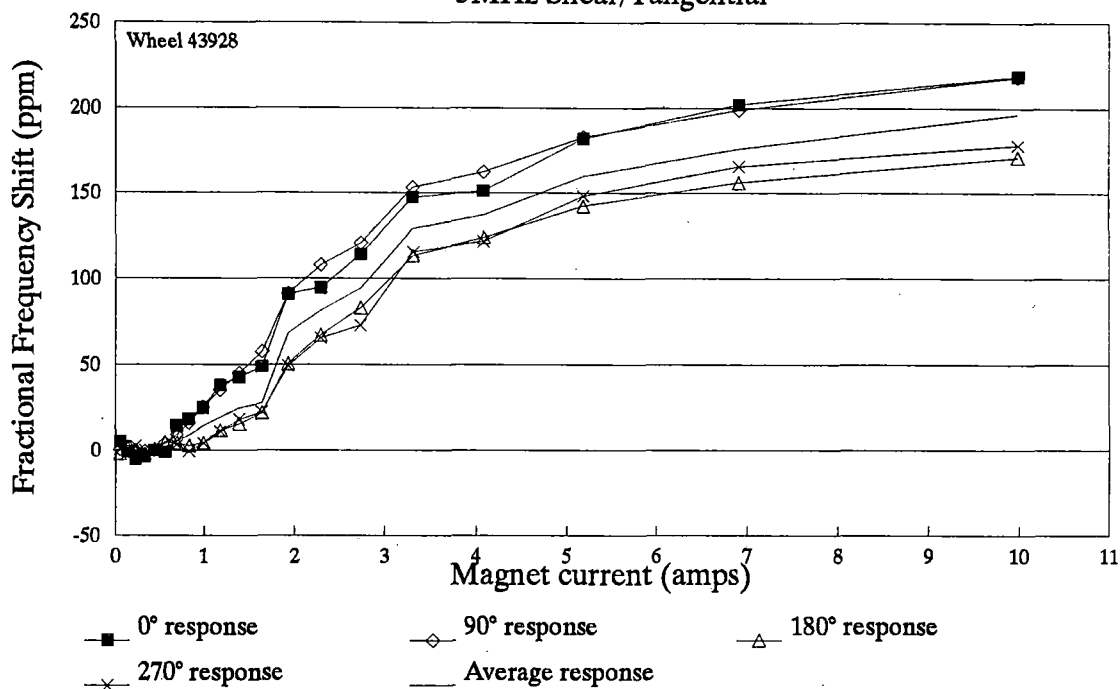
Magneto-Acoustic Data

5 MHz Shear/Tangential



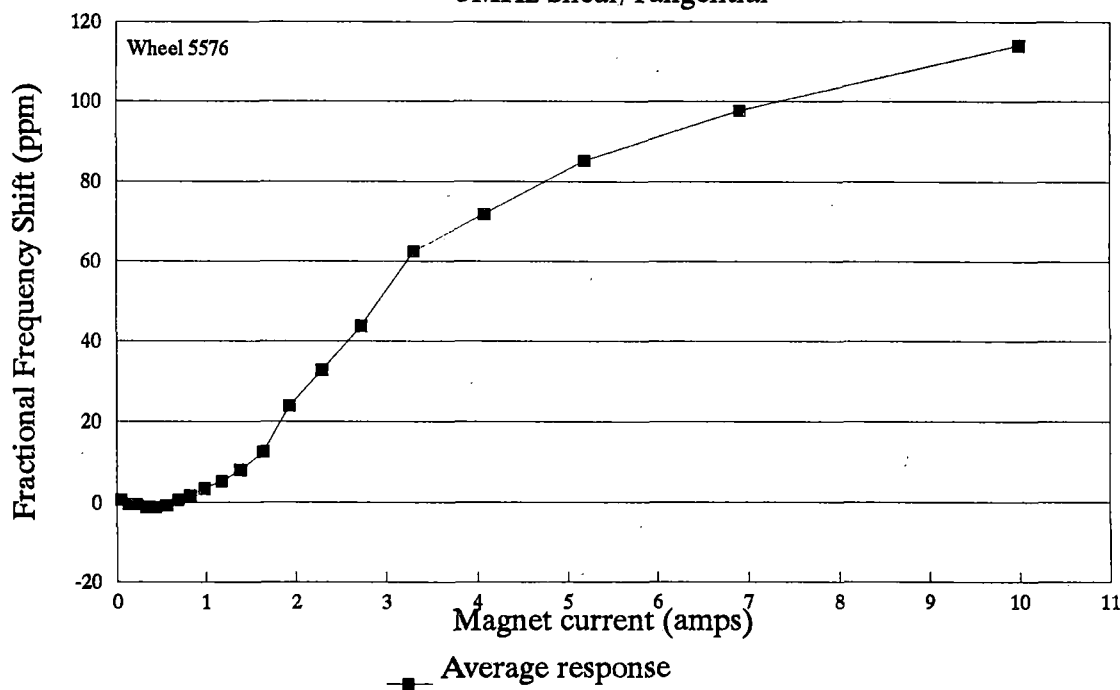
Magneto-Acoustic Data

5MHz Shear/Tangential



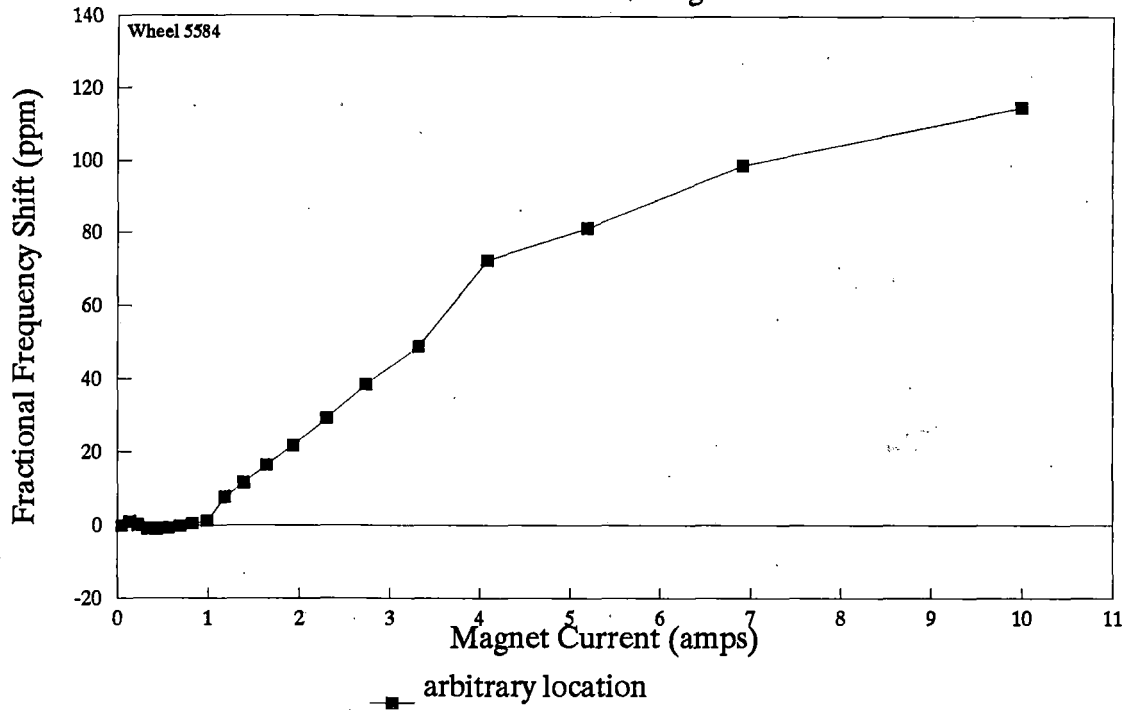
Magneto-Acoustic Data

5MHz Shear/Tangential



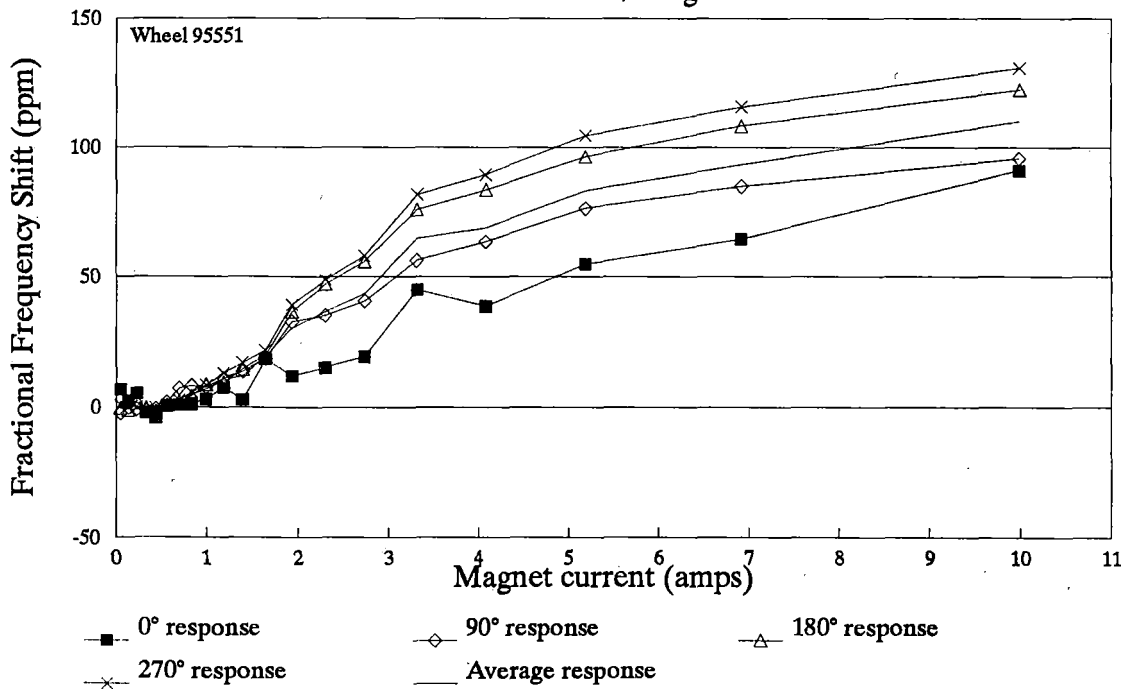
Magneto-Acoustic Data

5 MHz Shear/Tangential



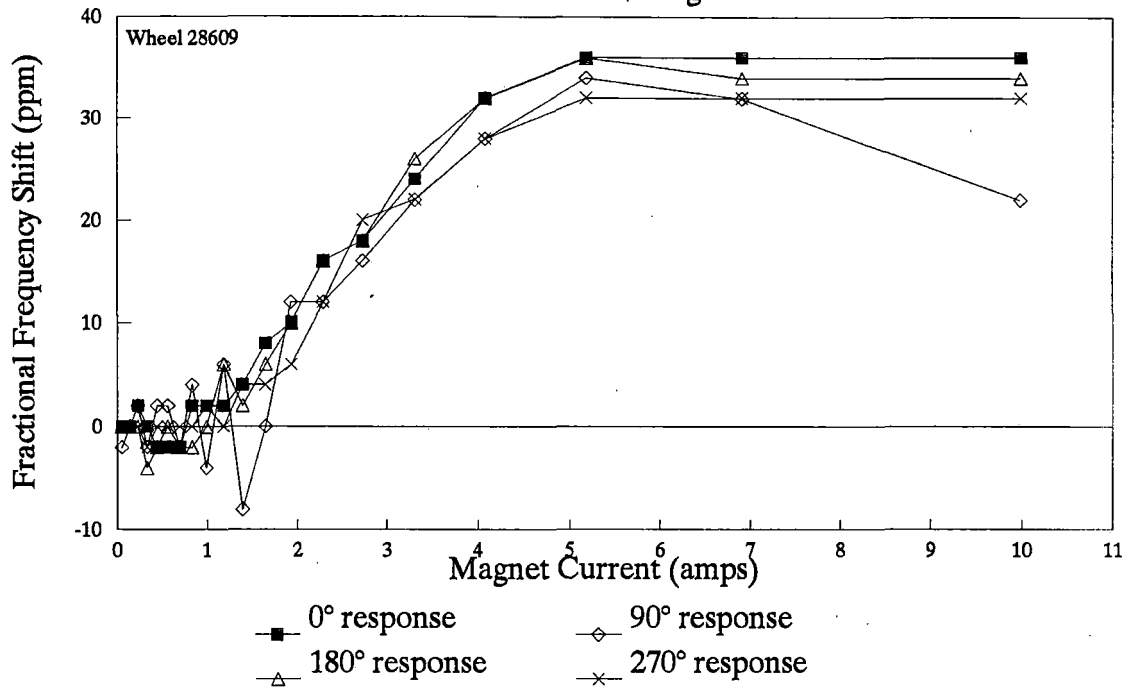
Magneto-Acoustic Data

5MHz Shear/Tangential



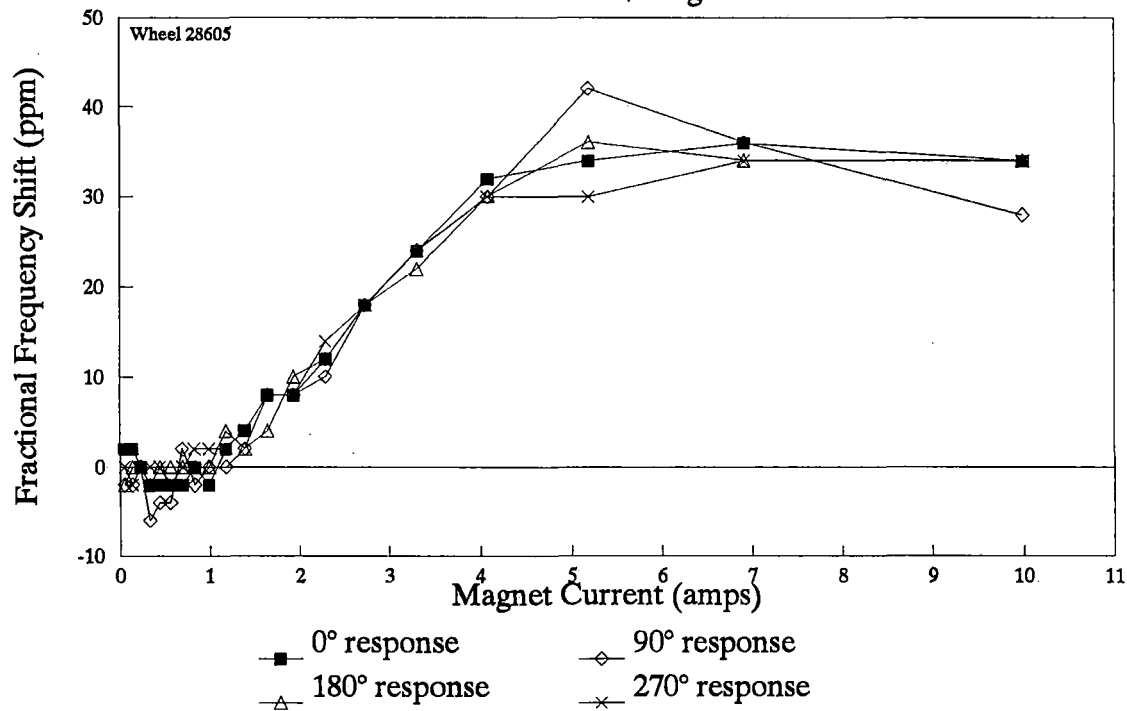
Magneto-Acoustic Data

5 MHz Shear/Tangential



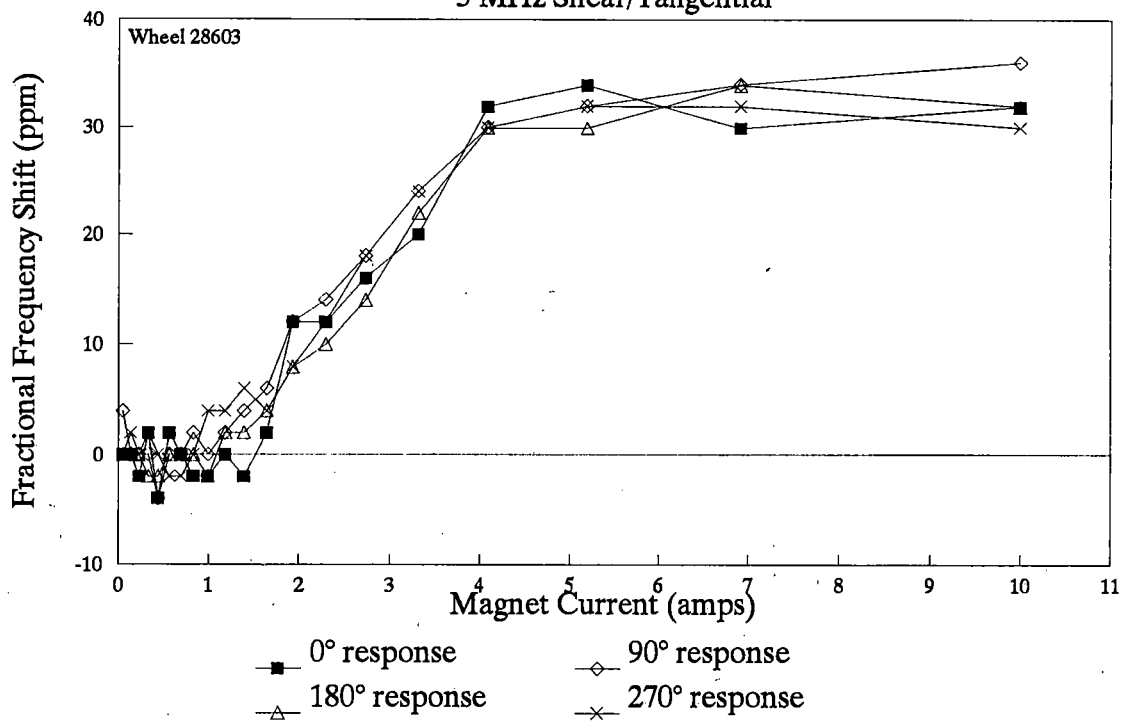
Magneto-Acoustic Data

5 MHz Shear/Tangential



Magneto-Acoustic Data

5 MHz Shear/Tangential



APPENDIX E

HOLE-DRILLING STRAIN-GAGE DATA

MEASUREMENTS GROUP RS-200 DATA FORM

WHEEL # 5550
12/12/15/19

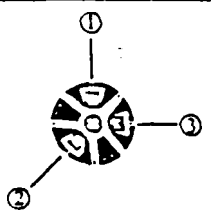
DEPTH		MEASURED STRAIN $\mu\epsilon$		PERCENT STRAIN RELIEVED	COEFFICIENTS Exponent of $(10)^{-4}$ with \bar{A} and \bar{B}		α	Equiv. Uniform Stress to Depth Z (1000 psi).	
Z (in)	Z/D ₀	ϵ_1	ϵ_2		\bar{a}	\bar{b}		σ_{min}	σ_{max}
0.010		ϵ_1	+94		\bar{a}	\bar{b}			
		ϵ_2	+109		\bar{A}	\bar{B}			
		ϵ_3	+104		$4\bar{A}$	$4\bar{B}$			
0.020		ϵ_1	+207		\bar{a}	\bar{b}			
		ϵ_2	+230		\bar{A}	\bar{B}			
		ϵ_3	+209		$4\bar{A}$	$4\bar{B}$			
0.030		ϵ_1	+288		\bar{a}	\bar{b}			
		ϵ_2	+326		\bar{A}	\bar{B}			
		ϵ_3	+284		$4\bar{A}$	$4\bar{B}$			
0.040		ϵ_1	+314		\bar{a}	\bar{b}			
		ϵ_2	+362		\bar{A}	\bar{B}			
		ϵ_3	+313		$4\bar{A}$	$4\bar{B}$			
0.050		ϵ_1	+326		\bar{a}	\bar{b}			
		ϵ_2	+380		\bar{A}	\bar{B}			
		ϵ_3	+326		$4\bar{A}$	$4\bar{B}$			
0.060		ϵ_1	+329		\bar{a}	\bar{b}			
		ϵ_2	+385		\bar{A}	\bar{B}			
		ϵ_3	+332		$4\bar{A}$	$4\bar{B}$			
0.070		ϵ_1	+330		\bar{a}	\bar{b}			
		ϵ_2	+387		\bar{A}	\bar{B}			
		ϵ_3	+335		$4\bar{A}$	$4\bar{B}$			
0.080		ϵ_1	+301		\bar{a}	\bar{b}			
		ϵ_2	+360		\bar{A}	\bar{B}			
		ϵ_3	+303		$4\bar{A}$	$4\bar{B}$			
0.090		ϵ_1	+299		\bar{a}	\bar{b}			
		ϵ_2	+354		\bar{A}	\bar{B}			
		ϵ_3	+308		$4\bar{A}$	$4\bar{B}$			
0.100		ϵ_1	+299		\bar{a}	\bar{b}			
		ϵ_2	+354		\bar{A}	\bar{B}			
		ϵ_3	+308		$4\bar{A}$	$4\bar{B}$			
1	2	3		4	5	6	7	8	9

12
13

changed bit.

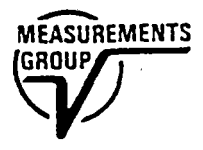
rotation bit changed

changed bit



$D_0 = \text{_____} \quad E = \text{_____} \quad \frac{1}{2E} = \text{_____} (10)^{-4}$
 $D/D_0 = \text{_____} \quad \nu = \text{_____}$
 $\frac{1+\nu}{2E} = \text{_____} (10)^{-4}$

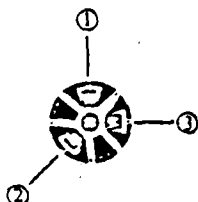
Material: _____



MEASUREMENTS GROUP RS-200 DATA FORM WHLZLZ 49619

DEPTH		MEASURED STRAIN $\mu\epsilon$		PERCENT STRAIN RELIEVED	COEFFICIENTS Exponent of $(10)^{-3}$ with \bar{A} and \bar{B}		α	Equiv. Uniform Stress to Depth Z (1000 psi)	
Z (in)	Z/D ₀	ϵ_1	ϵ_2		\bar{a}	\bar{b}		σ_{min}	σ_{max}
0.010		ϵ_1	+102		\bar{a}	\bar{b}			
		ϵ_2	+111		\bar{A}	\bar{B}			
		ϵ_3	+103		$4\bar{A}$	$4\bar{B}$			
0.020		ϵ_1	+192		\bar{a}	\bar{b}			
		ϵ_2	+202		\bar{A}	\bar{B}			
		ϵ_3	+206		$4\bar{A}$	$4\bar{B}$			
0.030		ϵ_1	+213		\bar{a}	\bar{b}			
		ϵ_2	+231		\bar{A}	\bar{B}			
		ϵ_3	+257		$4\bar{A}$	$4\bar{B}$			
0.040		ϵ_1	+221		\bar{a}	\bar{b}			
		ϵ_2	+250		\bar{A}	\bar{B}			
		ϵ_3	+289		$4\bar{A}$	$4\bar{B}$			
0.050		ϵ_1	+224		\bar{a}	\bar{b}			
		ϵ_2	+259		\bar{A}	\bar{B}			
		ϵ_3	+307		$4\bar{A}$	$4\bar{B}$			
0.060		ϵ_1	+223		\bar{a}	\bar{b}			
		ϵ_2	+262		\bar{A}	\bar{B}			
		ϵ_3	+315		$4\bar{A}$	$4\bar{B}$			
0.070		ϵ_1	+212		\bar{a}	\bar{b}			
		ϵ_2	+254		\bar{A}	\bar{B}			
		ϵ_3	+308		$4\bar{A}$	$4\bar{B}$			
0.080		ϵ_1	+210		\bar{a}	\bar{b}			
		ϵ_2	+254		\bar{A}	\bar{B}			
		ϵ_3	+309		$4\bar{A}$	$4\bar{B}$			
0.090		ϵ_1	+209		\bar{a}	\bar{b}			
		ϵ_2	+253		\bar{A}	\bar{B}			
		ϵ_3	+309		$4\bar{A}$	$4\bar{B}$			
0.100		ϵ_1	+204		\bar{a}	\bar{b}			
		ϵ_2	+252		\bar{A}	\bar{B}			
		ϵ_3	+308		$4\bar{A}$	$4\bar{B}$			
1	2	3		4	5	6	7	8	9

changed bit



$D_0 = \text{_____} \quad E = \text{_____} \quad \frac{1}{2E} = \text{_____} (10)^{-4}$
 $D/D_0 = \text{_____} \quad \nu = \text{_____}$
 $\frac{1+\nu}{2E} = \text{_____} (10)^{-4} \quad \text{Material: _____}$

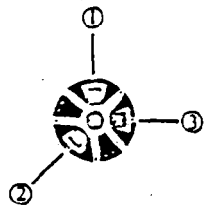


MEASUREMENTS GROUP RS-200 DATA FORM

W. MIT 0.1011
WHEEL #4434
12/12/90

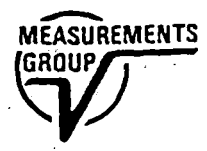
Ji

DEPTH		MEASURED STRAIN		PERCENT STRAIN RELIEVED	COEFFICIENTS			α	Equiv. Uniform Stress to Depth Z (1000 psi).	
Z (in)	Z/D ₀	$\mu\epsilon$			Exponent of (10) ⁻⁴ with \bar{A} and \bar{B}				σ_{min}	σ_{max}
0.010		ϵ_1	+114		\bar{a}	\bar{b}				
		ϵ_2	+99		\bar{A}	\bar{B}				
		ϵ_3	+67		$4\bar{A}$	$4\bar{B}$				
0.020		ϵ_1	+247		\bar{a}	\bar{b}				
		ϵ_2	+226		\bar{A}	\bar{B}				
		ϵ_3	+160		$4\bar{A}$	$4\bar{B}$				
0.030		ϵ_1	+301		\bar{a}	\bar{b}				
		ϵ_2	+280		\bar{A}	\bar{B}				
		ϵ_3	+199		$4\bar{A}$	$4\bar{B}$				
0.040		ϵ_1	+311		\bar{a}	\bar{b}				
		ϵ_2	+304		\bar{A}	\bar{B}				
		ϵ_3	+218		$4\bar{A}$	$4\bar{B}$				
0.050		ϵ_1	+324		\bar{a}	\bar{b}				
		ϵ_2	+314		\bar{A}	\bar{B}				
		ϵ_3	+227		$4\bar{A}$	$4\bar{B}$				
0.060		ϵ_1	+326		\bar{a}	\bar{b}				
		ϵ_2	+319		\bar{A}	\bar{B}				
		ϵ_3	+232		$4\bar{A}$	$4\bar{B}$				
0.070		ϵ_1	+327		\bar{a}	\bar{b}				
		ϵ_2	+322		\bar{A}	\bar{B}				
		ϵ_3	+235		$4\bar{A}$	$4\bar{B}$				
0.080		ϵ_1	+327		\bar{a}	\bar{b}				
		ϵ_2	+323		\bar{A}	\bar{B}				
		ϵ_3	+236		$4\bar{A}$	$4\bar{B}$				
0.090		ϵ_1	+327		\bar{a}	\bar{b}				
		ϵ_2	+323		\bar{A}	\bar{B}				
		ϵ_3	+236		$4\bar{A}$	$4\bar{B}$				
0.100		ϵ_1	+326		\bar{a}	\bar{b}				
		ϵ_2	+323		\bar{A}	\bar{B}				
		ϵ_3	+236		$4\bar{A}$	$4\bar{B}$				
1	2	3		4	5		6	7	8	9



$D_0 = \text{_____} E = \text{_____} \frac{1}{2E} = \text{_____} (10)^{-8}$
 $D/D_0 = \text{_____} \nu = \text{_____}$
 $\frac{1+\nu}{2E} = \text{_____} (10)^{-8}$

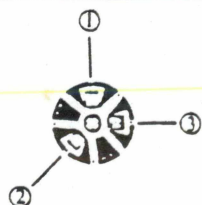
Material: _____



MEASUREMENTS GROUP RS-200 DATA FORM

W-5547955
12/10/20

DEPTH		MEASURED STRAIN		PERCENT STRAIN RELIEVED	COEFFICIENTS			α	Equiv. Uniform Stress to Depth Z (1000 psi).	
Z (in)	Z/D ₀	$\mu\epsilon$	$\mu\epsilon$		Exponent of (10) ⁻⁴ with \bar{A} and \bar{B}				σ_{min}	σ_{max}
0.010		ϵ_1	+97		\bar{a}	\bar{b}				
		ϵ_2	+70		\bar{A}	\bar{B}				
		ϵ_3	+35		$4\bar{A}$	$4\bar{B}$				
0.020		ϵ_1	+159		\bar{a}	\bar{b}				
		ϵ_2	+139		\bar{A}	\bar{B}				
		ϵ_3	+89		$4\bar{A}$	$4\bar{B}$				
0.030		ϵ_1	+248		\bar{a}	\bar{b}				
		ϵ_2	+176		\bar{A}	\bar{B}				
		ϵ_3	+106		$4\bar{A}$	$4\bar{B}$				
0.040		ϵ_1	+253		\bar{a}	\bar{b}				
		ϵ_2	+162		\bar{A}	\bar{B}				
		ϵ_3	+89		$4\bar{A}$	$4\bar{B}$				
0.050		ϵ_1	+267		\bar{a}	\bar{b}				
		ϵ_2	+178		\bar{A}	\bar{B}				
		ϵ_3	+107		$4\bar{A}$	$4\bar{B}$				
0.060		ϵ_1	+269		\bar{a}	\bar{b}				
		ϵ_2	+182		\bar{A}	\bar{B}				
		ϵ_3	+115		$4\bar{A}$	$4\bar{B}$				
0.070		ϵ_1	+269		\bar{a}	\bar{b}				
		ϵ_2	+184		\bar{A}	\bar{B}				
		ϵ_3	+119		$4\bar{A}$	$4\bar{B}$				
0.080		ϵ_1	+269		\bar{a}	\bar{b}				
		ϵ_2	+185		\bar{A}	\bar{B}				
		ϵ_3	+121		$4\bar{A}$	$4\bar{B}$				
0.090		ϵ_1	+269		\bar{a}	\bar{b}				
		ϵ_2	+185		\bar{A}	\bar{B}				
		ϵ_3	+121		$4\bar{A}$	$4\bar{B}$				
0.100		ϵ_1	+265		\bar{a}	\bar{b}				
		ϵ_2	+184		\bar{A}	\bar{B}				
		ϵ_3	+121		$4\bar{A}$	$4\bar{B}$				
1	2	3		4	5		6	7	8	9

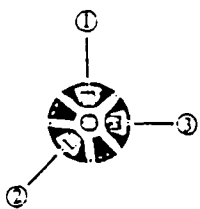


$D_0 = \text{_____}$ $E = \text{_____}$ $\frac{1}{2E} = \text{_____} (10)^{-4}$
 $D/D_0 = \text{_____}$ $\nu = \text{_____}$
 $\frac{1+\nu}{2E} = \text{_____} (10)^{-4}$ Material: _____



MEASUREMENTS GROUP RS-200 DATA FORM

DEPTH		MEASURED STRAIN		PERCENT STRAIN RELIEVED	COEFFICIENTS		α	Equiv. Uniform Stress to Depth Z (1000 psi).	
Z (in)	Z/D ₀	$\mu\epsilon$			Exponent of (10) ⁻⁴ with \bar{A} and \bar{B}			σ_{min}	σ_{max}
0.010		ϵ_1	+28		\bar{a}	\bar{b}			
		ϵ_2	+27		\bar{A}	\bar{B}			
		ϵ_3	+34		$4\bar{A}$	$4\bar{B}$			
0.020		ϵ_1	+39		\bar{a}	\bar{b}			
		ϵ_2	+38		\bar{A}	\bar{B}			
		ϵ_3	+54		$4\bar{A}$	$4\bar{B}$			
0.030		ϵ_1	+43		\bar{a}	\bar{b}			
		ϵ_2	+43		\bar{A}	\bar{B}			
		ϵ_3	+65		$4\bar{A}$	$4\bar{B}$			
0.040		ϵ_1	+446		\bar{a}	\bar{b}			
		ϵ_2	+487		\bar{A}	\bar{B}			
		ϵ_3	+6870		$4\bar{A}$	$4\bar{B}$			
0.050		ϵ_1	+45		\bar{a}	\bar{b}			
		ϵ_2	+48		\bar{A}	\bar{B}			
		ϵ_3	+76		$4\bar{A}$	$4\bar{B}$			
0.060		ϵ_1	+45		\bar{a}	\bar{b}			
		ϵ_2	+48		\bar{A}	\bar{B}			
		ϵ_3	+78		$4\bar{A}$	$4\bar{B}$			
0.070		ϵ_1	+44		\bar{a}	\bar{b}			
		ϵ_2	+48		\bar{A}	\bar{B}			
		ϵ_3	+77		$4\bar{A}$	$4\bar{B}$			
0.080		ϵ_1	+41		\bar{a}	\bar{b}			
		ϵ_2	+46		\bar{A}	\bar{B}			
		ϵ_3	+76		$4\bar{A}$	$4\bar{B}$			
0.090		ϵ_1	+38		\bar{a}	\bar{b}			
		ϵ_2	+45		\bar{A}	\bar{B}			
		ϵ_3	+74		$4\bar{A}$	$4\bar{B}$			
0.100		ϵ_1	+40		\bar{a}	\bar{b}			
		ϵ_2	+46		\bar{A}	\bar{B}			
		ϵ_3	+75		$4\bar{A}$	$4\bar{B}$			
1	2	3		4	5	6	7	8	9

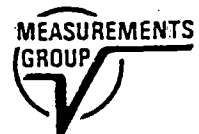


$D_0 = \text{_____}$ $E = \text{_____}$ $\frac{1}{2E} = \text{_____} (10)^{-4}$

$D/D_0 = \text{_____}$ $\nu = \text{_____}$

$\frac{1+\nu}{2E} = \text{_____} (10)^{-4}$

WHEEL # _____
 Material: Q43528
 10/24/91 - JM



P. A. 944

MEASUREMENTS GROUP RS-200 DATA FORM

WHEEL #5576
12/15/90

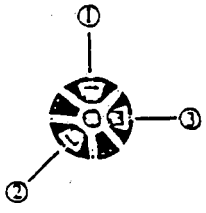
DEPTH		MEASURED STRAIN $\mu\epsilon$	PERCENT STRAIN RELIEVED	COEFFICIENTS Exponent of $(10)^{-4}$ with \bar{A} and \bar{B}		α	Equiv. Uniform Stress to Depth Z (1000 psi).	
Z (in)	Z/D ₀			\bar{a}	\bar{b}		σ_{min}	σ_{max}
0.010		ϵ_1 +126		\bar{a}	\bar{b}			
		ϵ_2 +130		\bar{A}	\bar{B}			
		ϵ_3 +101		$4\bar{A}$	$4\bar{B}$			
0.020		ϵ_1 +263		\bar{a}	\bar{b}			
		ϵ_2 +265		\bar{A}	\bar{B}			
		ϵ_3 +212		$4\bar{A}$	$4\bar{B}$			
0.030		ϵ_1 +299		\bar{a}	\bar{b}			
		ϵ_2 +310		\bar{A}	\bar{B}			
		ϵ_3 +240		$4\bar{A}$	$4\bar{B}$			
0.040		ϵ_1 +313		\bar{a}	\bar{b}			
		ϵ_2 +330		\bar{A}	\bar{B}			
		ϵ_3 +248		$4\bar{A}$	$4\bar{B}$			
0.050		ϵ_1 +318		\bar{a}	\bar{b}			
		ϵ_2 +338		\bar{A}	\bar{B}			
		ϵ_3 +250		$4\bar{A}$	$4\bar{B}$			
0.060		ϵ_1 +318		\bar{a}	\bar{b}			
		ϵ_2 +345		\bar{A}	\bar{B}			
		ϵ_3 +249		$4\bar{A}$	$4\bar{B}$			
0.070		ϵ_1 +319		\bar{a}	\bar{b}			
		ϵ_2 +317		\bar{A}	\bar{B}			
		ϵ_3 +249		$4\bar{A}$	$4\bar{B}$			
0.080		ϵ_1 +313		\bar{a}	\bar{b}			
		ϵ_2 +343		\bar{A}	\bar{B}			
		ϵ_3 +249		$4\bar{A}$	$4\bar{B}$			
0.090		ϵ_1 +314		\bar{a}	\bar{b}			
		ϵ_2 +374		\bar{A}	\bar{B}			
		ϵ_3 +250		$4\bar{A}$	$4\bar{B}$			
0.100		ϵ_1 +316		\bar{a}	\bar{b}			
		ϵ_2 +378		\bar{A}	\bar{B}			
		ϵ_3 +251		$4\bar{A}$	$4\bar{B}$			
1	2	3	4	5	6	7	8	9

changed bit

*changed bit
change*

*ch
ch
ch
ch*

ch



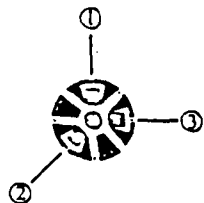
$D_0 = \text{_____} \quad E = \text{_____} \quad \frac{1}{2E} = \text{_____} (10)^{-4}$
 $D/D_0 = \text{_____} \quad \nu = \text{_____}$
 $\frac{1+\nu}{2E} = \text{_____} (10)^{-4} \quad \text{Material: _____}$



MEASUREMENTS GROUP RS-200 DATA FORM

WHEEL # 555
12/10/98 JM

DEPTH		MEASURED STRAIN $\mu\epsilon$	PERCENT STRAIN RELIEVED	COEFFICIENTS Exponent of $(10)^{-4}$ with \bar{A} and \bar{B}			α	Equiv. Uniform Stress to Depth Z (1000 psi).		
Z (in)	Z/D ₀			\bar{a}	\bar{A}	$4\bar{A}$		\bar{b}	\bar{B}	$4\bar{B}$
0.018		ϵ_1 +124		\bar{a}		\bar{b}				
		ϵ_2 +124		\bar{A}		\bar{B}				
		ϵ_3 +109		$4\bar{A}$		$4\bar{B}$				
0.020		ϵ_1 +242		\bar{a}		\bar{b}				
		ϵ_2 +240		\bar{A}		\bar{B}				
		ϵ_3 +217		$4\bar{A}$		$4\bar{B}$				
0.030		ϵ_1 +293		\bar{a}		\bar{b}				
		ϵ_2 +292		\bar{A}		\bar{B}				
		ϵ_3 +277		$4\bar{A}$		$4\bar{B}$				
0.040		ϵ_1 +308		\bar{a}		\bar{b}				
		ϵ_2 +311		\bar{A}		\bar{B}				
		ϵ_3 +303		$4\bar{A}$		$4\bar{B}$				
0.050		ϵ_1 +312		\bar{a}		\bar{b}				
		ϵ_2 +318		\bar{A}		\bar{B}				
		ϵ_3 +315		$4\bar{A}$		$4\bar{B}$				
0.060		ϵ_1 +312		\bar{a}		\bar{b}				
		ϵ_2 +320		\bar{A}		\bar{B}				
		ϵ_3 +321		$4\bar{A}$		$4\bar{B}$				
0.070		ϵ_1 +311		\bar{a}		\bar{b}				
		ϵ_2 +321		\bar{A}		\bar{B}				
		ϵ_3 +324		$4\bar{A}$		$4\bar{B}$				
0.080		ϵ_1 +311		\bar{a}		\bar{b}				
		ϵ_2 +321		\bar{A}		\bar{B}				
		ϵ_3 +325		$4\bar{A}$		$4\bar{B}$				
0.090		ϵ_1 +311		\bar{a}		\bar{b}				
		ϵ_2 +320		\bar{A}		\bar{B}				
		ϵ_3 +325		$4\bar{A}$		$4\bar{B}$				
0.100		ϵ_1 +311		\bar{a}		\bar{b}				
		ϵ_2 +321		\bar{A}		\bar{B}				
		ϵ_3 +325		$4\bar{A}$		$4\bar{B}$				
1	2	3	4	5	6	7	8	9		



$D_0 = \text{_____} \quad E = \text{_____} \quad \frac{1}{2E} = \text{_____} (10)^{-4}$
 $D/D_0 = \text{_____} \quad \nu = \text{_____}$
 $\frac{1+\nu}{2E} = \text{_____} (10)^{-4} \quad \text{Material: _____}$

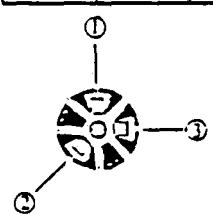


MEASUREMENTS GROUP RS-200 DATA FORM

11/21/96

DEPTH		MEASURED STRAIN $\mu\epsilon$	PERCENT STRAIN RELIEVED	COEFFICIENTS Exponent of $(10)^{-4}$ with \bar{A} and \bar{B}		α	Equiv. Uniform Stress to Depth Z (1000 psi).	
Z (in)	Z/D ₀			\bar{a}	\bar{b}		σ_{min}	σ_{max}
0.010		ϵ_1 +46		\bar{a}	\bar{b}			
		ϵ_2 +92		\bar{A}	\bar{B}			
		ϵ_3 +100		$4\bar{A}$	$4\bar{B}$			
0.020		ϵ_1 +74		\bar{a}	\bar{b}			
		ϵ_2 +172		\bar{A}	\bar{B}			
		ϵ_3 +193		$4\bar{A}$	$4\bar{B}$			
0.030		ϵ_1 +79		\bar{a}	\bar{b}			
		ϵ_2 +207		\bar{A}	\bar{B}			
		ϵ_3 +241		$4\bar{A}$	$4\bar{B}$			
0.040		ϵ_1 +74		\bar{a}	\bar{b}			
		ϵ_2 +218		\bar{A}	\bar{B}			
		ϵ_3 +265		$4\bar{A}$	$4\bar{B}$			
0.050		ϵ_1 +70		\bar{a}	\bar{b}			
		ϵ_2 +224		\bar{A}	\bar{B}			
		ϵ_3 +277		$4\bar{A}$	$4\bar{B}$			
0.060		ϵ_1 +67		\bar{a}	\bar{b}			
		ϵ_2 +226		\bar{A}	\bar{B}			
		ϵ_3 +282		$4\bar{A}$	$4\bar{B}$			
0.070		ϵ_1 +66		\bar{a}	\bar{b}			
		ϵ_2 +230		\bar{A}	\bar{B}			
		ϵ_3 +288		$4\bar{A}$	$4\bar{B}$			
0.080		ϵ_1 +65		\bar{a}	\bar{b}			
		ϵ_2 +231		\bar{A}	\bar{B}			
		ϵ_3 +291		$4\bar{A}$	$4\bar{B}$			
0.090		ϵ_1 +64		\bar{a}	\bar{b}			
		ϵ_2 +233		\bar{A}	\bar{B}			
		ϵ_3 +293		$4\bar{A}$	$4\bar{B}$			
0.100		ϵ_1 +63		\bar{a}	\bar{b}			
		ϵ_2 +233		\bar{A}	\bar{B}			
		ϵ_3 +293		$4\bar{A}$	$4\bar{B}$			
1	2	3	4	5	6	7	8	9

Temperature = 1
radius = 3
of sec = 2



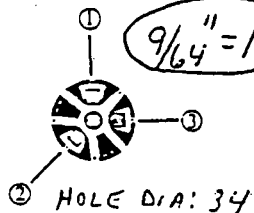
$D_0 = \text{_____} E = \text{_____}$
 $D/D_0 = \text{_____} \nu = \text{_____}$
 $\frac{1+\nu}{2E} = \text{_____} (10)^{-4}$
 Material: WHEEL #1



need diameter - and mass, long, dia.
3 10 2

MEASUREMENTS GROUP RS-200 DATA FORM

DEPTH		MEASURED STRAIN		PERCENT STRAIN RELIEVED	COEFFICIENTS		α	Equiv. Uniform Stress to Depth Z (1000 psi).	
Z (in)	Z/D ₀	$\mu\epsilon$			Exponent of (10) ⁻⁴ with \bar{A} and \bar{B}			σ_{min}	σ_{max}
0.010		ϵ_1	+36		\bar{a}	\bar{b}			
		ϵ_2	+73		\bar{A}	\bar{B}			
		ϵ_3	+125		$4\bar{A}$	$4\bar{B}$			
0.020		ϵ_1	+36		\bar{a}	\bar{b}			
		ϵ_2	+114		\bar{A}	\bar{B}			
		ϵ_3	+235		$4\bar{A}$	$4\bar{B}$			
0.030		ϵ_1	+27		\bar{a}	\bar{b}			
		ϵ_2	+126		\bar{A}	\bar{B}			
		ϵ_3	+227		$4\bar{A}$	$4\bar{B}$			
0.040		ϵ_1	+17		\bar{a}	\bar{b}			
		ϵ_2	+137		\bar{A}	\bar{B}			
		ϵ_3	+317		$4\bar{A}$	$4\bar{B}$			
0.050		ϵ_1	+9		\bar{a}	\bar{b}			
		ϵ_2	+139		\bar{A}	\bar{B}			
		ϵ_3	+336		$4\bar{A}$	$4\bar{B}$			
0.060		ϵ_1	+1		\bar{a}	\bar{b}			
		ϵ_2	+141		\bar{A}	\bar{B}			
		ϵ_3	+346		$4\bar{A}$	$4\bar{B}$			
0.070		ϵ_1	-5		\bar{a}	\bar{b}			
		ϵ_2	+140		\bar{A}	\bar{B}			
		ϵ_3	+350		$4\bar{A}$	$4\bar{B}$			
0.080		ϵ_1	-7		\bar{a}	\bar{b}			
		ϵ_2	+140		\bar{A}	\bar{B}			
		ϵ_3	+352		$4\bar{A}$	$4\bar{B}$			
0.090		ϵ_1	-8		\bar{a}	\bar{b}			
		ϵ_2	+138		\bar{A}	\bar{B}			
		ϵ_3	+353		$4\bar{A}$	$4\bar{B}$			
0.100		ϵ_1	-8		\bar{a}	\bar{b}			
		ϵ_2	+138		\bar{A}	\bar{B}			
		ϵ_3	+353		$4\bar{A}$	$4\bar{B}$			
1	2	3	4	5	6	7	8	9	



D/D₀ = _____ ν = _____ $\frac{1}{2E} =$ _____ (10)⁻⁴

$\frac{1+\nu}{2E} =$ _____ (10)⁻⁴

Material: WHEEL #895551
10/24/91 - JM

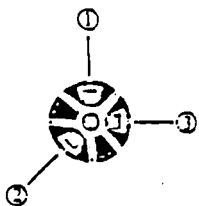


* CHANGED BIT

MEASUREMENTS GROUP RS-200 DATA FORM

11/21/92

DEPTH		MEASURED STRAIN $\mu\epsilon$	PERCENT STRAIN RELIEVED	COEFFICIENTS Exponent of $(10)^{-1}$ with \bar{A} and \bar{B}		α	Equiv. Uniform Stress to Depth Z (1000 psi).	
Z (in)	Z/D ₀			\bar{a}	\bar{b}		σ_{min}	σ_{max}
0.010		ϵ_1 +11		\bar{a}	\bar{b}			
		ϵ_2 +15		\bar{A}	\bar{B}			
		ϵ_3 +24		$4\bar{A}$	$4\bar{B}$			
0.020		ϵ_1 +18		\bar{a}	\bar{b}			
		ϵ_2 +30		\bar{A}	\bar{B}			
		ϵ_3 +55		$4\bar{A}$	$4\bar{B}$			
0.030		ϵ_1 +16		\bar{a}	\bar{b}			
		ϵ_2 +35		\bar{A}	\bar{B}			
		ϵ_3 +73		$4\bar{A}$	$4\bar{B}$			
0.040		ϵ_1 +12		\bar{a}	\bar{b}			
		ϵ_2 +37		\bar{A}	\bar{B}			
		ϵ_3 +87		$4\bar{A}$	$4\bar{B}$			
0.050		ϵ_1 +8		\bar{a}	\bar{b}			
		ϵ_2 +37		\bar{A}	\bar{B}			
		ϵ_3 +95		$4\bar{A}$	$4\bar{B}$			
0.060		ϵ_1 +7		\bar{a}	\bar{b}			
		ϵ_2 +39		\bar{A}	\bar{B}			
		ϵ_3 +99		$4\bar{A}$	$4\bar{B}$			
0.070		ϵ_1 +5		\bar{a}	\bar{b}			
		ϵ_2 +38		\bar{A}	\bar{B}			
		ϵ_3 +103		$4\bar{A}$	$4\bar{B}$			
0.080		ϵ_1 +2		\bar{a}	\bar{b}			
		ϵ_2 +38		\bar{A}	\bar{B}			
		ϵ_3 +105		$4\bar{A}$	$4\bar{B}$			
0.090		ϵ_1 6		\bar{a}	\bar{b}			
		ϵ_2 +37		\bar{A}	\bar{B}			
		ϵ_3 +105		$4\bar{A}$	$4\bar{B}$			
0.100		ϵ_1 -3		\bar{a}	\bar{b}			
		ϵ_2 +36		\bar{A}	\bar{B}			
		ϵ_3 +104		$4\bar{A}$	$4\bar{B}$			
1	2	3	4	5	6	7	8	9



$D_0 =$ _____ $E =$ _____ $\frac{1}{2E} =$ _____ $(10)^{-3}$

$D/D_0 =$ _____ $\nu =$ _____

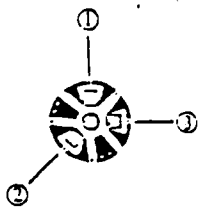
$\frac{1+\nu}{2E} =$ _____ $(10)^{-3}$ Material: WHEEL #5



Handwritten notes and scribbles at the bottom of the page.

MEASUREMENTS GROUP RS-200 DATA FORM 11/24/90

DEPTH		MEASURED STRAIN $\mu\epsilon$		PERCENT STRAIN RELIEVED	COEFFICIENTS Exponent of $(10)^{-3}$ with \bar{A} and \bar{B}			α	Equiv. Uniform Stress to Depth Z (1000 psi).	
Z (in)	Z/D ₀								σ_{min}	σ_{max}
0.010		ϵ_1	-20		\bar{a}	\bar{b}				
		ϵ_2	+33		\bar{A}	\bar{B}				
		ϵ_3	+36		$4\bar{A}$	$4\bar{B}$				
0.020		ϵ_1	+25		\bar{a}	\bar{b}				
		ϵ_2	+58		\bar{A}	\bar{B}				
		ϵ_3	+72		$4\bar{A}$	$4\bar{B}$				
0.030		ϵ_1	+30		\bar{a}	\bar{b}				
		ϵ_2	+68		\bar{A}	\bar{B}				
		ϵ_3	+87		$4\bar{A}$	$4\bar{B}$				
0.040		ϵ_1	-22		\bar{a}	\bar{b}				
		ϵ_2	+22		\bar{A}	\bar{B}				
		ϵ_3	+51		$4\bar{A}$	$4\bar{B}$				
0.050		ϵ_1	+25		\bar{a}	\bar{b}				
		ϵ_2	+10		\bar{A}	\bar{B}				
		ϵ_3	+37		$4\bar{A}$	$4\bar{B}$				
0.060		ϵ_1	-42		\bar{a}	\bar{b}				
		ϵ_2	+17		\bar{A}	\bar{B}				
		ϵ_3	+42		$4\bar{A}$	$4\bar{B}$				
0.070		ϵ_1	-42		\bar{a}	\bar{b}				
		ϵ_2	+20		\bar{A}	\bar{B}				
		ϵ_3	+47		$4\bar{A}$	$4\bar{B}$				
0.080		ϵ_1	-46		\bar{a}	\bar{b}				
		ϵ_2	+20		\bar{A}	\bar{B}				
		ϵ_3	+48		$4\bar{A}$	$4\bar{B}$				
0.090		ϵ_1	-48		\bar{a}	\bar{b}				
		ϵ_2	+18		\bar{A}	\bar{B}				
		ϵ_3	+46		$4\bar{A}$	$4\bar{B}$				
0.100		ϵ_1	-49		\bar{a}	\bar{b}				
		ϵ_2	+18		\bar{A}	\bar{B}				
		ϵ_3	+45		$4\bar{A}$	$4\bar{B}$				
1	2	3	4	5	6	7	8	9		



$D_0 = \text{_____} \quad E = \text{_____} \quad \frac{1}{2E} = \text{_____} (10)^{-3}$

$D/D_0 = \text{_____} \quad \nu = \text{_____}$

$\frac{1+\nu}{2E} = \text{_____} (10)^{-3}$

Material: WHEEL # 6
2ND LOCATION (150°)

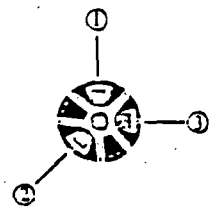


material = 1, -17, -17, -disc = 2

MEASUREMENTS GROUP RS-200 DATA FORM

11/20/70

DEPTH		MEASURED STRAIN $\mu\epsilon$	PERCENT STRAIN RELIEVED	COEFFICIENTS Exponent of $(10)^{-3}$ with \bar{A} and \bar{B}		α	Equiv. Uniform Stress to Depth Z (1000 psi).	
Z (in)	Z/D ₀			\bar{a}	\bar{b}		σ_{min}	σ_{max}
0.010		ϵ_1 +12		\bar{a}	\bar{b}			
		ϵ_2 +23		\bar{A}	\bar{B}			
		ϵ_3 +36		$4\bar{A}$	$4\bar{B}$			
0.020		ϵ_1 +11		\bar{a}	\bar{b}			
		ϵ_2 -37		\bar{A}	\bar{B}			
		ϵ_3 +75		$4\bar{A}$	$4\bar{B}$			
0.030		ϵ_1 +6		\bar{a}	\bar{b}			
		ϵ_2 +42		\bar{A}	\bar{B}			
		ϵ_3 +104		$4\bar{A}$	$4\bar{B}$			
0.040		ϵ_1 0		\bar{a}	\bar{b}			
		ϵ_2 +45		\bar{A}	\bar{B}			
		ϵ_3 +121		$4\bar{A}$	$4\bar{B}$			
0.050		ϵ_1 -7		\bar{a}	\bar{b}			
		ϵ_2 +45		\bar{A}	\bar{B}			
		ϵ_3 +130		$4\bar{A}$	$4\bar{B}$			
0.060		ϵ_1 -12		\bar{a}	\bar{b}			
		ϵ_2 +45		\bar{A}	\bar{B}			
		ϵ_3 +136		$4\bar{A}$	$4\bar{B}$			
0.070		ϵ_1 -15		\bar{a}	\bar{b}			
		ϵ_2 -44		\bar{A}	\bar{B}			
		ϵ_3 +139		$4\bar{A}$	$4\bar{B}$			
0.080		ϵ_1 -17		\bar{a}	\bar{b}			
		ϵ_2 +43		\bar{A}	\bar{B}			
		ϵ_3 +140		$4\bar{A}$	$4\bar{B}$			
0.090		ϵ_1 -19		\bar{a}	\bar{b}			
		ϵ_2 +43		\bar{A}	\bar{B}			
		ϵ_3 +141		$4\bar{A}$	$4\bar{B}$			
0.100		ϵ_1 -19		\bar{a}	\bar{b}			
		ϵ_2 +43		\bar{A}	\bar{B}			
		ϵ_3 +139		$4\bar{A}$	$4\bar{B}$			
1	2	3	4	5	6	7	8	9



$D_0 = \text{_____} E = \text{_____} \frac{1}{2E} = \text{_____} (10)^{-4}$
 $D/D_0 = \text{_____} \nu = \text{_____}$
 $\frac{1+\nu}{2E} = \text{_____} (10)^{-4}$
 Material: ALUMINUM #7
 $\sigma_1 = -15.2 \quad \sigma_2 = -3.1 \quad \sigma_3 = 7$

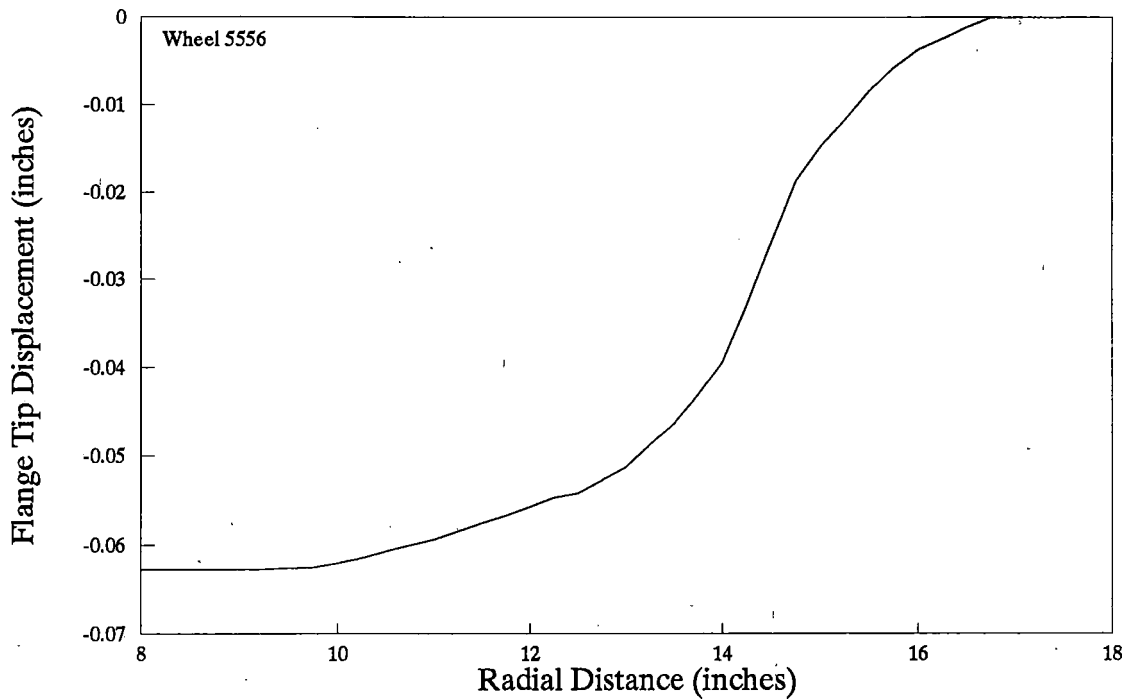


$\sigma_1 = -15.2 - 17 = \text{_____}$
 $\sigma_2 = -3.1 - 17 = \text{_____}$
 $\sigma_3 = 7 - 17 = \text{_____}$

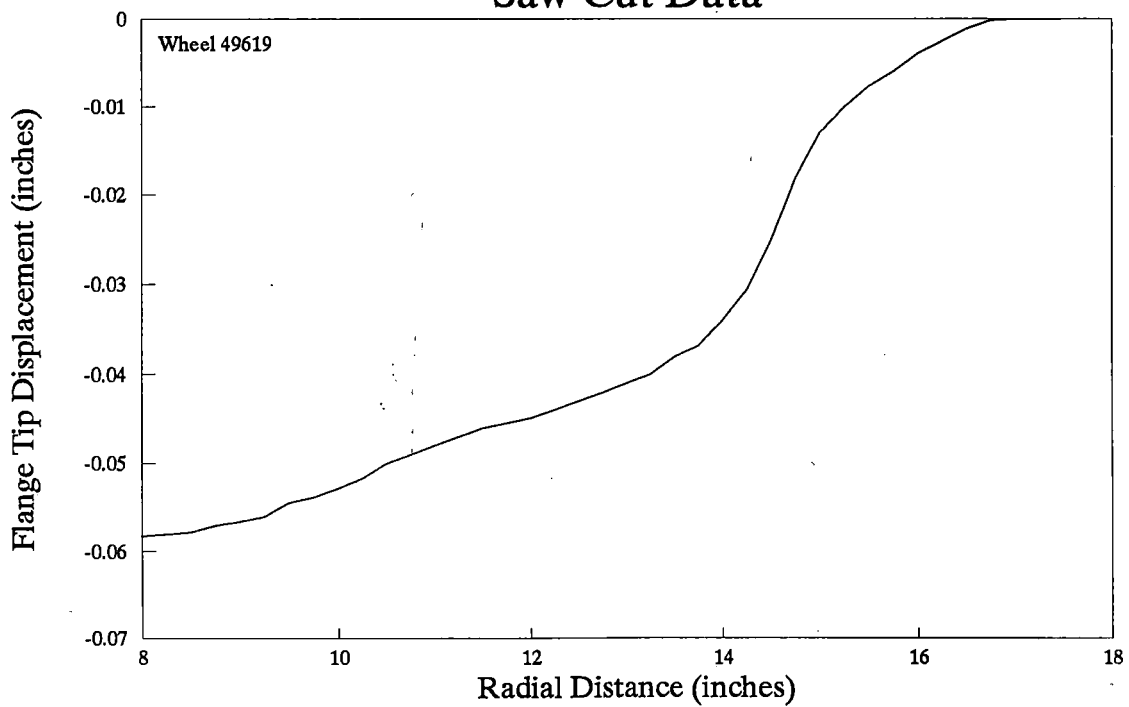
APPENDIX F

SAW-CUT DATA

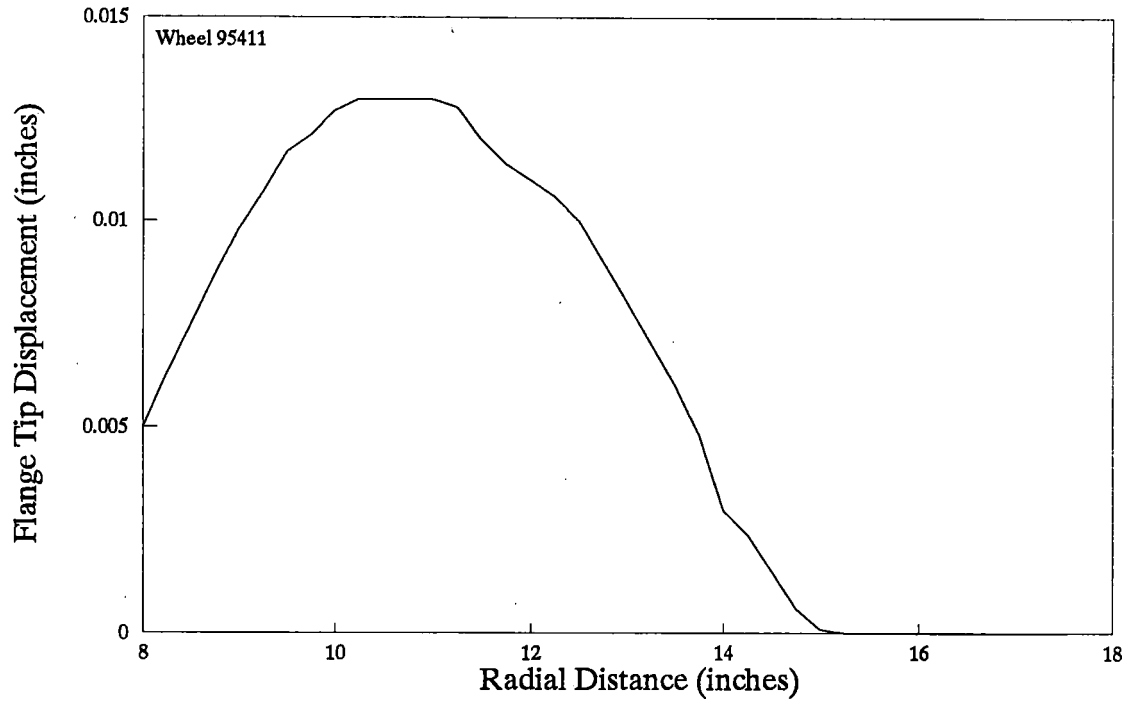
Saw Cut Data



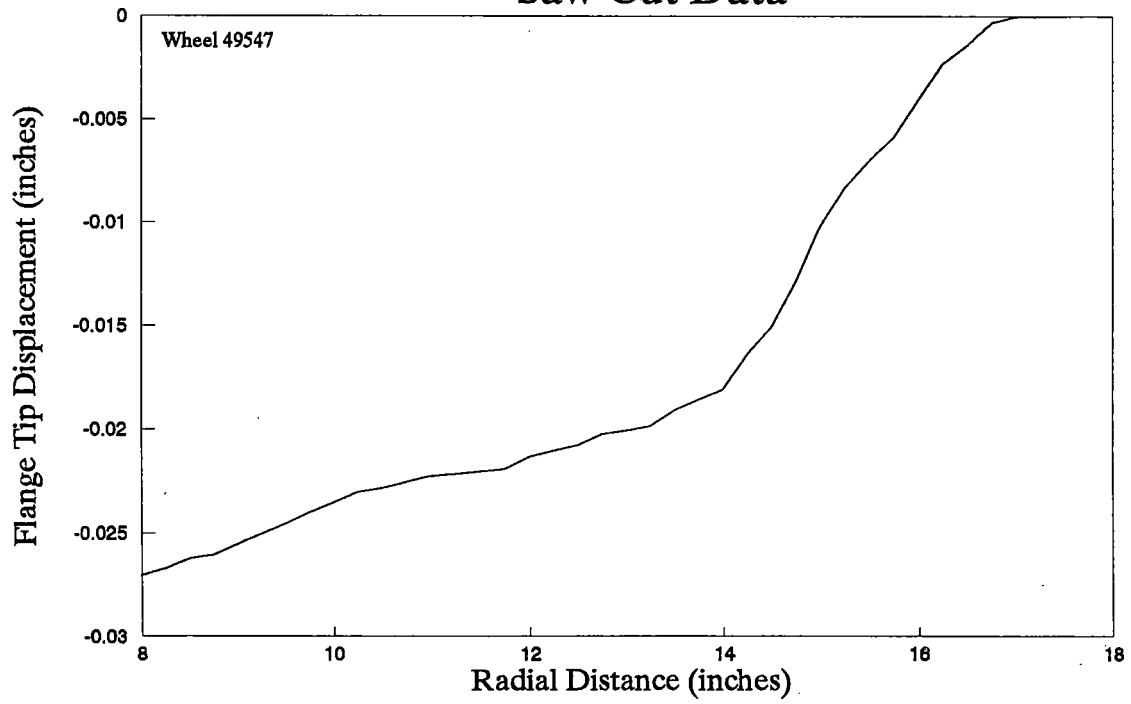
Saw Cut Data



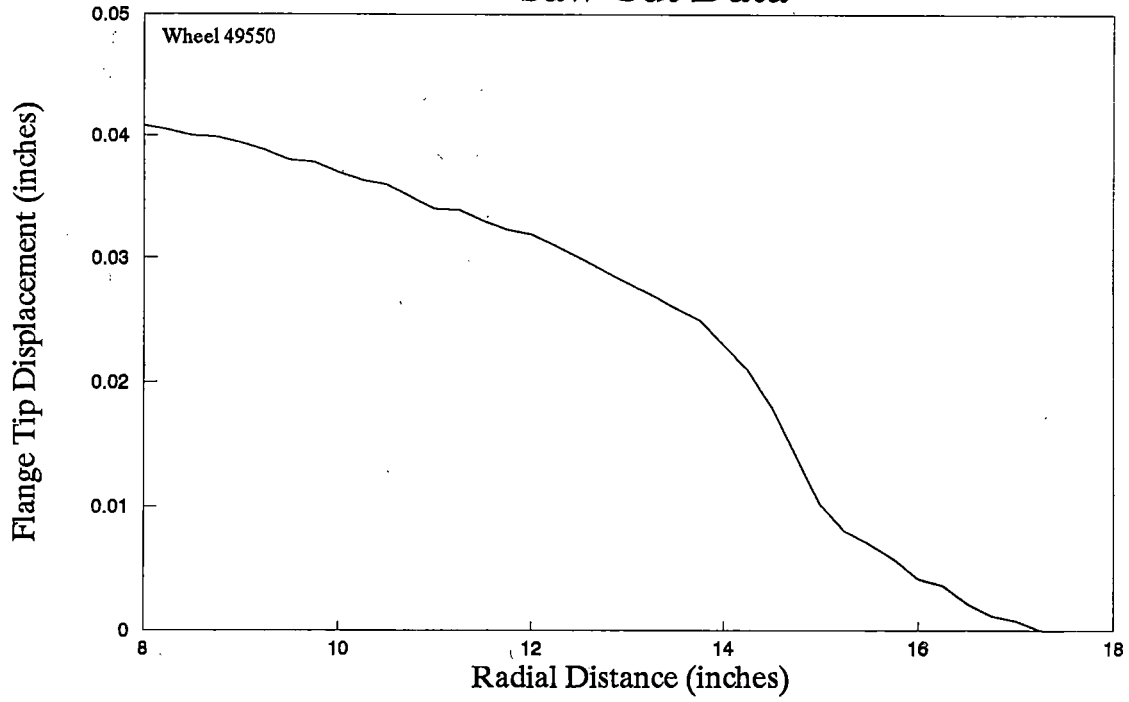
Saw Cut Data



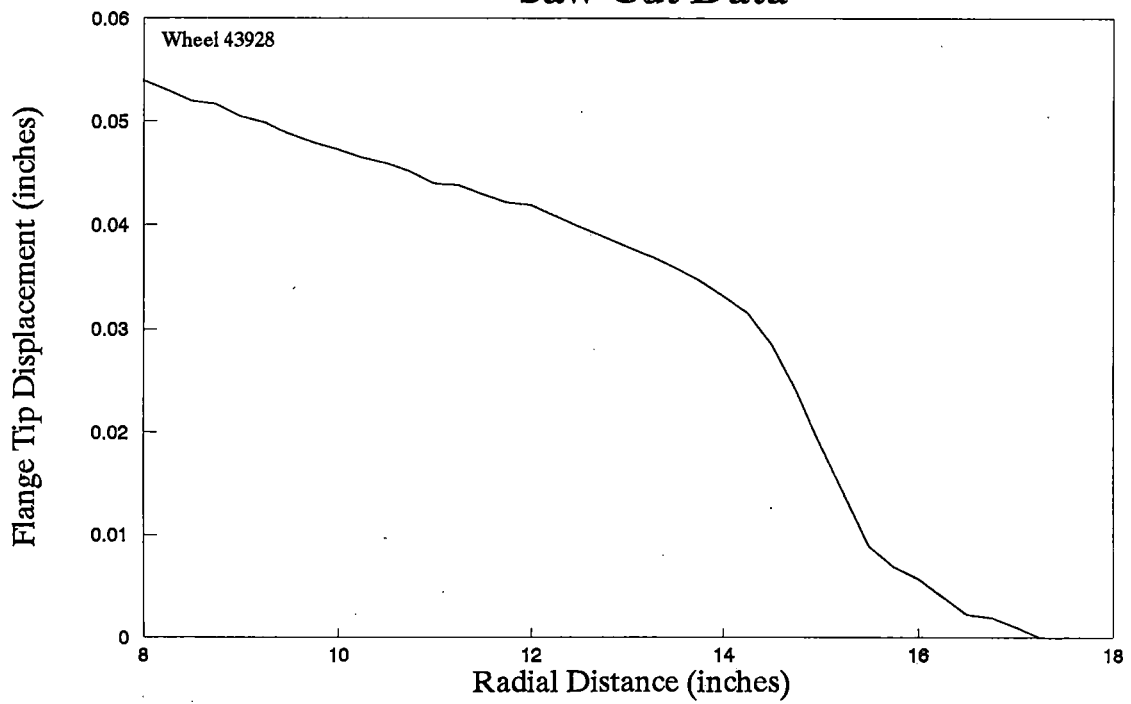
Saw Cut Data



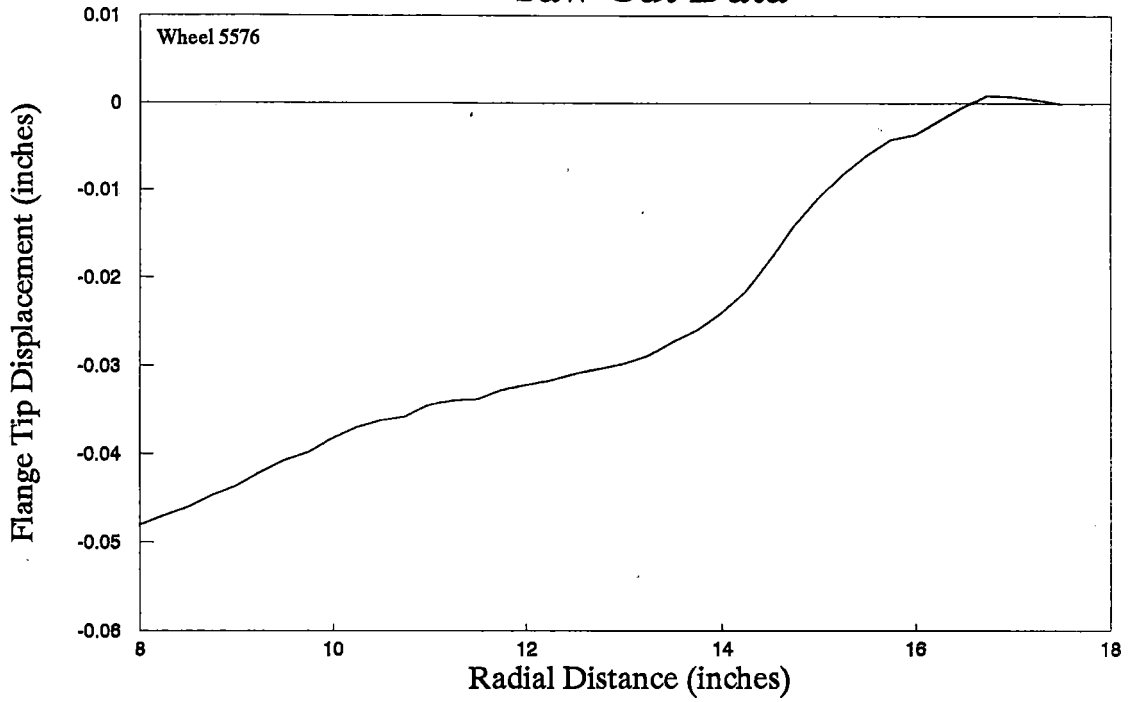
Saw Cut Data



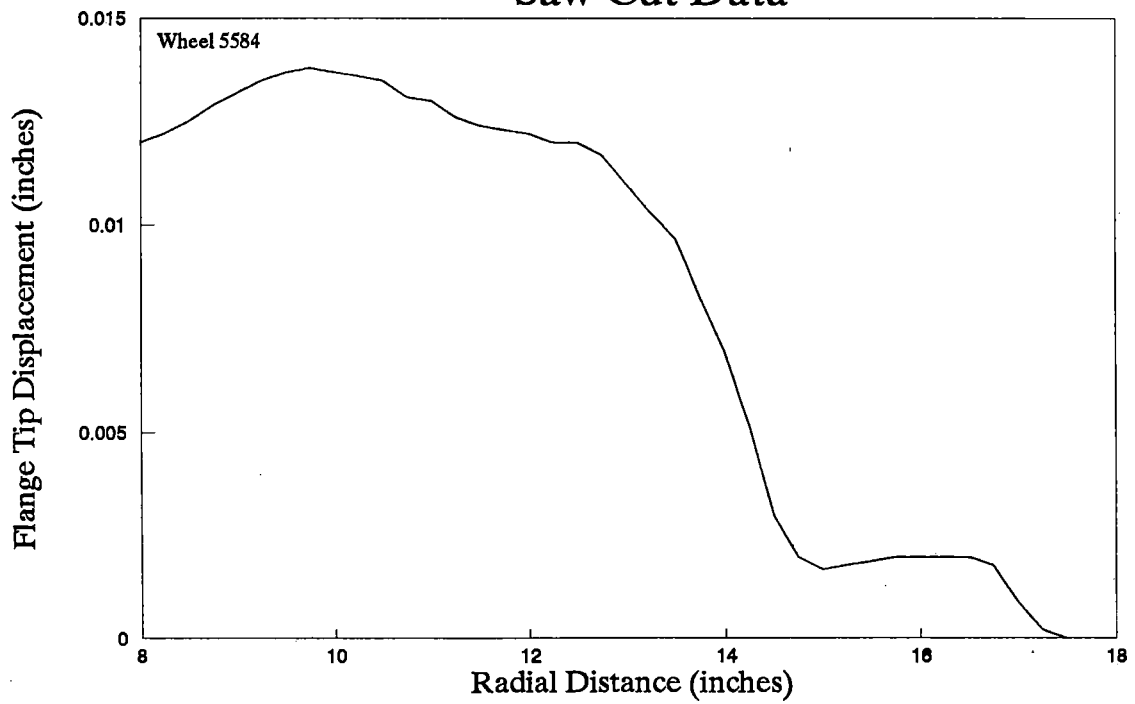
Saw Cut Data



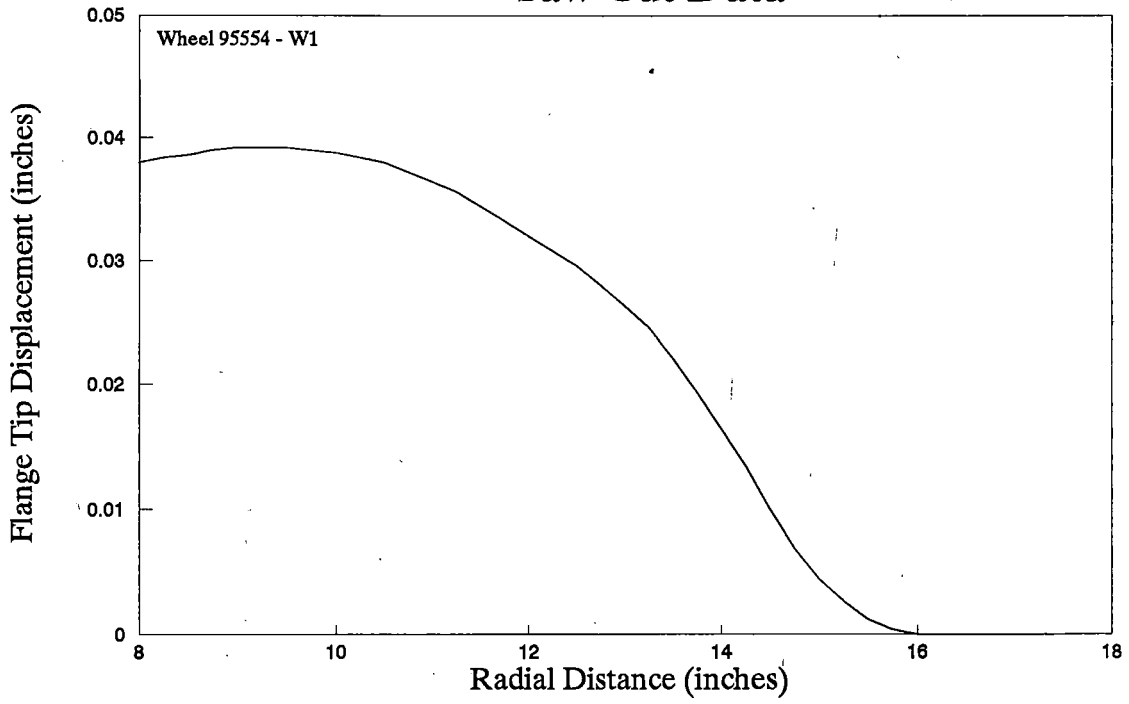
Saw Cut Data



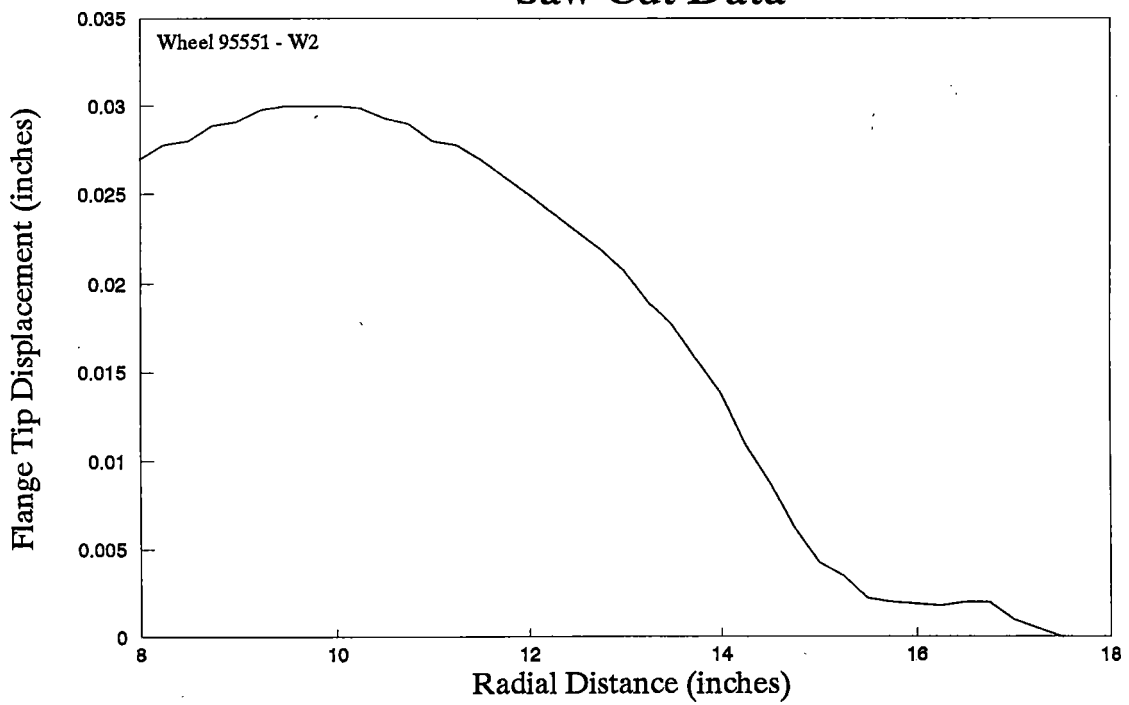
Saw Cut Data



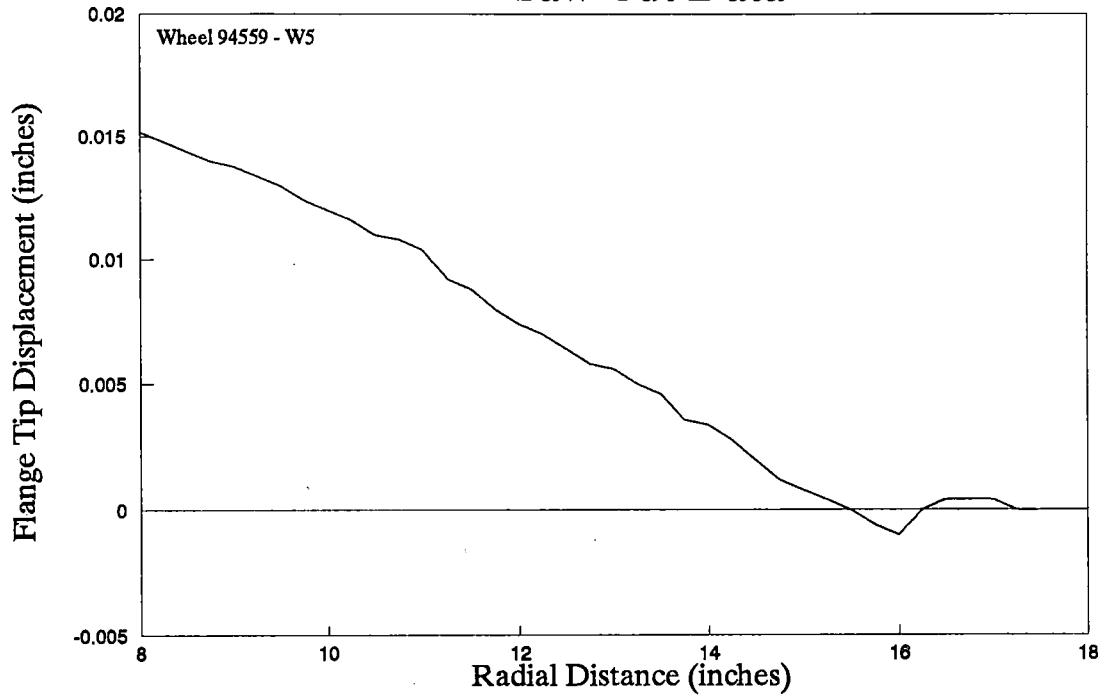
Saw Cut Data



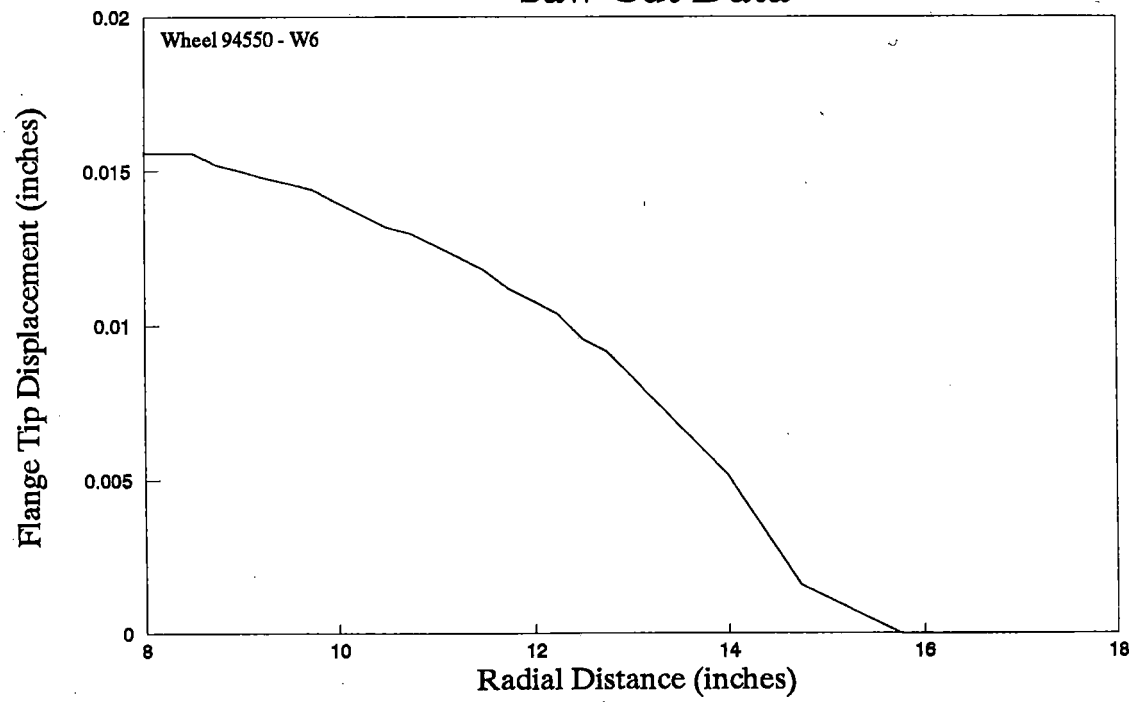
Saw Cut Data



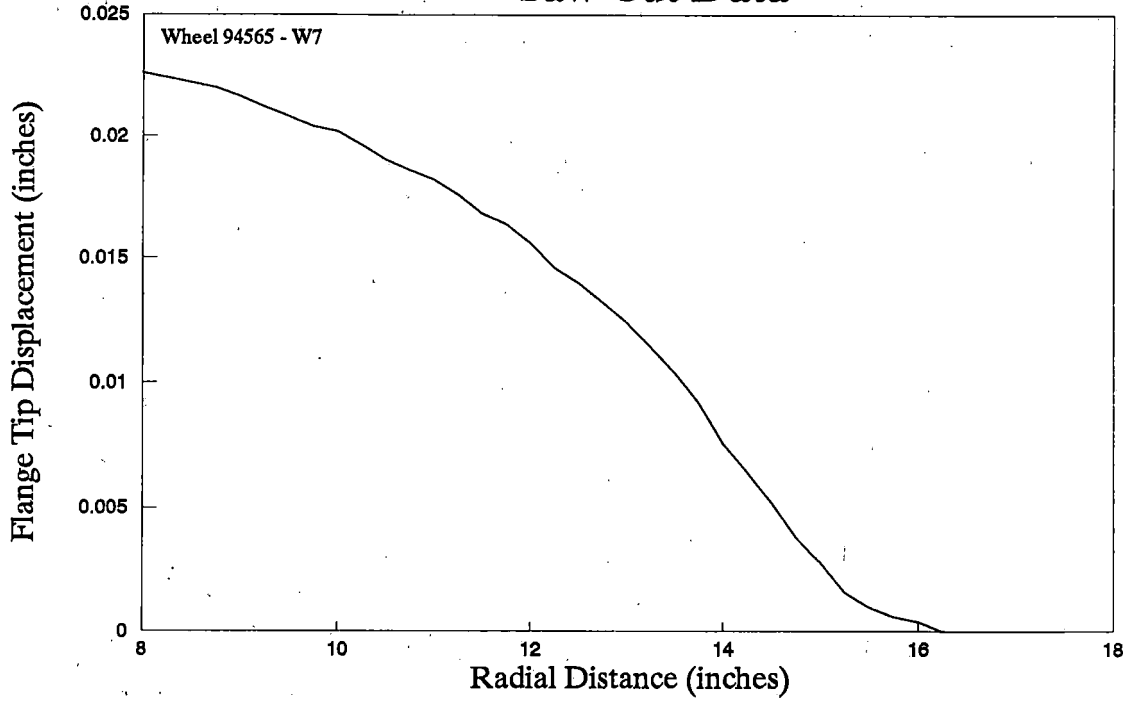
Saw Cut Data



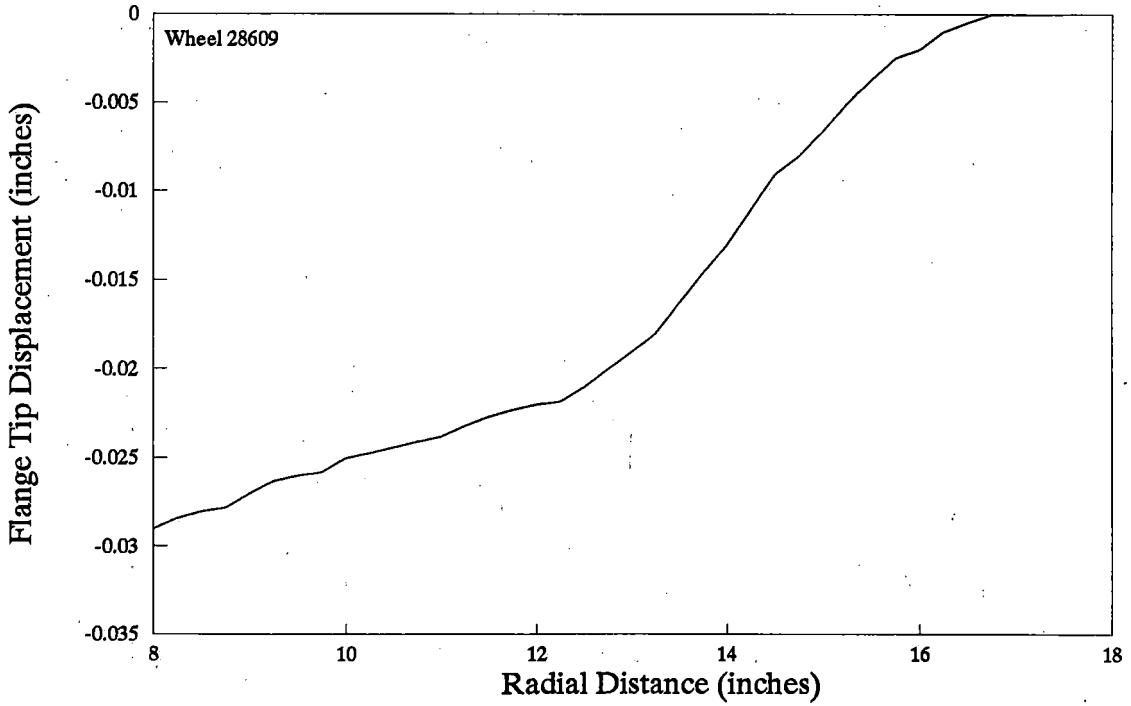
Saw Cut Data



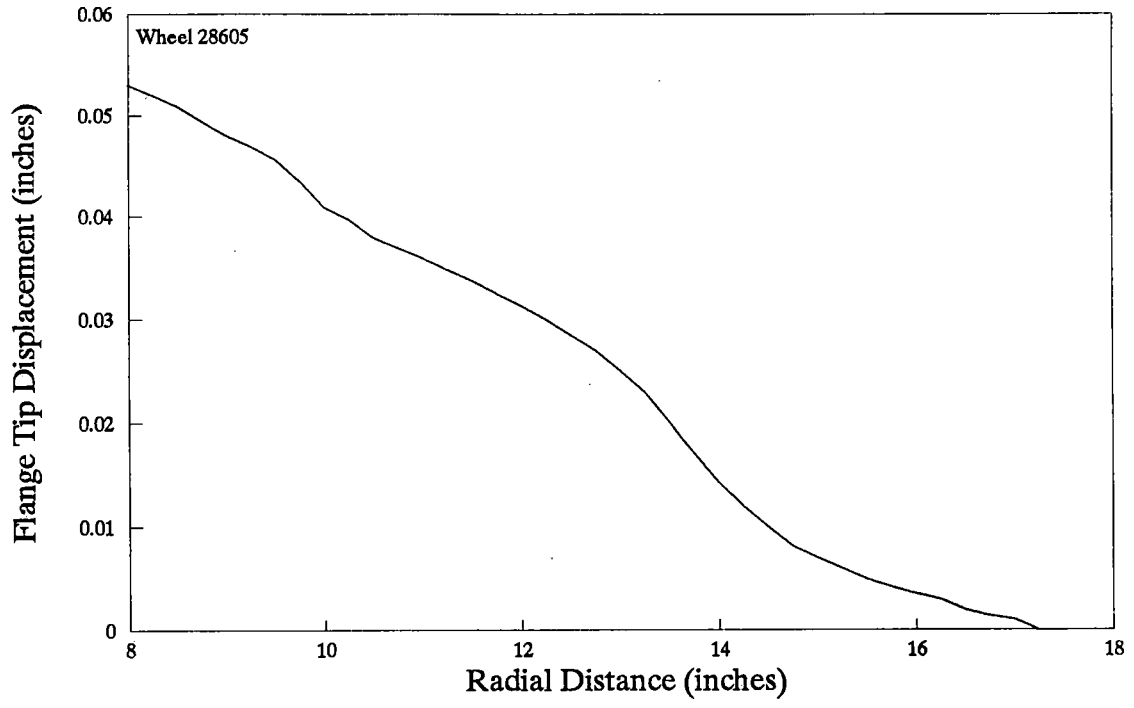
Saw Cut Data



Saw Cut Data



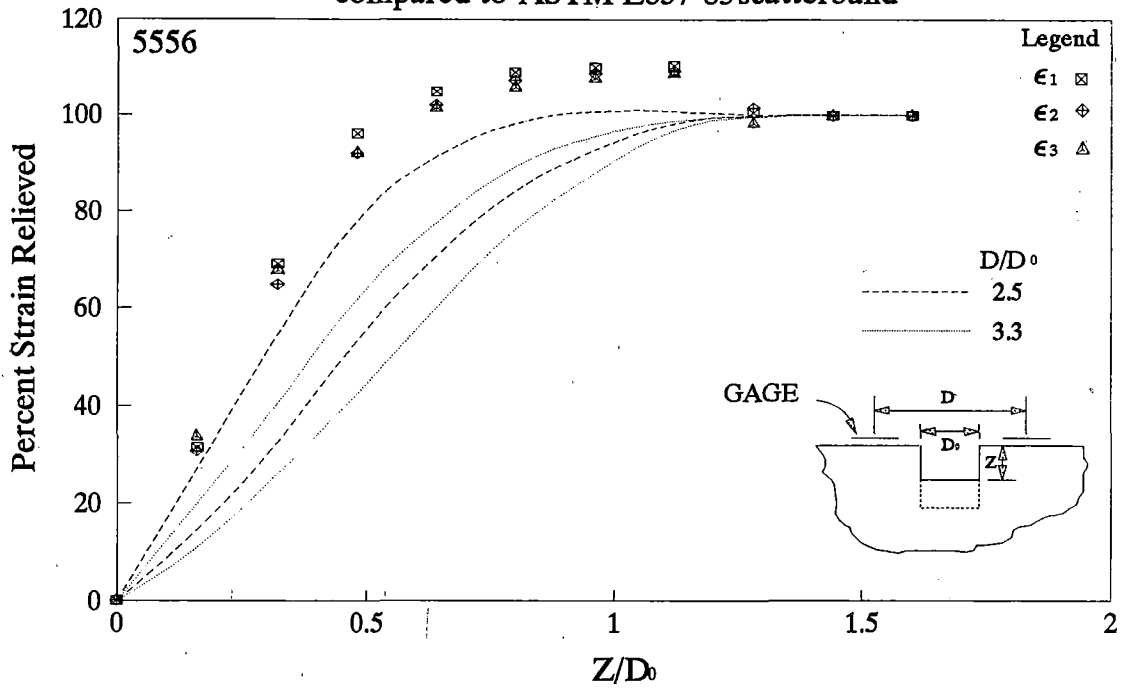
Saw Cut Data



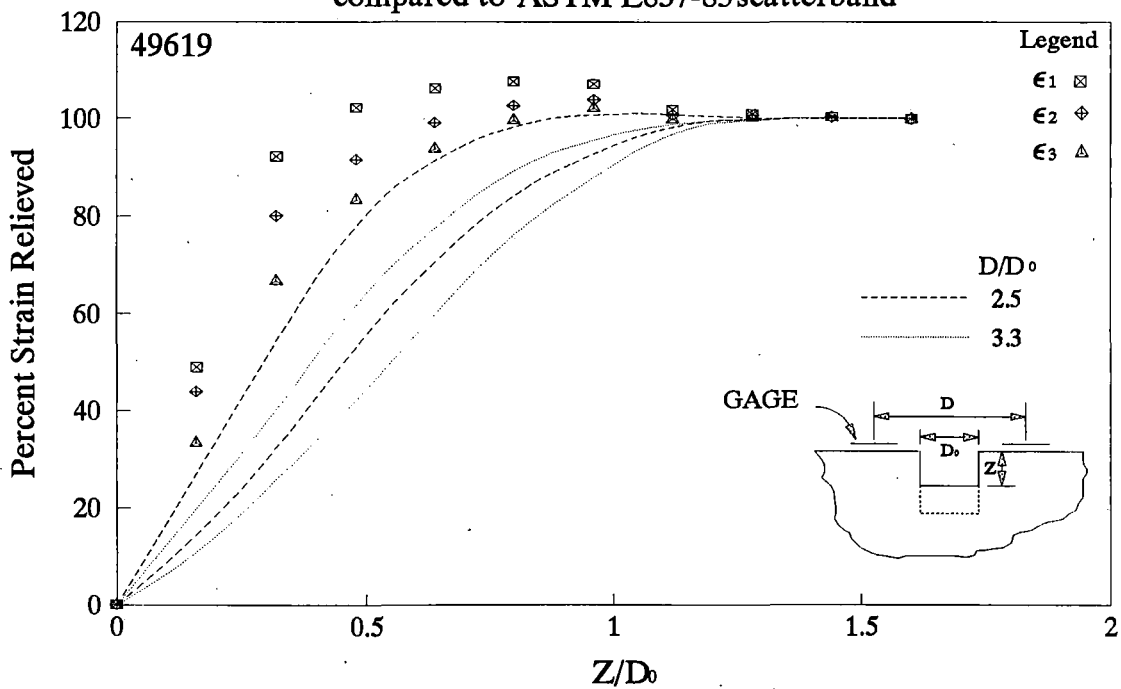
APPENDIX G

HOLE-DRILLING STRAIN-GAGE DATA ANALYSIS

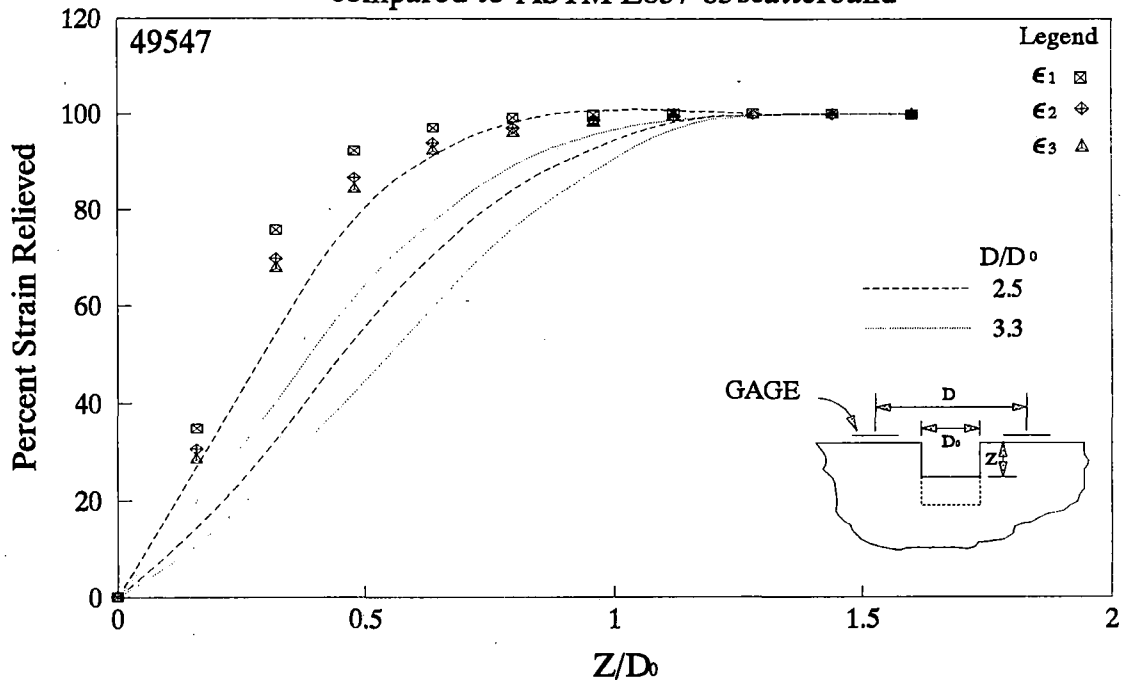
Normalized Relieved Strains compared to ASTM E837-85 scatterband



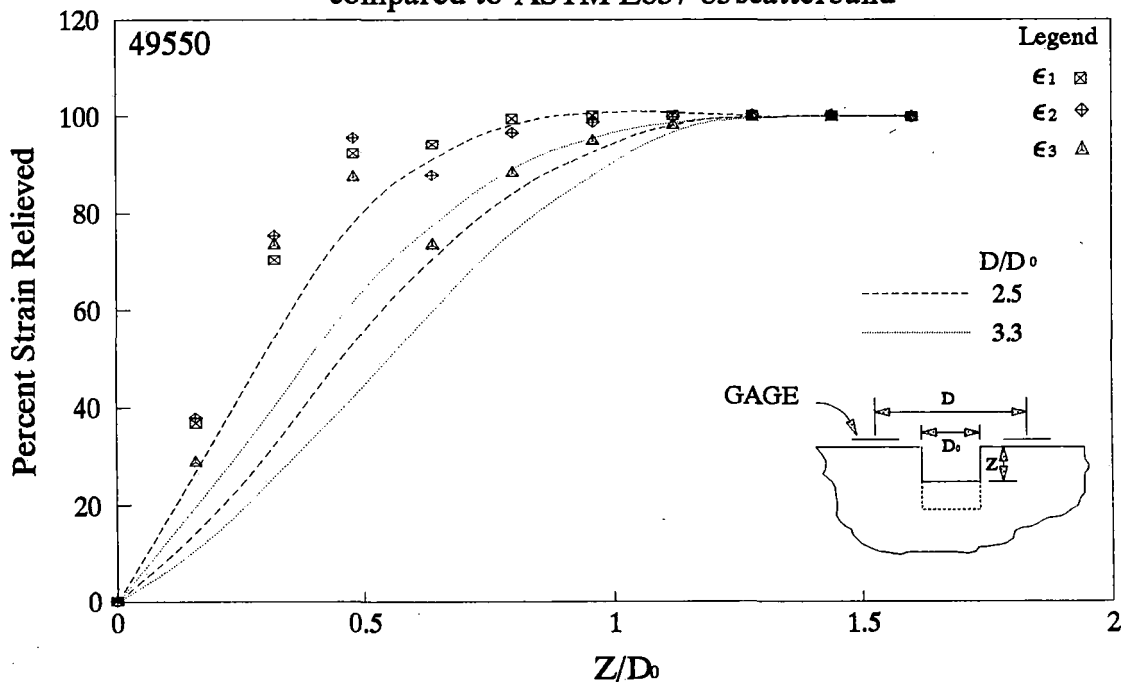
Normalized Relieved Strains compared to ASTM E837-85 scatterband



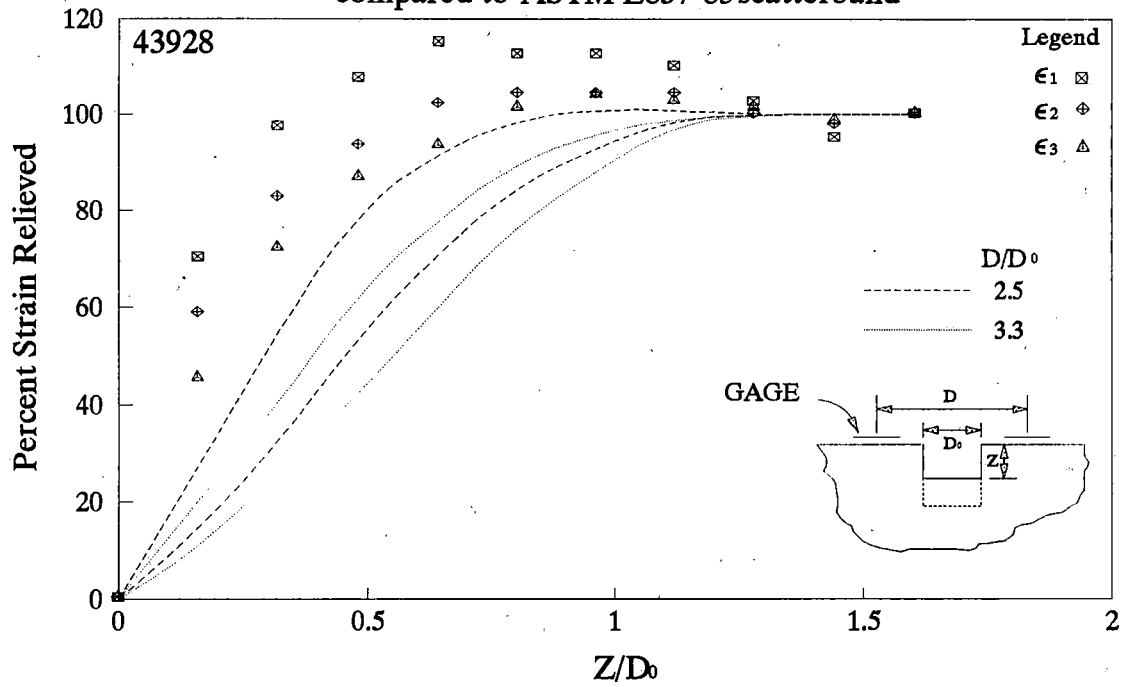
Normalized Relieved Strains compared to ASTM E837-85 scatterband



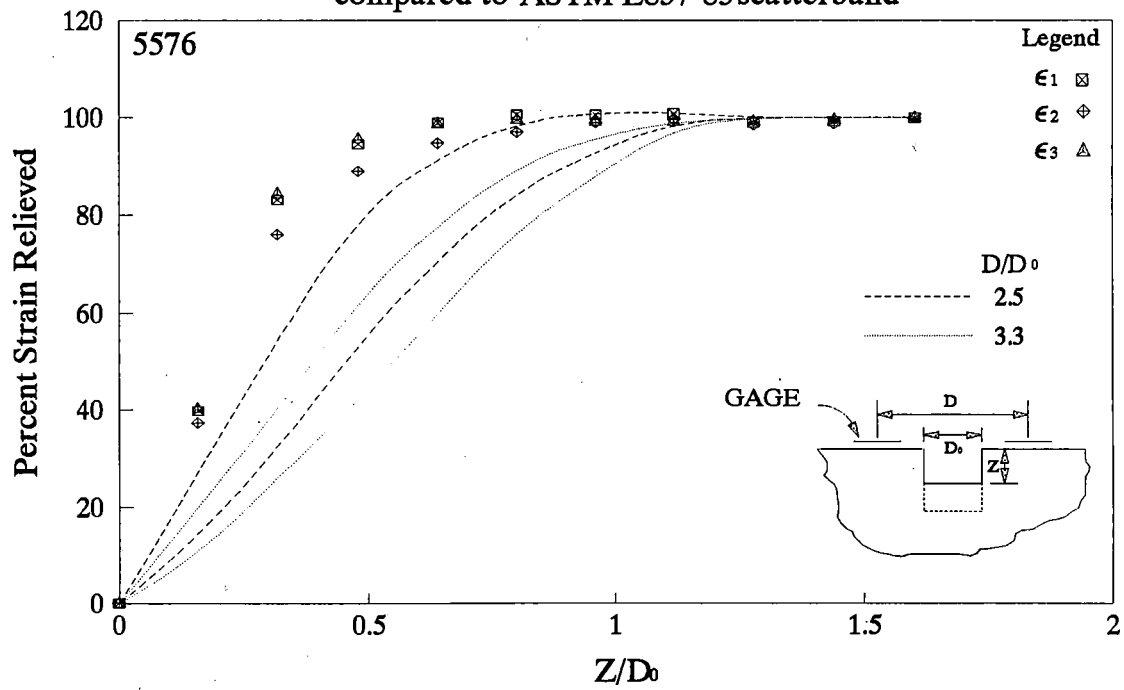
Normalized Relieved Strains compared to ASTM E837-85 scatterband



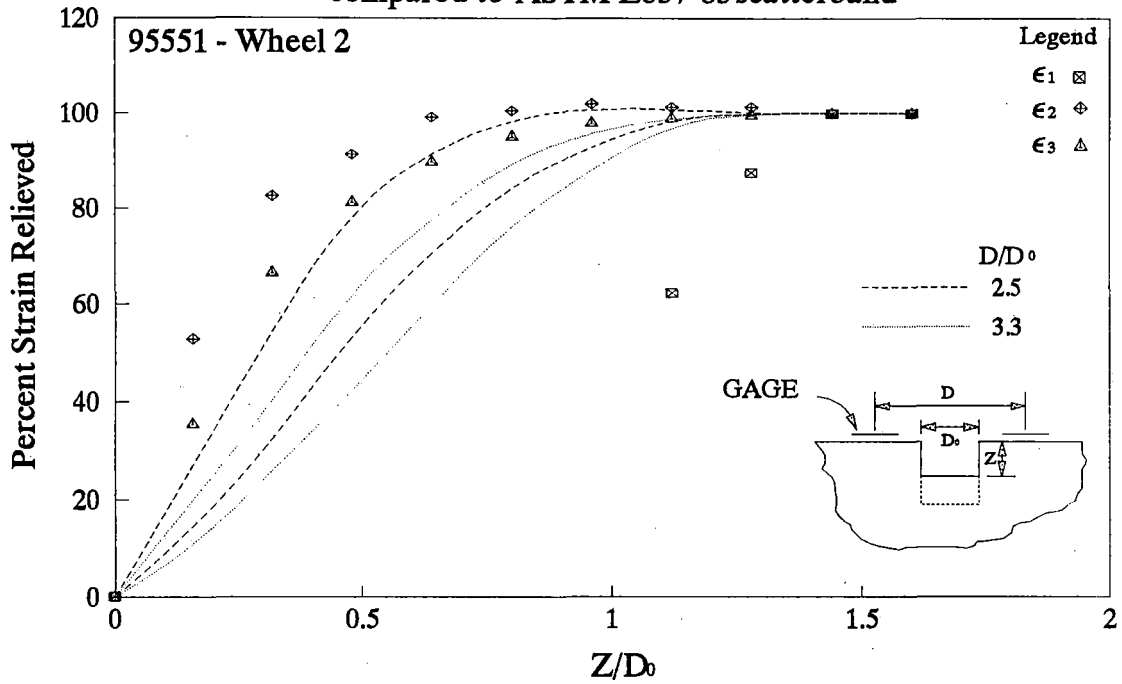
Normalized Relieved Strains compared to ASTM E837-85 scatterband



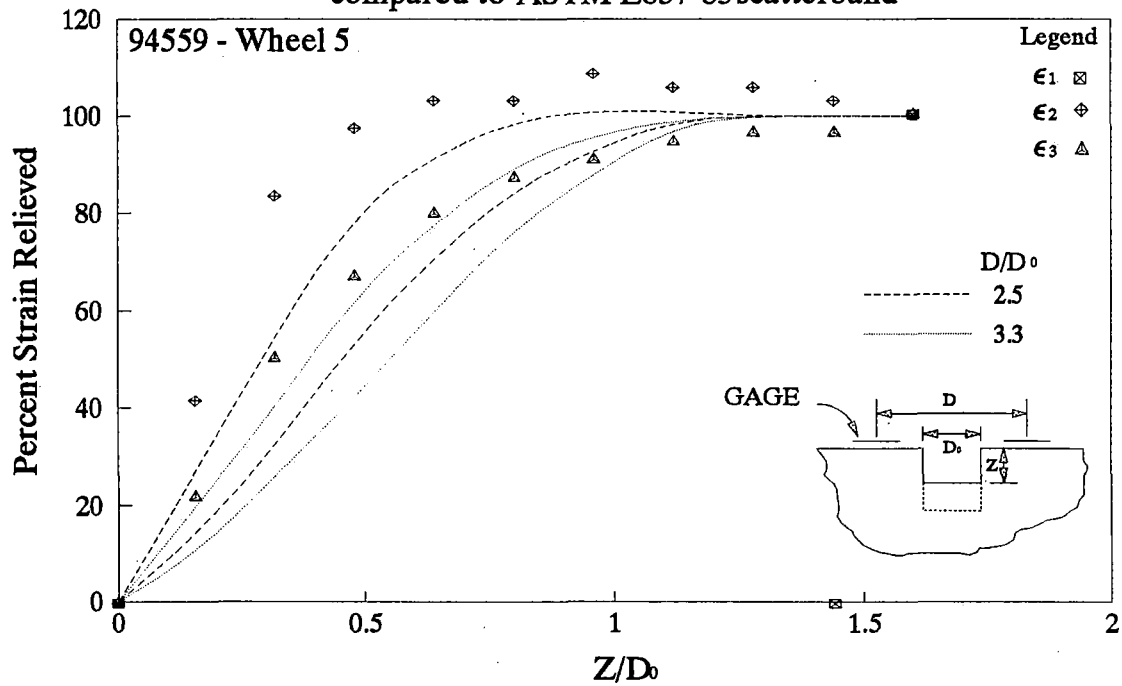
Normalized Relieved Strains compared to ASTM E837-85 scatterband



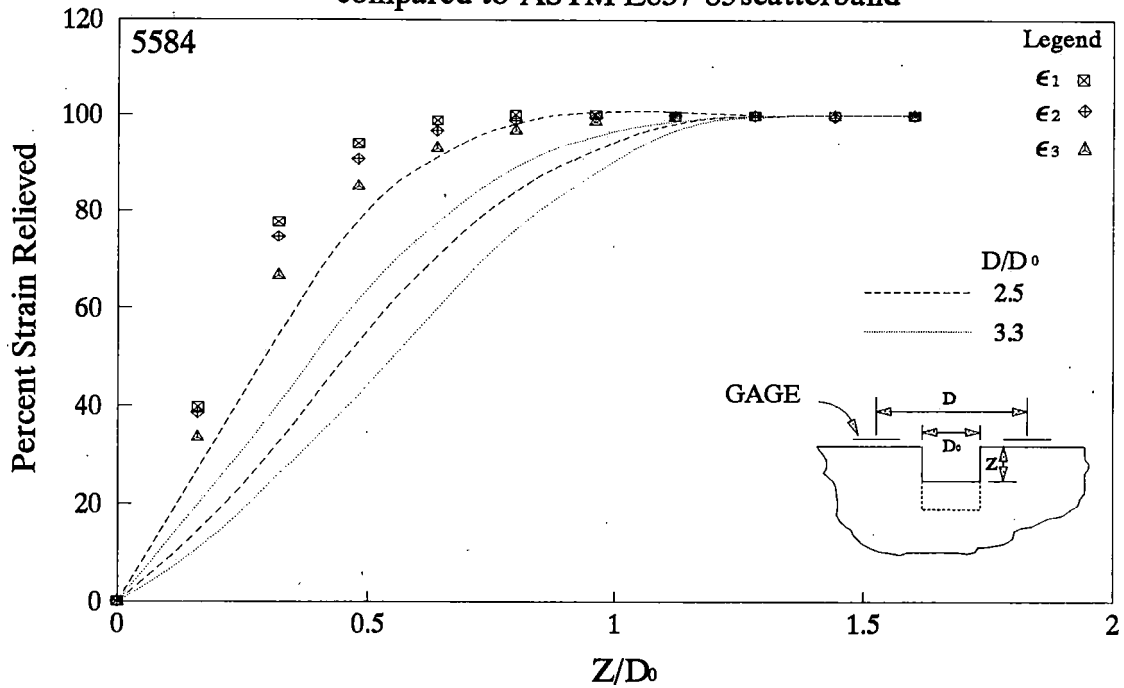
Normalized Relieved Strains compared to ASTM E837-85 scatterband



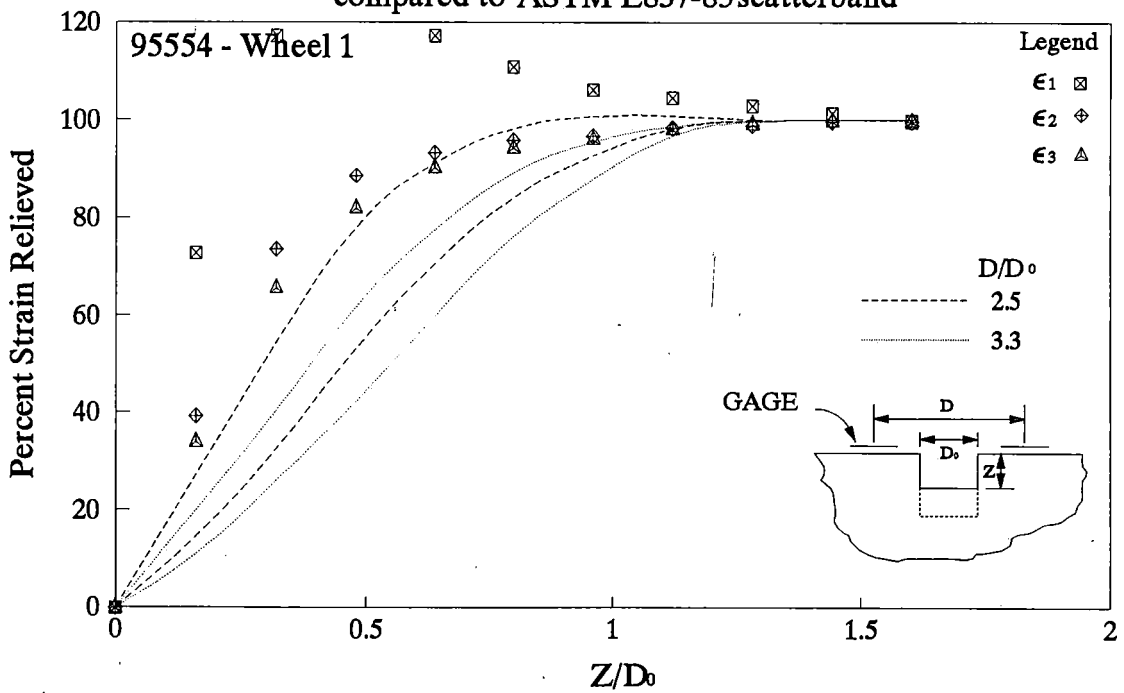
Normalized Relieved Strains compared to ASTM E837-85 scatterband



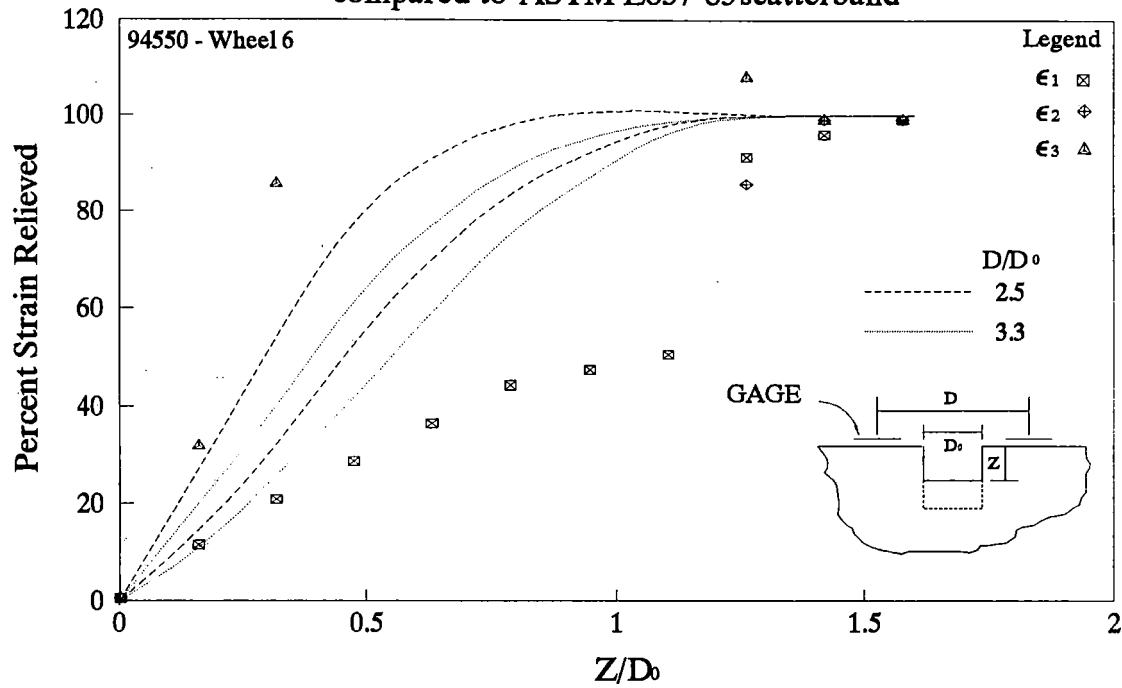
Normalized Relieved Strains compared to ASTM E837-85 scatterband



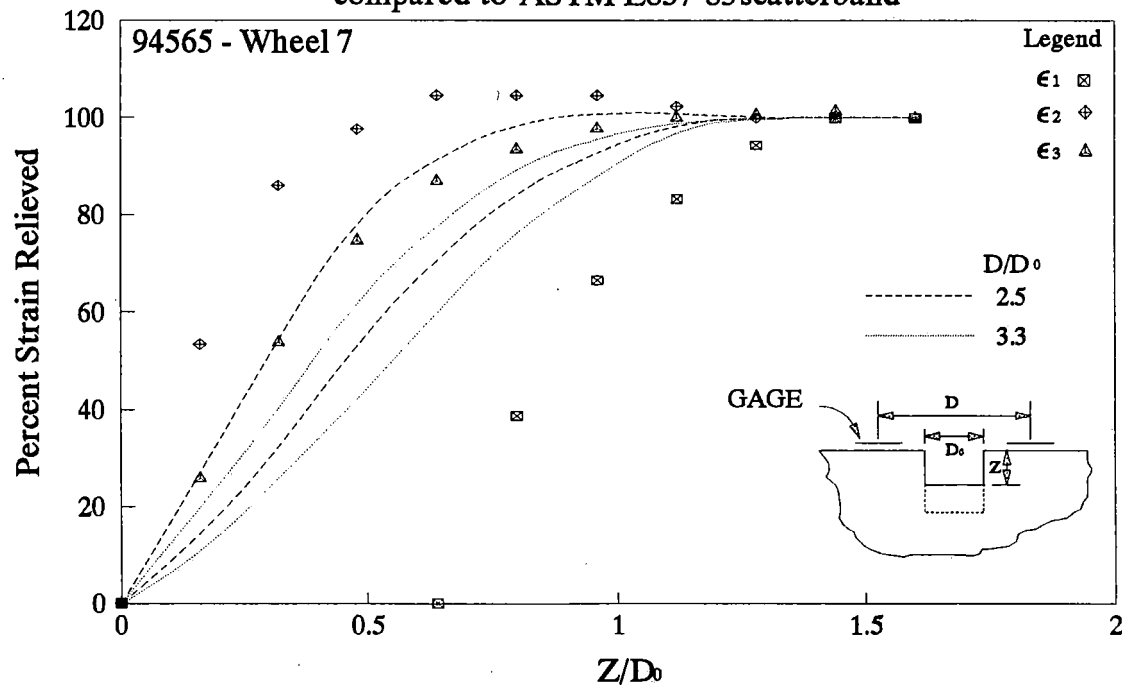
Normalized Relieved Strains compared to ASTM E837-85 scatterband



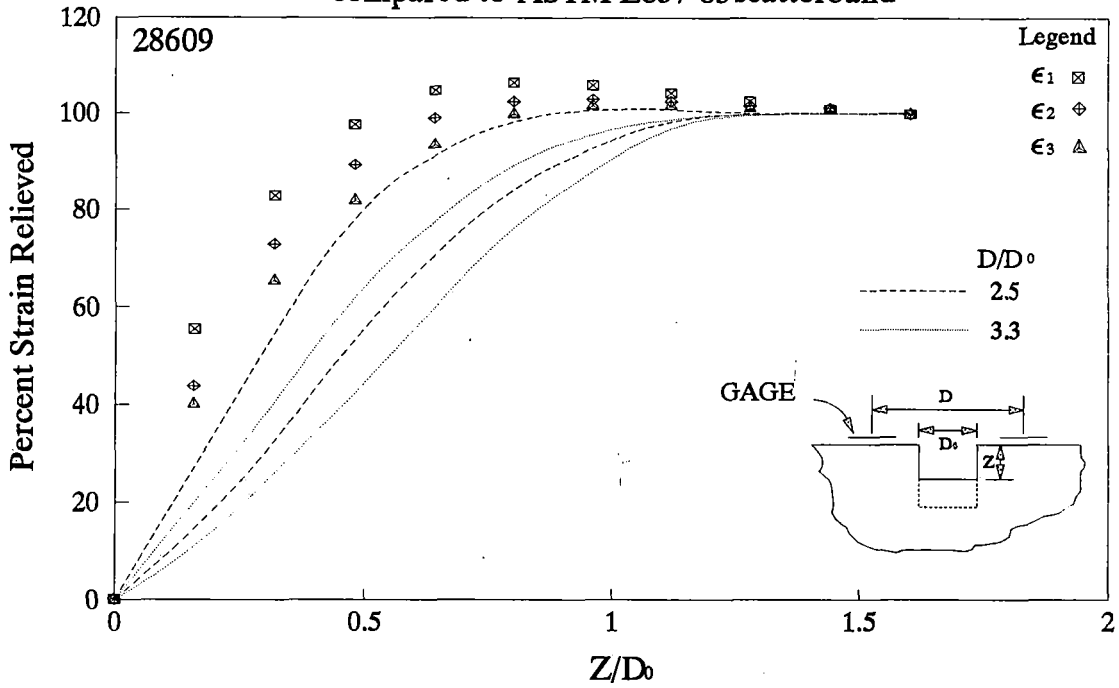
Normalized Relieved Strains compared to ASTM E837-85 scatterband



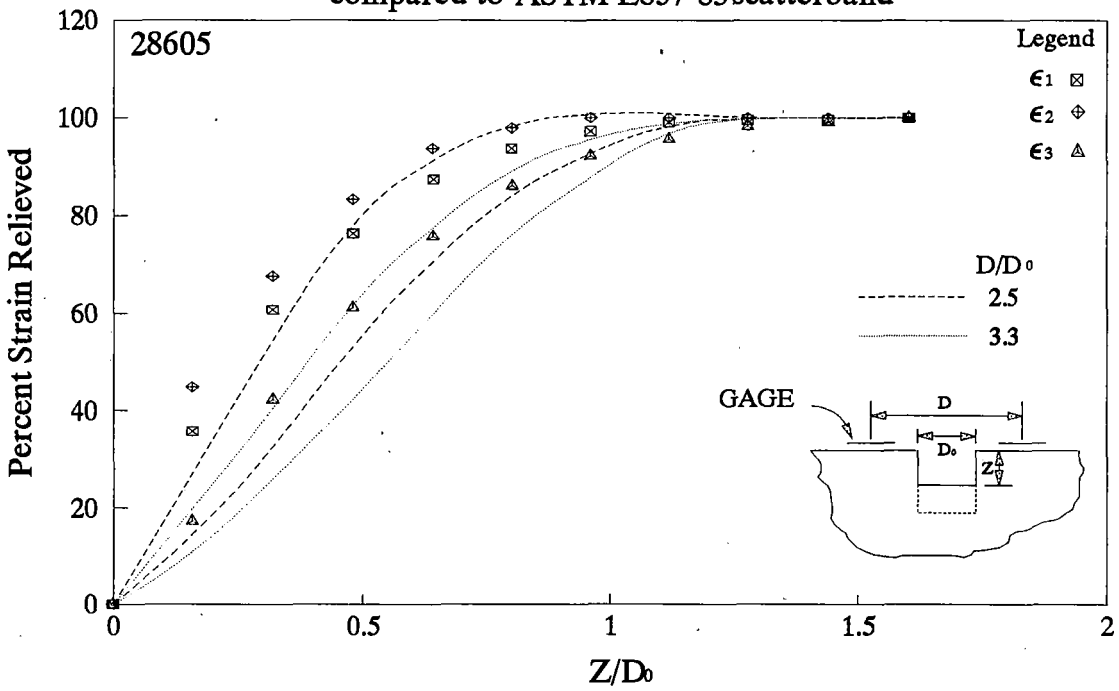
Normalized Relieved Strains compared to ASTM E837-85 scatterband



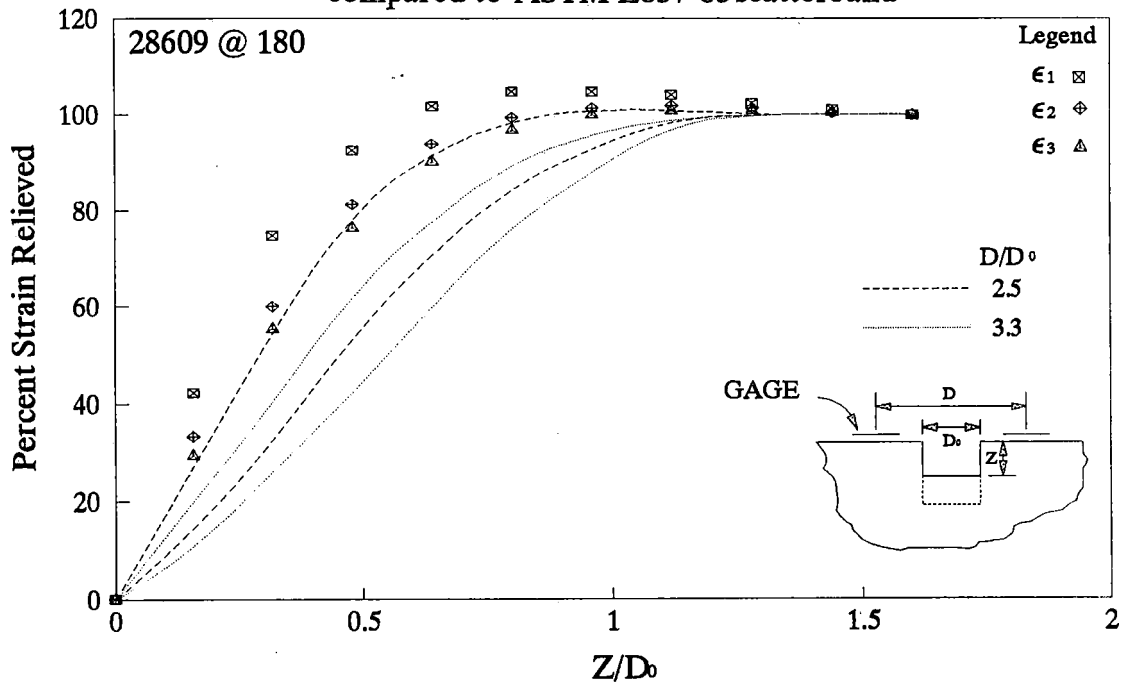
Normalized Relieved Strains compared to ASTM E837-85 scatterband



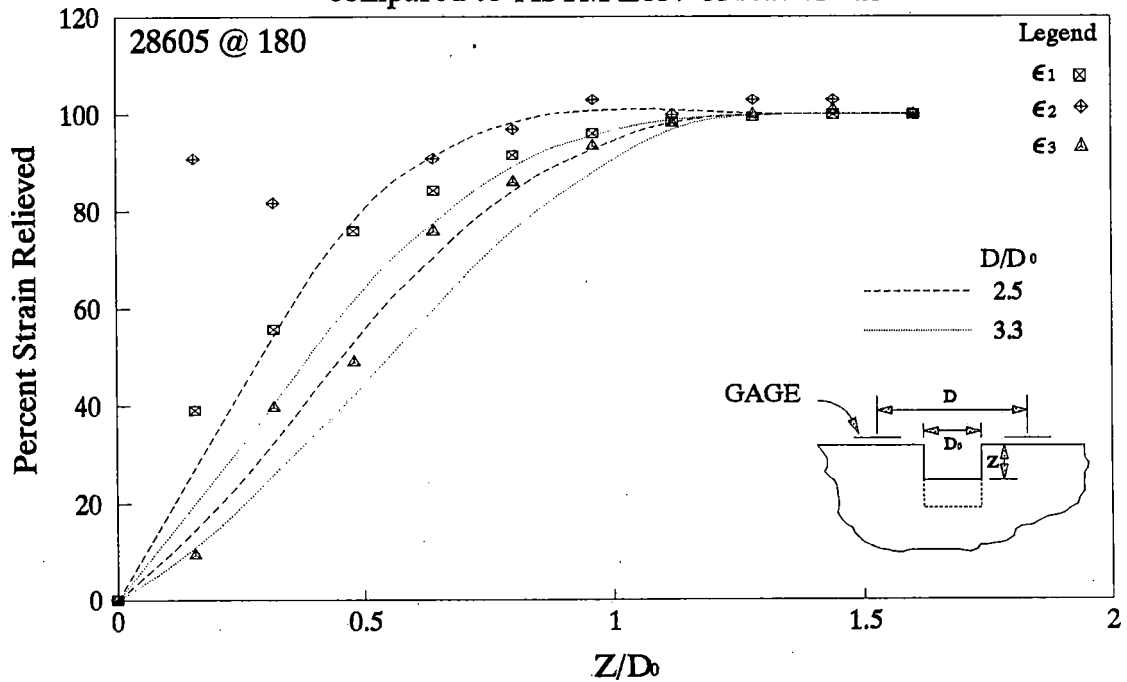
Normalized Relieved Strains compared to ASTM E837-85 scatterband



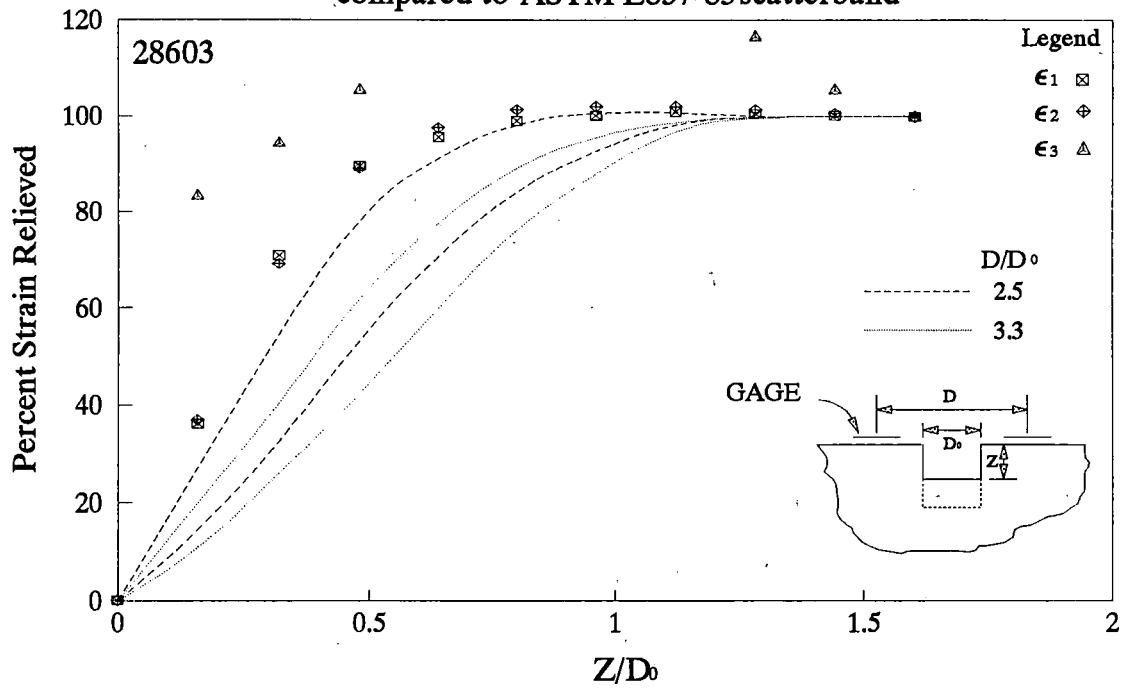
Normalized Relieved Strains compared to ASTM E837-85 scatterband



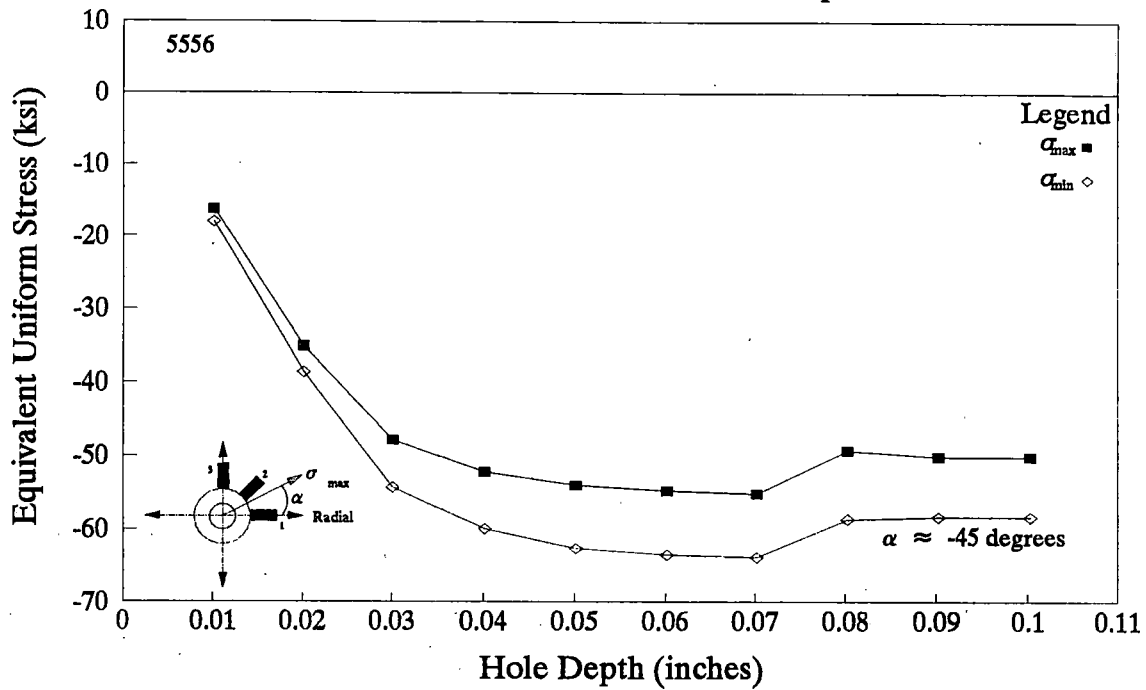
Normalized Relieved Strains compared to ASTM E837-85 scatterband



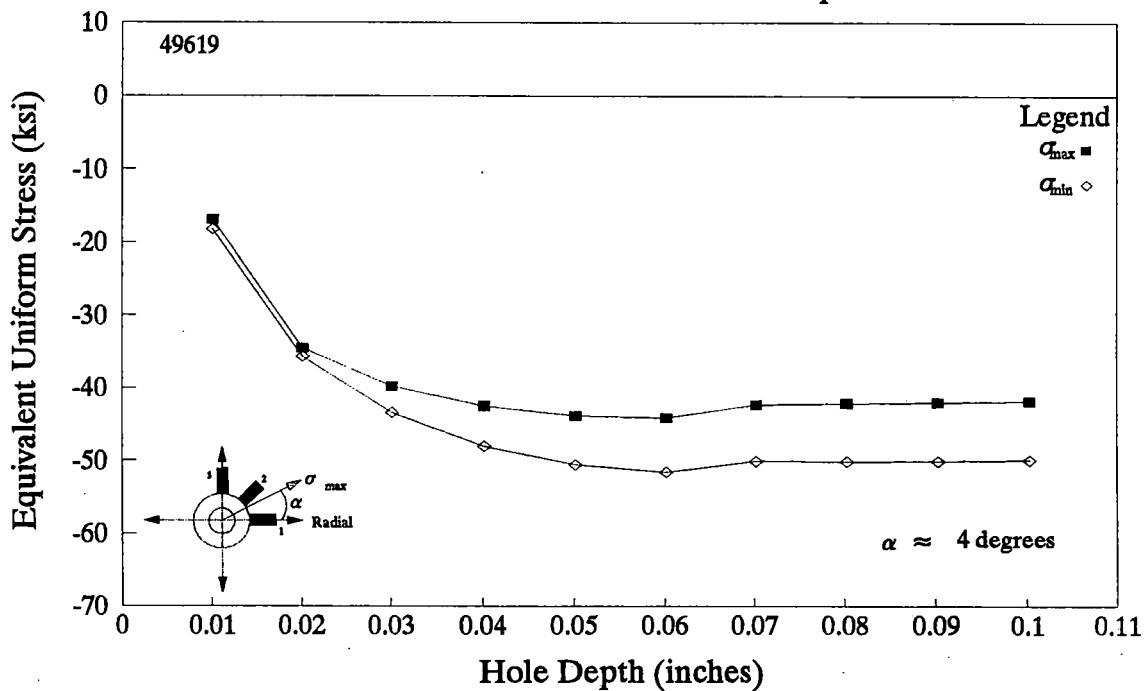
Normalized Relieved Strains compared to ASTM E837-85 scatterband



Computed Equivalent Uniform Stress as a function of absolute hole depth



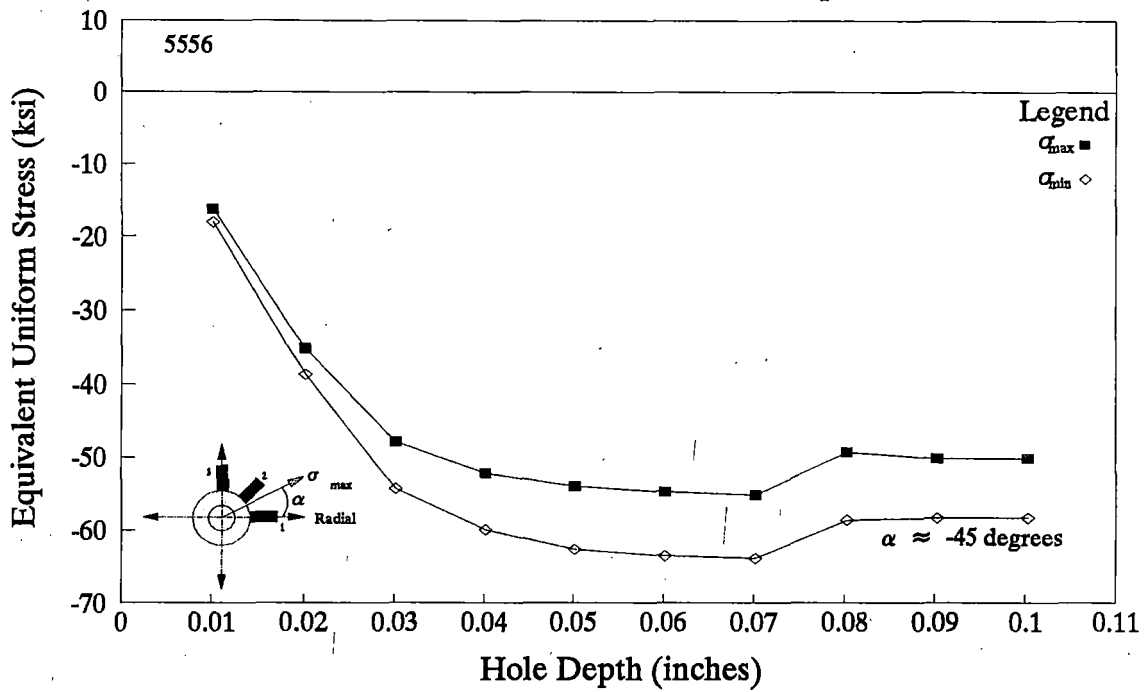
Computed Equivalent Uniform Stress as a function of absolute hole depth



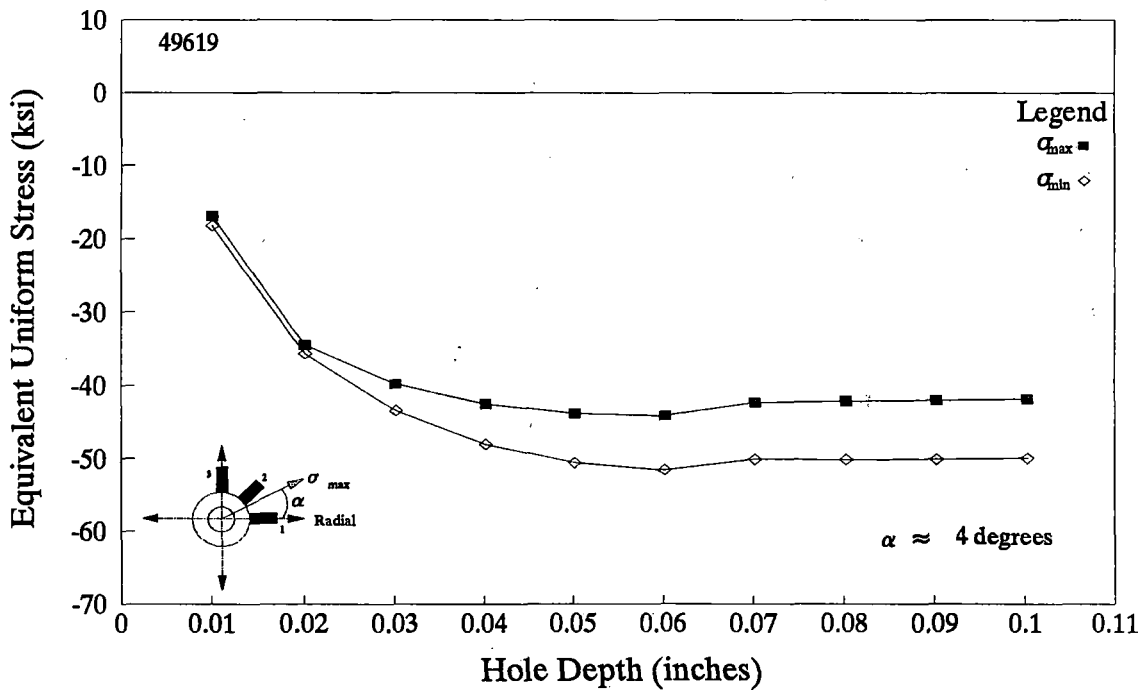
APPENDIX H

COMPUTED STRESSES FROM HOLE DRILLING STRAIN-GAGE DATA

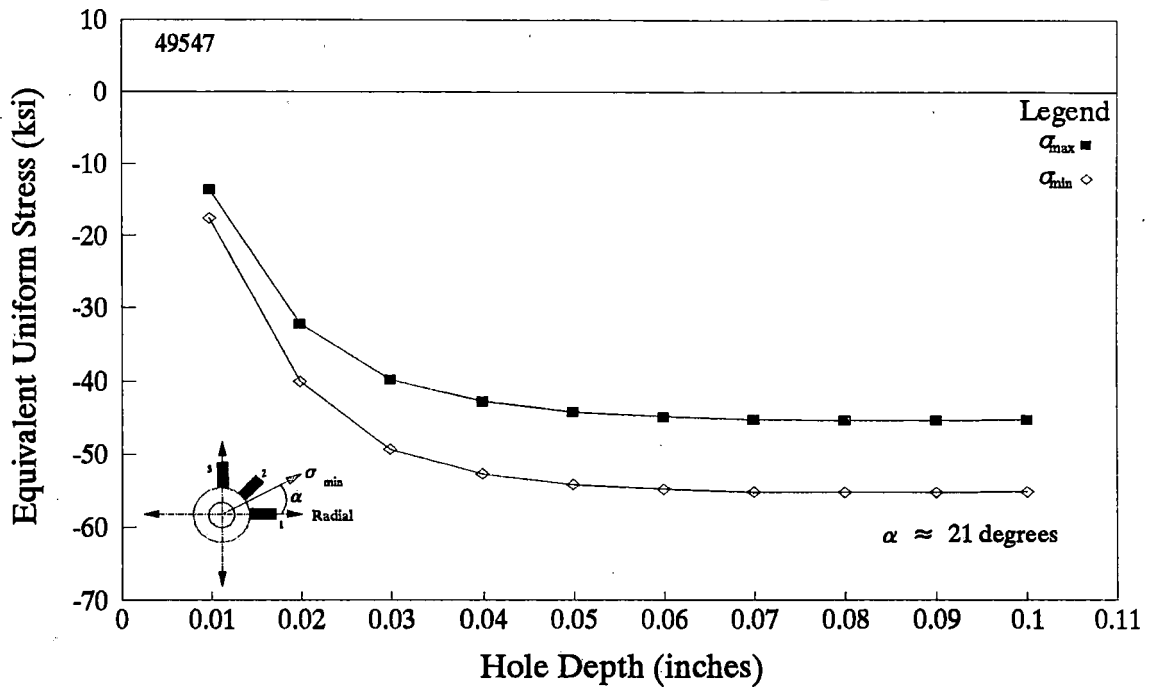
Computed Equivalent Uniform Stress as a function of absolute hole depth



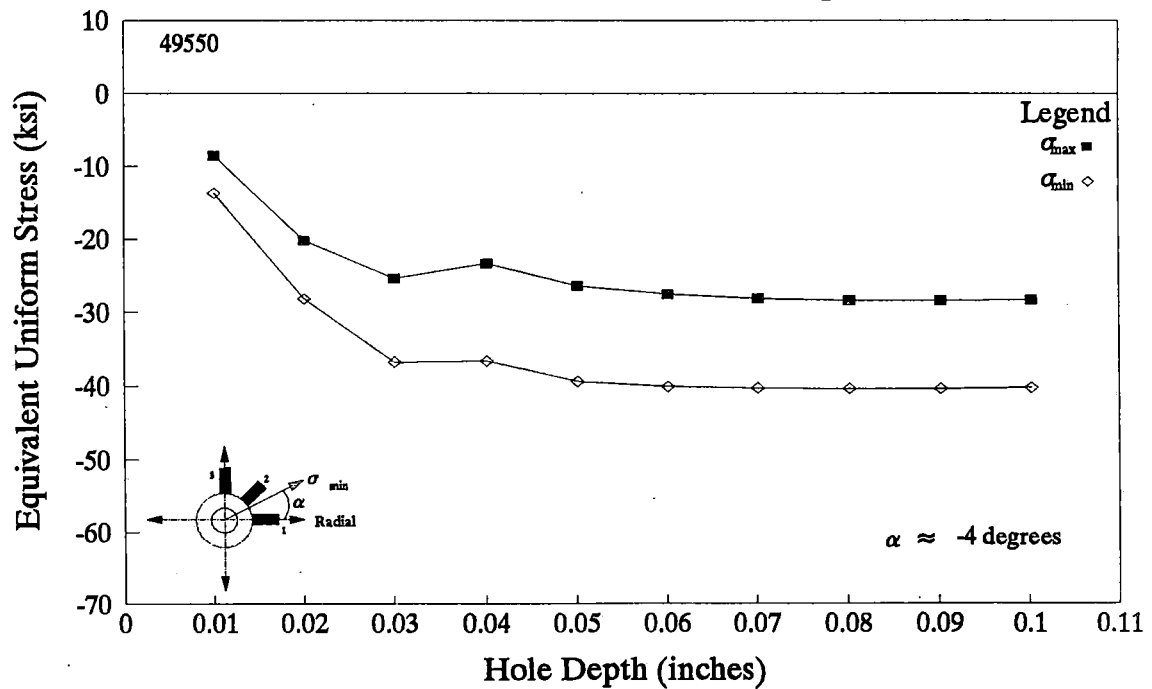
Computed Equivalent Uniform Stress as a function of absolute hole depth



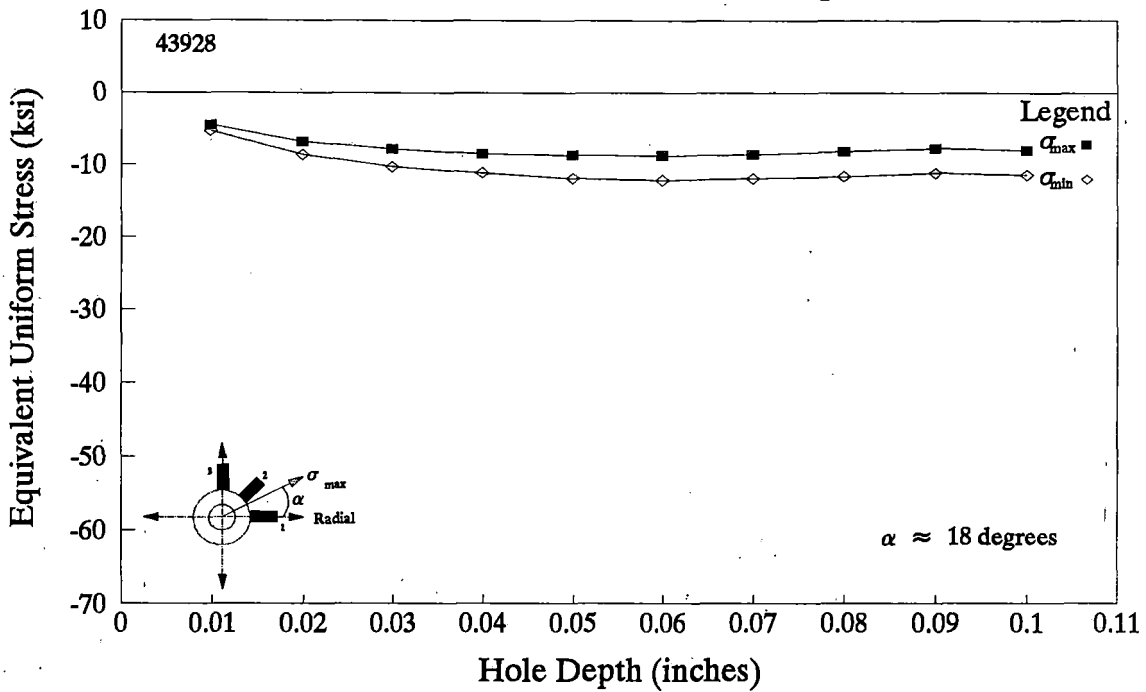
Computed Equivalent Uniform Stress as a function of absolute hole depth



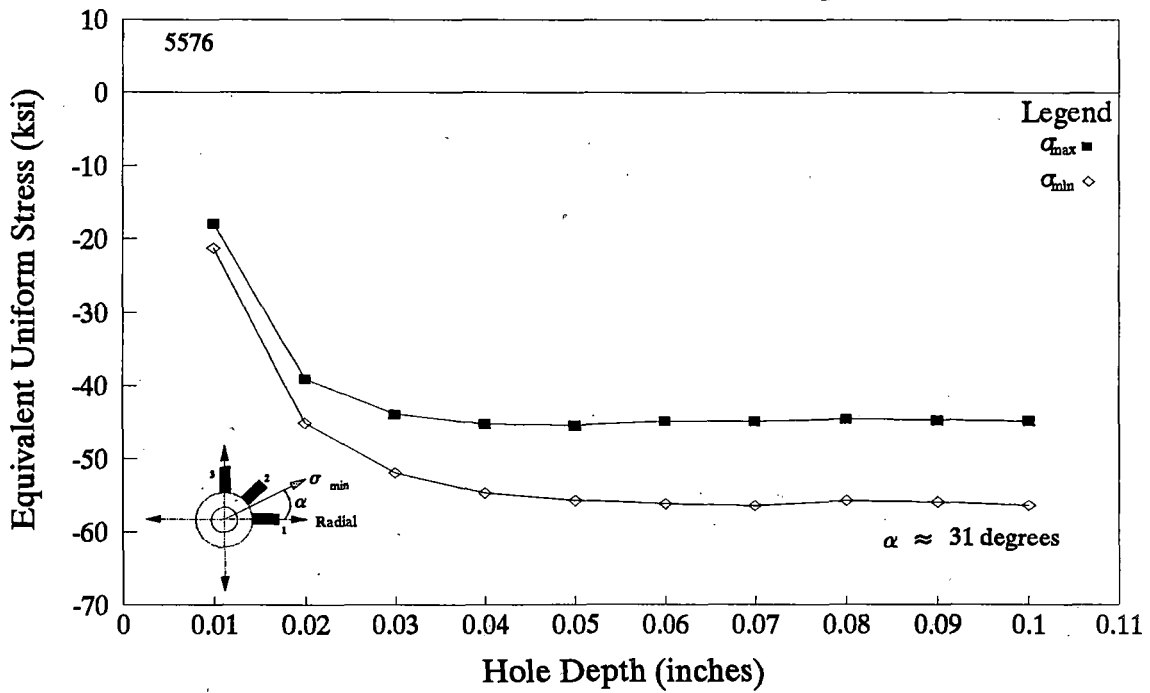
Computed Equivalent Uniform Stress as a function of absolute hole depth



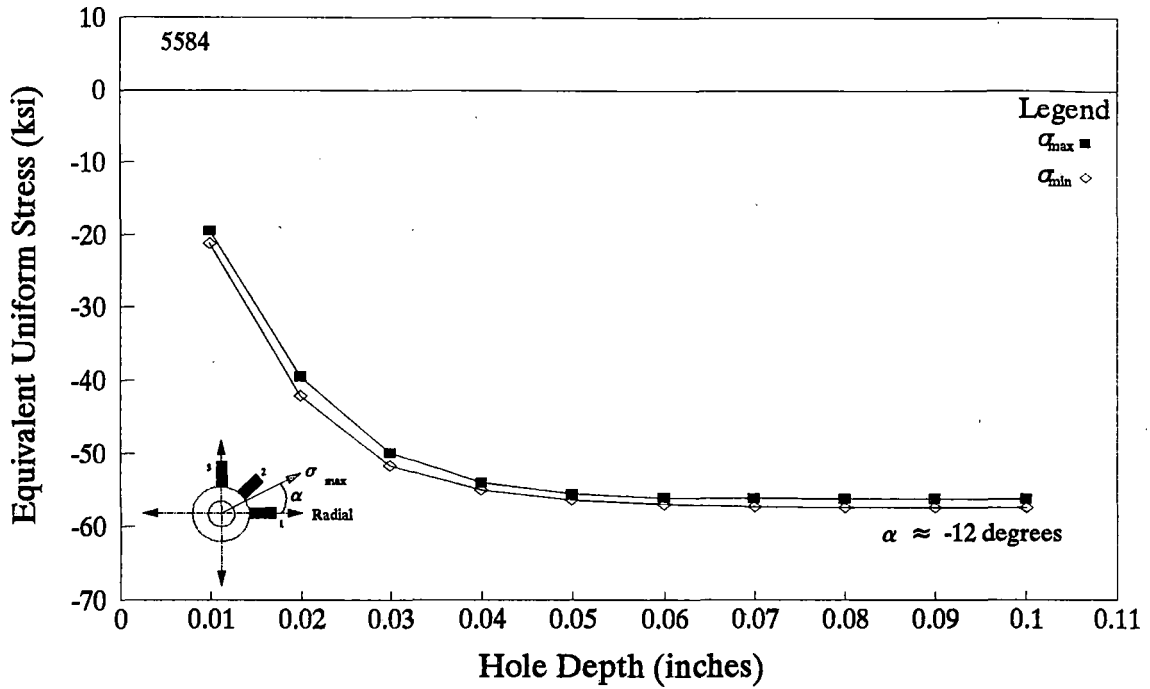
Computed Equivalent Uniform Stress as a function of absolute hole depth



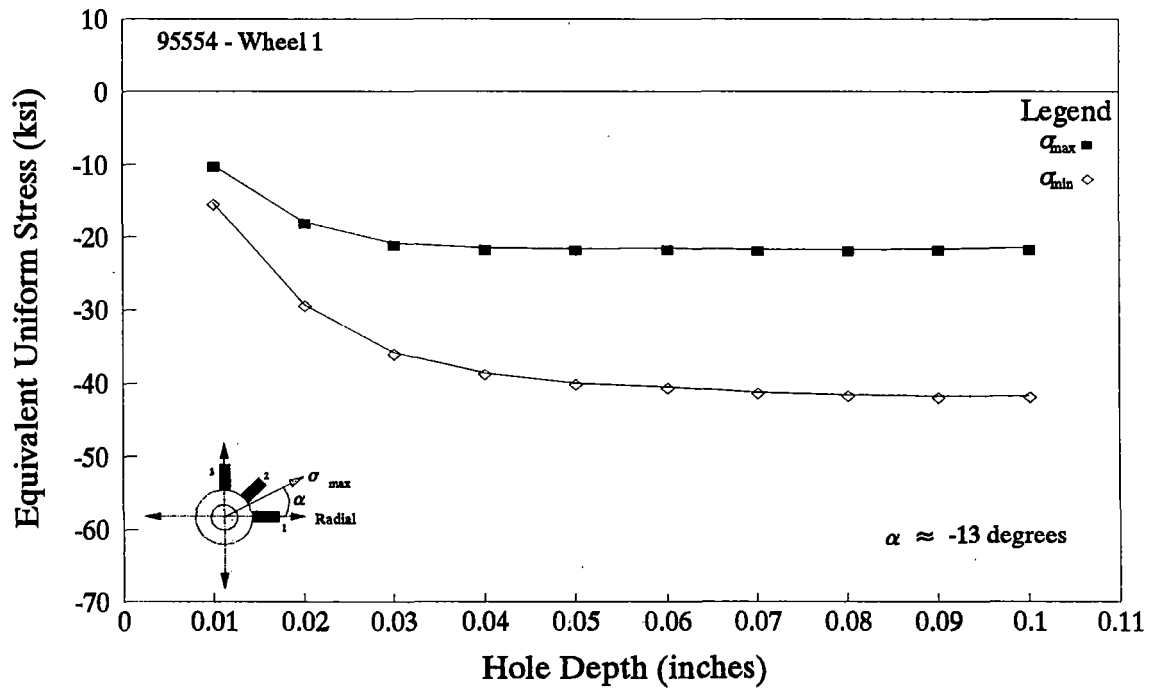
Computed Equivalent Uniform Stress as a function of absolute hole depth



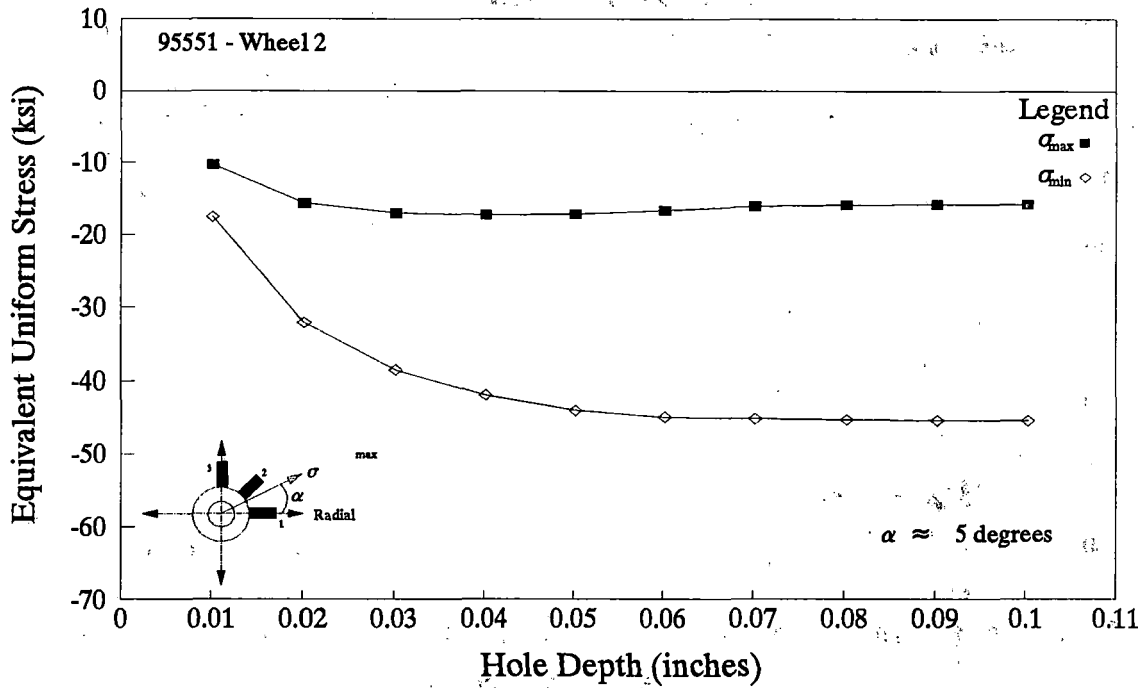
Computed Equivalent Uniform Stress as a function of absolute hole depth



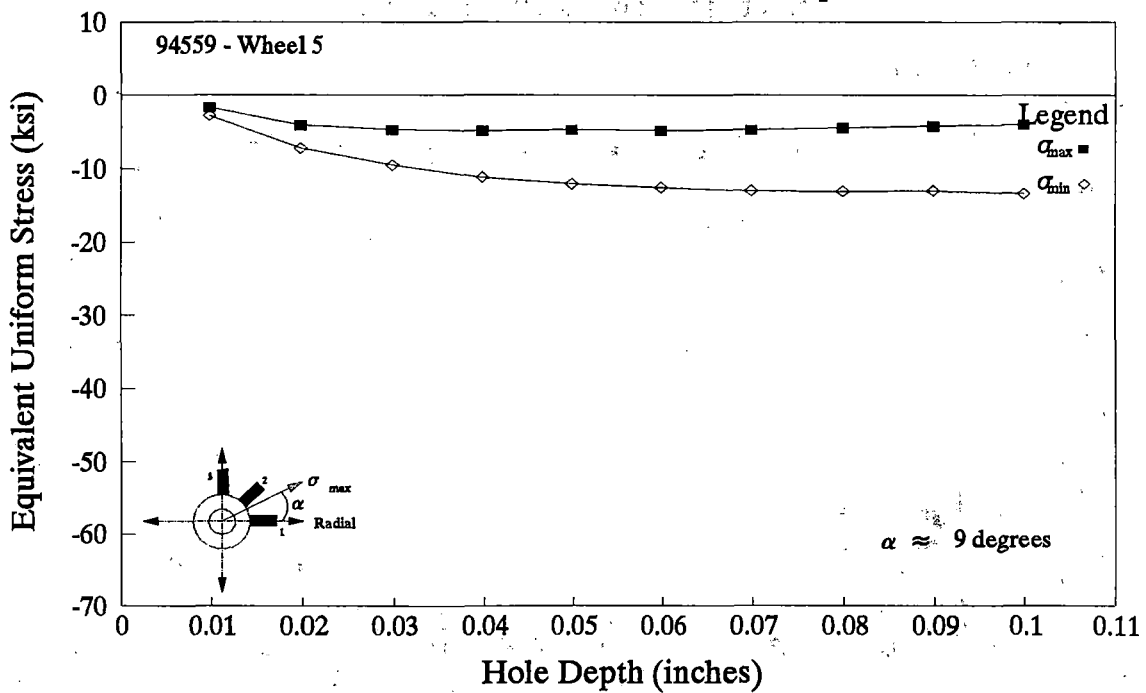
Computed Equivalent Uniform Stress as a function of absolute hole depth



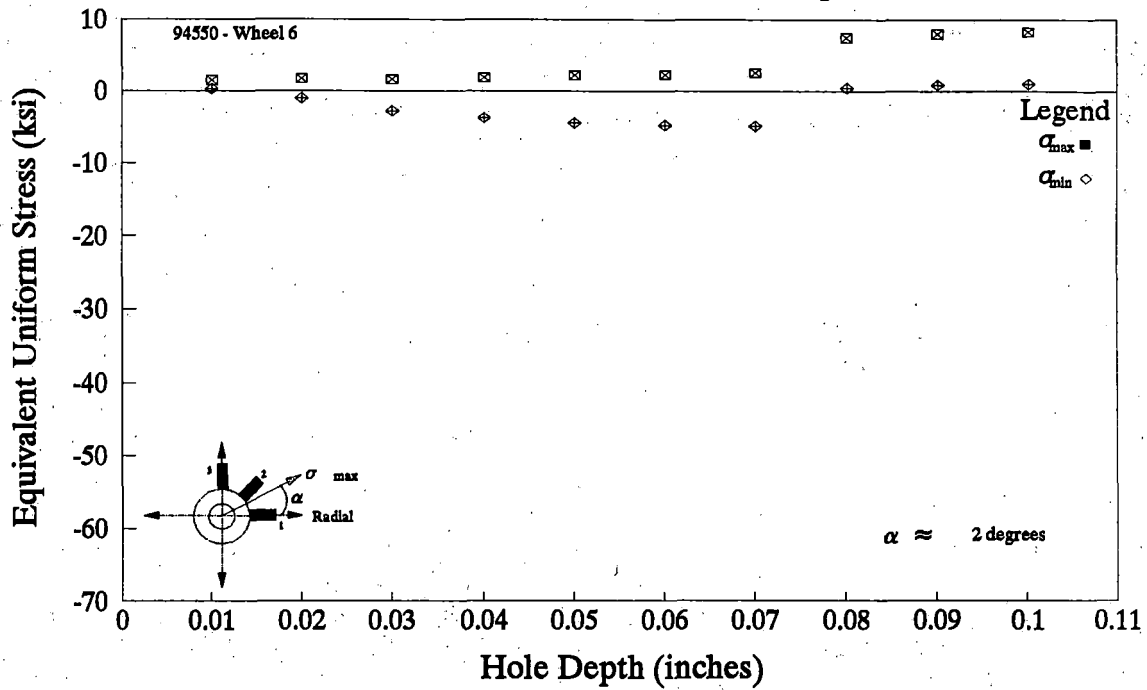
Computed Equivalent Uniform Stress as a function of absolute hole depth



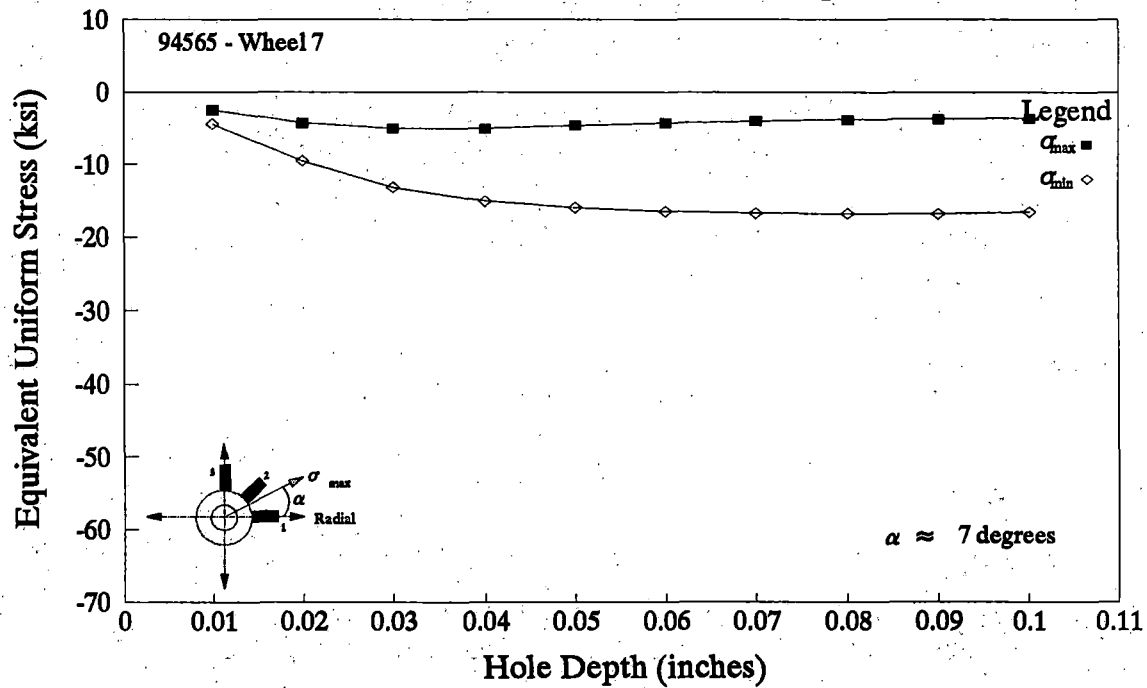
Computed Equivalent Uniform Stress as a function of absolute hole depth



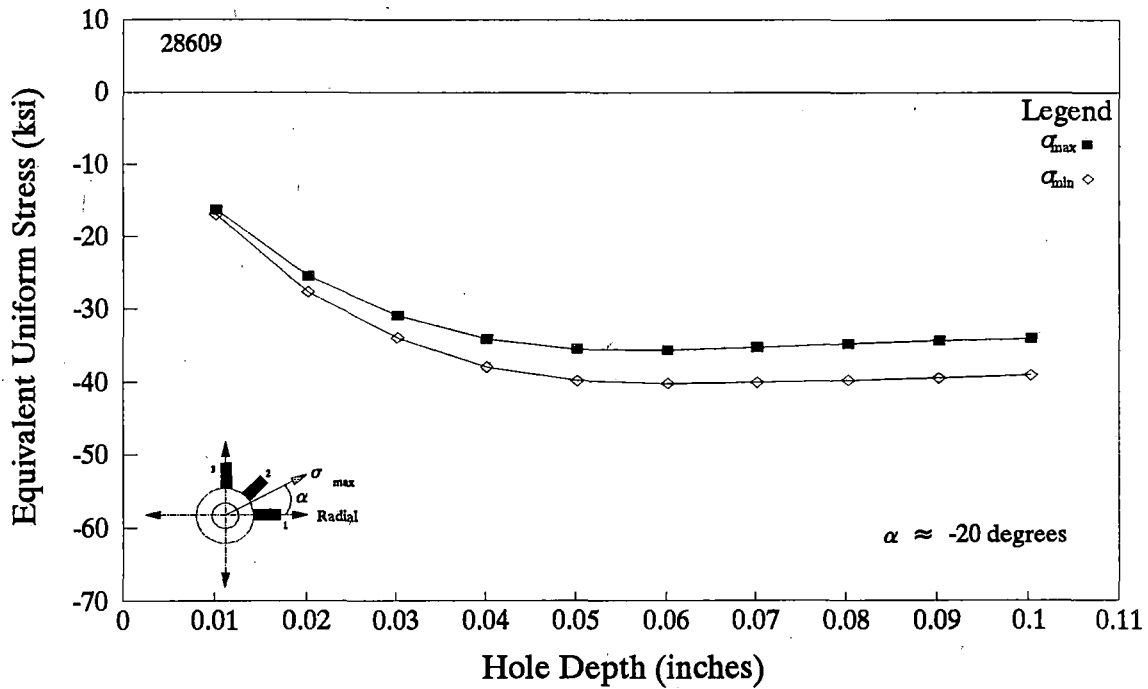
Computed Equivalent Uniform Stress as a function of absolute hole depth



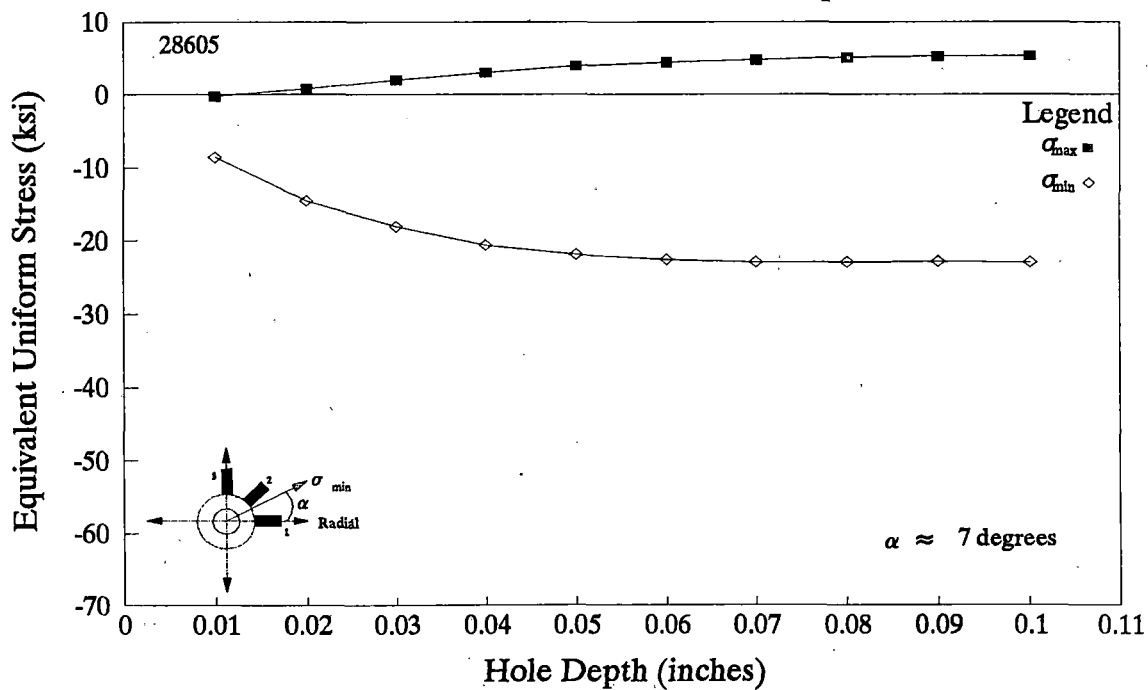
Computed Equivalent Uniform Stress as a function of absolute hole depth



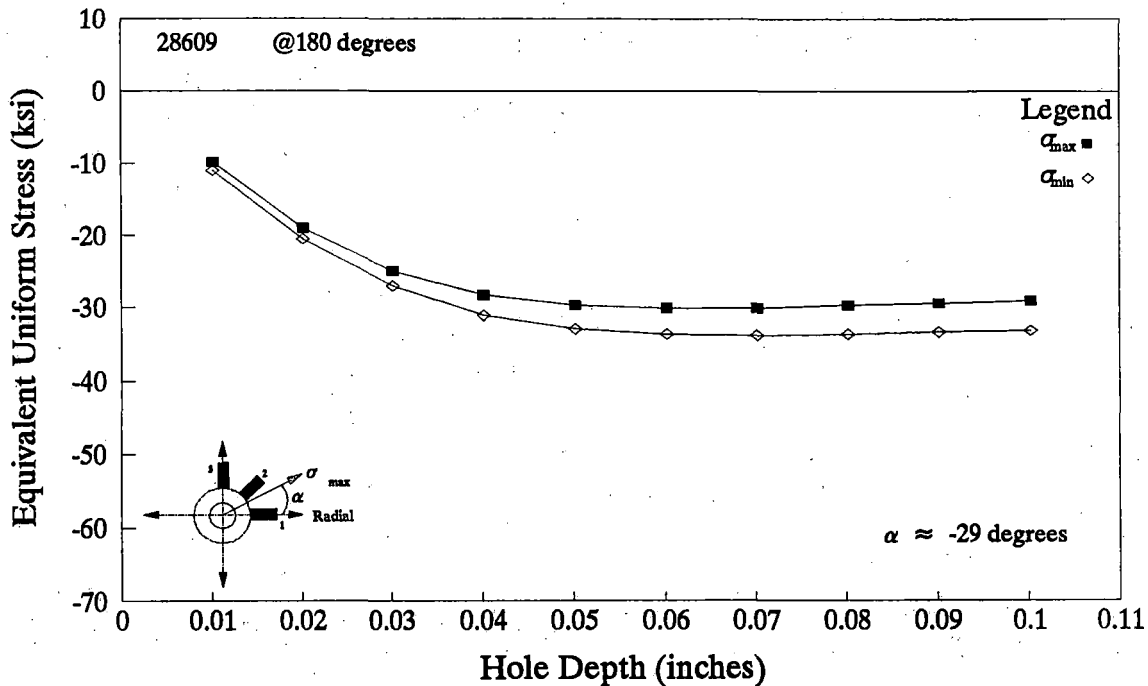
Computed Equivalent Uniform Stress as a function of absolute hole depth



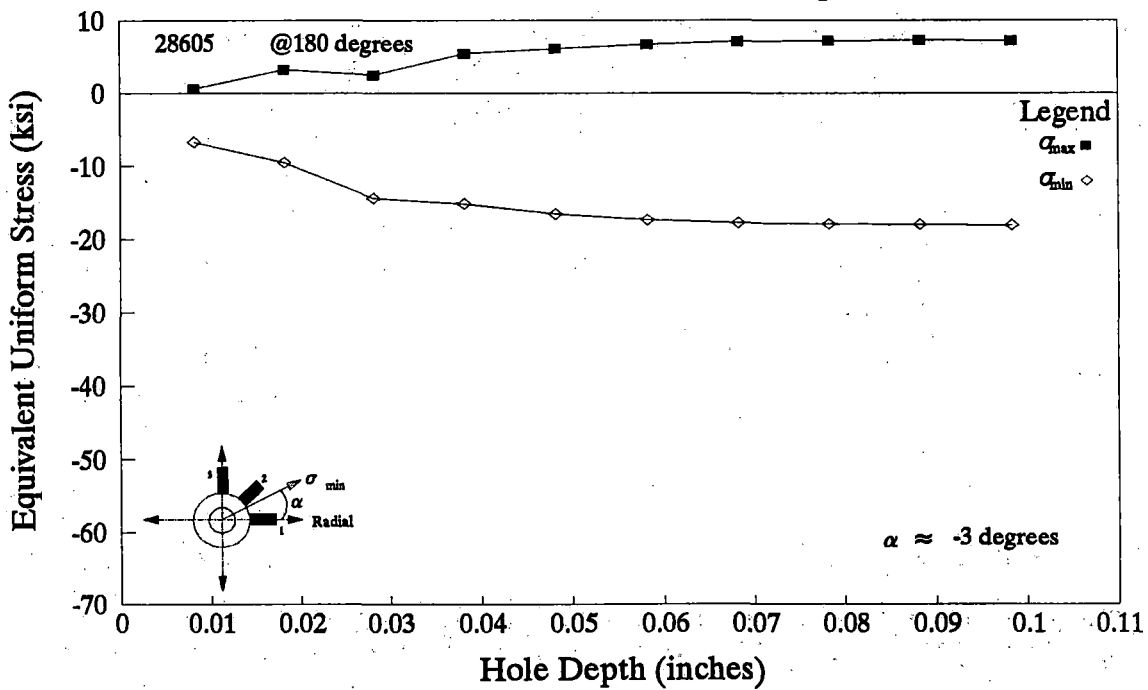
Computed Equivalent Uniform Stress as a function of absolute hole depth



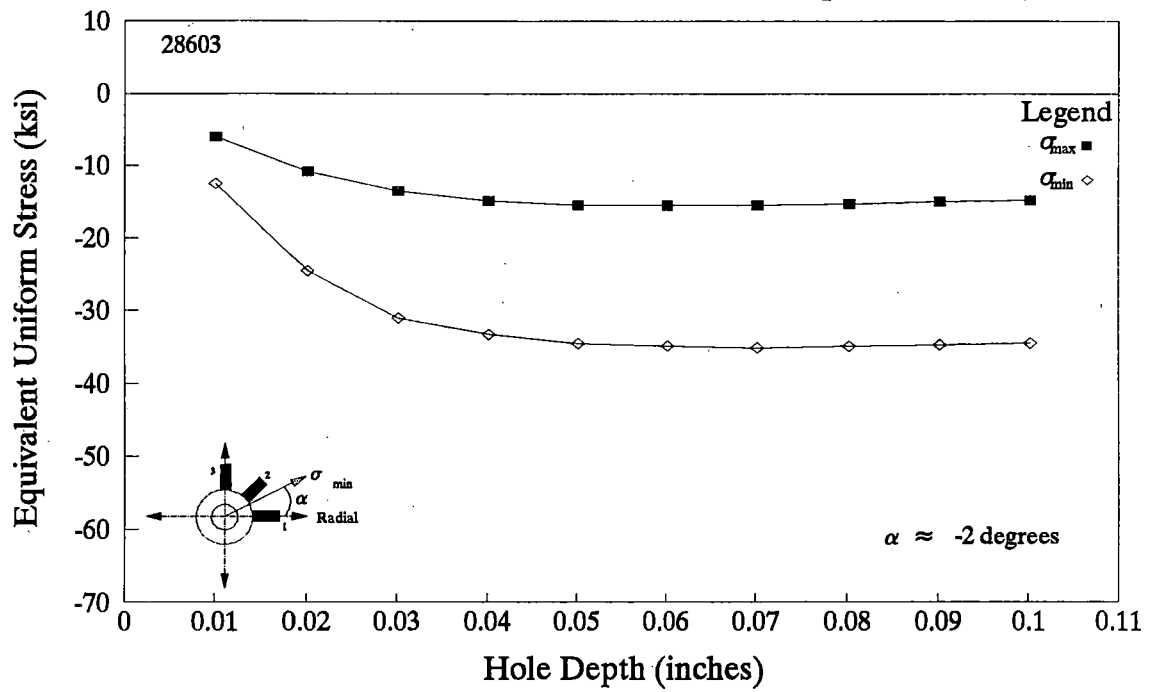
Computed Equivalent Uniform Stress as a function of absolute hole depth



Computed Equivalent Uniform Stress as a function of absolute hole depth



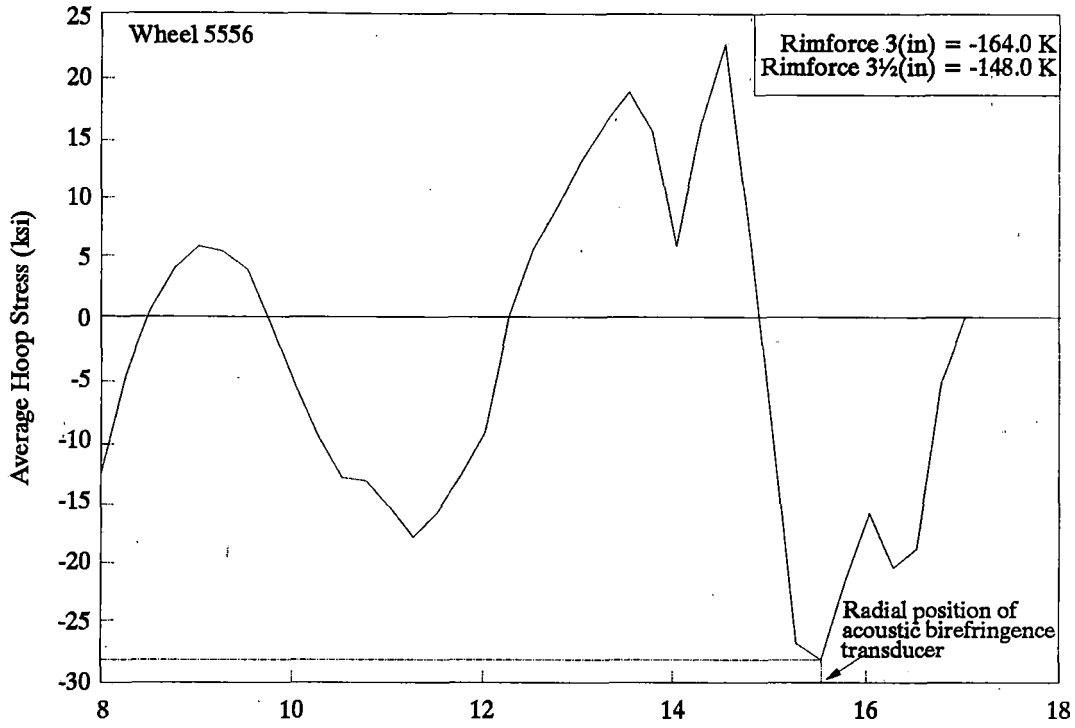
Computed Equivalent Uniform Stress as a function of absolute hole depth



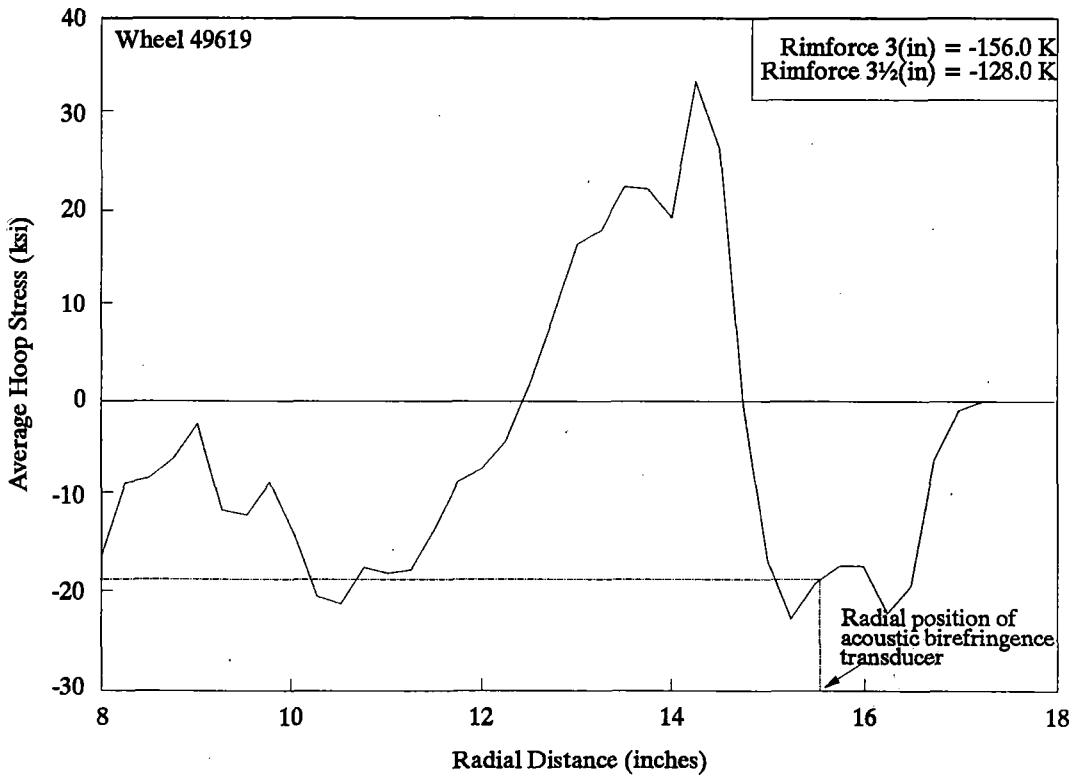
APPENDIX I

**RESIDUAL STRESSES COMPUTED FROM SAW-CUT DATA
USING TTC'S "CLOSED FORM" SOLUTION**

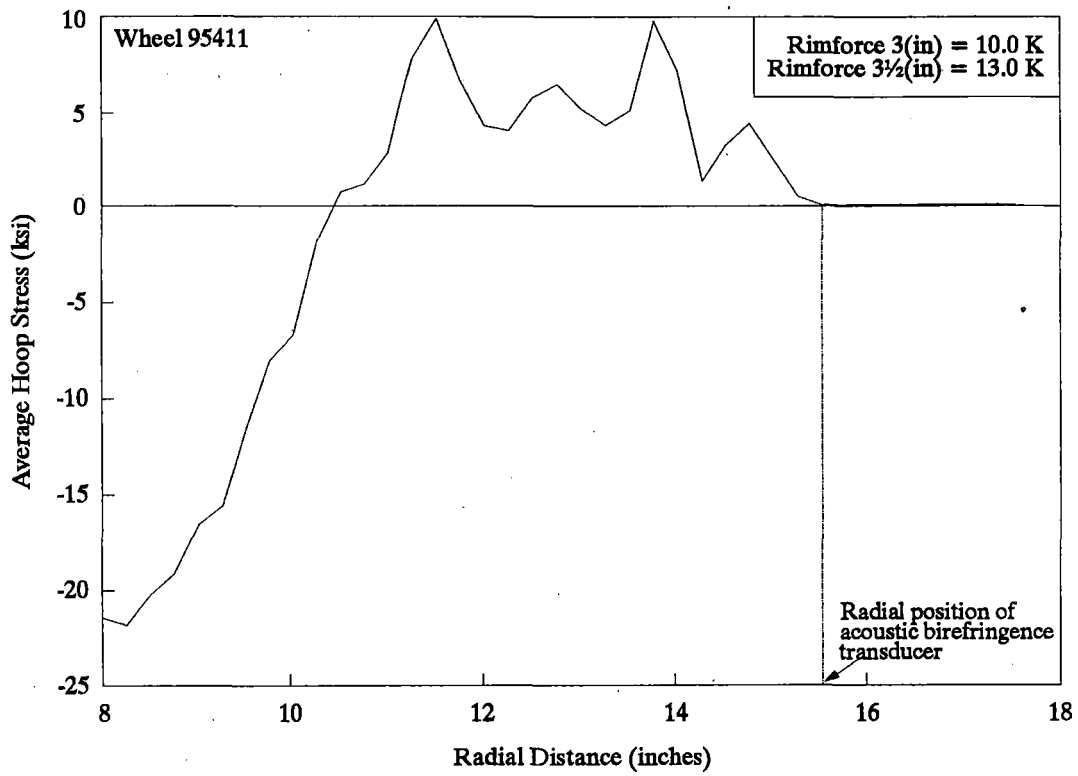
Computed Stress



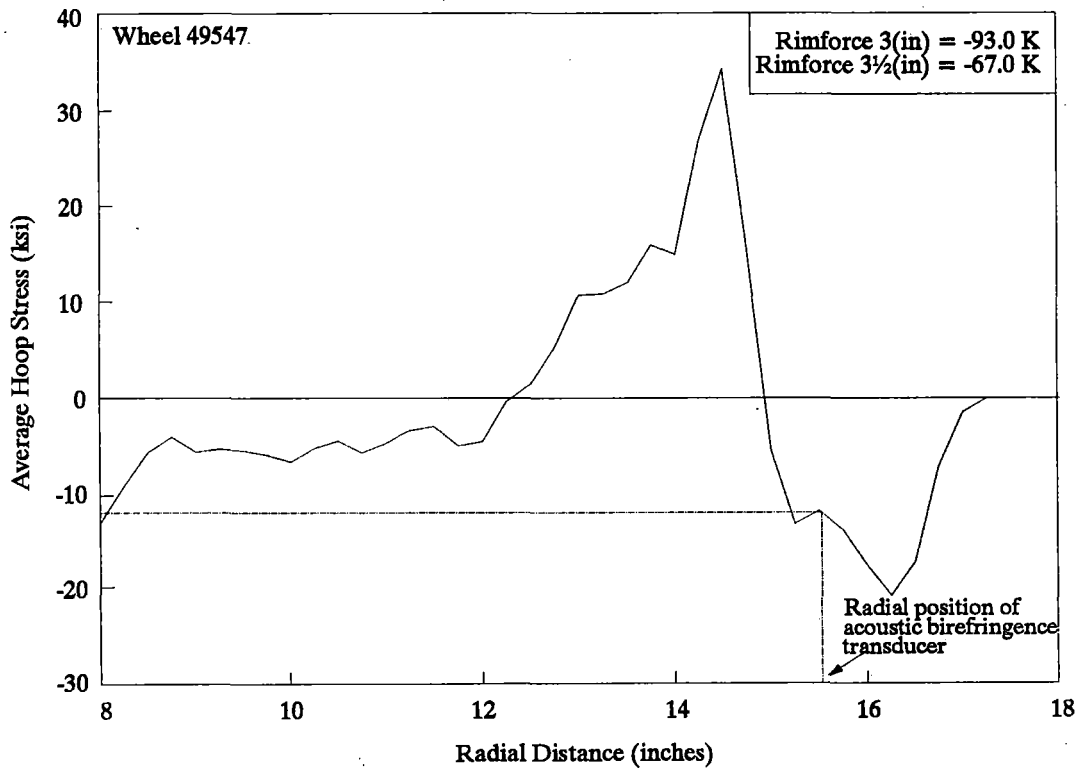
Computed Stress



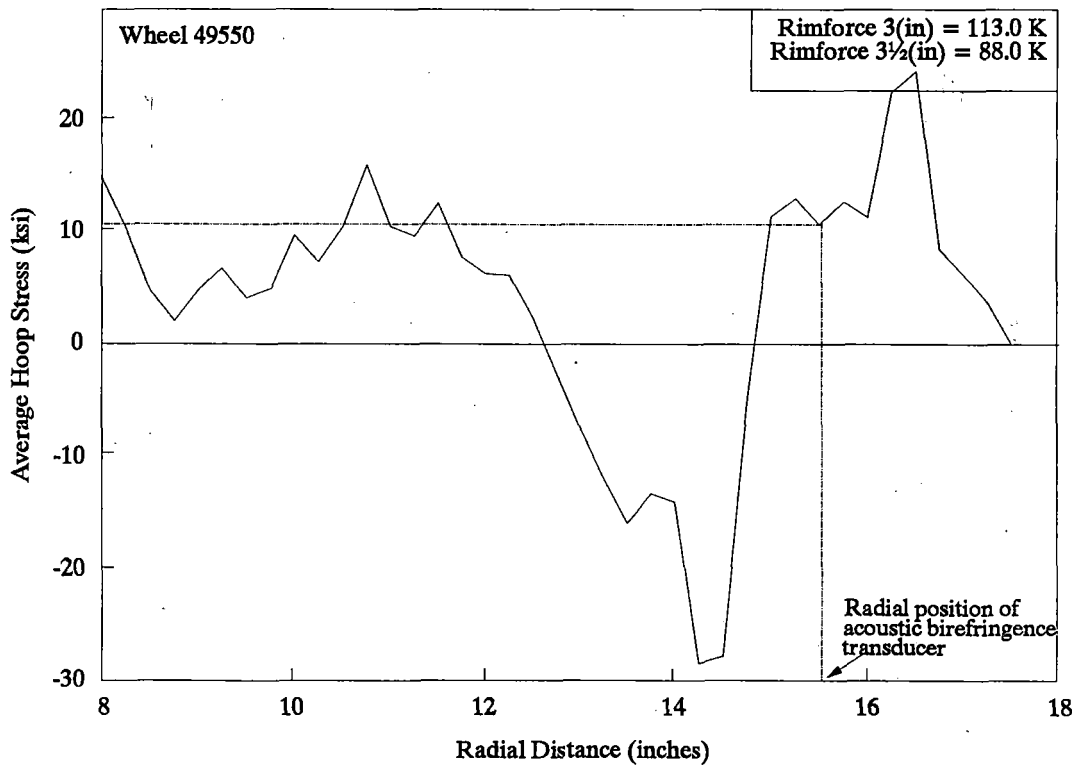
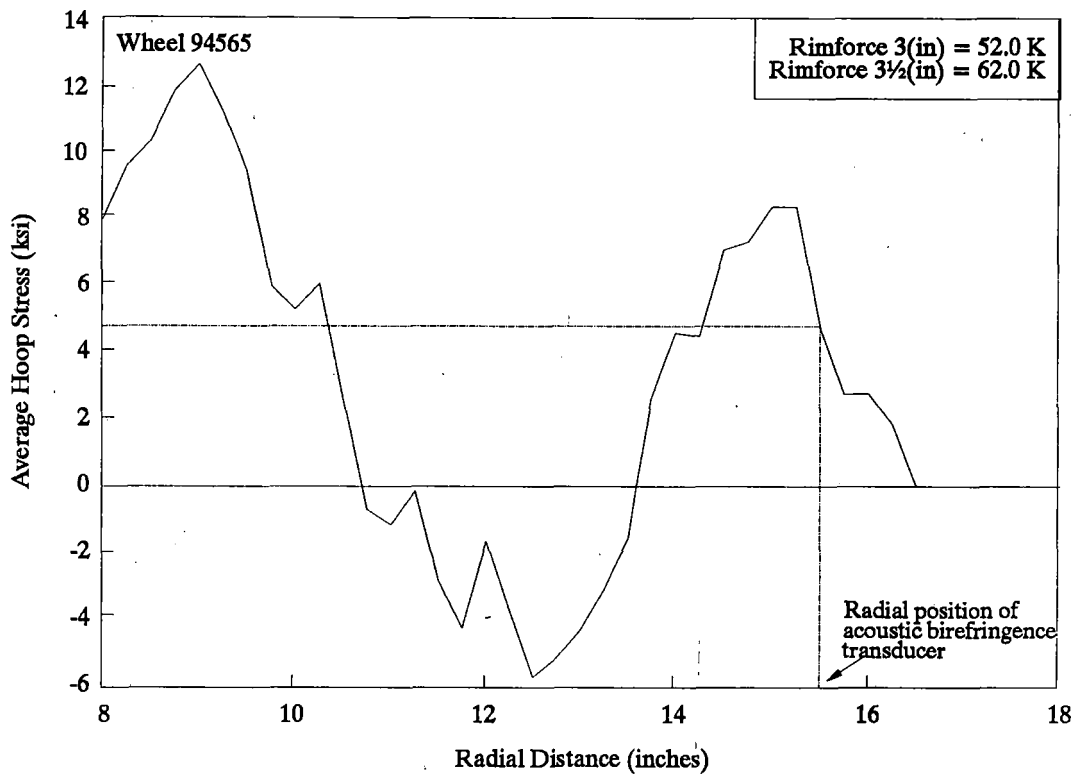
Computed Stress



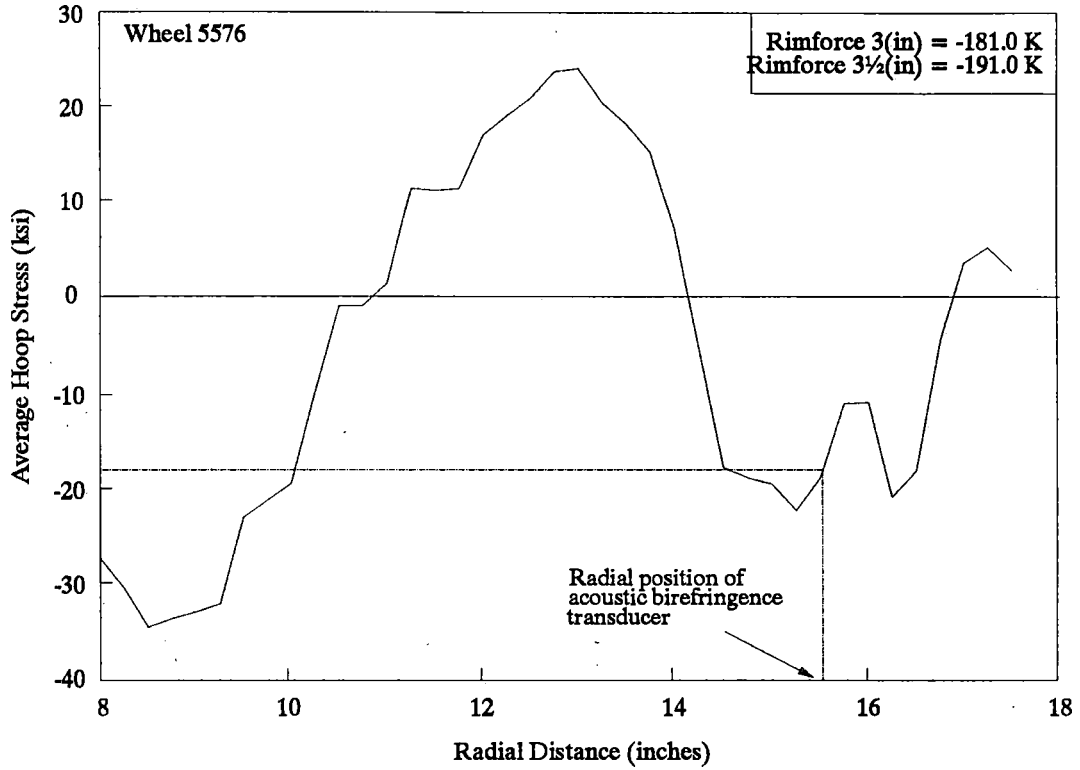
Computed Stress



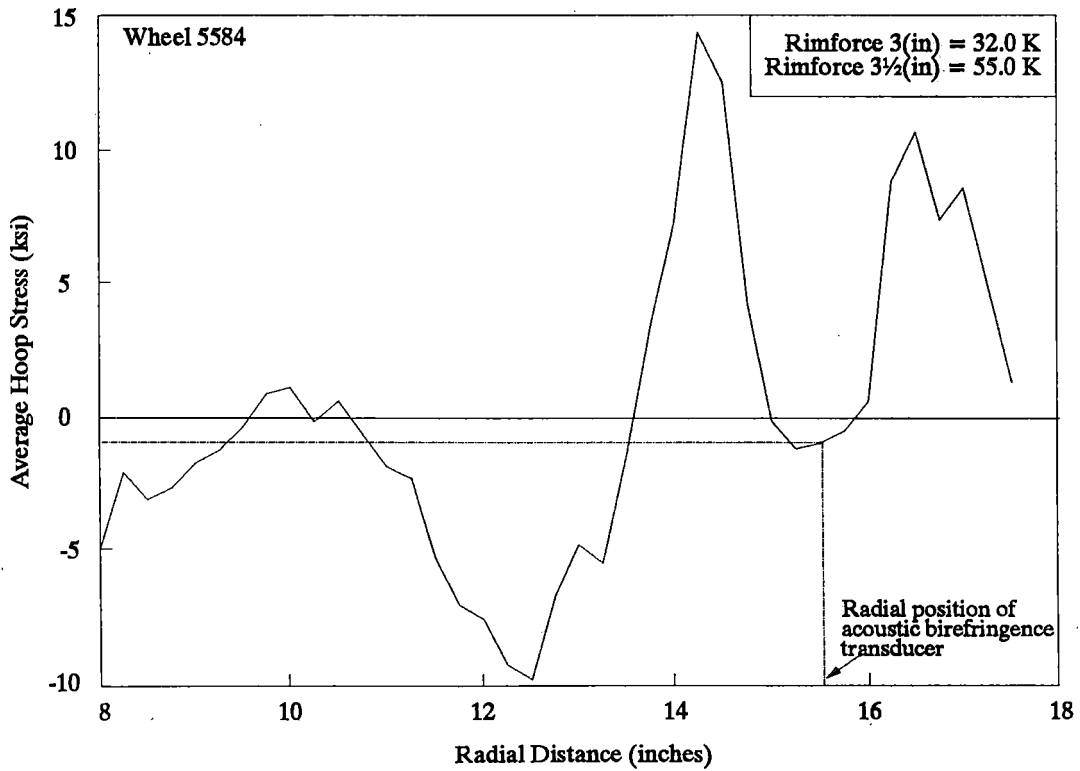
Computed Stress



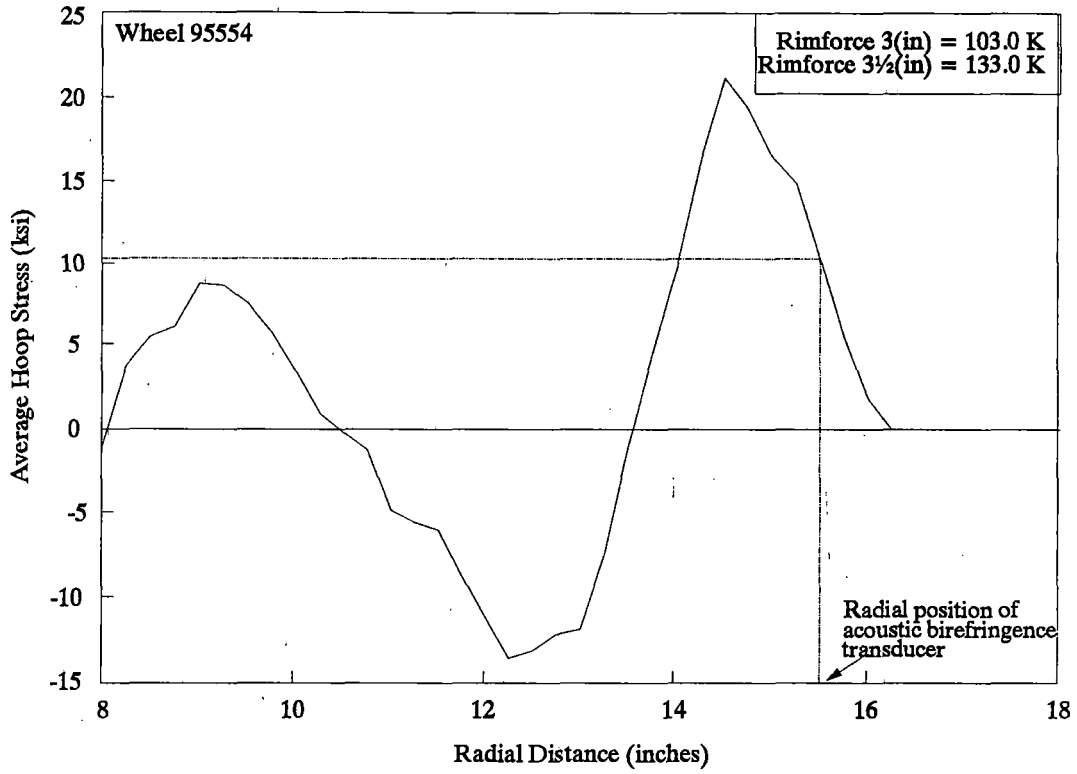
Computed Stress



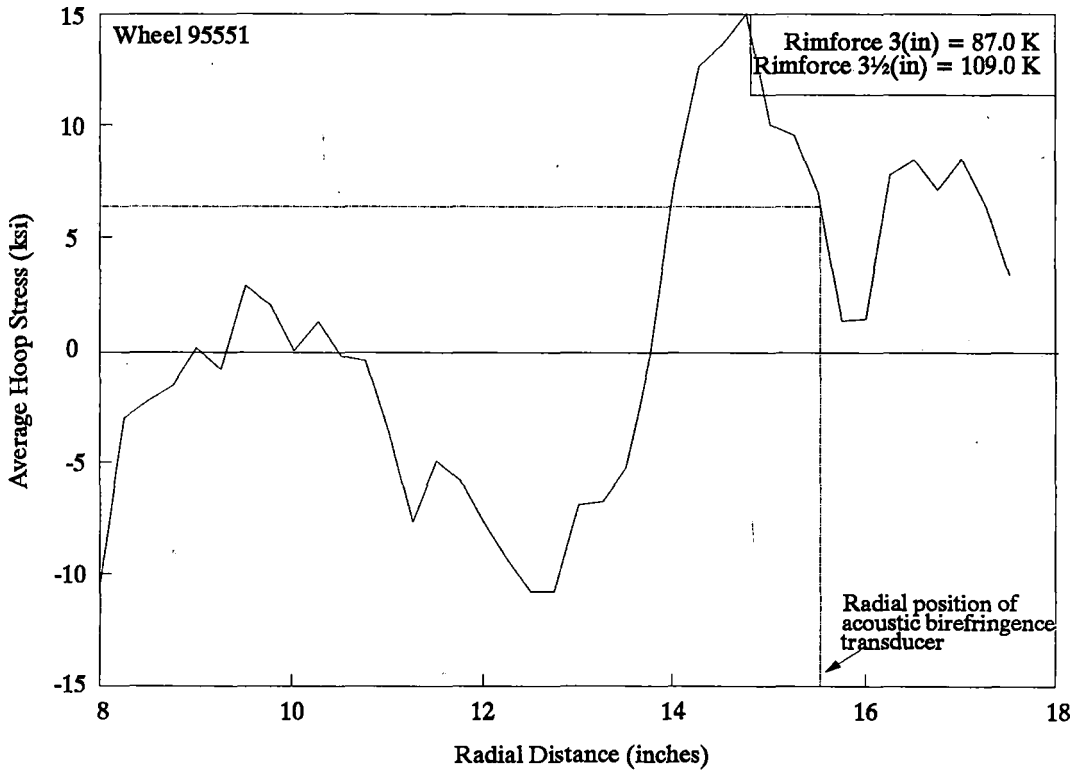
Computed Stress



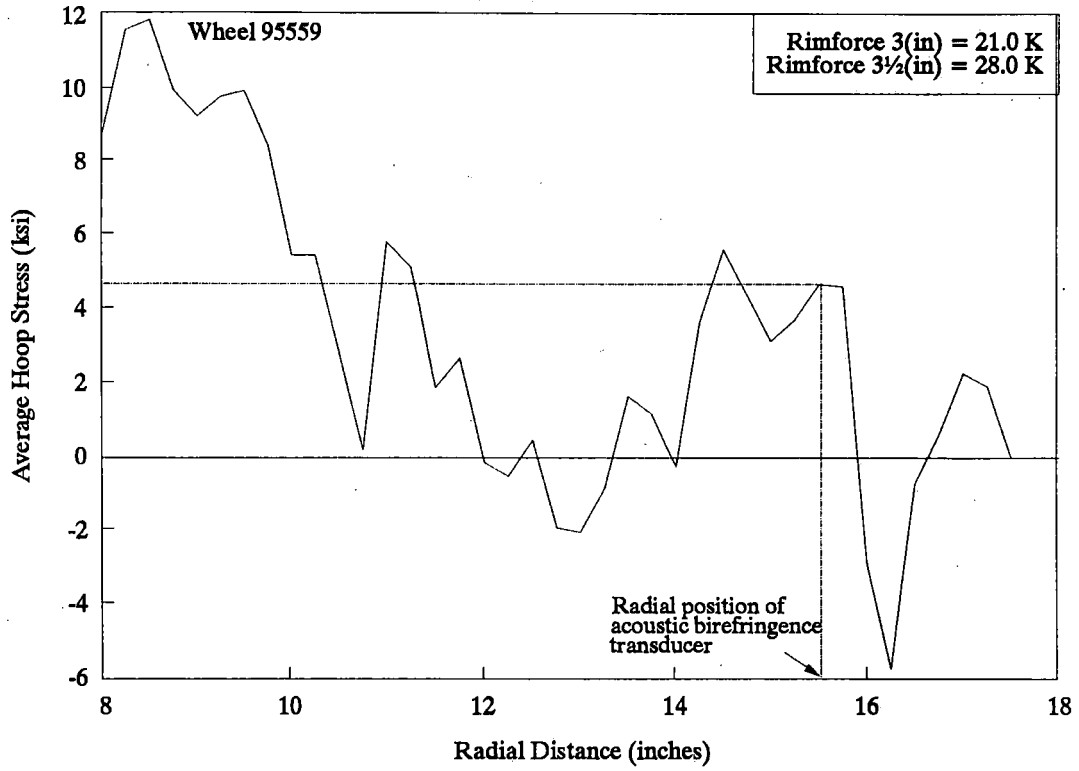
Computed Stress



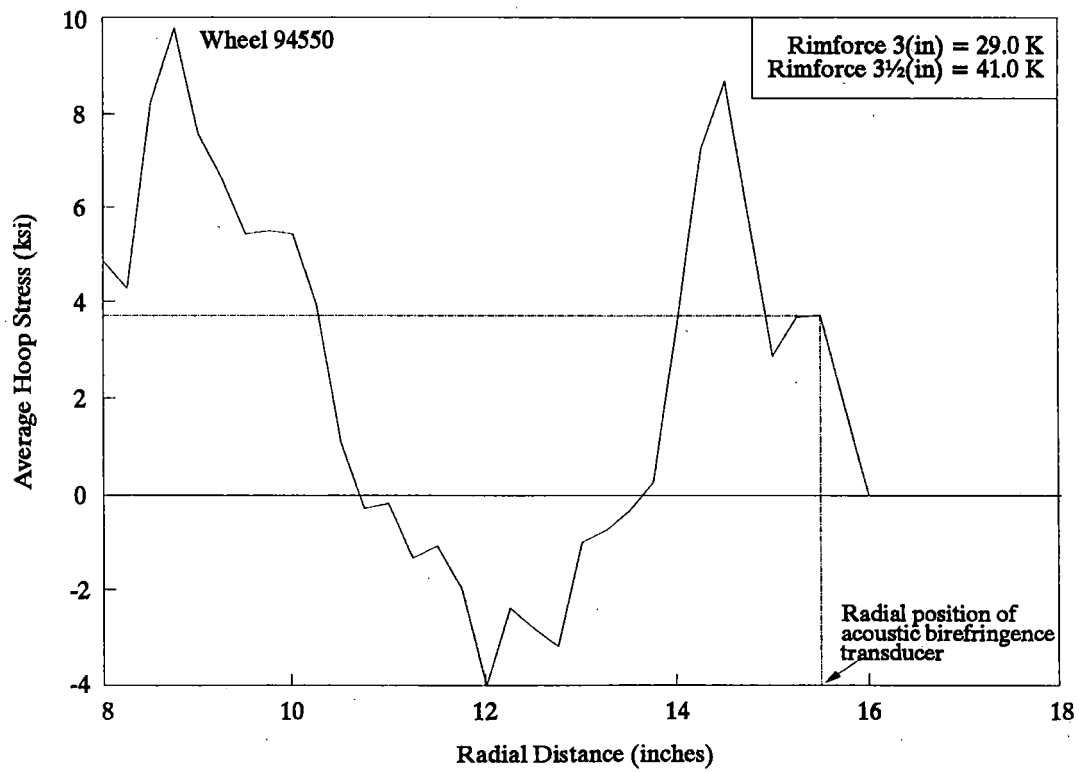
Computed Stress



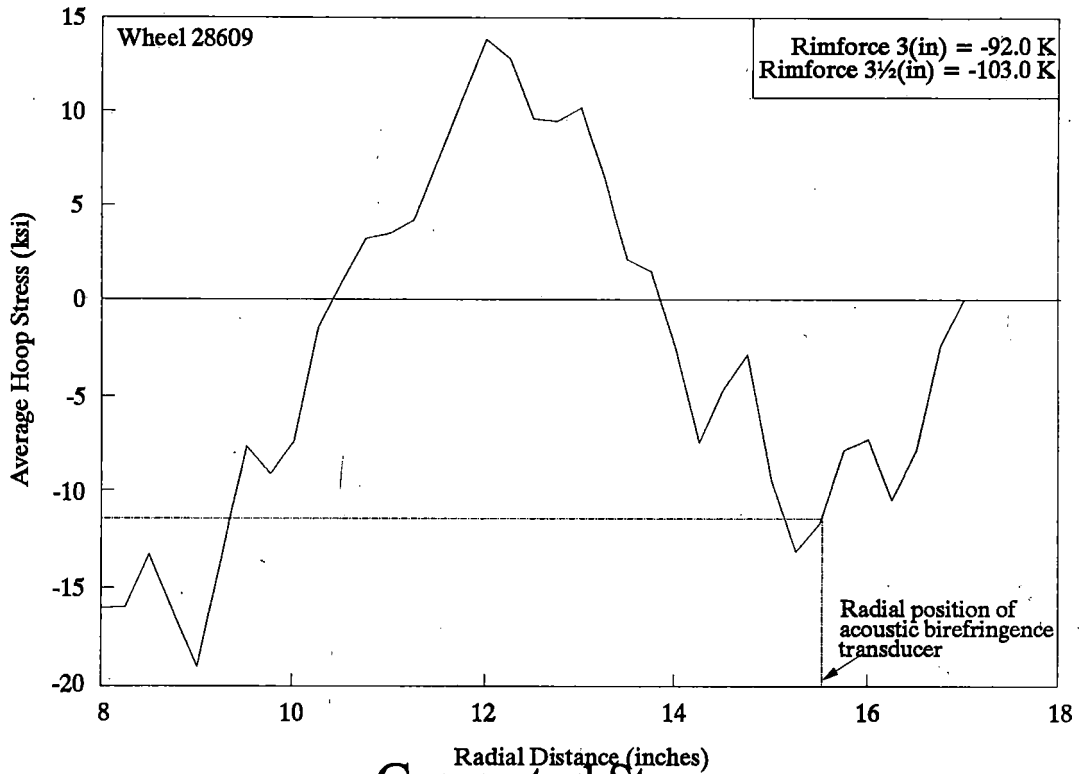
Computed Stress



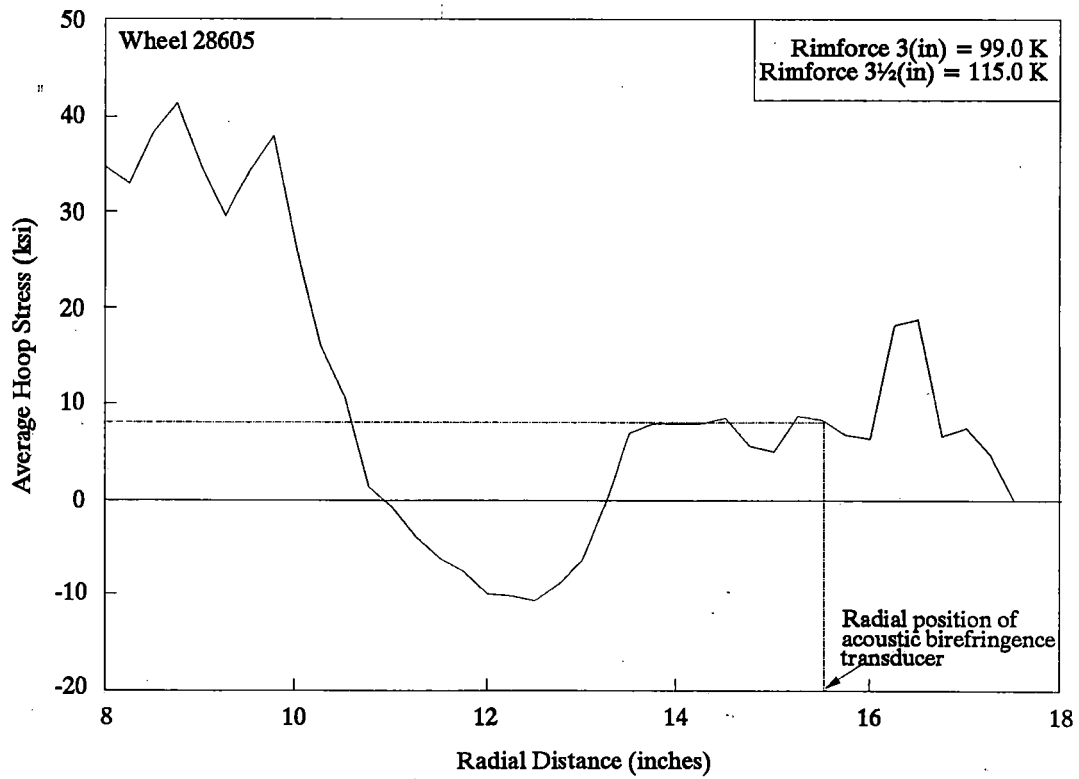
Computed Stress



Computed Stress



Computed Stress



APPENDIX J
INTERIM REPORT AND ANALYSIS OF WHEELS W1, W5, W6, AND W7 BY NIST

INTERIM REPORT:
PRELIMINARY COMPARISON BETWEEN NIST AND TTC STRESS DATA

This summarizes the results of measurements made at NIST on four drag-braked wheels labelled W1, W5, W6, and W7 by TTC. The original measurements (in drag-braked, stressed state) were made at NIST in 1987 (prior to the present task order). Recently, the wheels were destructively tested by saw cutting at TTC. Rim blocks were then cut out at four circumferential positions which corresponded to locations where birefringence measurements had previously been made. These locations were marked as the 0°, 90°, 180°, and 270° circumferential locations. These rim blocks were used to measure the (nominally) unstressed birefringence B_0 at both NIST and TTC. Measurements were made at TTC using equipment delivered by NIST early in 1991.

Several points can be made concerning these experiments. First, values of B_0 as measured at both labs were not in exact agreement. Overall, given the geometric assumptions about the reference marks used by the two labs (see below), the difference δB_0 in unstressed birefringence was equivalent to a stress difference of about 55 MPa (8 ksi) or less. This is an (approximate) average of the differences observed; these differences do not appear to be systematic. A typical plot of the data is shown in Fig. 1 for location 270°, wheel W6. Here the maximum discrepancy between NIST and TTC data is about 8×10^{-4} ; for a stress-acoustic constant C_A of $-9.5 \times 10^{-6} \text{ MPa}^{-1}$, we have, from

$$\delta B_0 / C_A = \delta \sigma_0,$$

a maximum stress difference, $\delta \sigma_0$, of about 80 MPa (11 ksi) between TTC and NIST data.

This raises some concerns about the differences between values of B_0 measured at NIST and TTC. The chief source of uncertainty in the measurement of B_0 appears to be lack of reproducibility in positioning the EMAT at exactly the same radial location. At NIST, we have done experiments which show that the precision (reproducibility) of these types of measurements (repositioning the EMAT at the same location) is about 3×10^{-4} , for a stress uncertainty $\delta \sigma_0$ of about 30 MPa (4 ksi).

Our consultation with TTC indicated two areas that may contribute to the observed differences:

1. Variations in the reference landmark or fiducial mark on the wheel rim. This makes it difficult to compare the several sets of data because of the radial gradient of the birefringence.
2. With the EMAT established at its radial location, there are two procedural difficulties in the data collection. The transducer must sit flat on the rim face and the arrival time measurement must be reliable to within a few nanoseconds.

There were several landmarks used for the current data (Fig. 2). At NIST, we have used the center of the of the flat part of the front rim face as the "0" radial position. In the course of the four years between the whole-wheel and the rim-block measurements, the original index marks were lost and had to be re-established. This represents some uncertainty because of the rounded edges of this face. TTC indexed their birefringence measurements to the inside edge of the front face. Again the rounded edge makes correlation of the data sets somewhat uncertain. The index for the DE measurements appears to be the flange tip.

We are now designing a mechanical aid to help us locate the face edge reproducibly. When both facilities have one of these, it will be possible to compare NIST and TTC data more confidently.

The EMAT fixture (Fig. 3) constructed a year ago helps to establish and maintain the radial location. In this first version, we have found that great care is necessary to keep the transducer flat on the rim face; this is necessary to assure the signal has maximum strength and constant phase. A modification of the fixture to address this problem is now in progress.

A very stable counter/timer is necessary to assure the essential timing accuracy. The unit delivered to TTC does not seem to have the necessary reliability. To relieve this problem, we are examining specifications for a replacement unit.

While the index marks vary among the measurements, it is possible to make some reasonable assumption to allow comparisons and calculations. Figures 4-7 show data taken on wheel W1 which showed the largest stress. Each figure shows a different circumferential location. It is clear that:

1. The original birefringence B (stressed state) was algebraically less than B_0 , indicating a state of tension for this wheel.
2. This pattern was observed for all four circumferential locations.
3. If the data points were connected, the NIST data for B_0 would appear to follow a "smoother" curve than the TTC data.
4. The (stressed) birefringence B appears to be relatively constant with radial position whereas the B_0 data have a larger gradient.

These data were used to produce a predicted stress, σ_0 , from the equation

$$B - B_0 = C_A \sigma_0. \quad (1)$$

To "smooth out" the apparent fluctuations in the data curves were "faired through" the B and B_0 data from NIST. The distances (B - B_0) between points on these lines was determined at various radial locations and inserted into equation (1) to obtain σ_0 .

The DE values σ_θ obtained from sawcutting are shown in Fig. 8. Here the right-hand side of the plot (at about a radial distance of 413 mm or 16.25 inches from the center of the hub) supposedly corresponds to the flange tip. The rim is about 62.5 mm (2.5 inches) wide, so the back rim face meets the parabolic region of the plate at about 356 mm (14 inches) on this plot.

At this point difficulties arose in comparing DE and NDE measurements. The problem here is this: the wheel is nominally 419 mm (16.5 inches) in diameter, as measured from hub center to a point on the tread, and the flange extends about 25 mm (1 inch) past this point. Thus, we expected the sawcut data to extend out to 445 mm (17.5 inches), rather than 413 mm (16.25 inches) as shown in Fig. 8.

In Fig. 9, we overlay the rim profile, sawcut (DE) data, and NDE data, assuming the sawcut data begins at the flange tip. The NDE and DE data have about the same peak σ_θ , but opposite gradient here. In Fig. 10, we have shifted the birefringence data for best correspondence with the sawcut data: now both DE and NDE data have about the same gradient, and the peak stress occurs at the inside edge of the inside rim face. In the figure we have used different symbols for the data taken at different circumferential locations. These show that the stress state is close to axisymmetric for this wheel (W1). In spite of these difficulties, it is encouraging to note that both DE and NDE measurements show that W1 was in tension in the rim area, and give about the same peak stress.

If we assume that for W6 the flange tip is at 406 mm (16 inches), then, since the DE data show a stress of about zero at 356 mm (14 inches), we would expect the NDE data to show small stress there also. In fact, to within experimental error (about 28 MPa or 4 ksi), we found that for all four circumferential positions $(B - B_0)/C_A$ was zero over the range of radial positions, r , for which $|r| \leq 4$ mm. Here $r=0$ (NIST definition) at TTC's "radial distance" of about 361 mm (14.2 inches). Thus, subject to the above assumption, we find that both the DE and NDE measurements give the same stress, to within the experimental error for this wheel.

It is difficult to conclude much about wheels W5 and W7, because $B - B_0$ was not of the same sign (for some radial positions) at all circumferential locations. This may mean that σ_θ is not axisymmetric, which may invalidate the DE data since they require an axisymmetric stress state. However, we can conclude that, if we average $B - B_0$ for all circumferential positions, it indicates once again that σ_θ is almost zero to within experimental error. This is in general agreement with the DE values of σ_θ . The DE values of σ_θ are also about -5 ksi for W5 over the range of

radial positions where $B - B_0$ was measured, and about +35 MPa (+5 ksi) for W7.

To conclude:

1. NIST and TTC values of B_0 are in general agreement, but the differences appear to be larger than the expected uncertainty by a factor of about two;
2. Some of the differences may be due to positioning errors in wheels with large B_0 gradients;
3. There is a problem in cross checking B_0 data, and also comparing DE and NDE data, due to differing schemes for determining fiducial marks;
4. For those wheels for which the DE values were such that $|\sigma_0| \leq 35$ MPa (5 ksi), the NDE values were essentially zero to within experimental error (estimated ± 28 MPa or ± 4 ksi);
5. For the one wheel having significant stress (W1), the DE and NDE peak σ_0 agree.

A. Van Clark
November 1991

Wheel 6 (270 degrees) 10-3-91

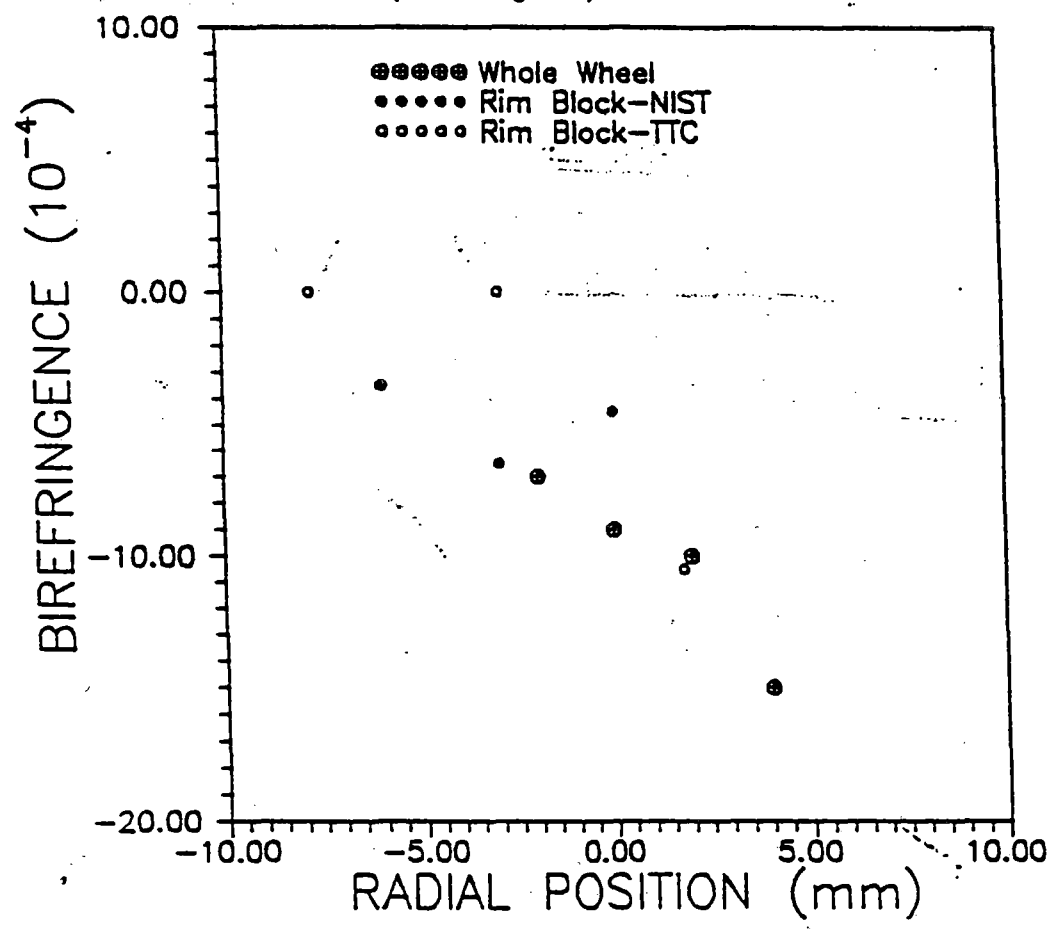


Fig. 1 Typical set of birefringence data comparing NIST and TTC measurements as well as whole wheel and rim block values. These data indicated the presence of very little stress in the drag-braked wheel W6.

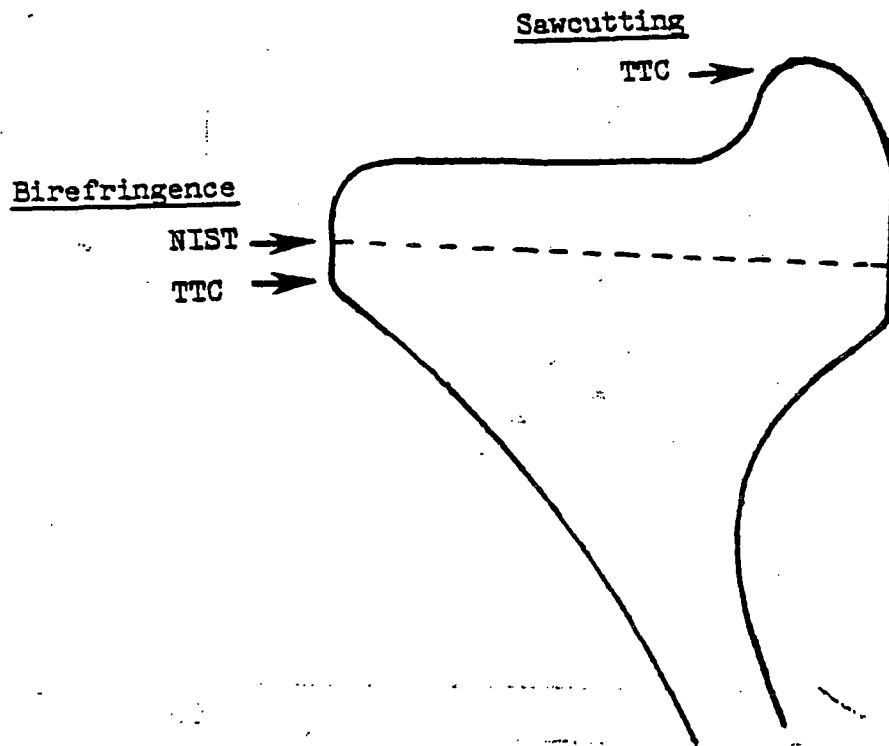


Fig. 2 Location of fiducial marks used for the various measurements noted in this report.

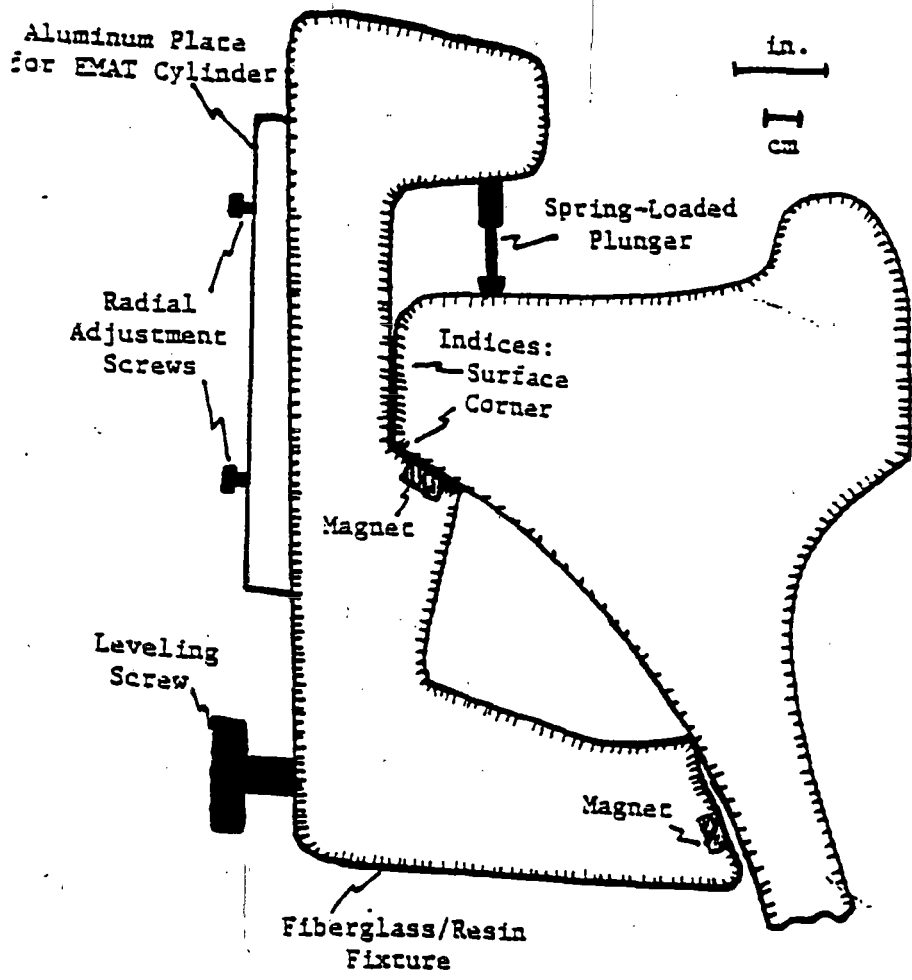


Fig. 3 Fixture used to position the EMAT on the front rim face.

Wheel 1 (0 degrees)

:10-3-91

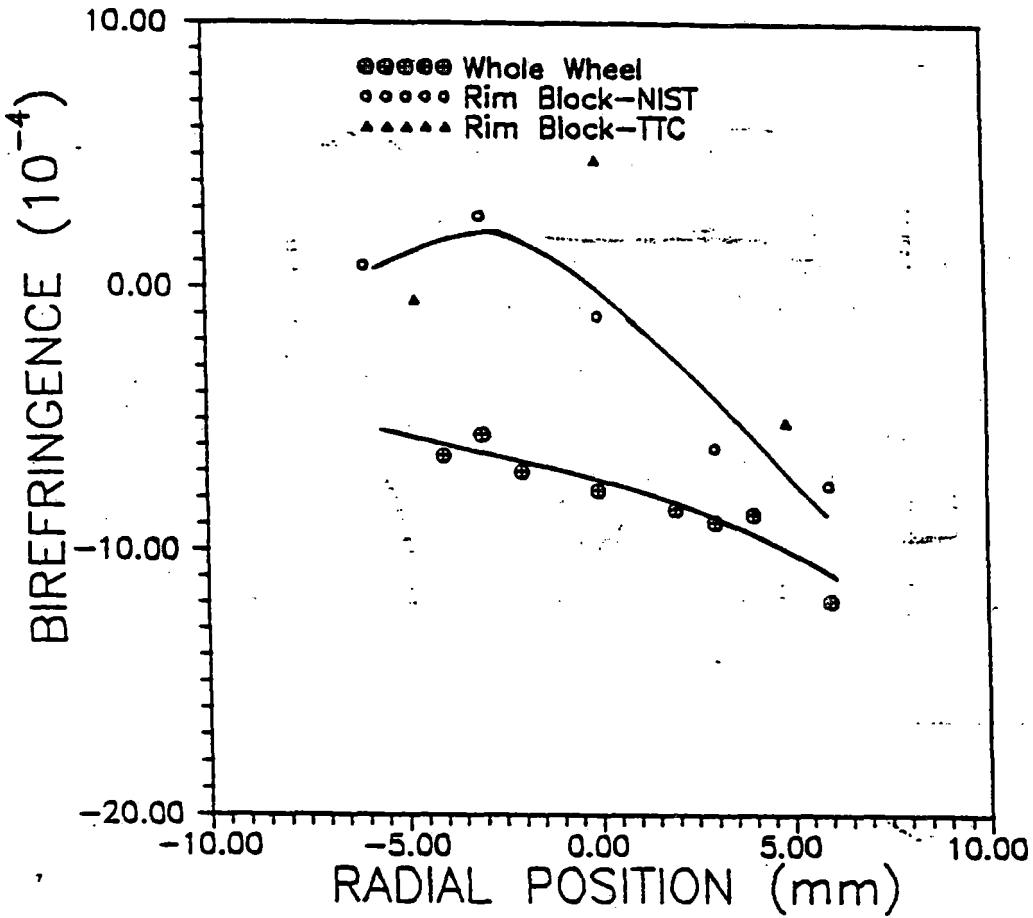


Fig. 4 Birefringence data for W1 at 0°. The curves are a smooth fit through the data and were used for the stress calculations.

Wheel 1 (90 degrees)

10-3-91

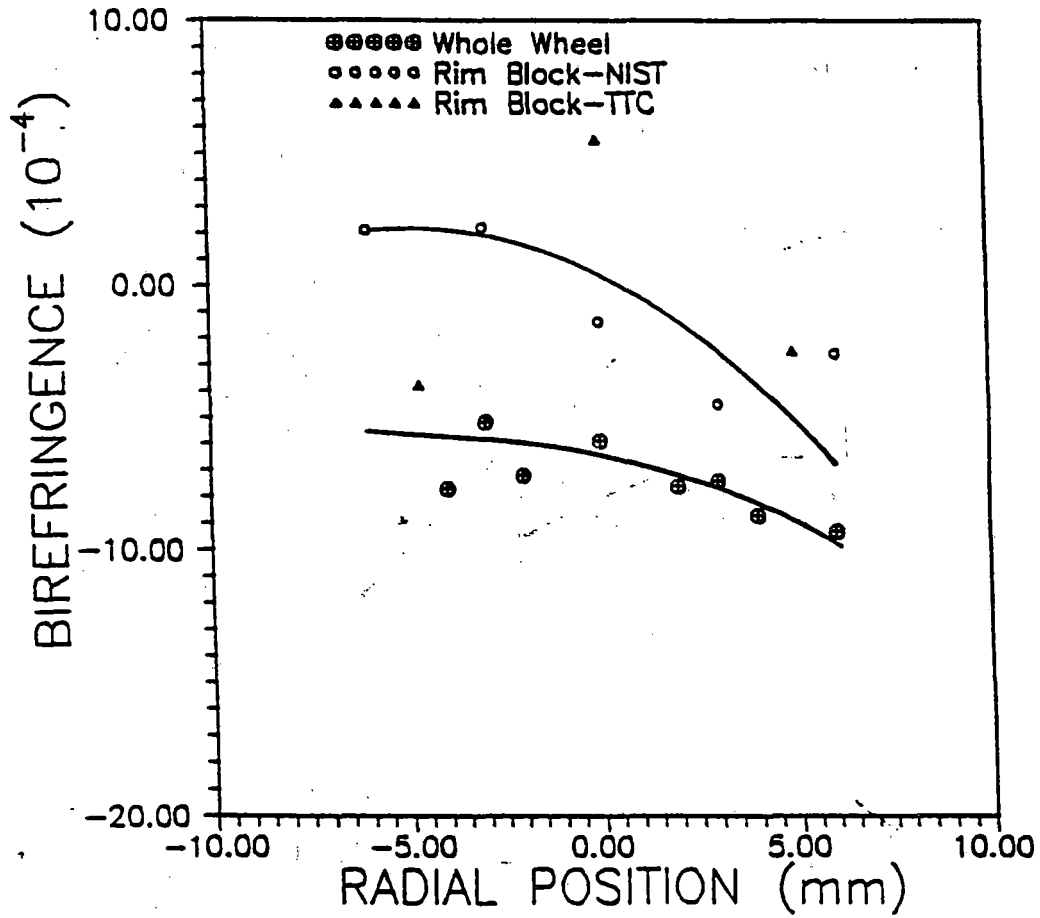


Fig. 5 Birefringence data for W1 at 90°. The curves are a smooth fit through the data and were used for the stress calculations.

Wheel 1 (180 degrees)

10-3-91

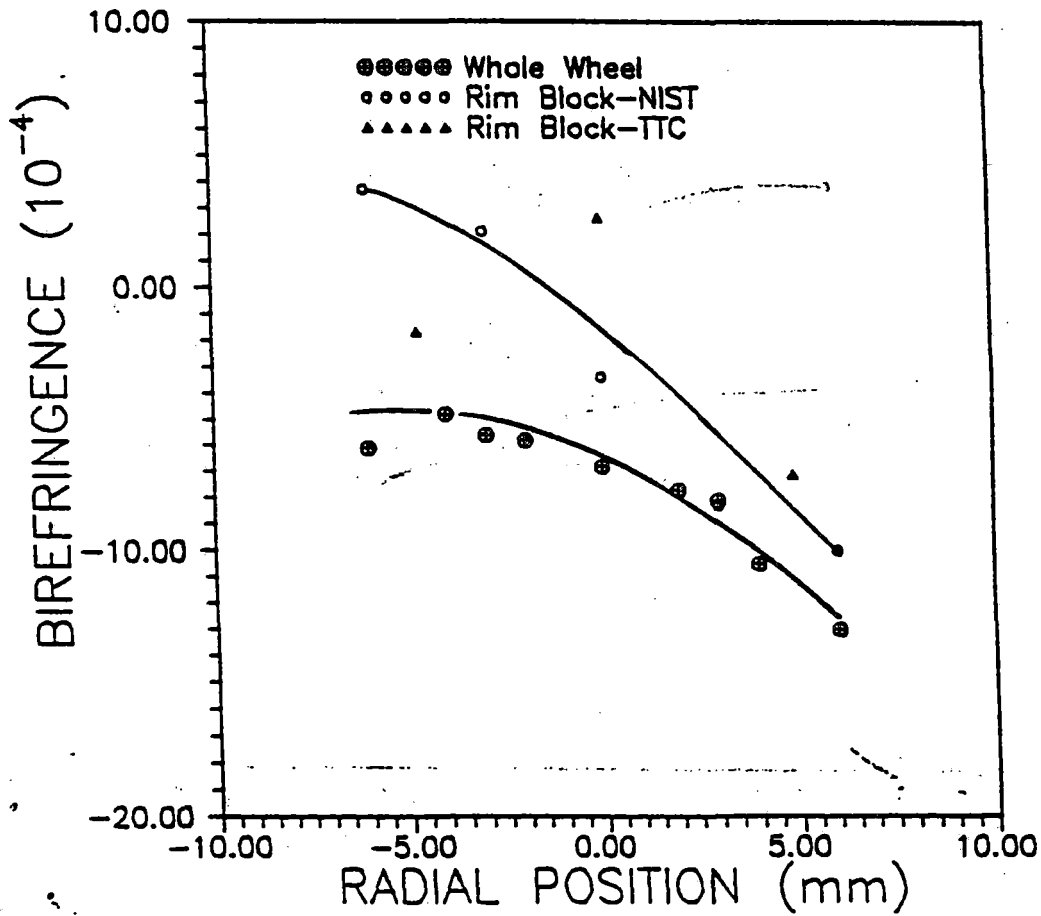


Fig. 6 Birefringence data for W1 at 180°. The curves are a smooth fit through the data and were used for the stress calculations.

Wheel 1 (270 degrees)

10-3-91

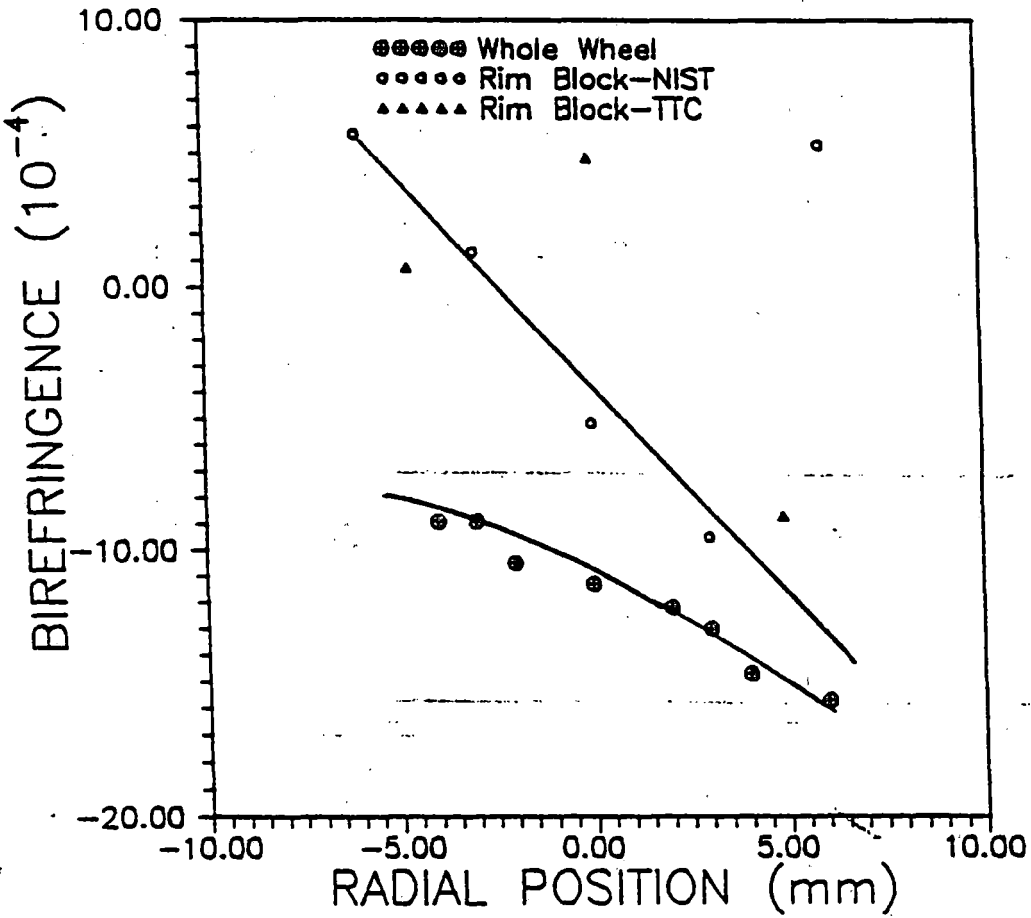


Fig. 7 Birefringence data for W1 at 270°. The curves are a smooth fit through the data and were used for the stress calculations.

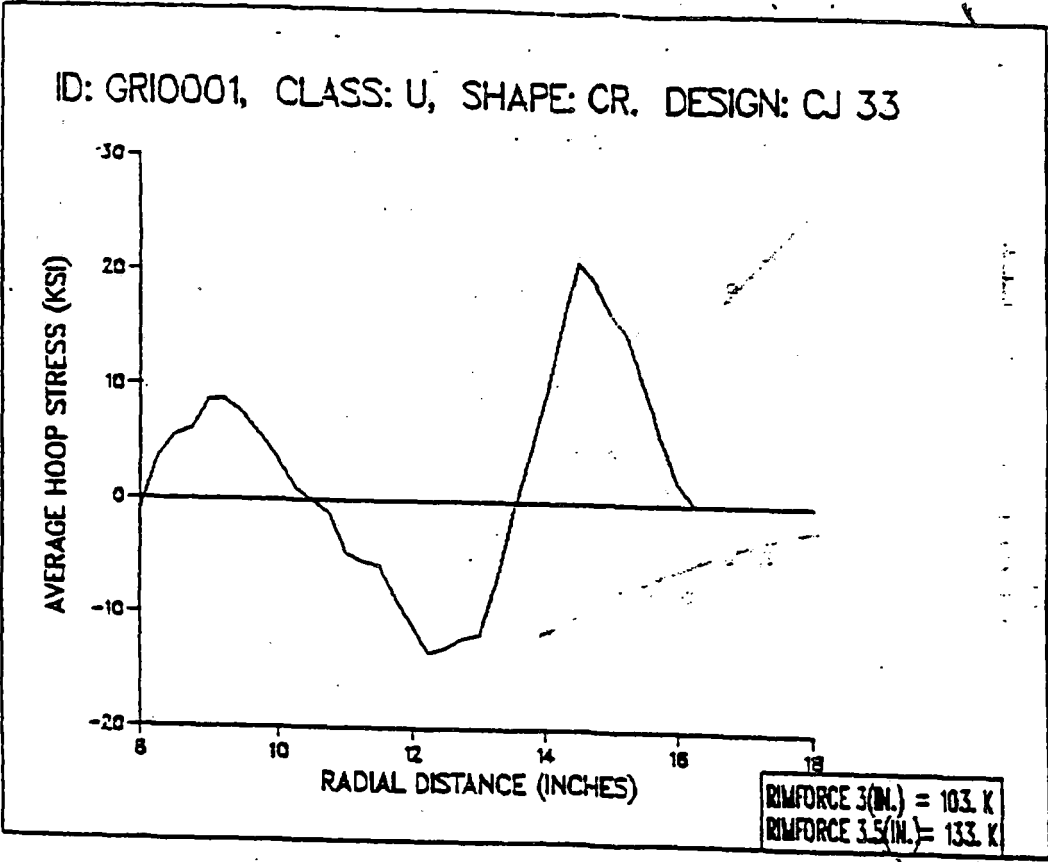


Fig. 8 TTC stress data for W1 calculated from sawcut displacement.

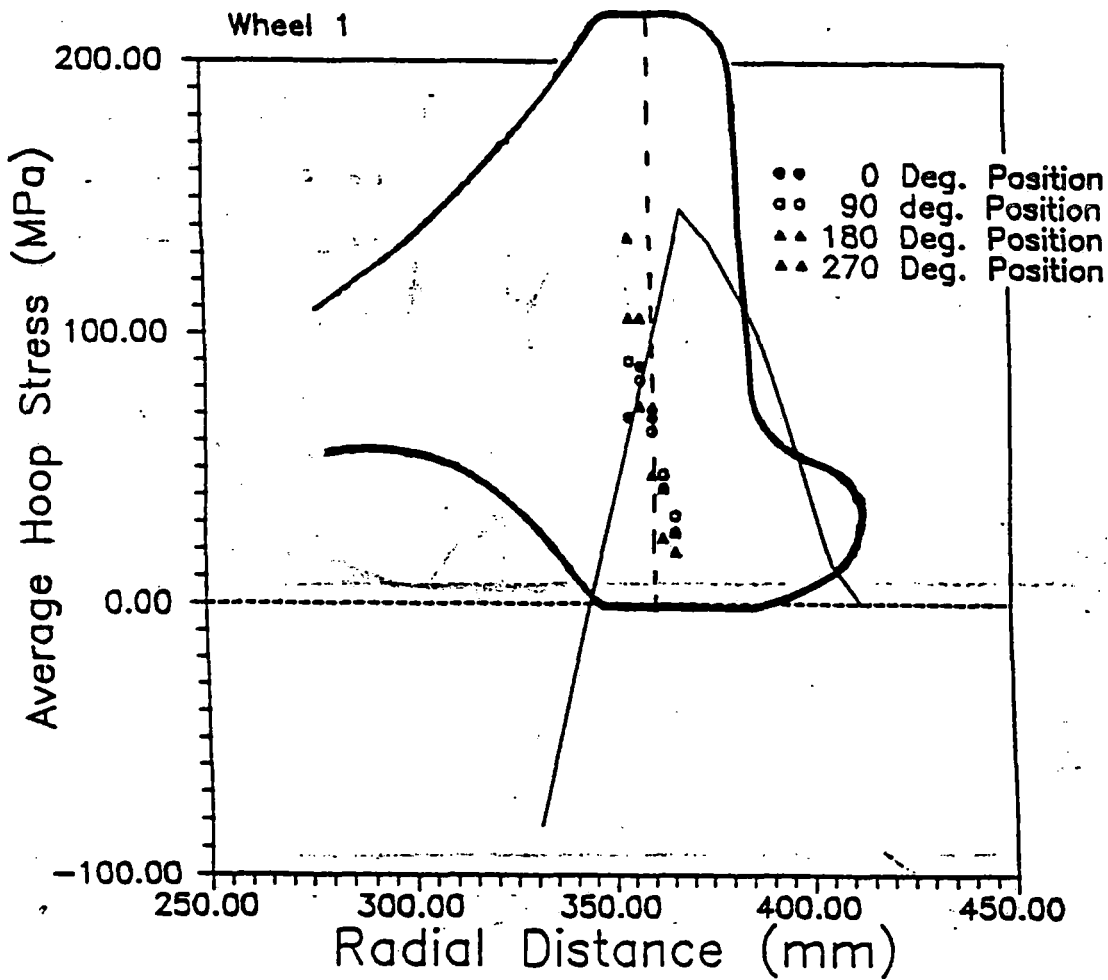


Fig. 9 Superposition of wheel profile over the stress data from TTC sawcutting and NIST birefringence. The assumption here is that the sawcut data begins at the flange tip.

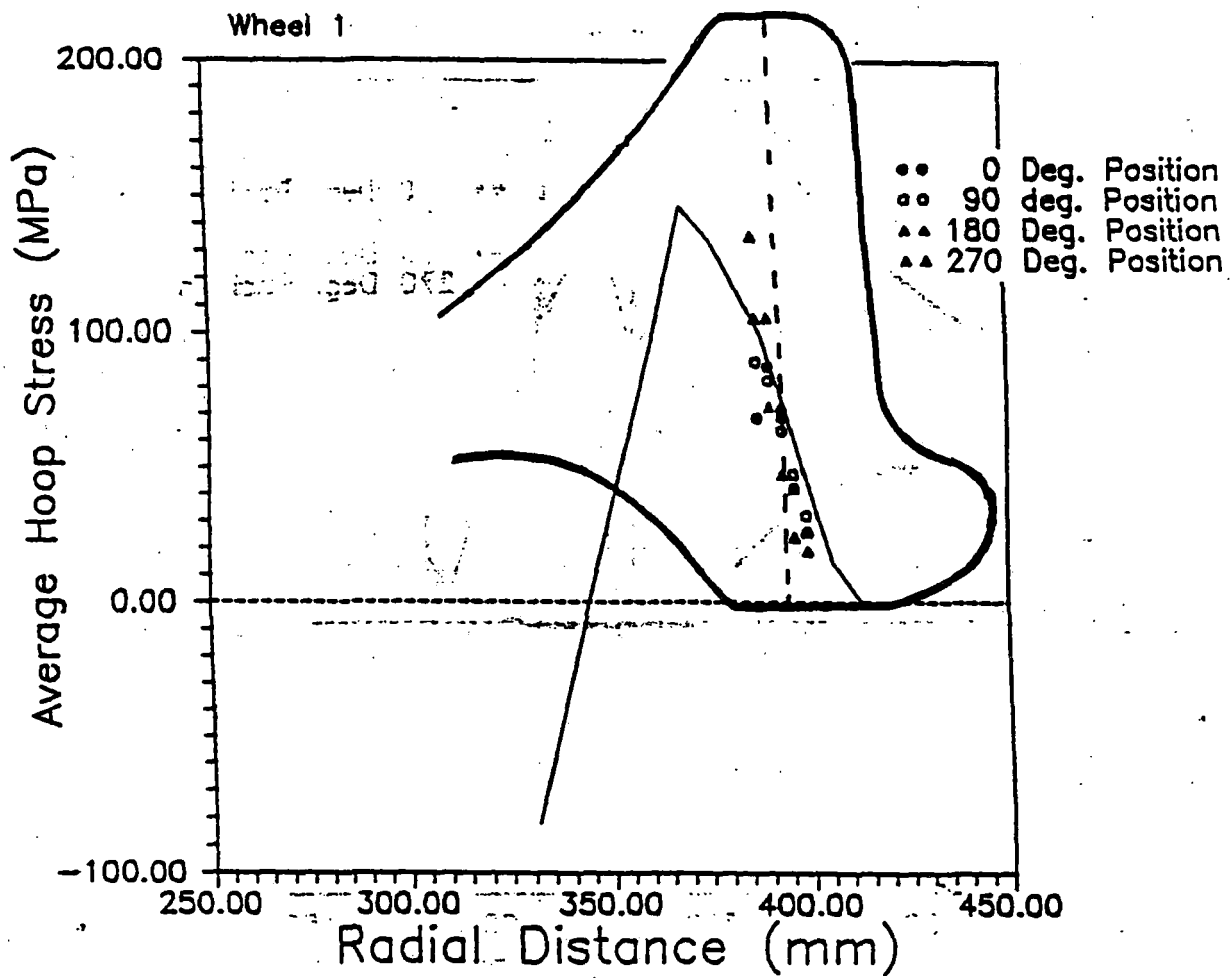


Fig. 10 Superposition of wheel profile over the stress data from TTC sawcutting and NIST birefringence. The assumption here is that the peak stress occurs at the inner edge of the inside rim face.

Evaluation of Two Prototypes
for Non-Destructively Measuring
Stresses in Railroad Wheels, 1992
US DOT, FRA, RL Higgins and BR Rajkumar

**Evaluation of Two Prototype Devices for
Non-Destructively Measuring Stresses in
Railroad Wheels, 1992**
US DOT, FRA, RL Higgins and BR Rajkumar

STP-D-00-78665